Microstructure Control of Si-based Non-Oxide Ceramics through Precursor Design

プレカーサーの化学構造設計を利用したケイ素基非酸化物セラミックスの組織制御

岩本　雄二

YUJI IWAMOTO

2004

Microstructure Control of Si-based Non-Oxide Ceramics through Precursor Design

Contents

Chapter 1

Introduction

1.1. General aspect of polymeric precursor route for Si-based non-oxide ceramics.

From a viewpoint of materials scientists with the background of chemistry, the design of high-performance ceramics based on atomic or molecular units is an ideal way to control structure and properties. An important approach to achieve this goal is the concept of the synthesis of ceramics from precursors [1-3]. Since the investigations of Verbeek *et al*. [4] and Yajima *et al*. [5] in the mid-1970s, the pyrolysis of an appropriate Si-based polymeric precursor has been known as a practicable method to produce Si-based non-oxide ceramics at noticeably low temperatures (800 to 1500 °C). This polymeric precursor route is composed of the following four steps, and sometimes denoted as hybrid processing [6] (Fig. 1-1):

(1) The synthesis of oligomers or polymers from monomer units.

(2) Chemical or thermal cross-linking of the as-synthesized precursors to form higher molecular compounds with preceramic network structure.

(3) Conversion of the cross-linked polymeric precursor into amorphous ceramics by pyrolysis.

(4) Crystallization of the amorphous ceramics into thermodynamically stable phases by an additional heat treatment.

The potential advantages of this route are the easy purification of starting materials and thus the effective reduction of impurities in the final ceramic product, and the formation of novel, metastable amorphous ceramics that can not be produced by conventional powder processing methods, as well as the low processing temperatures.

Furthermore, precursor synthesis, polymerization and cross-linking provide a means to vary the specific properties of the pre-ceramic compounds such as composition, solubility, fusibility or viscosity extensively providing the versatility in processing and shaping capabilities similar to that successfully achieved with polymer materials (Fig. 1-2). Ceramic powders and monoliths can be produced from highly cross-linked polymeric precursors. Soluble and fusible polymeric precursors with suitable viscosity are applied for the preparation of ceramic coatings and fibers as well as for the infiltration of porous materials, which are difficult or impossible by the conventional powder processing method. Moreover, polymeric precursors are expected to serve as binders for shaping conventional ceramic powders like silicon nitride (Si_3N_4) and silicon carbide (SiC), into green parts and act simultaneously as sintering additives. Instead of ceramic powders, active fillers like metal powders which reacts with gaseous and solid pyrolysis products can be also applied [7,8].

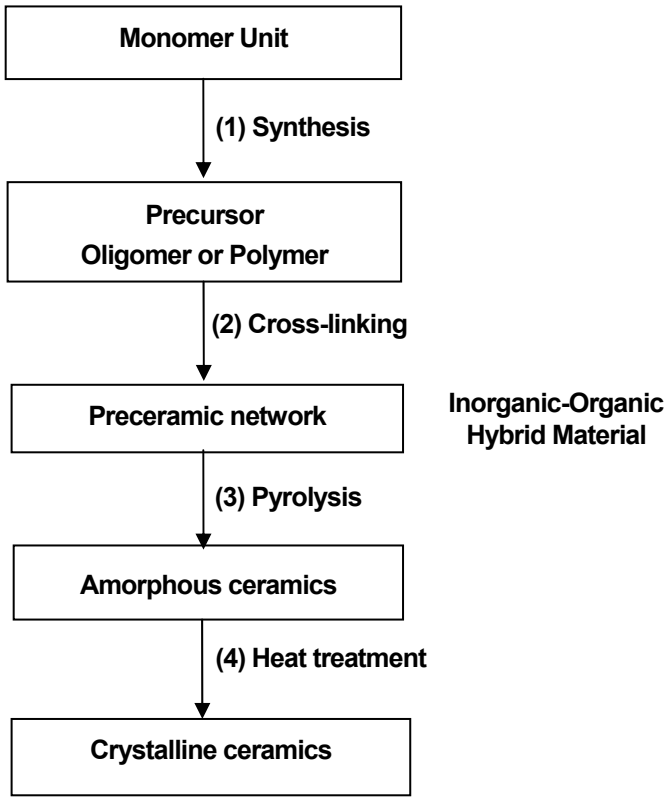

Fig. 1-1. Flow diagram showing synthesis of ceramics through polymeric precursor route.

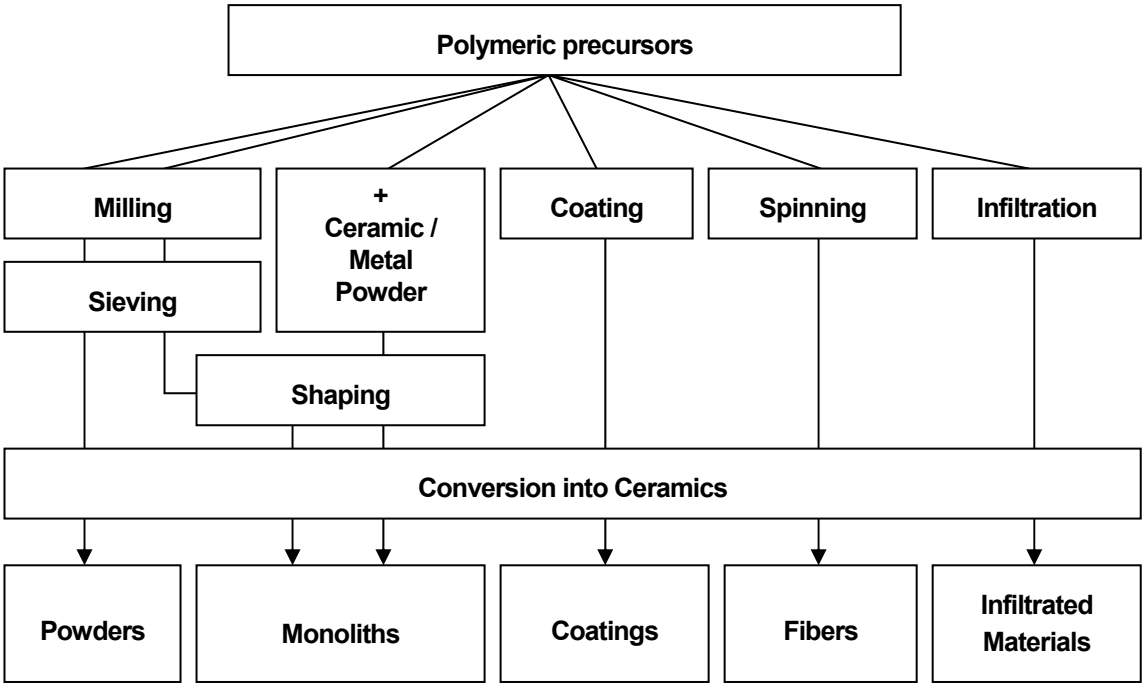

Fig. 1-2. Synthesis of ceramics from polymeric precursors.

1.1.1. Polymeric precursors for Si-based non-oxide ceramics

Figure 1-3 shows an overview of the different types of polymeric precursors for Si-based non-oxide ceramics. The polymeric precursors are built up from monomer units. Si can be linked with Si-, C-, and N-containing units to form polymers with a variety of molecular structures. The polymeric precursors can be subdivided into four groups: (1) polysilanes ($[-R^1R^2Si-]_n$), (2) polycarbosilanes ($[-R^1R^2Si-CH_2-]_n$), (3) polysilazanes ($[-R^1R^2Si-NH-]_n$) and (4) polysilylcarbodiimides ($[-R^1R^2Si-N=C=N-]_n$), where R, R^1, R^2=H, CH_3, C_6H_5 (phenyl) or $CH=CH_2$ (vinyl).

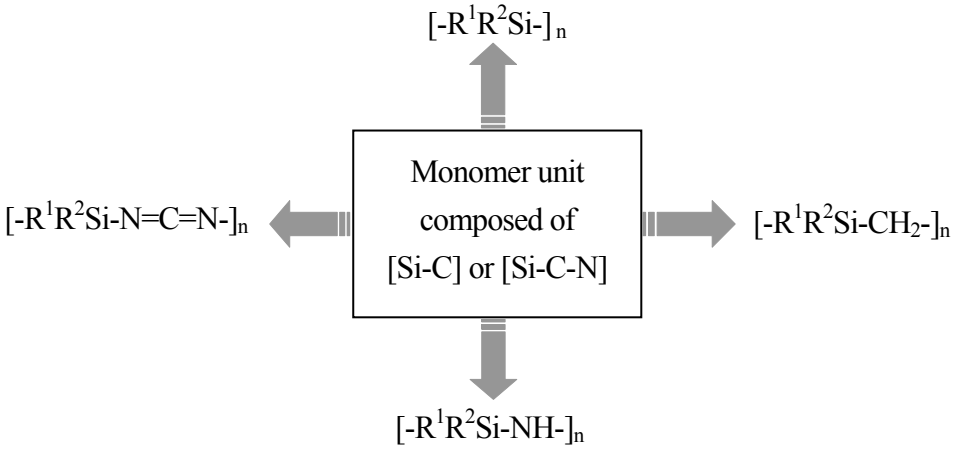

Fig. 1-3. Polymeric precursors from monomer units.

1.1.1.A. Polymeric precursors for SiC ceramics

Polydiorganosilanes, which have a backbone composed entirely of silicon atoms, have long been known. In 1921, Kipping *et al*. first synthesized polydiphenylsilanes by the Wurtz-Fittig analogous reaction of dichlorodiphenylsilane with molten sodium in xylene [9]:

$$nPh_2SiCl_2 \xrightarrow{Na} [-Ph_2Si-]_n + nNaCl \qquad (1.1)$$

Polydimethylsilane, synthesized by the similar dechlorination reaction in benzene, was reported by Burkhardt in 1949 [10]:

$$n(CH_3)_2SiCl_2 \xrightarrow{Na} [-(CH_3)_2Si-]_n + nNaCl \qquad (1.2)$$

However, these polymers were characterized only in terms of the chemical composition at that time. Consequently, the field of polydiorganosilane synthesis was not further pursued until the investigations of Verbeek *et al*. [4] and Yajima *et al*. [5] on the thermal conversion of polydimethylsilanes into SiC ceramics published in 1974 and 1975, respectively.

Prior to the conversion into SiC, the polydimethylsilanes undergo rearrangement into polycarbosilanes by heat treatment above 400 °C (Eq. 1.3) [11] (Kumada rearrangement [12]), which can also be promoted by Lewis acid catalysts [13,14].

$$[\text{-}(CH_3)_2Si\text{-}]_n \xrightarrow{T < 400\ °C} [\text{-}(CH_3)SiH\text{-}CH_2\text{-}]_m \qquad (1.3)$$

Polycarbosilanes can also be directly synthesized by the potassium metal dechlorination of mixtures of vinylmethylchlorosilanes with methylchlorosilanes [15], or by platinum catalyzed polymerization using vinyl- or allylchloroailanes as starting materials and subsequent reduction by $LiAlH_4$ [16].

The pyrolysis above 1000 °C of polycarbosilanes results in the formation of SiC ceramic residues containing an excess of carbon (Eq. 1.4), which limits the high-temperature properties like the oxidation resistance of the SiC ceramics [13].

$$[\text{-}(CH_3)SiH\text{-}CH_2\text{-}]_m \xrightarrow{T<1000\ °C} mSiC + mH_2 + mCH_4 \qquad (1.4)$$

Therefore, a main objective for the preparation of near stoichiometric SiC is the synthesis of polymeric precursors with lower carbon content, and the synthesis of polymethylsilanes ($[\text{-}(CH_3)SiH\text{-}]_n$) by polymerization of CH_3SiH_3 applying metallocenes [16] as well as by the Na condensation of CH_3SiHCl_2 and subsequent treatment with metallocenes [17] has been developed.

1.1.1.B. Polymeric precursors for ternary Si-C-N ceramics

(1) Polysilazanes and related compounds

Contrary to the expensive dechlorination reaction of chlorodiorganosilanes with Na or K used to synthesize the polysilanes, the polysilazanes are much more easily accessible in high amounts by the ammonolysis of R_2SiCl_2 and subsequent base-catalysed cross-linking of the received oligosilazane according to the method reported by Seyferth *et al*. [18]:

$$n CH_3SiHCl_2 + 3n NH_3 \xrightarrow{-2n NH_4Cl} [CH_3SiH\text{-}NH]_n \ (n=3 \text{ or } 4) \qquad (1.5)$$

$$n[CH_3SiH\text{-}NH]_4 \xrightarrow[-mH_2]{KH} [CH_3SiH\text{-}NH]_{4n-m}[CH_3SiN]_m \qquad (1.6)$$

The molecular composition of the polysilazanes can be varied either by the substitution of the methyl groups by other alkyl, aryl or vinyl groups, or by the coammonolysis of $RSiH_3$ and R_2SiCl_2 ($R=CH_3$).

The cyclic oligosilazanes have been converted, by the reaction with urea, to another higher molecular weight compound, poly(ureidosilazane) with the following simplified polymer structure [19]:

$$\{-[HN\text{-}SiH(CH_3)]_x\text{-}NH\text{-}[(C=O)\text{-}NH\text{-}SiH(CH_3)]_y\text{-}\}_n \qquad (1.7)$$

This synthetic route was developed on the basis of an older report about the reaction of hexamethyldisilazane with urea to give N,N-bis(trimethylsilyl)urea [20]:

$$[(CH_3)_3Si]_2NH + (H_2N)_2C=O \xrightarrow{\Delta} NH_3 + ((CH_3)_3SiHN)_2C=O \qquad (1.8)$$

Laine *et al*. developed another process based on transition metal catalysed dehaydrocoupling reaction, and poly(N-methylsilazane) has been successfully synthesized by the following synthetic route using $Ru_3(CO)_{12}$ [21]:

$$n H_2SiCl_2 + 3n CH_3NH_2 \xrightarrow[-2CH_3NH_3Cl]{Et_2O,\ -78\ ^\circ C} CH_3NH\text{-}[H_2Si\text{-}N(CH_3)]_n\text{-}H$$

$$\xrightarrow[-H_2]{Ru_3(CO)_{12},\ 65\ ^\circ C} CH_3NH\text{-}[H_2Si\text{-}N(CH_3)]_x\text{-}[HSi\text{-}N(CH_3)_{1.5}]_y\text{-}H \qquad (1.9)$$

Mocaer *et al*. synthesized a new kind of silazanes where the backbones of the polymer contain Si-N as well as Si-Si bonds by reaction of dimethyldichlorosilane and 1,3-dichloro-1,3-dimethyldisilazane in the presence of Na (Eq. 1.10) [22].

$$(1\text{-}x)(CH_3)_2SiCl_2 + xCl(CH_3)HSi\text{-}NH\text{-}SiH(CH_3)Cl \xrightarrow{\text{Na, Toluene}} [\text{-}(CH_3)_2Si\text{-}]_{1\text{-}x}[\text{-}(CH_3)SiH\text{-}NH\text{-}HSi(CH_3)\text{-}]_x \quad (1.10)$$

Similar to the transformation of the polysilanes into polycarbosilanes, the polymers can be transformed by thermal treatment to polycarbosilazanes by the insertion of methylene groups into Si-Si bonds to form backbones consisted of Si-CH_2-Si-N bonds.

He *et al*. also synthesized another new kind of silazanes, poly(methylsiladiazane) by copolymerization of methyldichlorosilane with hydrazine in 1:1.4 molar ratio [23]:

$$nCH_3SiHCl_2 + 1.4nH_2NNH_2 \xrightarrow[-\,2Et_3NHCl]{2Et_3N,\ \text{Toluene}} [\text{-}(CH_3)SiH\text{-}NH\text{-}NH\text{-}]_n \quad (1.11)$$

Pyrolysis of polysilazanes in an inert atmosphere at around 1000 °C yields ternary Si-C-N ceramics, while that in a reactive ammonia atmosphere yields binary Si-N ceramics according to the following simplified reactions equations:

$$[CH_3SiH\text{-}NH]_{4n\text{-}m}[CH_3SiN]_m \xrightarrow{1000\ ^\circ C,\ Ar\ \text{or}\ N_2} Si_xC_yN_z + H_2 + CH_4 \quad (1.12)$$

$$[CH_3SiH\text{-}NH]_{4n\text{-}m}[CH_3SiN]_m \xrightarrow{1000\ ^\circ C,\ NH_3} Si_xN_y + H_2 + CH_4 \quad (1.13)$$

Carbon-free polysilazanes, $[\text{-}SiH_2\text{-}NH\text{-}]_n$ have been also developed by the reaction of dichlorosilane and trichlorosilane with ammonia [24] as well as by the reaction of dichlorosilane-pyridine adducts ($SiH_2Cl_2{\cdot}2C_5H_5N$) with ammonia [25]. These perhydropolysilazanes can be directly pyrolyzed to yield binary Si-N ceramics under an inert atmosphere.

(2) Polysilylcarbodiimides

In 1993, Kienzle *et al*. developed the synthesis of $Si_xC_yN_z$ ceramics by pyrolysis of a novel class of polymeric precursors, the polysilylcarbodiimides [26]. The novel precursors can be synthesized by the reaction of dichloroorganosilanes with cyanamide and C_5H_5N:

$$nR(CH_3)SiCl_2 + H_2N\text{-}C{\equiv}N \xrightarrow[-\ C_5H_5N{\bullet}HCl]{C_5H_5N} [-R(CH_3)Si\text{-}N{=}C{=}N\text{-}]_n \qquad (1.14)$$

$R = CH_3, CH{=}CH_2, H$

The three-dimensional networks of silylcarbosiimides can be built up by the reaction of tetrachlorosilane ($SiCl_4$) with bis(trimethylsilyl)carbodiimide ($((CH_3)_3Si\text{-}N{=}C{=}N\text{-}Si(CH_3)_3$) in toluene with a catalytic amount of C_5H_5N [27] (Eq. 1.15).

$$nSiCl_4 + 2n(CH_3)_3Si\text{-}N{=}C{=}N\text{-}Si(CH_3)_3 \xrightarrow{C_5H_5N} [Si(N{=}C{=}N)_2]_n + 4nMe_3SiCl \qquad (1.15)$$

The reaction proceeds via the substitution of Si-Cl by $Si\text{-}N{=}C{=}N\text{-}Si(CH_3)_3$ groups and the subsequent condensation to poly(silicondicarbodiimide) ($[Si(N{=}C{=}N)_2]_n$). This reaction mechanism is completely analogous to the reaction of $SiCl_4$ and H_2O to SiO_2, and can be considered a novel sol-gel process route to non-oxidic Si-C-N ceramic materials (Fig. 1-4).

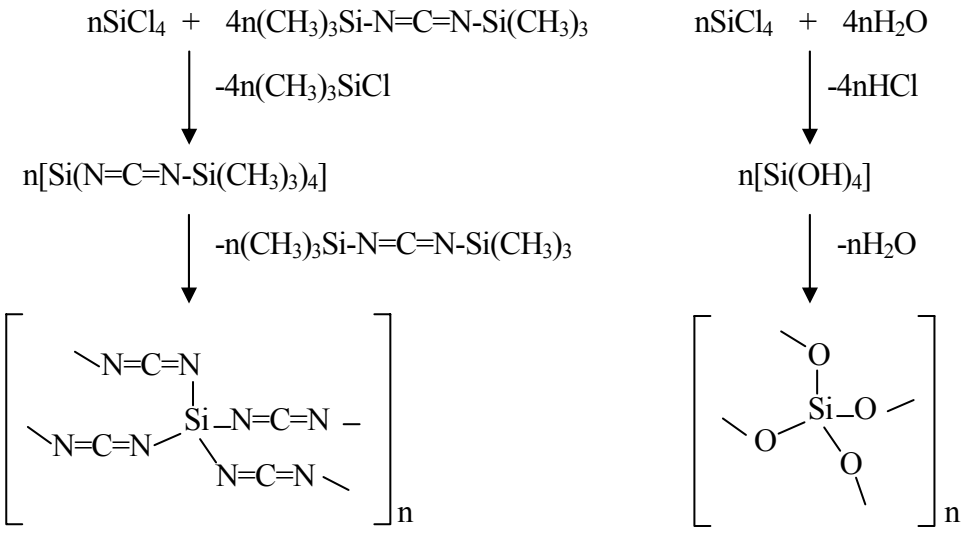

Fig. 1-4. Analogy of the reaction of $SiCl_4$ with $(CH_3)_3Si\text{-}N{=}C{=}N\text{-}Si(CH_3)_3$ and H_2O, respectively.

1.1.1.C. Polymeric precursors for multicomponent Si-M-C-N(O) ceramics

In the field of multicomponent ceramic materials, the following two aspects are important: (1) The synthesis of multicomponent amorphous ceramic powders is suitable to develop composite materials comprised of two or more binary compounds. For that purpose, the desired elements are subjected to heat treatment wherein the densification, crystallization and phase partitioning take place. (2) Some multicomponent amorphous materials can keep amorphous state even at extraordinarily high temperatures and thus can be used for high-temperature application.

However, the synthesis of multicomponent ceramic materials by the conventional powder processing has much difficulty, owing to the thermodynamic instability of their solid solutions. In contrast, thermodynamically metastable solid solution can be synthesized by the pyrolysis of polymeric precursors containing appropriate elements. The synthesis of multicomponent ceramic materials through the polymeric precursor route can be realized by following three different methods.

(1) Polymeric precursors with reactive powders

Mixing polycarbosilane or polysilazane with metal powders (Al, Ti, Zr, V, Nb, Ta, W) to form homogeneous polymer-metal composite powders, and subsequent pyrolysis under Ar or ammonia up to 1500 °C yields multiphase ceramic composites composed of silicides, nitrides and carbides of the applied metal [7].

Si-M-C(N)-O (M=Ti, Cr, V, Mo, B, Cr, Mo, etc.) multicomponent bulk ceramic components have been also successfully synthesized from Si-based polymeric precursors (polycarbosilane, polysilazane and polysiloxane) with reactive filler particles of metals (Ti, Cr, V, Zr, Nb, Ta, Mo, W, Al, B, Si) or silicides ($CrSi_2$, $MoSi_2$) [8].

During pyrolysis and the subsequent heat treatment, the filler particles react with carbon from Si-based polymeric precursor or nitrogen from the reaction gas atmosphere to form new (oxy)carbide or (oxy)nitride embedded in a nanocrystalline Si-C(N)-O matrix. The selective volume expansion encountered in the filler phase reaction can be used to compensate for the volume shrinkage of the polymeric precursor-derived material during the pyrolytic conversion process, and near-net forming of bulk ceramic components, even with complex geometry, is possible.

(2) Preparation of polymeric precursors from M-containing monomer units

Polymeric precursor-derived Si-B-C-N ceramics have a number of advantages compared to Si-C-N system, including thermal stability, oxidation resistance [28] and higher crystallization temperatures [29-31]. Therefore, the fabrication of the Si-B-C-N ceramics, including fibers and coatings has received an increasing attention.

Polyborosilazanes have been synthesized by a dehydrocoupling reaction of tetrakis(methylamino)silane and trimethylamine-borane with the Si/B atomic ratios in the range of 10 to 1 [32]:

$$n\mathrm{Si(NHCH_3)_4} + n\mathrm{BH_3{\bullet}N(CH_2CH_3)_3} \xrightarrow[-n\mathrm{N(CH_2CH_3)_3}]{\text{Toluene, reflux}} [\text{-N(CH}_3\text{)-Si(NHCH}_3\text{)}_2\text{-N(CH}_3\text{)-BH-}]_n + 2n\mathrm{H_2} \quad (1.16)$$

Hydroboration of reactive molecules containing double bonds such as C=C and C=N are an alternative route for the preparation of useful Si-B-C monomers for polyborosilazanes. The hydroboration of dichloromethylvinylsilane with dimethylsulfide-borane leads to a boron-containing dichlorosilane in high yield. The monomer can be ammonolysed to give a polyborosilazane with the Si/B atomic ratio of 3 (Eq. 1.17) [29]. The boron content of the polyborosilazane can be increased by use of the hydroboration reactions of the vinylsilanes and dimethyl-sulfide addacts of chloroboranes like $ClBH_2$ (Eq. 1.18) or Cl_2BH (Eq. 1.19) [30]. The resulting replacement of borane by mono- and dichloroborane is monomers with decreased Si/B atomic ratios of 2 and 1, compared to 3 for BH_3.

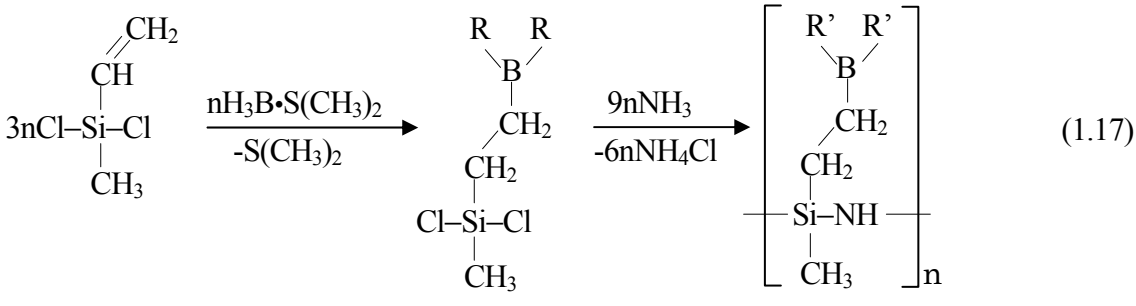

(1.17)

R= –CH(CH$_3$)–Si(CH$_3$)Cl$_2$ R'= –CH(CH$_3$)–Si(CH$_3$)(NH–)–NH–

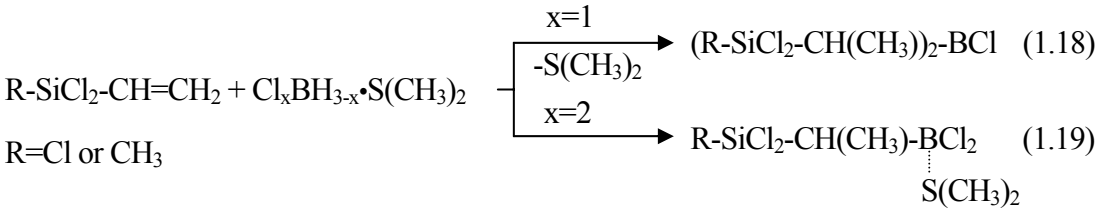

Hydroboration of bis(trimethylsilyl)carbodiimide with dimethylsulfide leads to highly cross-linked boron-containing polymers [33] (Fig. 1-5). In a first step, the carbodiimde unit is hydoroborated by 2 mol of borane. Further intermolecular hydroboration of the residual $–BH_2$ groups with unreacted bis(trimethylsilyl)carbodi-imide results in the formation of polymethylborocarbosilazanes.

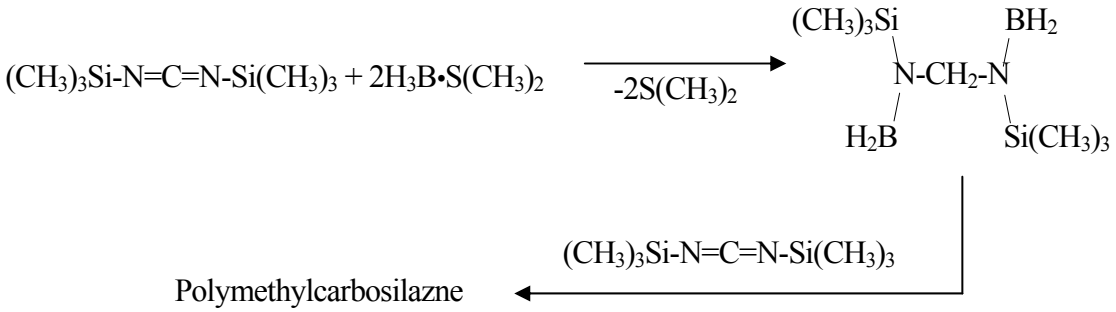

Fig. 1-5. Synthesis of polymethlyborocarbosilazane.

Polyborosilazane from a boron-containing monomer unit has been also described by Baldus *et al*. [31]. The reaction of hexamethyldisilazane with tetrachlorosilane yields 1,1,1,3,3,3-trichlorotrimethyldisilazane (TTDS). TTDS forms (trichlorosilylamino)-dichloroborane (TADB) upon treatment with BCl_3 (Eq. 1.20). Ammonolysis with liquid ammonia at –78 °C provides a polyborosilazane as an insoluble white solid, which forms $Si_3B_3N_7$ after pyrolysis. A yellow solid with a softening point of 130 °C is obtained by aminolysis using methylamine. This soluble N-methylpolyborosilazane is isolated at 80 % yield (Fig. 1-6).

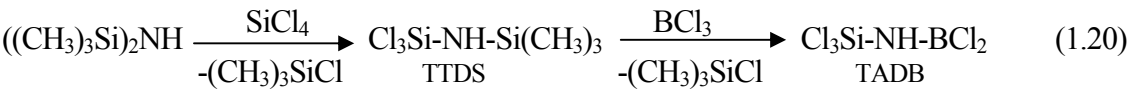

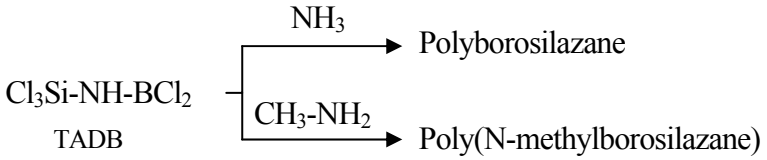

Fig. 1-6. Ammonolysis and aminolysis of TADB.

Besides boron, other elements have been introduced into Si-based polymeric precursors in order to synthesize precursors for mulicomponent ceramic systems. A promising candidate is aluminum since AlN, Al_2O_3, SiAlONs and other Al-containing materials show interesting properties such as high-strength, hardness or resistance to thermal shock and oxidation. Aluminum-doped silazane polymers can be synthesized, analogous to the reactions described above of borane with tetrakis(methylamino)silane [32]. The alane Lewis-base adduct, $AlH_3{\cdot}N(CH_3)_3$ and $Si(NHCH_3)_4$ in toluene at –78 °C yield solid polymer containing 12.4 wt % aluminum:

$$nSi(NHCH_3)_4 + nAlH_3{\bullet}\ N(CH_3)_3 \xrightarrow[-nN(CH_3)_3]{\text{Toluene, reflux}} [\text{-}N(CH_3)\text{-}Si(NHCH_3)_2\text{-}N(CH_3)\text{-}AlH\text{-}]_n + 2nH_2 \quad (1.21)$$

Transition metals like titanium or zirconium can be also incorporated in Si-based polymeric precursors. This is a useful task since cross-linking and curing may be positively influenced by the presence of these elements, for example, giving higher ceramic yields. Polytitanocarbosilanes are already used for the production of Si-Ti-C-O fiber “Tyrano” by UBE Ltd. in Japan [34]. This fiber exhibits enhanced high-temperature mechanical properties compared to the Si-C “Nicalon” fiber. Moreover, TiN or Ti(C,N) mico/nano particle-dispersed Si_3N_4 ceramics have been suggested as structural materials because of their mechanical properties [35-37]. However, only a few molecular Si-Ti-C-N precursors have been developed and thermally converted into ceramic materials. As was shown above for the synthesis of the Si-B-C-N polymeric precursor TADB, an analogous titanium compound can be provided by the reaction shown in Eq. 1.22 to give red-orange colored crystalline solid. It was pyorolyzed in nitrogen at 600 °C to 1000 °C to give TiN [38]:

$$TiCl_4 + (CH_3)_3Si\text{-}NH\text{-}Si(CH_3)_3 \longrightarrow (CH_3)_3Si\text{-}NH\text{-}TiCl_3 + ClSi(CH_3)_3 \quad (1.22)$$

(3) Chemical modification of Si-based polymers with a monomer containing desired element M

As mentioned above, polytitanocarbosilanes have been developed for the production of Si-Ti-C-O fiber [34, 39]. The polymeric precursor was synthesized by chemical modification of polycarbosilanes with titanium alkoxides. The reaction yields Si-O-Ti bonds accompanied by evolution of alkane gas:

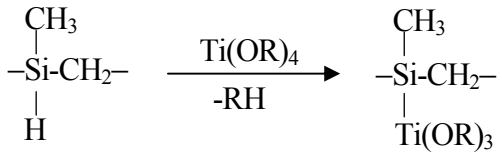

(1. 23)

R= -$(CH_2)_3CH_3$, - $CH(CH_3)_2$, -$CH_2CHR''(CH_2)_4CH_3$ (R''= -CH_2CH_3)

After that, chemical modification of polycarbosilanes using various metal alkoxides ($Al(OCH(CH_3)CH_2CH_3)_3$ [40], $Zr(O(CH_2)_3CH_3)_4$ [41], $Ta(O(CH_2CH_3)_5$ [42]) have been investigated. However, the Si-M-O (M=Al, Zr, Ta) bond formations could not be clearly detected by nuclear magnetic resonance (NMR) and fourier transform infra red (FT-IR) spectroscopic analyses.

For the synthesis of multicomponent ceramic systems through the chemical modification route, oligosilazanes [43-45], polysilazanes [46] and perhydro-polysilazanes [47, 48] have also been used as a starting precursor. Seyferth *et al.* studied the reaction of cyclic oligosilazanes with borane adducts [43]. Based on the B-NMR spectroscopic analysis, it was concluded that the reaction can be described as a dehydrocondensation between N-H and B-H groups, followed by rearrangements to borazine rings and SiH_2-(CH_3) groups (Eq. 1.24). The silazanyl side-chains in the product can react further with $H_3B{\cdot}S(CH_3)_2$ to give boron-containing polysilazanes.

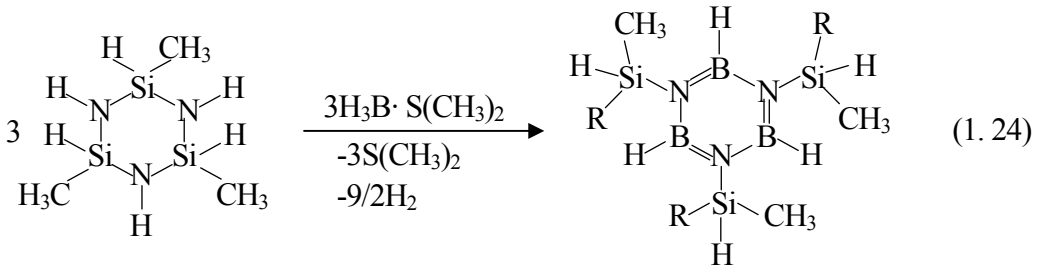

(1. 24)

Schmidt *et al.* investigated the reaction of the cyclic oligosilazanes with aluminum compounds like triethylaluminum [44,45]. Si-Al-C-N polymers were formed by Al-N bond formations with evolution of ethane (Eq. 1.25). The Si/Al atomic ratios were varied from 1 to 0.2 for R=CH_3. The polymers were pyrolyzed and crystallized up to 1900 °C, yielding SiC-AlN composites.

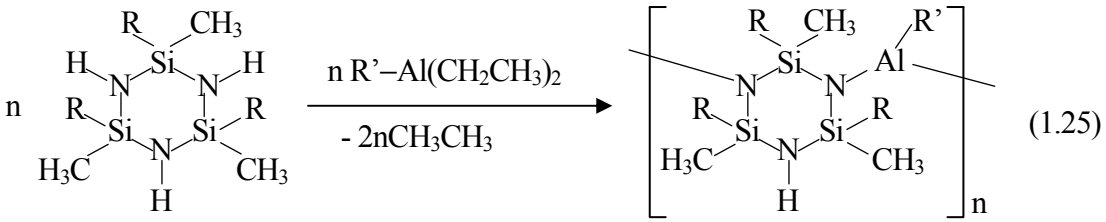

(1.25)

R= -CH_3, -CH=CH_2 R'= NH_2, CH_2CH_3

Bill *et al.* [46] suggested that the transamination of polyhydridomethylsilazane with dimethylamide ($M[N(CH_3)_2]_3$, M=B or P), resulting in an appropriate M-containing polyhydridomethylsilazane. Further intermolecular transamination reaction leads to the formation of highly cross-linked network via N-M-N bridges (Eq. 1.26).

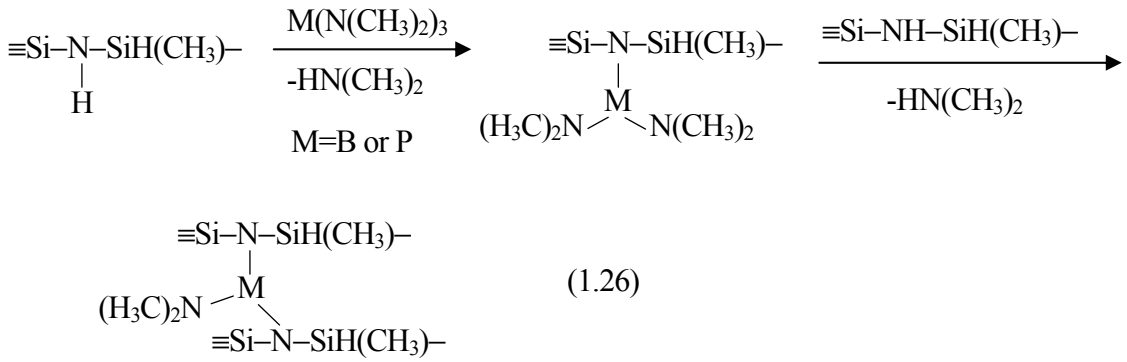

(1.26)

Funayama *et al.* investigated the reaction of perhydropolysilazane with trimethoxyborane [47] or (ethylacetoacetate)aluminumdiisopropoxide [48], and successfully synthesized Si-M-O-N (M=B or Al) multicompoment ceramic systems. According to the FT-IR and NMR spectroscopic analyses, the reaction of perhydropolysilazane with trimethoxyborane results in the formation of B-N bonds (Eq. 1.27) rather than the reaction of the borane at the silicon atom forming Si-O-B bonds (Eq. 1.28). Further elemental analyses revealed that the polymer predominantly contains =N-B(OCH_3)-N= units [47].

$$-H_2Si\text{-}NH- + B(OCH_3)_3 \longrightarrow -H_2Si\text{-}N(B(OCH_3)_2)- + CH_3OH \quad (1.27)$$

$$-H_2Si\text{-}NH- + B(OCH_3)_3 \longrightarrow -HSi(B(OCH_3)_2)\text{-}NH- + CH_4 \quad (1.28)$$

1.1.2. Cross-linking and prolysis

The transformation of linear polymeric precursor chains into branched structures prevents the loss of lower molecular weight compounds during pyrolysis, which can increase the ceramic yield [49]. Moreover, fragmentation and depolymerization reactions leading to the volatilization of oligomers can be avoided. Accordingly, the precursors have to be transformed into highly cross-linked preceramic network prior to pyrolysis. Furthermore, this process provides a means to transform the precursors into infusible materials which prevents the degradation of their shape by melting during pyrolysis at higher temperature.

1.1.2.A. Polycarbosilanes

Polycarbosilanes are normally cross-linked by air oxidation (Eq. 1.29). The FT-IR spectroscopic analysis revealed that Si-H bonds are oxidized rather than C-H bonds, and the reactions of Eqs. 1.30-1.34 can be assumed as the oxdation mechanism [50, 51].

$$2\,(CH_3)SiH\text{-}CH_2\text{-}SiH= \xrightarrow[190\ ^\circ C]{O_2} (CH_3)Si\text{-}CH_2\text{-}Si(O)(O)\text{-}Si(CH_3)\text{-}CH_2\text{-}Si= \quad (1.29)$$

$$\equiv Si\text{-}H \rightarrow \equiv Si\cdot + H\cdot \quad (1.30)$$

$$\equiv Si\cdot + O_2 \rightarrow \equiv Si\text{-}O\text{-}O\cdot \quad (1.31)$$

$$\equiv Si\text{-}O\text{-}O\cdot + \equiv Si\text{-}H \rightarrow \equiv Si\text{-}O\text{-}O\text{-}H + Si\equiv\cdot \quad (1.32)$$

$$\equiv Si\text{-}O\text{-}O\text{-}H + \equiv Si\text{-}H \rightarrow 2Si\text{-}O\text{-}H \quad (1.33)$$

$$2Si\text{-}O\text{-}H \rightarrow \equiv Si\text{-}O\text{-}Si\equiv + H_2O \quad (1.34)$$

The pyrolysis behavior above 200 °C of polycarbsilanes is composed of the following six stages [50, 51]:

(1) 200 °C < T ≤ 400 °C: Low molecular polycabosilanes are removed by evaporation.

(2) 400 °C < T ≤ 550 °C: Si-H bonds condense with Si-CH_3 groups through the radical reactions (Eqs. 1.30, 1.35-1.38) leading to the formation of Si-CH_2-Si linkages.

$$\equiv Si–CH_3 + H\cdot \rightarrow \equiv Si–CH_2\cdot + H_2 \quad (1.35)$$

$$\equiv Si–CH_3 \rightarrow \equiv Si\cdot + \cdot CH_3 \quad (1.36)$$

$$\equiv Si–CH_3 + \cdot CH_3 \rightarrow \equiv Si–CH_2\cdot + CH_4\uparrow \quad (1.37)$$

$$\equiv Si\cdot + \cdot CH_2–Si\equiv \rightarrow \equiv Si–CH_2–Si\equiv \quad (1.38)$$

(3) 550 °C < T ≤ 850 °C: Transformation into SiC materials with the elimination of Si-H, Si-CH_3 and Si-CH_2-Si moieties. The conversion of the highly cross-linked network into an inorganic SiC network is shown in Eq. 1 39.

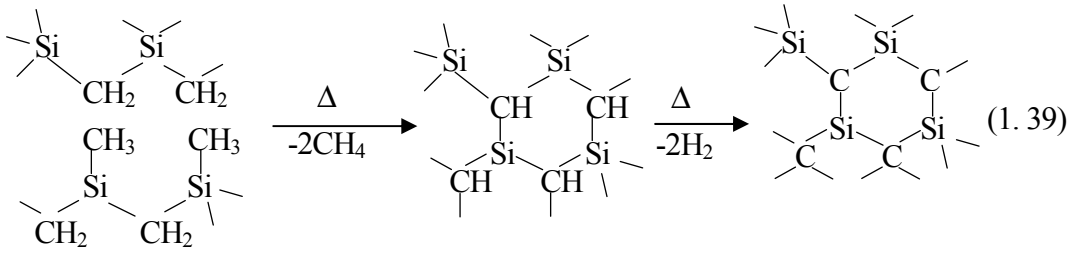

(1. 39)

(4) 850 °C < T ≤ 1000 °C: This stage has been characterized as a minimal weight loss without gas evolution.

(5) 1000 °C < T ≤ 1200 °C: Onset of crystallization

(6) 1200 °C < T: This stage corresponds to the crystal growth occurring with CO evaporation due to the reaction of Si-C bonds with excess oxygen (about 10 wt%).

As the "Nicaron" fibers have been produced using the cross-linking process by air oxidation, the mechanical strength of the fibers apparently decreases at around 1200 °C caused by the crystallization.

After that, amorphous SiC fibers with low oxygen content (below 1wt%) have been successfully

synthesized by a novel cross-linking process using electron beam irradiation in a helium atmosphere followed by pyrolysis at 1000 to 1200 °C [52,53]. This synthetic rote has lead to the production of "Hi-Nicaron" SiC fibers with excellent mechanical properties up to 1400 °C. Recently, polycarbosilanes with higher molecular weight fraction are also commercially available [54]. The polymers show no specific melting point, and can be expected as useful for the synthesis of SiC ceramics without the air oxidation cross-linking process.

1.1.1.B. Polysilazanes and related compounds

The oligomeric silazanes can be thermally cross-linked into non-volatile polysilazanes. On consideration of the control of elemental and phase composition of final ceramic products, the thermal cross-linking is favorable because no additional elements are introduced to the polymeric precursors. The cross-linking reactions of silazanes have been investigated by FT-IR, NMR and mass spectroscopic analyses [55-59]. The major reactions are dehydrogenation via Si-H and N-H (Eq. 1.40), dehydrocoupling (Eq. 1.41) and trasaminations (Eq. 1.42). In the case of silazanes including active vinyl groups, hydrosilylation (Eq. 1. 43) and polymerization (Eq. 1.44) reactions also proceed. The cross-linking conditions and the associated cross-linking reactions of several kinds of commercial polysilazanes are shown in Table 1-1.

$$\equiv Si{-}H + H{-}N{=} \rightarrow \equiv Si{-}N + H_2 \quad (1.40)$$

$$\equiv Si{-}H + \equiv Si{-}NH{-}Si\equiv \rightarrow \equiv Si{-}N(Si\equiv){-}Si\equiv + H_2 \quad (1.41)$$

$$3 \equiv Si{-}NH{-}Si\equiv \rightarrow 2 \equiv Si{-}N(Si\equiv){-}Si\equiv + NH_3 \quad (1.42)$$

$$\equiv Si{-}H + \equiv Si{-}CH{=}CH_2 \begin{cases} \xrightarrow{\alpha\text{-addition}} \equiv Si{-}CH(CH_3){-}Si\equiv \\ \xrightarrow{\beta\text{-addition}} \equiv Si{-}CH_2{-}CH_2{-}Si\equiv \end{cases} \quad (1.43)$$

$$2n \equiv Si{-}CH{=}CH_2\cdot \rightarrow [{-}CH(Si\equiv){-}CH_2{-}]_{n-1}{-}CH(Si\equiv){=}CH_2 + [{-}CH(Si\equiv){-}CH_2{-}]_{n-1}{-}CH(Si\equiv){-}CH_2 \quad (1.44)$$

Table 1-1. Cross-linking conditions and reactions of polysilazanes.

Polymeric precursor (Name, Distributor)	Cross-linking conditions Major reactions (Eq. No.)	References
$[(CH_3)_2Si\text{-}NH]_x[(CH_3)SiH\text{-}NH]_y[CH_3SiN]_z$ (NCP 200, Chisso Co., Japan)	300-400°C in Ar (1.40), (1.41)	[55, 56]
$[(CH_2{=}CH\text{-}Si(NH)_{1.5}]_x$ (VT 50, Hoechst AG, Germany)	200-300°C in Ar (1.42), (1.43), (1.44)	[55]
$Si(CH_3)(CH{=}CH_2)\text{-}NH\text{-}(CH_3)SiH$ $HN\text{-}[(CH_3)(R)Si\text{-}NH]_n\text{-}C(=O)\text{-}N(R)$ (Ceracet, Lanxide Co., USA)	250-400°C in Ar (1.43) 90-130°C in Ar, 0.1%-peroxide (1.44)	[57] [58, 59]

Further pyrolysis reactions above 500 °C of polysilazanes are investigated using NMR, FT-IR and TG/MS characterization techniques. Bill *et al*. [55] and Seitz *et al*. [60] studied the pyrolysis reactions of commercial polysilazanes (NCP 200). The ^{13}C NMR spectroscopic analysis indicates the presence of Si-CH_2-Si units around 550 °C. TG/MS proved the evolution of methane at this temperature suggesting reactions among Si-H and Si-CH_3 groups. The pyrolysis reactions involving N-H groups proceeded at 550 to 600 °C leading to the formation of SiN_4 units by the replacement of methyl groups reacting with N-H groups. Above 625 °C, major reactions involve elimination of Si-H and Si-CH_3 groups. This is in accordance with the FT-IR spectra, and the increase of the number of Si-N and Si-C bonds with pyrolysis temperature was supported by the ^{13}C NMR and ^{29}Si NMR spectroscopic data. At even higher temperatures, the hydrogen content of the material further decreases and single phase amorphous silicon carbonitride which contains tetrahedral SiC_xN_y (x+y=4) units is formed.

Seitz *et al*. [60] discussed various possible pyrolysis reactions between Si-CH_3, Si-H and Si_2N-H groups in the polysilazanes by estimating the reaction enthalpies ΔE which were calculated based on the dissociation energies and the assumption of CH_4 and H_2 formation (Table 1-2). The results show that the formation of new Si-C (Eq. 1.45-1.50) and Si-N (Eq. 1.51, 1.52) is favorable, while that of C-C (Eq. 1.53), C-N (Eq. 1.54) and C=C or C≡C (Eq. 1.55, 1.56) is less favorable. This result is agreement with the spectroscopic analysis showing the formation of Si-C and Si-N bonds in the pyrolyzed products. However, the Si-N bond formation was detectable above 600 °C by ^{29}Si NMR spectra which contradicts to the low ΔE values of the related reactions (Eq. 1.51, 1.52).

Table 1-2. Various possible pyrolysis reactions among N-H, Si-CH_3, Si-H groups and the calculated reaction enthalpy ΔE (kJ/mol) [60].

Pyrolysis reactions	ΔE (kJ/mol)	Eq. No.
$\equiv SiCH_2–H + H–Si\equiv \rightarrow \equiv SiCH_2–Si\equiv + H_2$	-2	(1.45)
$\equiv Si–CH_3 + H–CH_2Si\equiv \rightarrow \equiv Si–CH_2Si\equiv + CH_4$	0	(1.46)
$\equiv Si–H + H–CH(Si\equiv)_2 \rightarrow \equiv Si–CH(Si\equiv)_2 + H_2$	-2	(1.47)
$\equiv Si–CH_3 + H–CH(Si\equiv)_2 \rightarrow \equiv Si–CH(Si\equiv)_2 + CH_4$	0	(1.48)
$\equiv Si–H + H–C(Si\equiv)_3 \rightarrow \equiv Si–C(Si\equiv)_2 + H_2$	-2	(1.49)
$\equiv Si–CH_3 + H–C(Si\equiv)_3 \rightarrow \equiv Si–C(Si\equiv)_2 + CH_4$	0	(1.50)
$(\equiv Si)_2N–H + H–Si\equiv \rightarrow (\equiv Si)_2N–Si\equiv + H_2$	-55	(1.51)
$\equiv Si–CH_3 + H–N(Si\equiv)_2 \rightarrow \equiv Si–N(Si\equiv)_2 + CH_4$	-54	(1.52)
$\equiv SiCH_2–H + H–CH_2Si\equiv \rightarrow \equiv SiCH_2–CH_2Si\equiv + H_2$	+51	(1.53)
$\equiv SiCH_2–H + H–N= \rightarrow \equiv SiCH_2–N= + H_2$	+66	(1.54)
$\equiv SiCH_3 + H–CH_2Si\equiv \rightarrow \equiv SiCH=CHSi\equiv + 2H_2$	+177	(1.55)
$\equiv SiCH_3 + CH_3Si\equiv \rightarrow \equiv SiC\equiv CSi\equiv + 3H_2$	+296	(1.56)

Bill *et al.* and Seitz *et al.* [55, 60] also investigated the pyrolysis reactions of commercial vinyl group-containing polysilazanes (VT 50). Above 350 °C, the carbon chains formed by the vinyl-polymerization (Eq. 1.44) transformed into sp^2-carbon, while the number of Si-N bond increased by the reactions of Si-H or Si-CH_3 and N-H groups (Eq. 1.51 or 1.52). At 1050 °C, the polysilazanes were converted into amorphous silicon carbonitride consisted of SiN_4 tetrahedral units and sp^2-hybridised carbon.

1.1.2.C. Polysilylcarbodiimides

Compared to polysilazanes, the structural difference of $[Si(N=C=N)_2]_n$ can lead to different behavior during pyrolysis, resulting in the formation of new phases, SiC_2N_4 and Si_2CN_4 [27]. The in-situ X-ray diffractometry (XRD), Si-NMR and FT-IR spectroscopic analyses revealed that the $[Si(N=C=N)_2]_n$-derived amorphous material transformed to crystalline SiC_2N_4 at about 400 °C, which decomposes at 920 to 1000 °C to give polycrystalline Si_2CN_4 composed of tetrahedral $N_3Si(N=C=N)$ units (Eq. 1.57). Above 1000 °C, Si_2CN_4 gradually decomposes to give amorphous Si-C-N materials.

$$4[Si(N=C=N)_2] \xrightarrow{T=400\ ^\circ C} 4SiC_2N_4 \xrightarrow{T=920\text{-}1000\ ^\circ C} 2Si_2CN_4 + N_2 + 3C_2N_2 \quad (1.57)$$

In contrast to the thermal decomposition behavior of $[Si(N=C=N)_2]_n$, poly(methylsilsesquicarbodiimide) ($[CH_3Si(N=C=N)_{1.5}]_n$) derived from CH_3SiCl_3 and $(CH_3)_3Si\text{-}N=C=N\text{-}Si(CH_3)_3$ (Eq. 1.58) decomposes at 570 to 800 °C to give an amorphous Si-C-N material composed of three kinds of tetrahedral $N_{4-x}Si(N=C=N)_x$ ($0 \le x \le 2$) units [61] (Eq. 1.59).

$$nCH_3SiCl_3 + 1.5n(CH_3)_3Si\text{-}N=C=N\text{-}Si(CH_3)_3 \xrightarrow{C_5H_5N} [CH_3Si(N=C=N)_{1.5}]_n + 3nMe_3SiCl \quad (1.58)$$

$$4[CH_3Si(N=C=N)_{1.5}] \xrightarrow{T=570\text{-}800\ °C} 4Si_{1.0}C_{1.25}N_{2.5}\ [N_{4-x}Si(N=C=N)_x\ (0 \le x \le 2)] + 2CH_3CN + CH_4 + H_2 \quad (1.59)$$

1.1.3. Crystallization

1.1.3.A. Ternary Si-C-N system

One interesting property of the polymeric precursor-derived Si-C-N ceramics is that they remain amorphous up to 1400-1500 °C in inert atmospheres of N_2 [21, 23, 62-64] or Ar [19, 22, 65-67]. They also exhibit excellent oxidation [68] and creep resistance [69] at very high temperatures due to the absence of metal oxide additives. These findings indicate that the amorphous Si-C-N ceramics are good candidates for high temperature applications.

The polymeric precursor-derived amorphous Si-C-N ceramics were found to show higher thermal stability compared to the binary Si-N or Si-C amorphous ceramics derived from C-free or N-free Si-based polymeric precursors, respectively. In order to clarify the enhanced thermal stability, an increasing number of studies on the understanding of the amorphous network structure has been recently reported [22]. Various structural characterization techniques were performed to provide information about the structure of the amorphous Si-C-N network on an atomic level including NMR, FT-IR, Raman and neutron diffraction as well as high resolution transmission electron microscopy (HRTEM). Solid state NMR and FT-IR analyses of the X-ray amorphous Si-C-N ceramics derived from poly(hydridomethyl)silazane (PHMS) and polyvinylsilazane (PVS) revealed two different amorphous network structures: The PHMS-derived amorphous ceramics synthesized at around 1000 °C had a short-range order of the elements consisting mainly of tetrahedral SiC_xN_y

(x+y=4) units with some SiN_2CH tetrahedra. In contrast, the PVS-derived amorphous ceramics synthesized at 1050 °C consisted of SiN_4 tetrahedral units and sp^2-hybridised carbon [55,70,71]. A similar structure of the SiN_4 units mixed with amorphous carbon was proposed for X-ray amorphous Si-C-N ceramics derived from poly(N-methylsilazane). The amorphous Si-C-N ceramics were synthesized at 1400 °C and characterized by FT-IR, NMR and Raman analyses [21]. Neutron diffraction analysis of the PVS-derived ceramics revealed an average SiN_3C tetrahedral unit [72]. Contrarily, X-ray and neutron diffraction analyses of the PHMS-derived amorphous ceramics synthesized at 1050 °C showed the existence of amorphous Si-N and graphite-like amorphous carbon [73]. HRTEM investigations of the crystallization behavior of polycarbosilzane-derived amorphous Si-C-N ceramics revealed that free carbon was the first phase to nucleate as so-called basic structural units (BSU) at 1100 °C followed by subsequent SiC crystallization at 1200 °C, which originated upon the thermochemical degradation of the amorphous Si-C-N network [74]. The diversity of network structures might be due to the differences in precursor chemistry, pyrolysis conditions and the heat treatment, which makes it difficult to understand and interpret the results comprehensively.

Recently, Iwamoto *et al*. [75] reported the first direct comparison of the crystallization behavior under N_2 atmosphere of amorphous Si-C-N ceramics derived from polysilazanes and polysilylcarbodiimides, as well as the effects of carbon content and the utilization of polymer blends versus single source precursors. Amorphous Si-C-N ceramics with a C/Si atomic ratio in the range of 0.34 to 1.13 were prepared using the polymeric precursors (Table 1-3).

Table 1-3. Chemical composition of polymeric precursor-derived ceramics synthesized by pyrolysis at 1100 °C.

Name	Precursors	Empirical formula
Si-N	$[-SiH_2-NH-]_n$ (PHPS)	$SiN_{0.96}C_{0.00}O_{0.01}$
SNC	$[-(CH_3)SiH-NH-]_n[-SiH_2-NH-]_m$ (MHOS)	$SiN_{0.69}C_{0.34}O_{0.01}$
SNSC-1	$[-(CH_3)SiH-CH_2-]_n$ (PCS)/PHPS=0.5	$SiN_{0.36}C_{0.42}O_{0.06}$
SNSC-2	PCS/PHPS=0.7	$SiN_{0.57}C_{0.53}O_{0.05}$
PSC	$[Si(N=C=N)_2]_n$	$SiN_{1.78}C_{0.56}O_{0.10}$
PMSC	$[CH_3Si(N=C=N)_{1.5}]_n$	$SiN_{1.52}C_{1.13}O_{0.05}$

The XRD study indicated that the crystallization temperature of Si_3N_4 increased consistently with the C/Si atomic ratio and reached 1500 °C at C/Si atomic ratios ranging from 0.53 to 1.13. This temperature was 300 °C higher than that of the C-free amorphous Si-N material. In contrast, the SiC crystallization temperature showed no clear relation with the C/Si atomic ratio (Fig. 1-7).

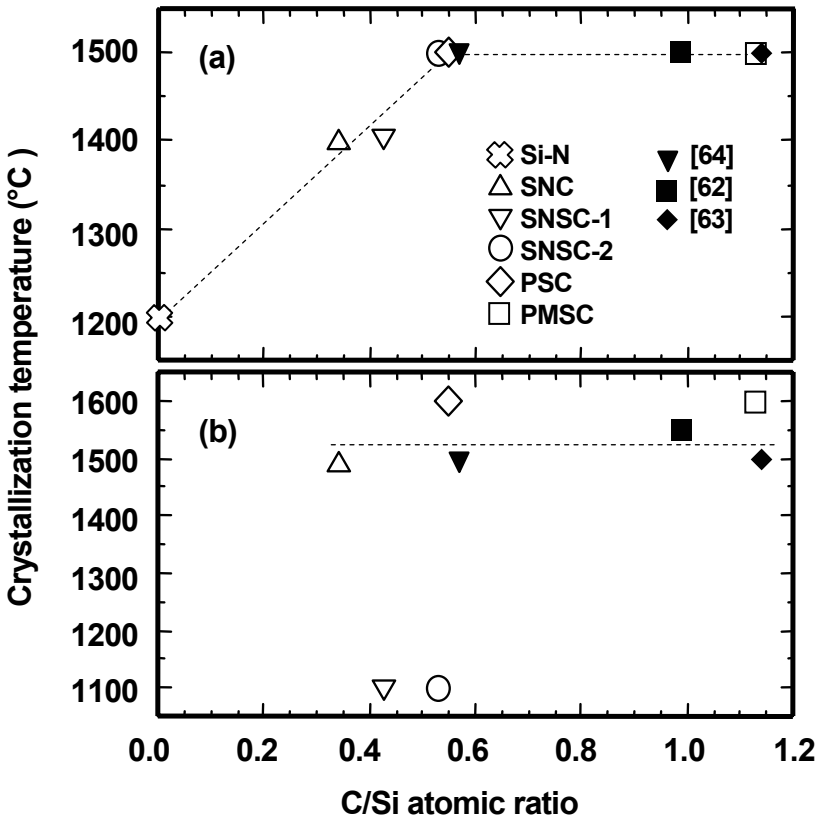

Fig. 1-7. Crystallization temperature of polymeric precursor-derived Si-C-N as a function of C/Si atomic ratio. (a) Si_3N_4 phase and (b) SiC phase.

The ^{29}Si MAS NMR analysis of the amorphous Si-C-N exhibited two different structures: The polyorganosilazane-derived Si-C-N ceramics were composed of SiC_xN_y (x+y=4) units, while the polyorganosilylcarbodiimide-derived ceramics mainly consisted of SiN_4 units interconnected with amorphous carbon (Fig. 1-8).

The formation of these particular structures could retard the crystallization and phase partitioning processes of the thermodynamically stable phases Si_3N_4 and SiC. Amorphous Si-C-N derived from polysilylcarbodiimides formed crystalline SiC around 1600 °C, which was 50-100 °C higher than the crystallization temperatures found corresponding polysilazane derived-materials with the same C/Si ratio. This might be due to the formation of SiN_4 tetrahedra separated by the remaining carbon, and it was concluded that the crystallization of amorphous Si-C-N was governed by carbon content, as well as chemical homogeneity and molecular structure of the amorphous Si-C-N network.

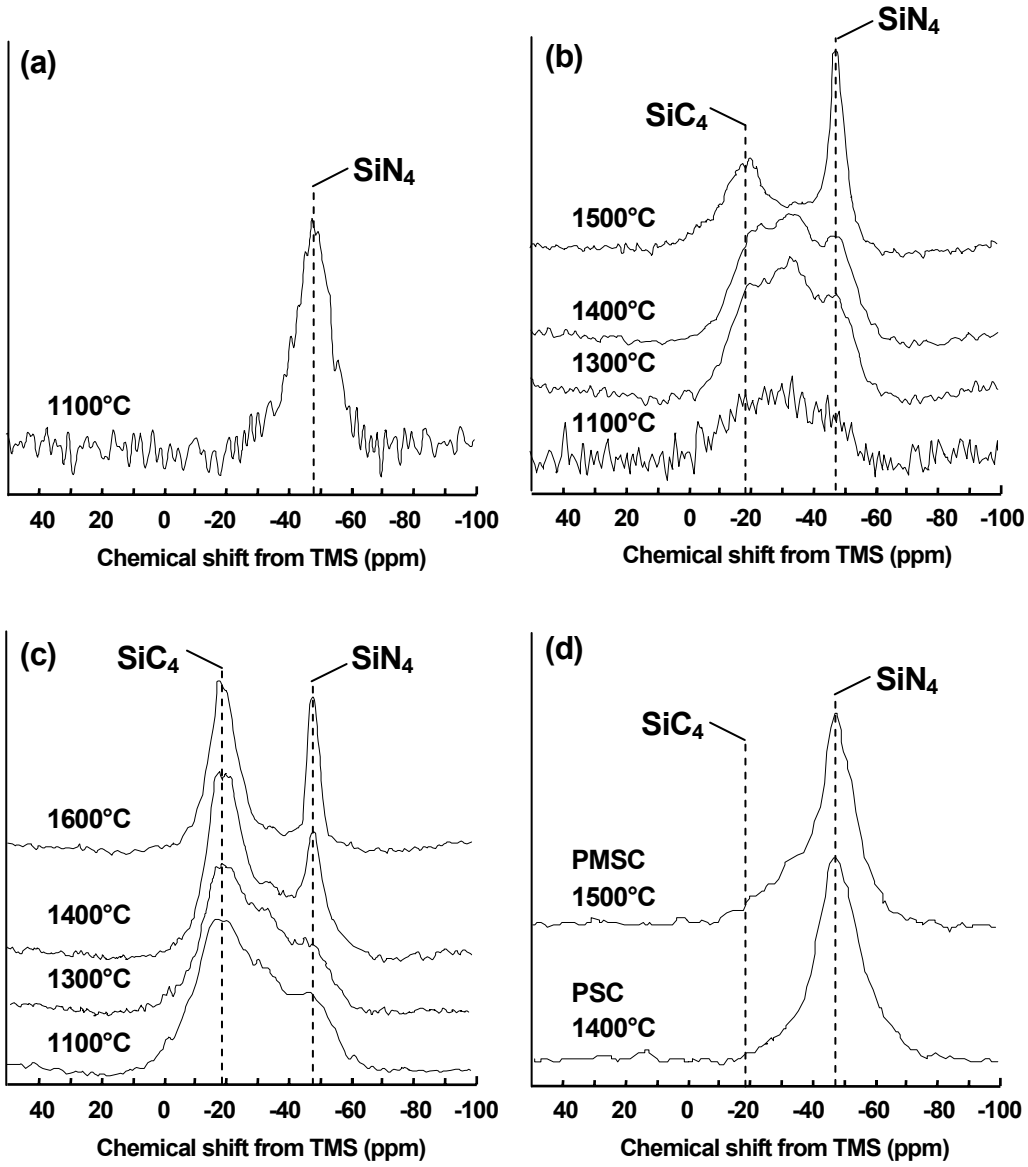

Fig. 1-8. ^{29}Si MAS NMR spectra of (a) 1100 °C pyrolyzed-PHPS, (b) SNC, (c) SNSC-2 and (d) Si-C-N ceramics polyorganosilylcarbodiimides.

1.1.3.B. Multicomponent Si-M-C-N systems

Incorporation of hetero element into the ternary Si-C-N system also strongly influences the crystallization behavior of amorphous Si-C-N materials to Si_3N_4/SiC composite materials. As mentioned in the section 1.2.3.B, the B element can stabilize the amorphous state of Si-C-N ceramics at higher temperatures [29-31]. The reported results showed that the crystallization temperature of Si_3N_4 phase from the amorphous Si-B-C-N is 1700 to 1800 °C. This temperature is at least 200 °C

higher than that of the amorphous Si-C-N. In contrast, the element P did not show such a remarkable enhancement of the thermal stability of amorphous Si-C-N, and the XRD and TEM analysis revealed that the P element was found to rather accelerate the Si_3N_4 crystallization [70]. The difference in the crystallization behavior can offer an opportunity to control the microstructure development of the Si_3N_4/SiC composite materials. Bill *et al*. prepared amorphous Si-(M)-C-N ceramics (M=B, P) by pyrolysis of chemically modified PHMS using $M(N(CH_3)_2)_3$ (Eq. 1.26) [46]. The atomic Si/M ratio was about 2. The TEM analysis of the 1400 °C heat-treated samples resulted in the formation of completely different microstructures: The crystallization of the Si-B-C-N yielded a nano/nano composite consisting of nanocrystallites of Si_3N_4 and SiC with the crystallite sizes smaller than 50 nm. The Si-C-N yielded nanoclrystalline SiC embedded in a crystalline Si_3N_4 matrix, while the microstructure of the Si-P-C-N samples consisted of microcrystallites of Si_3N_4 and SiC with the crystallite sizes around 0.5 μm [55,70].

1.2. General background of Si_3N_4 and SiC ceramics

Engineering ceramics have become important as structural materials based on their chemical stability and wear resistance. These materials have been expected to use in areas in which the typical metallic materials show weakness such as wear, high temperature creep and oxidation. The most widely studied ceramic materials are silicon-based non-oxides such as Si_3N_4 and SiC.

1.2.1. Si_3N_4 ceramics

Si_3N_4 has been known to crystallize in the two hexagonal modifications α and β which differ in that the lattice distance in the direction of the crystallographic *c*-axis is α-Si_3N_4 for about twice as large as for the β-Si_3N_4 [76]. The compound α-Si_3N_4, with a density of $\rho=3.183 \times 10^4$ kg/m^3 has been synthesized at ambient pressure and temperatures below 1527 °C, while the β-Si_3N_4 ($\rho=3.200 \times 10^4$ kg/m^3) requires higher temperatures [77,78]. With increasing temperature, the α-phase becomes unstable with respect to β-Si_3N_4. However, the α/β-Si_3N_4 phase transformation is reconstructive and can occur with solution-precipitation by means of a liquid phase. The relative stability of these phases and the influence of oxygen on the stability of α-Si_3N_4 are not fully understood [79]. Recently, a third polymorph with a cubic spinel structure (c-Si_3N_4) has been synthesized at pressures above 15 GPa and temperatures exceeding 1727 °C. The new phase, c-Si_3N_4, has been found to persist metastably in air at ambient pressure to at least 427 °C [80].

Si_3N_4 powder can be produced in a large scale by following four main methods [81].

(1) Nitridation of metallic silicon powder:

$$3Si + 2N_2 \rightarrow Si_3N_4 \quad (1.60)$$

(2) Gas phase deposition:

$$3SiCl_4 + 4NH_3 \rightarrow Si_3N_4 + 12HCl\uparrow \quad (1.61)$$

(3) Carbothermal reduction of silicon dioxide (SiO_2) in N_2 atmosphere:

$$3SiO_2 + 6C + 2N_2 \rightarrow Si_3N_4 + 6CO\uparrow \quad (1.62)$$

(4) Precipitation of silicon diimide and thermal decomposition:

$$3SiCl_4 + 4NH_3 \rightarrow Si(NH)_2 + 4NH_4Cl\uparrow \quad (1.63)$$

$$3Si(NH)_2 \rightarrow Si_3N_4 + 2NH_3\uparrow \quad (1.64)$$

Because of the high degree of covalent bonding (about 70 %), classical sintering is not applicable to produce pure dense Si_3N_4 ceramics. As a consequence, alternative techniques have been developed such as nitridation of silicon powder compacts (reaction-bonding) or the addition of sintering aids to Si_3N_4 powders to promote liquid-phase sintering with or without the application of pressure to assist the sintering process [82]. The reaction-bonding results in a still porous material. Fully dense Si_3N_4 ceramics, however, can be produced by the liquid phase sintering with the use of different oxide or non-oxide sintering additives, such as the frequently used MgO, Y_2O_3 or Y_2O_3-Al_2O_3 [82, 83]. In these cases, the densification and microstructure development are controlled by the mechanisms of liquid phase sintering formulated by Kingary: rearrangement, solution-diffusion-precipitation, and coalescence [84]. Figure 1-9 shows a schematic drawing of the solution-precipitation model for the liquid phase sintering of Si_3N_4 [82].

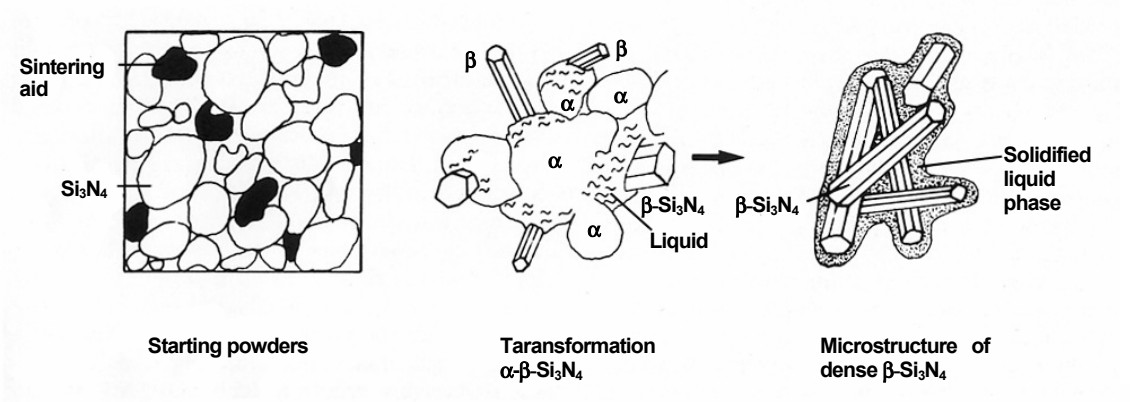

Fig. 1-9. Solution-precipitation model for the liquid phase sintering of Si_3N_4 [82].

The sintering additives react with the phases containing oxygen, SiO_2 or oxynitride, which are always present on the powder surfaces of commercially available Si_3N_4 powders, to form the liquid phase. Generally, the liquid phase starts to form at around 1400 to 1600 °C, which depends on the liquid phase composition. When the amount of liquid phase is high enough and the viscosity at sintering temperature is sufficiently low, the rearrangement process will occur induced by capillary forces. With increasing temperature, the α-Si_3N_4 dissolves in liquid phase and elongated β-Si_3N_4 grains precipitate from the liquid phase. After α/β-Si_3N_4 phase transformation is complete, the coalescence starts as the third stage of the liquid phase sintering process, which is due to the effort for minimizing the surface energy of β-Si_3N_4 grains.

The liquid phase solidifies during cooling mostly to amorphous or partially crystalline phases arranged at the grain boundaries in thin layer or at the grain boundary triple junctions of β-Si_3N_4 elongated grains. The grain boundary phase influences the mechanical properties of ceramics, especially at elevated temperatures, due to the softening to cause intergranular fracture, grain boundary sliding and slow crack growth. The mechanical properties strongly depend on the size and aspect ratio of β-Si_3N_4 grains [85], as well as the qualities of the grain boundary phases. Accordingly, microstructure control through the liquid phase sintering plays an important role for fabrication of high-performance Si_3N_4 ceramics.

1.2.2. SiC ceramics

SiC has been known to crystallize in the two modifications, β- and α-phases [86]. The β-SiC is crystallographically face centered cubic and assigned as 3C, while the α-SiC exists in either hexagonal or rhombohedral symmetry, such as 4H, 6H, 15R and 21R. It has been reported that the β-/α-phase transformation and morphological development in SiC ceramics are greatly influenced by local crystallographic coherence between the β- and α-phases, which controls the anisotropic grain growth [87,88]. The polytypic transformation has been also investigated, and the results show that the transformation is greatly affected by the sintering additives and chemical environment in which the SiC ceramics are heat-treated. Typically, the polytypic transformation of 6H to 4H has been reported when SiC ceramics are heat-treated in as aluminum-rich environment [89,90].

SiC powder is commercially produced by the "Acheson Process" which is the reaction between SiO_2 and carbon [86]:

$$SiO_2 + 3C \rightarrow SiC + 2CO \qquad (1.65)$$

High purity fine SiC powder can be synthesized by gas phase reactions [86]. Inorganic silicon monomer (SiX_4, X=H or Cl) can be reacted with hydrocarbon (C_nH_{2n+2}, n=1, 3), or organosilicon monomers such as $Si(CH_3)_4$ or H_3CSiCl_3 can be thermally pyrolysed in gas phase.

Due to the high degree of covalent bonding (about 80%), densification of pure SiC could not be achieved by classical sintering, and SiC ceramics were used to be produced by the reaction-bonding method using SiC, Si and C powders, or hot pressing method. In 1956, Alliegro *et al*. discovered that Al_2O_3 was an effective sintering additive of SiC ceramics, and fully dense SiC-based ceramics was fabricated by hot pressing [91]. In 1975, Lange *et al*. reported that the additive of Al_2O_3 and the impurity of SiO_2 existed in SiC starting powders promoted the liquid phase sintering of SiC [92,93]. Then, various additives of Al_2O_3-Y_2O_3 [94-96], Al_2O_3-Y_2O_3-CaO [97,98] as well as Al_2O_3 [99,100] have been investigated for liquid phase sintering of SiC ceramics. However, the glassy phase existing at the grain boundaries of the liquid phase sintered SiC ceramics limits their high-temperature application.

The solid state sintering of SiC has been also investigated extensively to produce a structural ceramic material for high-temperature applications. In 1974, Prochaszka *et al.* first discovered that very fine SiC powders with low oxygen content could be sintered in the presence of small amount of boron and carbon without applied pressure at 1950 to 2100 °C [101,102]. Boron may contribute to decreasing the grain boundary energy, while carbon may contribute to increasing the surface energy. After that, some combinations of aluminum (Al), boron (B) and carbon (C) have been also reported as effective to fabricate fully dense SiC ceramics [87], then the SiC-(Al)-B-C systems have been investigated for fabrication of SiC-based ceramic components for high-temperature applications.

1.3. Objective of the present study

Since the investigations of SiC synthesis from polyorganosilanes in the mid-1970s, various types of Si-based polymeric precursors have been designed and synthesized for the fabrication of Si-based non-oxide amorphous ceramics in the form of fibers and coatings at low processing temperatures. Amorphous Si-C-O and Si-Ti-C-O fibers have been successfully developed, and they are now commercially available as “Nicaron” fibers [50,51] and “Tyrano” fibers [34,39], respectively. Novel thermally stable amorphous Si-B-C-N ceramics have been also successfully synthesized by the thermal conversion of polyborosilazanes [29-32]. However, for the development of novel technologies to fabricate high-performance Si-based non-oxide ceramic bulk materials by polymeric precursor route, it is essential that the relationships between chemical structure/composition of polymeric precursors, chemical reactions during the conversion to ceramics, and microstructure development of the final polycrystalline ceramics be clarified. In the previous studies, such

investigations have been only performed and discussed on the polycrystalline powder syntheses [55,70], or other studies briefly reported a tendency of the microstructure homogeneity and refinement of the polymeric precursor-derived SiAlON [41,48] and Si_3N_4 ceramics [103] compared to those fabricated by the conventional powder processing.

In the present study, novel polymeric precursors are designed and synthesized for fabrication of Si_3N_4- and SiC-based ceramic bulk materials. As a means to develop novel technologies for controlling their chemical composition and microstructure, two different synthesis routes are investigated using the designed polymeric precursors as shown in Fig. 1-10. One is the synthesis of Si_3N_4-based composites from polymeric precursor-derived multicomponent amorphous ceramic powders. The other is the synthesis of SiC ceramics by using polymeric precursors which can act as a compaction binder during green body forming and an in-situ source for microstructure control during sintering. Polymeric precursors for Si_3N_4-based composites and SiC ceramics are designed and synthesized by chemical modification of Si-based polymeric precursors. The polymeric precursors are successfully refined and utilized for synthesizing the Si-based non-oxide ceramics with controlled microstructure.

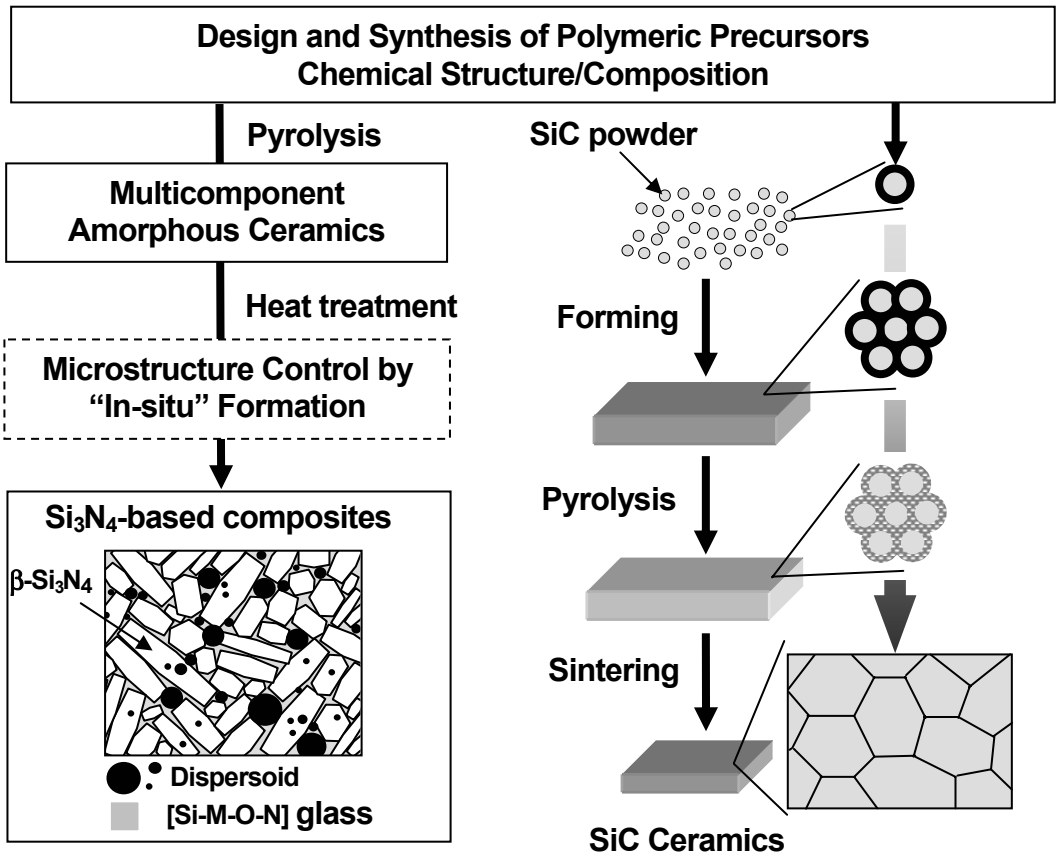

Fig. 1-10. Development of novel microstructure control technologies for Si_3N_4- and SiC-based ceramics through polymeric precursor route.

1.3.1. Study on the microstructure development of Si_3N_4-based composites from polymeric precursor-derived multicomponent amorphous powders

Composites like Si_3N_4/SiC ceramics are interesting materials because they combine the characteristics of the single components, an advantage that can be used to tailor the properties of ceramic materials. The crystallization of amorphous ceramic materials represents a completely powder-free process for the preparation of composite materials. Compared to the conventional powder metallurgical techniques, no nanocrystalline powders have to be applied which prevents problems like agglomeration and contamination of the materials due to the high surface area of nanocrystalline powders. Additionally, the design, synthesis and controlled conversion of polymeric precursors into ceramics can serve an opportunity to control the chemical composition, homogeneity of the ceramics at atomic or molecular size level, leading to the development of a novel nano/microstructure control technology for Si_3N_4-based composites through precursor design.

In this study, polymeric precursors for Si_3N_4-based composites are designed and synthesized by chemical modification of polysilazanes. The polymeric precursors are composed of all the elements for Si_3N_4 matrix, secondary phase as reinforcement and additives for liquid phase sintering of Si_3N_4 matrix. The polymeric precursors are successfully converted into Si_3N_4-based composites, and found to be useful for synthesizing nano/micro particle-dispersed Si_3N_4-based composites. A novel nano/micro-structure control technology for Si_3N_4-based composites is also proposed by controlling the chemical composition and structure of the polymeric precursors.

1.3.2. Design and synthesis of a novel “self-binder” for SiC ceramics, chemically modified polycarbosilanes

SiC ceramics fabricated by solid state sintering are attractive for high-temperature application. However, the reliability of the SiC is not so high due to their low fracture toughness, which limits applications of the SiC ceramics. To enhance the reliability, it is effective to decrease total amount of defects and the defect size [104,105]. Basically, an important method to decrease the number and size of defects in ceramics is to fabricate well-densified powder compacts.

As mentioned in the section 1.1.1.A, polycarbosilane is the most typical polymeric precursor for SiC ceramics. If a polymeric SiC precursor is applied for the conventional powder metallurgy route of the SiC ceramics, the polymeric precursor can act both a compaction binder during forming and an in-situ source for microstructure control during sintering, which is expected to develop high quality SiC ceramics. Such a novel “self-binder” [106] can be flexibly designed and synthesized by chemical modification of polycarbosilanes.

In this study, chemically modified polycarbosilanes with fluoro-alkoxy or -alkyl side chains are designed and synthesized. This is expected to be essential for improving green density of SiC powder compacts when combined with SiC powders. The polymeric precursors are successfully applied for fabrication of SiC ceramics by conventional powder processing, and found to be useful as a novel "self-binder" for fabrication of SiC ceramics with uniform microstructure.

References

[1] R. W. Rice, Am. Ceram. Soc. Bull., **62**, 889-892 (1983).
[2] K. J. Wynne and R. W. Rice, Annu. Rev. Mater. Sci., **14**, 297-334 (1984).
[3] R. Riedel and W. Dressler, Ceram. Int., **22**, 233-39 (1996).
[4] W. Verbeek and G. Winter, German Patent, 2236078, **1974**.
[5] S. Yajima, J. Hayashi and M Omori, Chem. Lett., 931-934 (1975).
[6] R. Riedel, G. Passing, H. Schonfelder and R. J. Brooks, Nature, **355**, 714-716 (1992).
[7] D. Seyferth, N. Bryson, D. P. Workman and C. A. Sobon, J. Am. Chem. Soc., **74**, 2687-89 (1991).
[8] P. Greil, J. Am. Chem. Soc., **78**, 835-48 (1995).
[9] F. S. Kipping and J. E. Sands, J . Chem. Soc., 119, 830-833 (1921).
[10] C. A. Burkhardt, J. Am. Chem. Soc., **74**, 963-967 (1949).
[11] S. Yajima, J. Hayashi, M Omori and K. Okamura, Nature, **261**, 683-685 (1976).
[12] H. Sakurai, R. Koh, A. Hosomi and M. Kumada, Bull. Chem. Soc. Japan, **39**, 2050-51 (1966).
[13] S. Yajima, Am. Ceram. Soc. Bull., **62**, 893-898 (1983).
[14] R. M. Laine and F. Babonneau, Chem. Mater, **5**, 260-279 (1993).
[15] C. L. Schilling Jr., J. P. Wesson and T. C. Williams, Am. Ceram. Soc. Bull., **62**, 912-915 (1983).
[16] B. Boury, R. J. P. Corriu and W. E. Douglas, Chem. Mater, **3**, 487-489 (1991).
[17] D. Seyferth, T. G. Wood, H. J. Tracy and J. L. Robinson, J. Am. Chem. Soc., **75**, 1300-1302 (1992).
[18] D. Seyferth and G. H. Wiseman, J. Am. Chem. Soc., **67**, C132-133 (1984).
[19] D. Seyferth, C. Strohmann, N. R. Dando and J. Perrotta, Chem. Mater, **7**, 2058-66 (1995).
[20] U. Wannagat, H. Bürger, C. Krüger, J. Pump, Z. Anorg. Allg. Chem., **321**, 208-212 (1963).
[21] R. M. Laine, F. Babonneau, K. Y. Blowhowiak, R. A. Kennich, J. A. Rhan, G. J. Exarhos and K. Waldner, J. Am. Chem. Soc., **78**, [1], 137-45 (1995).
[22] D. Mocaer, R. Pailler, R. Naslain, C. Richard, J. P. Pillot, J. Dunogues, C. Gerardin and F.

Taulelle, J. Mater. Sci., **28**, 2615-31 (1993).

[23] J. He, M. Scarlete and J. F. Harrod, J. Am. Ceram. Soc., **78**, 3009-17 (1995).

[24] C. R. Blanchar and S. T. Schwab, J. Am. Ceram. Soc., **77**, 1729-39 (1994).

[25] O. Funayama, Y.Tashiro, T. Aoki and T. Isoda, J. Ceram. Soc. Japan, **102**, 908-912 (1994).

[26] A. Kinienzle, A. Obermayer, A. Simon, R. Riedel, and F. Aldinger, Chem. Ber., **126**, 2569-71 (1993).

[27] R. Riedel, A. Greiner, G. Miehe, W. Dreβler, H. Fueβ, J. Bill, and F. Aldinger, Angew. Chem., Int. Ed. Engl., **36**, 603-606 (1997).

[28] H.-P. Baldus, M. Jansen and D. Sporn, SCIENCE, **285**, 699-703 (1999).

[29] R. Riedel, A. Kienzle, W. Dressler, L. Ruwisch, J. Bill and F. Aldinger, Nature (London), **382**, 796-798 (1996).

[30] L. Ruwisch, "Synthese und Hochtemperaturverhalten borhaltiger Silicium-carbonitride", PhD. Thesis, Technische Universität Darmstadt, Darmstadt, Germany, July 17, 1998.

[31] H.-P. Baldus, M. Jansen and O. Wagner, "New Materials in the system Si-(N,C)-B and their characterization", pp. 75-80 in Silicon Nitride '93, Key Engineering materials Vol. 89-91, edited by M. J. Hoffmann, P. F. Becher and G. Petzow (Trans Tech Publications, Aedermannsdorf, Switzerland), 1994.

[32] J. Löffelholz and M. Jansen, Adv. Mater, **7**, 289-292 (1995).

[33] K. Kienzle, PhD. Thesis, Universität Stuttgart, Stuttgart, Germany, 1994.

[34] S. Yajima, T. Iwai, T. Yamanaka, K. Okamura and Y. Hasegawa, J. Mater. Sci., **16**, 1349-55 (1981).

[35] A. Bellosi, S. Guicciardi and A. Tampieri, J. Europ. Ceram. Soc., **9**, 83-97 (1992).

[36] M. Herrmann, B. Balzer, Chr. Schbert and W. Hermel, J Europ. Ceram. Soc., **12**, 287-296 (1993).

[37] J. L. Huahg, M. T. Lee, H. H. Lu and D. F. Lii., Mater. Chem. Phys., **45**, 203-210 (1996).

[38] C. K. Narula, B. G. Demczyk, P. Czubarow and D. Seyferth, J. Am. Ceram. Soc., **78**, 1247-51 (1995).

[39] S. Yamamura, Y. Ishikawa, M. Shibuya, T. Hisayuki and K. Okamura, J. Mater. Sci., **23**, 2589-94 (1988).

[40] G. D. Sorarú, A. Ravagni and R. Campostrini, J. Europ. Ceram. Soc., **8**, 29-34 (1991).

[41] G. D. Sorarú, A. Ravagni, R. D. Maschio and G. Arturan, J. Am. Ceram. Soc., **74**, 2220-23 (1991).

[42] K. Thorne, E. Limatta and J. D. Mackenzie, Chem. Mater, **6**, 2199-2207 (1995).

[43] D. Seyferth, G. Brodt and B. Boury, J. Am. Ceram. Soc., **73**, 2131-33 (1990).

[44] W. R. Schmit, W. J. Hurley Jr., R. H. Doremus, L. V. Interrante and P. S. Marchetti, "Novel Polymeric Precursors to Si-C-Al-O-N ceramic composites," pp.19-25 in Ceramic Transactions, Vol. 19, Advanced Composite Materals, edited by M. D. Sacks (The American Ceramic Society, Westerville, OH), 1991.

[45] G. Verdecia, K. L. O'Brien, W. R. Schmit and T. M. Apple, Chem. Mater, **10**, 1003-09 (1998).

[46] J. Bill, M. Friess, F. Aldinger and R. Riedel, "Doped Silicon Carbonitride: Synthesis, Characterization and Properties", pp. 605-615 in Better Ceramics Through Chemistry VI, Mat. Res. Soc. Symp. Proc. Vol. 346, edited by A. K. Cheetham, C. J. Brinker, M. L. Mecartney and C. Sanchez (Materials Research Society, Pittsburgh, PA), 1994.

[47] O. Funayama, T. Kato, Y. Tashiro and T.Isoda, J. Am. Cerm. Soc., **76**, 717-723 (1993).

[48] O. Funayama, Y. Tashiro, T. Aoki and T. Isoda, J. Ceram. Soc. Japan, **102**, 908-912 (1994).

[49] Y. D. Blum, K. B. Schwartz and R. M. Laine, J. Mater. Sci., **24**, 1707-11 (1989).

[50] Y. Hasegawa, M. Iimura and S. Yajima, J. Mater. Sci., **15**, 720-728 (1980).

[51] K. Okamura, "Continuous silicon carbide fibers", pp.73-88 in "Silicon carbide ceramics", edited by S. Somiya and Y. Inomata (Uchida Rokakuho, Tokyo, Japan), 1988.

[52] M. Takeda, Y. Imai, H. Ichikawa, T. Ishikawa, T. Seguchi and K. Okamura, Ceram. Eng. Sci. Proc., **12**[7-8], 1007-18 (1991).

[53] M. Takeda, Y. Imai, H. Ichikawa, T. Ishikawa, N. Kasai, T. Seguchi and K. Okamura, Ceram. Eng. Sci. Proc., **13**[7-8], 209-217 (1992).

[54] Nippon Carbon Co., LTD, Technical information, Polycarbosilanes "Nipusi®", 19, May, 1995.

[55] J. Bill, J. Seitz, G. Thurn, J. Dürr, J. Canel, B. Z. Janos, A. Jalowiecki, A. Sauter, S. Schempp, H. P. Lamparter, J. Mayer and F. Aldinger, Phys. Stat. Solidi (a), **166**, 269-296 (1998).

[56] Y. Li, R. Riedel, J. Steiger, and H. Seggern, Adv. Eng. Mater., **2**, 290-293 (2000).

[57] J. M. Schwark, US Patent 4,929,704 (1990).

[58] J. M. Schwark, US Patent 5,032,649 (1991).

[59] Lanxide Company, Technical Bulletin of CERASET™ SN Inorganic Polymer, 1997.

[60] J. Seitz, J. Bill, N. Egger, and F. Aldinger, J. Europ. Ceram. Soc., **16**, 885-91 (1996).

[61] A. Gabriel, "Darstellung und keramisierung sauerstofffreier Polysilylcarbodiimid-Gele"; Ph.D. Thesis, Technische Universität Darmstadt, Darmstadt, Germany, June 5, 1998.

[62] J. Luecke, J. Hacker, D. Suttor, and G. Ziegler, Appl. Organomett. Chem., **11**, 181-94 (1997).

[63] G. Boden, A. Neumann, T. Breuning, E. Tschernikova and W. Hermel, J. Europ. Ceram. Soc., **18**, 1461-69 (1998).

[64] E. Kroke, Y-L. Li, C. Konetschny, E. Lecomte, C. Fasel, and R. Riedel, Mater. Sci. Eng., **R26**, 97-199 (2000).

[65] D. Bahloul, M. Pereira and P. Gourdsat, J. Am. Ceram. Soc., **76**[5], 1163-68 (1995).

[66] R. Riedel, "Advanced Ceramics from Inorganic Polymers," pp. 1-50 in Materials Science and Technology Vol. 17B, edited by. R. J. Brook (Wiley-VCH, Weinheim, Germany), 1996.

[67] A. O. Gabriel and R. Riedel, Angew. Chem., Int. Ed. Engl., **36**, 384-86 (1997).

[68] R. Riedel, H.-J. Kleebe, H. Schönfelder and F. Aldinger, Nature (London), **374**, 5264-28 (1995).

[69] L. An, R. Riedel, C. Konetschny, H.-J. Kleebe, and R. Raj, J. Am. Ceram. Soc., **81**, 1349-52 (1998).

[70] J. Bill and F. Aldinger, Adv. Mater., **7**, 775-87 (1995).

[71] J. Seitz, J. Bill, N. Egger, and F. Aldinger, J. Europ. Ceram. Soc., **16**, 885-891 (1996).

[72] J. Dixmer, R. Bellissent, D. Baholoul, and P. Goursat, J. Europ. Ceram. Soc., **13**, 293-298 (1994).

[73] S. Schempp, J. Durr, P. Lamparter, J. Bill, and F. Aldinger, Z. Naturforsch, **53** a, 127-133 (1998).

[74] M. Monthioux, O. Delverdier, J. Europ. Ceram. Soc., **16**, 721-737 (1996).

[75] Y. Iwamoto, W. Völger, E. Kroke, T. Saitou, K. Matsunaga and R. Riedel, J. Am. Ceram. Soc., **84**, 2170-78 (2002).

[76] D. Hardie and K. H. Jack, Nature, **180**, 332-336 (1980).

[77] R. S. Bradley, D. C. Munro and M. Whitfield, J. Inorg. Nucl. Chem., **28**, 1803-12 (1966).

[78] N. Wada, S. A. Solin, J. Wong and S. Prochazka, J. Non-Cryst. Solids, **43**, 7-15 (1981).

[79] K. Komeya and M Matsui, pp. 518-565 in Materials Science and Technology, edited by R. W. Cahn, P. Haasen, and E. J. Kramer (Wiley-VCH, Weinheim, Germany), 1994.

[80] A. Zerr, G. Mieche, G. Serghiou, A. Schwarz, E. Kroke, R. Riedel, H. Fueβ, P. Kroll and R. Boehler, Nature, **340**, 340-342 (1999).

[81] T. Ishii, I. Imai, A. Sano and M. Komatsu, "A New Method of Manufacturing a-Si_3N_4 Powder", pp. 11-19 in Silicon nitride ceramics 2, edited by M. Mitomo and S. Somiya (Uchida Rokakuho, Tokyo, Japan), 1990.

[82] G. Ziegler, J. Heinrich and G. Wötting, J. Mater. Sci., **22**, 3041-86 (1987).

[83] M. Mitomo, "Microstructural Development During Liquid Phase Sintering of Silicon Nitride", pp. 93-108 in Silicon nitride ceramics 2, edited by M. Mitomo and S. Somiya (Uchida Rokakuho, Tokyo, Japan), 1990.

[84] W. D. Kingary, J. Appl. Phys., **30**, 301-306 (1983).

[85] K. Kawashima, H. Okamoto, H. Yamamoto and A. Kitamura, "Characteristic Variety of Silicon Nitride Made Through Microstructural Control", pp. 135-146 in Silicon nitride ceramics 2, edited by M. Mitomo and S. Somiya (Uchida Rokakuho, Tokyo, Japan), 1990.

[86] K. Yamada and M. Mohri, "Properties and Application of Silicon Carbide Ceramics", pp. 9-30

in Silicon carbide ceramics, edited by S. Somiya and Y. Inomata (Uchida Rokakuho, Tokyo, Japan), 1988.

[87] S. Shinozaki, J Hangas, W. T. Donlon, R. M. Williams and B. N. Juterbock, "Analytical Electron Microscopy on the Effects of Sintering Aids in Pressureless Sintered SiC Materials ", pp. 7-28 in Advanced Ceramics II, edited by S. Somiya (Elsevier Applied Science, London and New York), 1986.

[88] L.U. Ogbugi, T. E. Mitchell and A. H. Heuer, J. Am. Ceram. Soc., **78**, 3145-48 (1995).

[89] Y. Tajima and W. D. Kingery, J. Am. Ceram. Soc., **65**, C-27 (1982).

[90] M. Mitomo, Y. Inomata and M. Kumanomido, J. Ceram. Soc. Japan, 78, 224-228 (1970).

[91] R. A. Alliegro, L. B. Coffin and J. R. Tinklepaugh, J. Am. Ceram. Soc., **39**, 386-389 (1956).

[92] F. F. Lange, J. Mater. Sci., **10**, 314-320 (1975).

[93] S. C. Singhal and F. F. Lange, J. Am. Ceram. Soc., **58**, 433-435 (1975).

[94] M. Ohmori and H. Takei, J. Am. Ceram. Soc., **65**, C-92 (1982).

[95] M. A. Mulla and V. D. kristic, Am. Ceram. Soc. Bull., **70**, 429-443 (1991).

[96] N. P. Padture, J. Am. Ceram. Soc., **77**, 519-523 (1994).

[97] Y.-W. Kim, M. Mitomo and H. Hirotsuru, J. Am. Ceram. Soc., **78**, 3145-48 (1995).

[98] Y.-W. Kim and M. Mitomo J. Ceram. Soc. Japan, **104**, 816-818 (1996).

[99] K. Suzuki, Rep. Res. Lab., Asahi Glass Co. Ltd., **36**, 25-36 (1986).

[100] K. Suzuki, "Pressureless Sintering of Silicon Carbide Ceramics with Addition of Aluminum Oxide", pp. 345-360 in Silicon carbide ceramics, edited by S. Somiya and Y. Inomata (Uchida Rokakuho, Tokyo, Japan), 1988.

[101] S. Prochaszka and P. C. Smith, G. E. Report, SRD-74-040 (1974).

[102] S. Prochaszka and R. J. Charles, Am. Ceram. Soc. Bull., **52**, 885-891 (1974).

[103] Y. Iwamoto, H. Matsubara and R. J. Brook, "Microstructural Development of Si_3N_4-Y_2O_3 Ceramics derived from Polymer Precursors", pp.193-197 in Ceramic Transactions, Vol. 51, Ceramic Processing Science and Technology, edited by H. Hausner, G. L. Messing and S. Hirano (The American Ceramic Society, Westerville, OH), 1995.

[104] K. Hirao, T. Nagaoka, M. E. Brito and S. Kanzaki, J. Am. Ceram. Soc., **77**, 1857-62 (1994).

[105] K. Ueno, Bull. Ceram. Soc. Japan, **18**, 1040-46 (1983).

[106] S. Hirano, Y. Iwamoto, Y. Sawai and T. Nagaoka, pp. 9-18 in "Synergy Ceramics," edited by Fine Ceramics Research Association (Gihoudo, Tokyo, Japan), 2000.

Chapter 2

Synthesis of chemically modified perhydropolysilazane and conversion into Si_3N_4-SiC-Y_2O_3 ceramics

2.1. Introduction

Si_3N_4 ceramics have been intensively studied for their excellent mechanical properties at both room and medium temperatures. However, application of this material at higher temperatures (>1000 °C) is still limited by the softening of the glassy phase which is located at Si_3N_4 matrix grain boundaries. As one of the possible ways to overcome this problem, the fabrication of Si_3N_4/SiC composites has been suggested. SiC has been applied for the composites in the form of particles, platelets, and whiskers. More recently, Si_3N_4/SiC nanocomposites have been developed. Especially, SiC nano/micro-particle dispersed Si_3N_4-Y_2O_3 ceramics exhibit excellent mechanical properties up to 1500 °C [1-4].

On the other hand, increasing attention has been directed to using silicon-based metal-organic precursors for the manufacture of Si_3N_4 ceramics [5-9], and there have been some reports on the synthesis of Si_3N_4-based ceramic composites using oligosilazanes [10-12], polysilazanes [13-15] and perhydropolysilazanes [16-18]. Among these starting precursors, perhydropolysilazane (PHPS) has some advantages in high purity and high ceramic yield [9]. Furthermore, PHPS contains many reactive Si-H and N-H groups which can react with chemical modifiers such as metal alkoxides ($M(OR)_x$, M=B [16], Al [17]) and metal amides ($M(NR_2)_x$, M=B [18]).

In this chapter, a novel polymeric precursor for SiC nano/micro-particle dispersed Si_3N_4-Y_2O_3 has been designed and synthesized by chemical modification of commercially available PHPS with molecular carbon source of n-decyl alcohol ($CH_3(CH_2)_9OH$) for SiC nano/micro-particles, and yttrium tri-methoxide ($Y(OCH_3)_3$) as a precursor for sintering additive of Y_2O_3. The chemical structures of the polymeric precursors are characterized by FT-IR and ^{1}H-NMR spectroscopic analyses. The crystallization behavior and microstructure development of the precursor-derived [Si-Y-O-C-N] multicomponent amorphous ceramics are studied by XRD analysis and electron microscopic observations.

2. 2. Experimental procedure

2.2.1. Precursor synthesis

Figure 2-1 shows the synthesis route of the polymeric precursor for Si_3N_4-SiC-Y_2O_3 ceramics.

Commercially available PHPS (Tonen Co. N-N410, mean molecular weight of 800, Tokyo, Japan) was used as a starting polymer. As shown in Fig. 2-1, this polymer mainly consists of structural units of $HSiN_3$, H_2SiN_2, H_3SiN, Si_2NH and also contains some $N(Si(CH_3)_3)_2$ groups which are introduced to stabilize PHPS toward ambient moisture. Reagents of $CH_3(CH_2)_9OH$ (Nakarai chemical, reagent grade, Tokyo, Japan) and $Y(OCH_3)_3$ (Kojundo Chemical Laboratory Co., Saitama, Japan) were used as-received. Organic solvents of xylene and pyridine were distilled and dried before use.

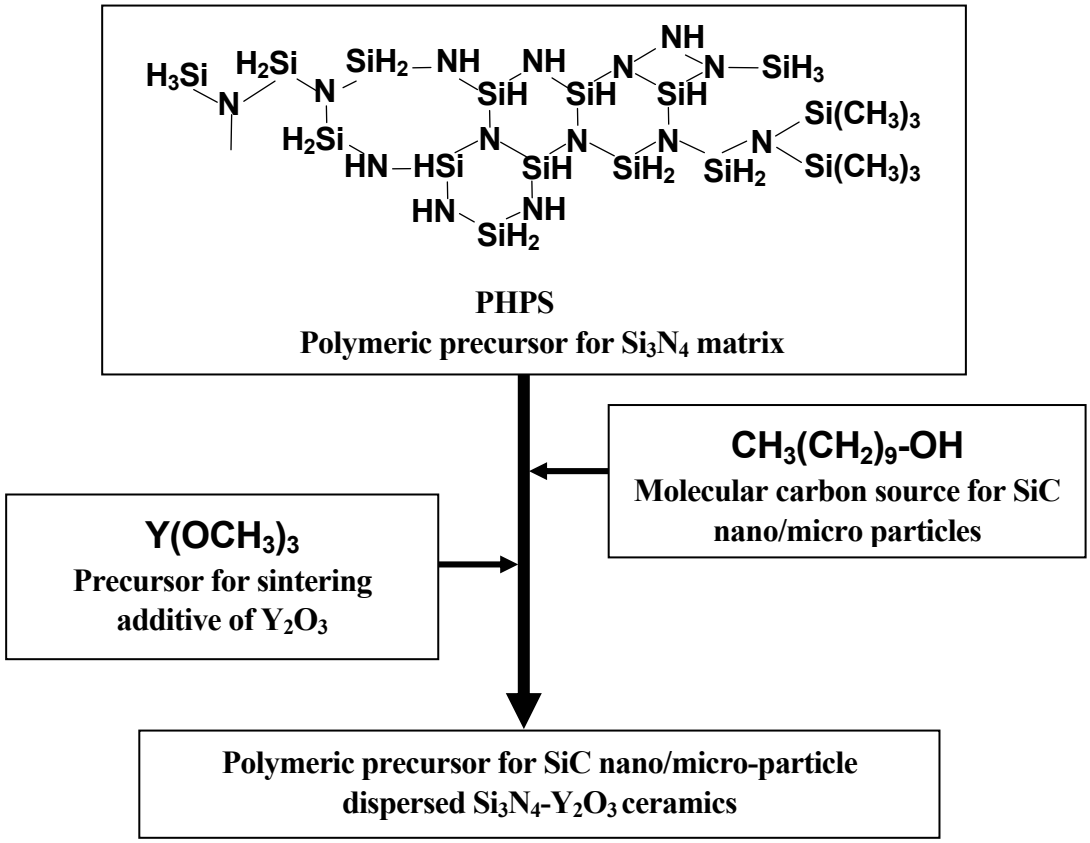

Fig. 2-1. Design and synthesis of a polymeric precursor for SiC nano/micro-particle dispersed Si_3N_4-Y_2O_3 ceramics through chemical modification route.

The chemical modification reactions of PHPS were carried out under N_2 atmosphere. The chemical yield was evaluated by weight % (wt%) based on the total amount of PHPS and reagents used in each chemical modification reaction.

As-received PHPS (14.6 g: Si, 57.7; N, 23.9; O, 0.8; C, 4.1wt%, hence Si=300) was dissolved in dry xylene (100 ml). To this solution, $CH_3(CH_2)_9OH$ (10 mmol, hence a total atomic ratio of Si/C=2) was added dropwise with stirring at room temperature. After the addition was completed, the mixture was refluxed at 125 °C for 1h with stirring. After cooling down to room temperature, the reaction mixture was concentrated in a rotary evaporator, then the residue was dried under vacuum to give an alcohol adduct (DEOPHPS, 15.9 g, 98 %) as a viscous liquid.

The DEOPHPS and $Y(OCH_3)_3$ (2g, 11 mmol, hence an atomic ratio of Si/Y=27) were mixed with dry pyridine (250 ml). The solution was refluxed at 125 °C for 2h with stirring. After concentration of the reaction solvent under the same manner as DEOPHPS, the reaction residue turned to be gel. Since the residue contained large amount of pyridine, dry xylene was added to the residue. Then, the mixture was again concentrated in a rotary evaporator to get rid of the residual pyridine. The residue was dried under vacuum to give an yttrium modified DEOPHPS (Y-DEOPHPS, 17.3 g, 96 %) as a white solid. This polymer was found almost insoluble in organic solvents such as toluene, ether and chloroform ($CHCl_3$).

To examine the chemical structure of Y-DEOPHPS, as-received PHPS was reacted with methanol (CH_3OH (100 mmol), Nakarai chemical, reagent grade, Tokyo, Japan) under the same reaction condition as PHPS with $CH_3(CH_2)_9OH$ to give another alcohol adduct (MEOPHPS, 14.2 g, 80 %) as a viscous liquid.

2.2.2. Pyrolysis and heat treatment

Pyrolysis of precursors was performed in an alumina tube furnace (Toukaikounetsukogyo, Tokyo, Japan) under flowing N_2 (500 ml/min). The precursor sample was ground to a fine powder using a mortar and pestle in a glove box under N_2 atmosphere. The powdered-precursor was pyrolyzed at 1000 °C for 3h with heating rate of 100 °C/h followed by cooling down with the same rate to room temperature.

The pyrolyzed sample was ground to a fine powder using a mortar and pestle, then sieved through a 250 μm screen before forming by uniaxial pressing at 150 MPa (15 mm diameter, 1.5g) and cold isostatic pressing at 300 MPa. The green compacts were placed on a BN plate within a Si_3N_4 crucible and heat treated in a graphite resistance-heated furnace (Model High Multi 10000, Fujidempa Kogyo, Osaka, Japan) at selected temperatures from 1200 °C to 1800 °C for 1h under a nitrogen pressure of 392 kPa.

2.2.3. Characterization

FT-IR spectra were recorded on KBr pellets containing precursor samples (Model System 2000, Perkin Elmer, Connecticut, USA). ^{1}H-NMR spectra were recorded for precursor samples in $CDCl_3$ solution at room temperature (Model EX-270, JEOL, Tokyo, Japan). All the chemical shifts were quoted relative to the signal of tetramethylsilane ($Si(CH_3)_4$, TMS).

Thermogravimetric analysis (TGA) was performed on the precursor samples up to 1000 °C at a heating rate of 10 °C/min under N_2 flow (Model TG8110D, Rigaku, Tokyo, Japan).

Elemental analyses were performed on the pyrolyzed and heat treated-samples for Si and Y (ICP spectrometry, Model ICAP-757V, Nippon Jarrell-Ash, Kyoto, Japan), C (high-temperature combustion method, Model EMGA 110, HORIBA, Kyoto, Japan), N and O (inert gas fusion method, Model EMGA 650, HORIBA, Kyoto, Japan).

XRD measurements were performed on the pyrolyzed- and heat treated-samples with CuKα radiation using an automated powder diffractometer equipped with a monochrometer (Model RINT 2500, Rigaku, Tokyo, Japan).

Apparent density of the heat treated-samples was measured by the Archimedes method. Relative density was evaluated using the theoretical density (3.275×10^3 kg/m^3) calculated from the composition of the 1800 °C heat treated-sample.

Microstructure of the heat treated-samples was studied using a scanning electron microscopy (SEM, Model S-800, Hitachi, Tokyo, Japan and Model JSM-6000F, JEOL, Tokyo, Japan) and a transmission electron microscopy (TEM, Model 4000FX, JEOL, Tokyo, Japan, operating at 400 kV).

2.3. Results and discussion

2.3.1. Chemical structure of precursors

FT-IR spectrum of as-received PHPS is shown in Fig. 2-2 (a). The absorption bands at 3400 cm^{-1} (N-H) [19], 2950-2900 cm^{-1} (C-H) [20], 2150 cm^{-1} (Si-H) [19], 1250 cm^{-1} (Si-CH_3) [20], 1180 cm^{-1} (N-H) [19] and 840-1020 cm^{-1} (Si-N-Si) [19] are observed. In the spectrum of DEOPHPS (Fig. 2-2 (b)), the absorption intensity of C-H groups at 2950-2850 cm^{-1} increases in comparison with that of as-received PHPS and a week shoulder is observed at 1090 cm^{-1} (marked by an arrow), which is assigned to Si-O groups [20].

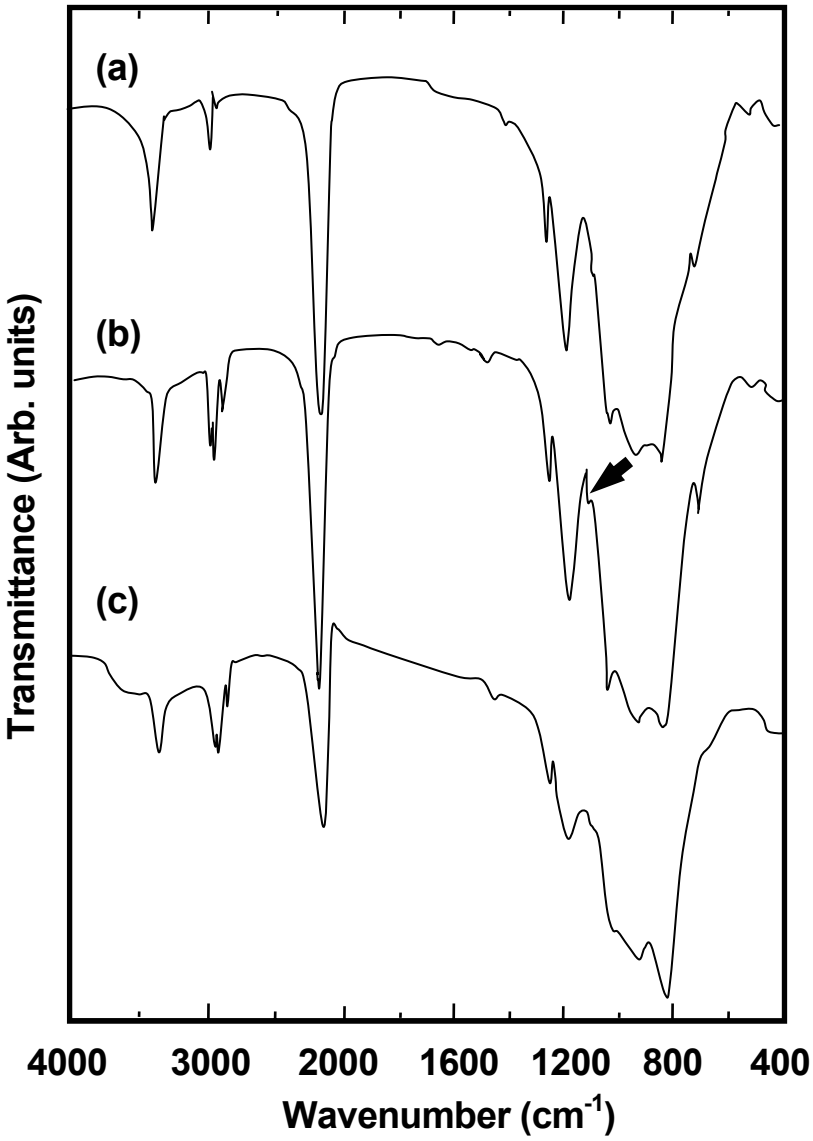

Fig. 2-2. FT-IR spectra of (a) as-received PHPS, (b) DEOPHPS obtained by the reaction of PHPS with $CH_3(CH_2)_9OH$ and (c) Y-DEOPHPS.

The ^1H NMR spectra of as-received PHPS and $CH_3(CH_2)_9OH$ are shown in Fig. 2-3 (a) and Fig 2-3 (b), respectively. The peak assignment for $CH_3(CH_2)_9OH$ is also shown in Fig. 2-3 (b) [20]. As-received PHPS presents four peaks at 4.8, 4.3, 1.4 (broad) and 0.1-0.2 ppm assigned to SiH/SiH_2, SiH_3, NH and $Si-CH_3$, respectively [19, 20].

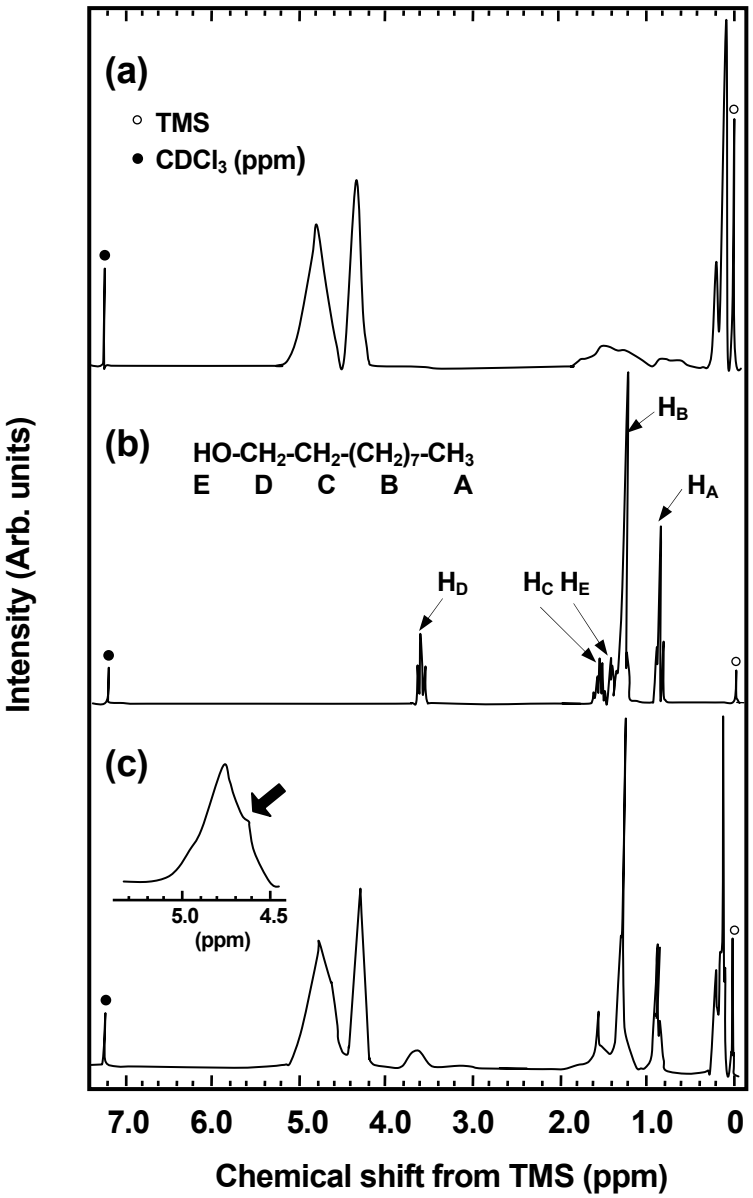

Fig. 2-3. ^{1}H-NMR spectra of (a) as-received PHPS, (b) $CH_3(CH_2)_9OH$ and (c) DEOPHPS obtained by the reaction of PHPS with $CH_3(CH_2)_9OH$.

The ^{1}H NMR spectrum of DEOPHPS (Fig. 2-3 (c)) mainly consists of the peaks of PHPS and $CH_3(CH_2)_9O$- group. However, a small shoulder at 4.7 ppm is observed on the peak of $HSiN_3/H_2SiN_2$ (marked by an arrow), which is assigned to $HSiON_2$ groups [16]. The peak of an alcoholic proton (H_E) at 1.44 ppm disappears and the peaks of the $CH_3(CH_2)_9O$- group are broader in comparison with those of as-received $CH_3(CH_2)_9OH$ (Fig. 2-3 (b)), indicating the influence of

the polymer network of PHPS. The ratio of the peaks of H_3SiN at 4.3 ppm to that of Si-CH_3 group at 0.1-0.2 ppm for DEOPHPS is 2.84, which is almost the same value of as-received PHPS (2.89).

These spectroscopic data indicate that $CH_3(CH_2)_9OH$ mainly reacted with H_2SiN_2 groups (not SiH_3 groups) of PHPS to yield $CH_3(CH_2)_9O$-Si(H)= groups:

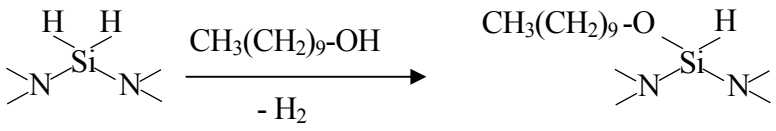

(2.1)

The FT-IR spectrum of Y-DEOPHPS is shown in Fig. 2-2 (c). Compared with the spectrum of DEOPHPS (Fig. 2-2 (b)), a remarkable decrease in absorption intensity at 3400, 1180 cm^{-1} (N-H) and 2150 cm^{-1} (Si-H) is observed. It should be noted that, during this reaction process, pyridine was also considered to behave as a basic catalyst of dehydrocondensation of PHPS and a decrease in absorption intensity of N-H and Si-H groups might be observed. However, such remarkable intensity changes were not observed in the FT-IR spectrum of DEOPHPS after heat treatment in pyridine without $Y(OCH_3)_3$ and isolation under the same condition as mentioned in the experimental section. These changes in the FT-IR spectrum indicate that $Y(OCH_3)_3$ reacted with N-H and Si-H groups of DEOPHPS.

As mentioned in the experimental section, Y-DEOPHPS was almost insoluble in organic solvents and we could not get further information for this sample by ^1H NMR spectroscopy. To examine this reaction step in more detail, as-received PHPS was directly reacted with $Y(OCH_3)_3$ in pyridine at 60 °C for 5h, then the reaction mixture was immediately diluted with $CDCl_3$ and analyzed before further solidification occurred.

The ^1H NMR spectrum of the reaction mixture is shown in Fig. 2-4 (a). In addition to the peaks of as-received PHPS (Fig. 2-4 (b)), two extra peaks are observed at 4.7 ppm and at 3.7-3.5 ppm. The decrease in peak intensity of H_3SiN at 4.3 ppm is also observed. The peak at 4.7 ppm is assigned to $HSiON_2$, while the peaks at 3.7-3.5 ppm are assigned as Si-OCH_3 [20] and Y-OCH_3 group [21].

These changes in this spectrum are quite similar to those of the MEOPHPS obtained by the reaction of PHPS with CH_3OH as shown in Fig. 2-4 (c). In addition to the peaks of PHPS, the MEOPHPS presents two extra peaks at 4.7 ppm and 3.5 ppm assigned to $HSiON_2$ and CH_3O, respectively. These extra peaks indicate that CH_3OH reacted with H_2SiN_2 groups of PHPS and CH_3O-$SiHN_2$ groups were formed. However, the relative peak intensity of H_3SiN group to Si-CH_3 group for MEOPHPS is 1.90, while that for as-received PHPS is 2.89. The decrease of the amount

of H_3SiN groups in PHPS reveals that CH_3OH also reacted with these groups of PHPS. During the reaction of PHPS with CH_3OH, cleavage of Si-N bonds occurred as well as CH_3O-$SiHN_2$ formation [16].

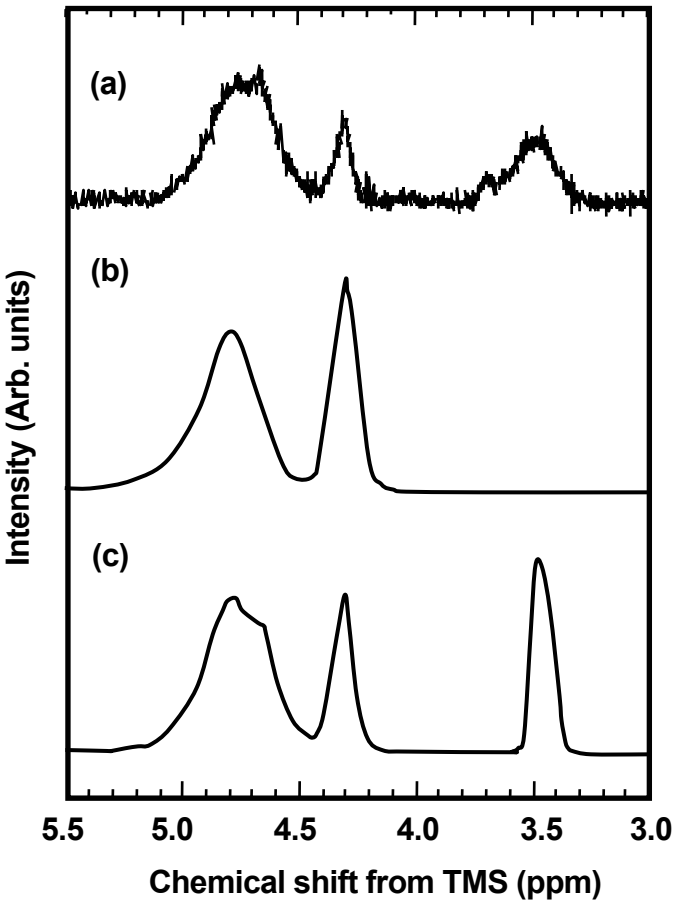

Fig. 2-4. ^{1}H-NMR spectra of (a) the reaction mixture of as-received PHPS with $Y(OCH_3)_3$ in pyridine at 60 °C for 5 h (b) as-received PHPS and (c) MEOPHPS obtained by the reaction of PHPS with CH_3OH.

One possible reason for the decrease of the amount of H_3SiN groups is considered to be due to the reaction of CH_3OH with some H_3SiN groups of PHPS followed by the cleavage of Si-N bonds, elimination and evolution of alkoxysilane compounds such as CH_3OSiH_3 as shown Eq. 2.2.

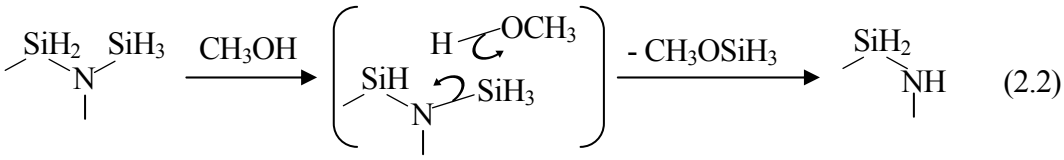

(2.2)

According to these spectroscopic analyses, $Y(OCH_3)_3$ was thought to react with N-H bonds in DEOPHPS followed by the elimination of CH_3OH as shown in Eq. 2.3, then the produced CH_3OH reacted with H_2SiN_2 and H_3SiN groups in PHPS as mentioned above.

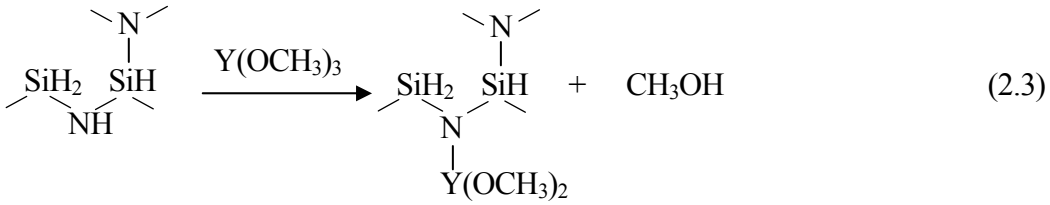

(2.3)

Funayama *et al.* reported that the reactions of PHPS with trimethoxy borate [16], and PHPS with (ethyl acetoacetate) aluminumdiisopropoxide [17] formed N-B bonds and N-Al bonds, respectively, and PHPS with $Y(OCH_3)_3$ seemed to form N-Y bonds as analogously as boron or aluminum alkoxide. Since Y-DEOPHPS was almost insoluble solid toward organic solvents, further cross-linking of PHPS moieties in Y-DEOPHPS is considered to be occurred via functional groups such as $NY(OCH_3)N$. Based on the results obtained by the spectroscopic analyses, the proposed chemical structure of Y-DEOPHPS is shown in Fig. 2-5.

2.3.2. Conversion of precursor into amorphous [Si-Y-O-C-N] ceramics

The TGA curves of as-received PHPS and the Y-DEOPHPS are shown in Fig. 2-6. The weight loss of these samples starts at around 100 °C and completed at around 600 °C in N_2. As-received PHPS shows a continuous weight loss from 100 to 600 °C, while the weight loss of the Y-DEOPHPS is mainly observed below 200 °C, then, rather stable up to 400 °C and the total weight loss of Y-DEOPHPS is suppressed in comparison with that of as-received PHPS.

The weight loss of Y-DEOPHPS observed below 200 °C is considered to be due to the residual solvent used in the chemical modification as mentioned in the experimental section, and the total weight loss is thought to be suppressed by the highly cross-linked structure via functional groups, such as $NY(OCH_3)N$.

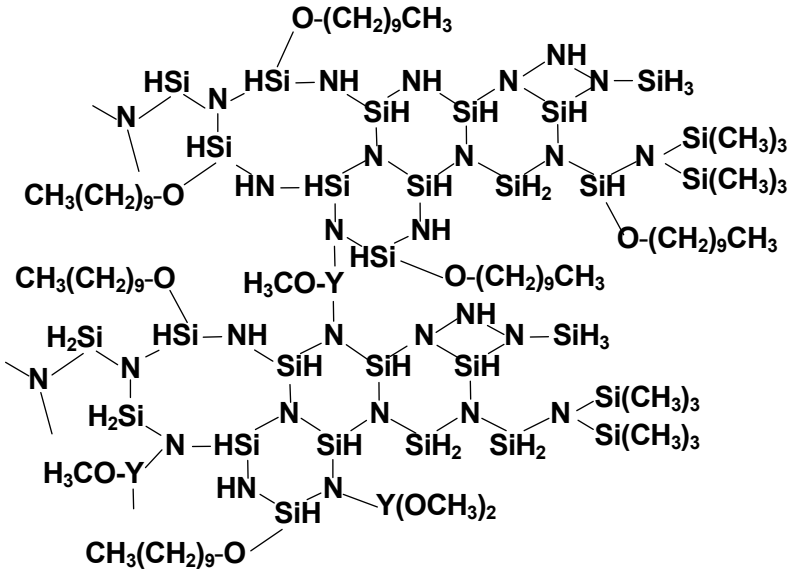

Fig. 2-5. Proposed chemical structure of Y-DEOPHPS.

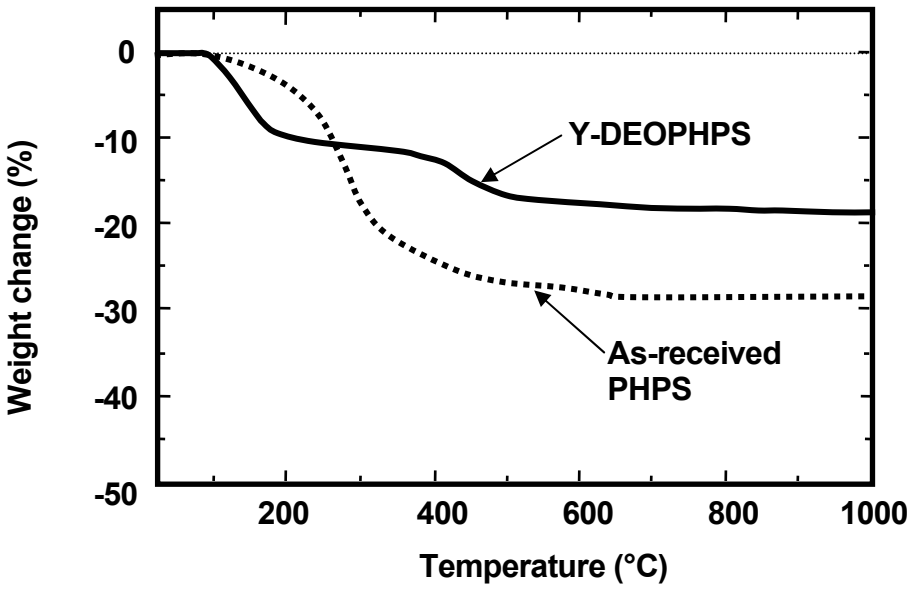

Fig. 2-6. TGA of as-received PHPS and Y-DEOPHPS from room temperature to 1000 °C at a heating rate of 10 °C/min under a N_2 flow of 100 ml/min.

The pyrolysis of larger quantities in the alumina tube furnace almost resulted in the same ceramic yield (above 75 %). The chemical composition analysis of the pyrolyzed samples and the resulting empirical atomic ratios are shown in Table 2-1. The Si/Y atomic ratio of [Si-Y-O-C-N] amorphous is 25, which is slightly smaller than the calculated value of 27. During the chemical modification reaction of PHPS, silicon content was thought to be reduced by the side reaction as shown in Eq. 2-2.

The Si/C atomic ratio of [Si-Y-O-C-N] amorphous is 3.8 and carbon content of the pyrolyzed sample is also smaller than the calculated content. However, in comparison with as-received PHPS, carbon and yttrium were successfully doped in the pyrolyzed sample by the two-step chemical modification of PHPS.

Table 2-1. Chemical composition of 1000 °C pyrolyzed-samples.

Precursor	Composition (wt%)					Atomic ratio
	Si	Y	O	C	N	
Y-DEOPHPS	52.8	6.0	7.1	7.2	25.9	$Si_{1.0}Y_{0.04}O_{0.24}C_{0.27}N_{0.98}$
PHPS	73.9	--	0.4	3.1	21.6	$Si_{1.0}Y_{0.00}O_{0.01}C_{0.09}N_{0.56}$

2.3.3. Crystallization and microstructure development of amorphous [Si-Y-O-C-N] ceramics

The XRD patterns of the precursor-derived [Si-Y-O-C-N] ceramics are shown in Fig. 2-7. At 1200 °C, $YSiO_2N$ crystallization is observed before Si_3N_4 crystallization occurs. At 1400 °C, both α- and β-Si_3N_4 and Si_2N_2O peaks begin to appear. The Si_2N_2O peaks disappears at 1600 °C, then the α-/β-Si_3N_4 phase transformation is completed at 1800 °C. In addition to Si_3N_4, β-SiC is observed above 1700 °C as a minor phase.

The crystallization behavior observed below 1600 °C indicates that [Si-Y-O-N] liquid phase promoted both α-Si_3N_4 crystallization and α-/β-Si_3N_4 phase transformation below 1400 °C. The formation of Si_2N_2O at 1400 °C is due to the excess oxygen introduced in the Y-DEOPHPS from $Y(OCH_3)_3$ (O/Y=3), and the resulting amorphous [Si-Y-O-C-N] powders may be highly reactive towards ambient moisture, which lead to an increase of total oxygen content (Table 2-1). During heating process from 1400 °C to 1600 °C, Si_2N_2O was decomposed to form Si_3N_4 and volatile SiO and O_2.

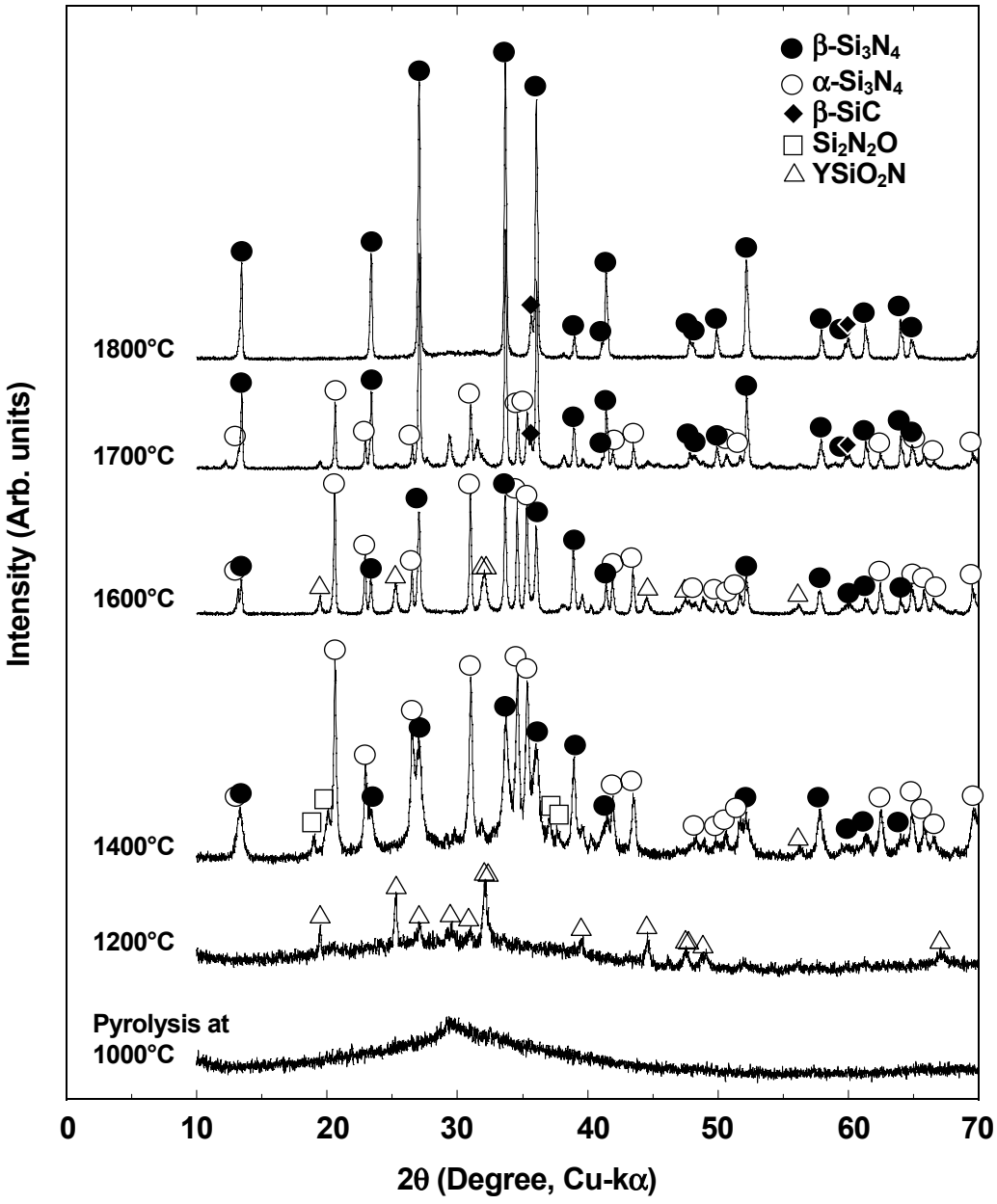

Fig. 2-7. The crystallization behavior of [Si-Y-O-C-N] amorphous powder compact.

Figure 2-8 shows the microstructure development of the amorphous [Si-Y-O-C-N] powder compact. At 1400 °C, several round and shallow holes are observed on the surface of large particles, which are thought to be generated by volatile fragments in heat treatment. At 1600 °C, needle like fine crystallites are observed on the surfaces of large particles. Above 1600 °C, the needle like fine crystallites grows up continuously, while large particles disappears and finally, [Si-Y-O-C-N] amorphous powders yields a unique fibrous microstructure composed of whiskers with submicron in diameter and more than 10 μm in length. As shown in Fig. 2-9 (a), the whiskers grew uniformly inside of the compact. The whisker tips were surrounded with facets (Fig. 2-9 (b)) and a polycrystalline was found at the root of whiskers (Fig. 2-9 (c)).

Figure 2-10 shows the changes in chemical composition and weight of the [Si-Y-O-C-N] compact during heat treatment up to 1800 °C. The silicon content slightly decreases up to 1600 °C, then increases above this temperature. After heat treatment at 1800 °C, the silicon content almost regains the initial content. The yttrium content is almost constant during heat treatment up to 1800 °C. However, both carbon and oxygen contents decrease with increasing temperature. Especially, remarkable decreases of carbon and oxygen contents are observed at 1400 to 1600 °C, while nitrogen content increases above 1600 °C. During these composition changes, weight loss of the compact increases up to 1600 °C, then the weight loss is suppressed above this temperature. After heat treatment at 1800 °C, the weight of the compact almost regains the initial weight.

The composition change of the [Si-Y-O-C-N] compact indicates that the weight loss observed below 1600 °C is due to the volatilization of gases such as CO and SiO. This is also suggested by the microstructure observation as shown in Fig. 2-8 (b). The amorphous [Si-Y-O-C-N] powders were thought to be thermodynamically metastable and were able to give off these gases during heat treatment.

Since nitrogen content increased above 1600 °C, the weight loss is considered to be mainly compensated by direct nitridation of silicon remaining in the amorphous [Si-Y-O-C-N] powders above 1600 °C [22].

The change in silicon content observed up to 1800 °C suggest the formation of Si_3N_4 whiskers from the vapor phase composed of gases from the [Si-Y-O-C-N] amorphous powders and atmosphere of N_2. In many whisker syntheses using metallic agents, small spherical droplets have been observed on the whisker tips, and the VLS (vapor-liquid- solid) mechanism [23] has been proposed for the whisker growth. However, no droplets were observed on the whisker tips as shown in Fig. 2-8 (a). Even at the very initial growth stage, no droplets were observed as shown in Fig. 2-7 (c). Accordingly, the growth of whiskers in this study seems to occur by the VS (vapor-solid) mechanism from the initial stage of the whisker growth.

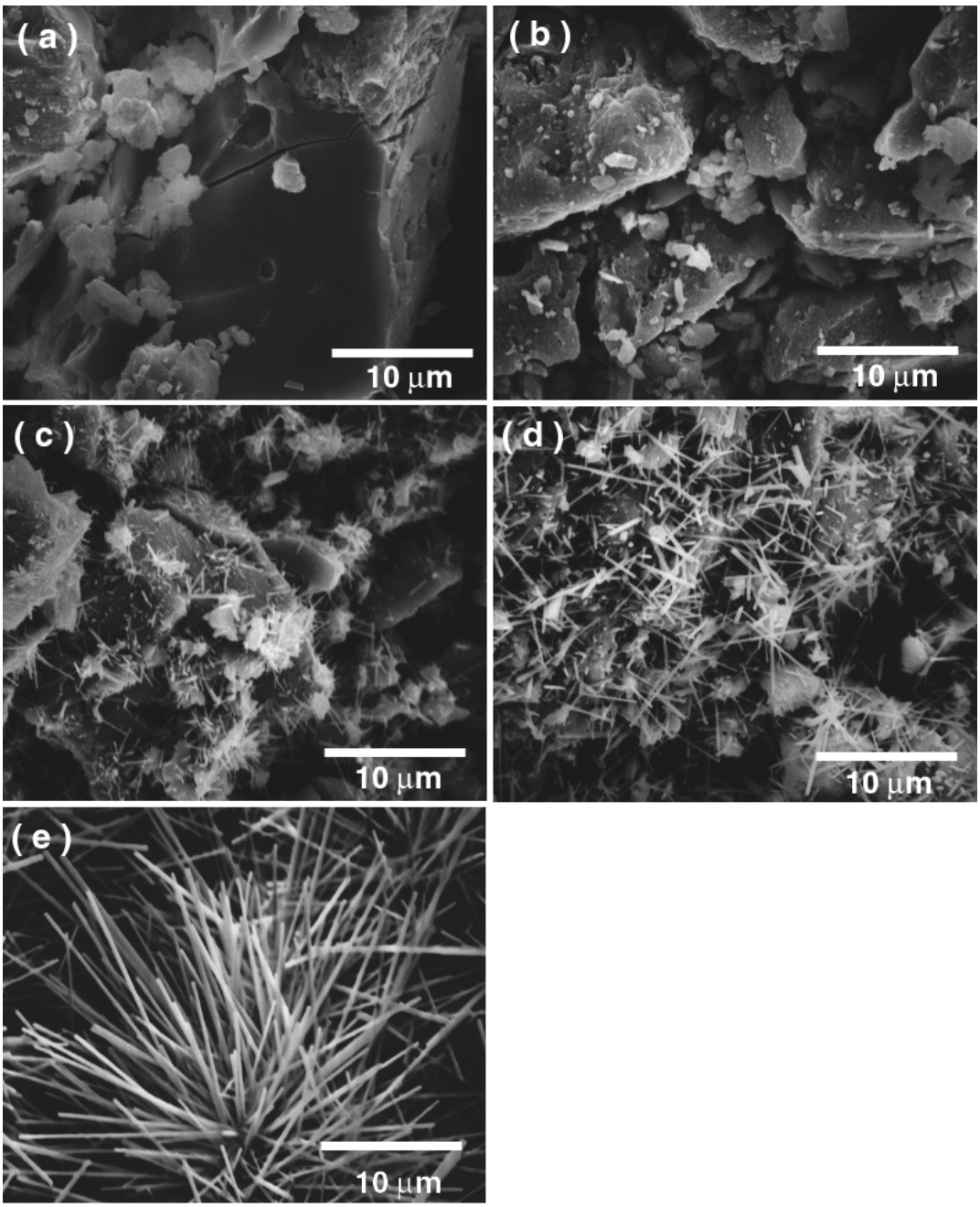

Fig. 2-8. Microstructures of polymeric precursor-derived [Si-Y-O-C-N] ceramics heat treated at (a) 1200 °C, (b) 1400 °C, (c) 1600 °C, (d) 1700 °C and (e) 1800 °C for 1h.

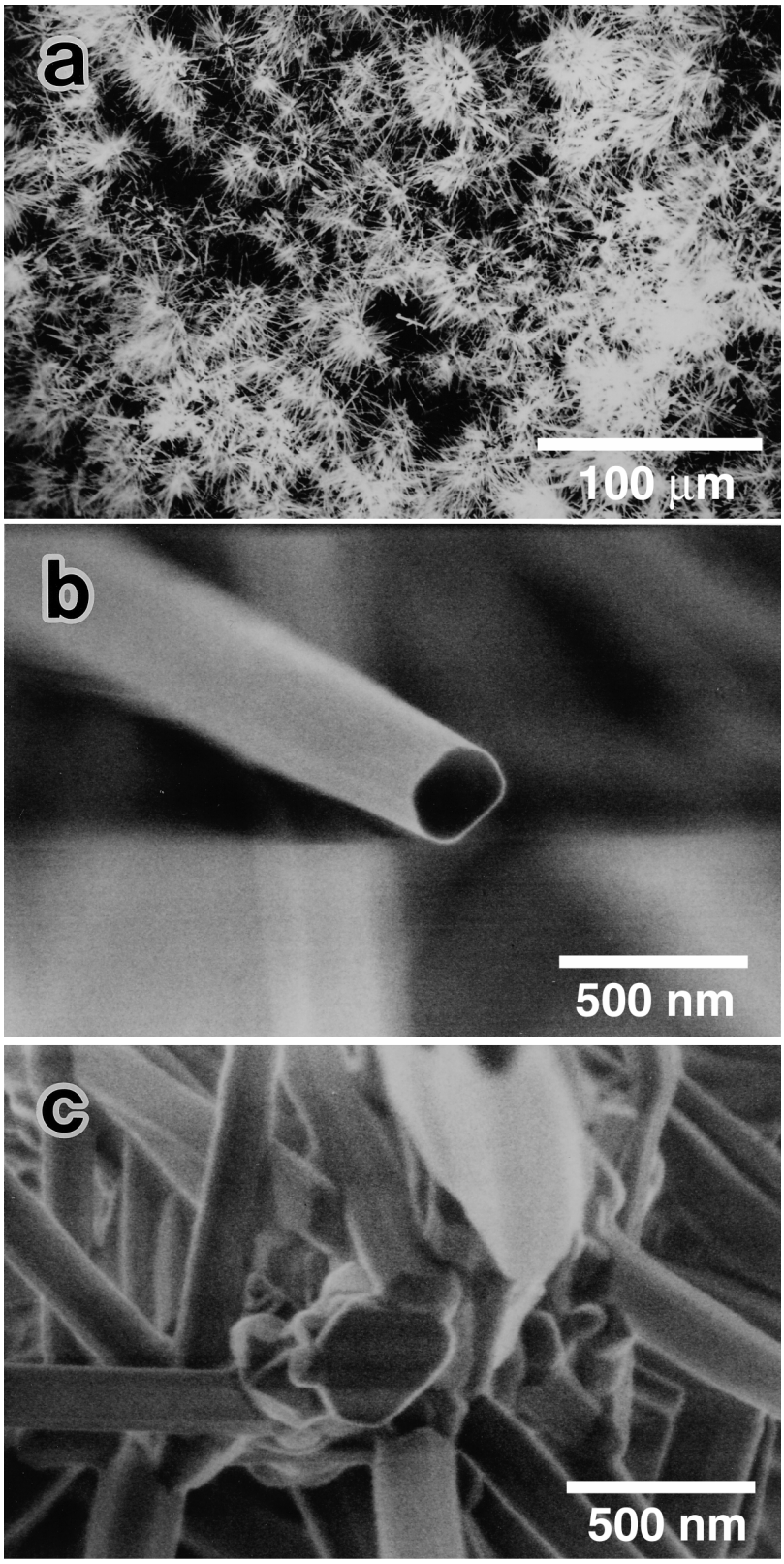

Fig. 2-9. SEM micrograph showing (a) β-Si_3N_4 whiskers uniformly grown in the compact, (b) facets without droplet at the tip of β-Si_3N_4 whisker and (c) polycrystalline at the root of β-Si_3N_4 whiskers.

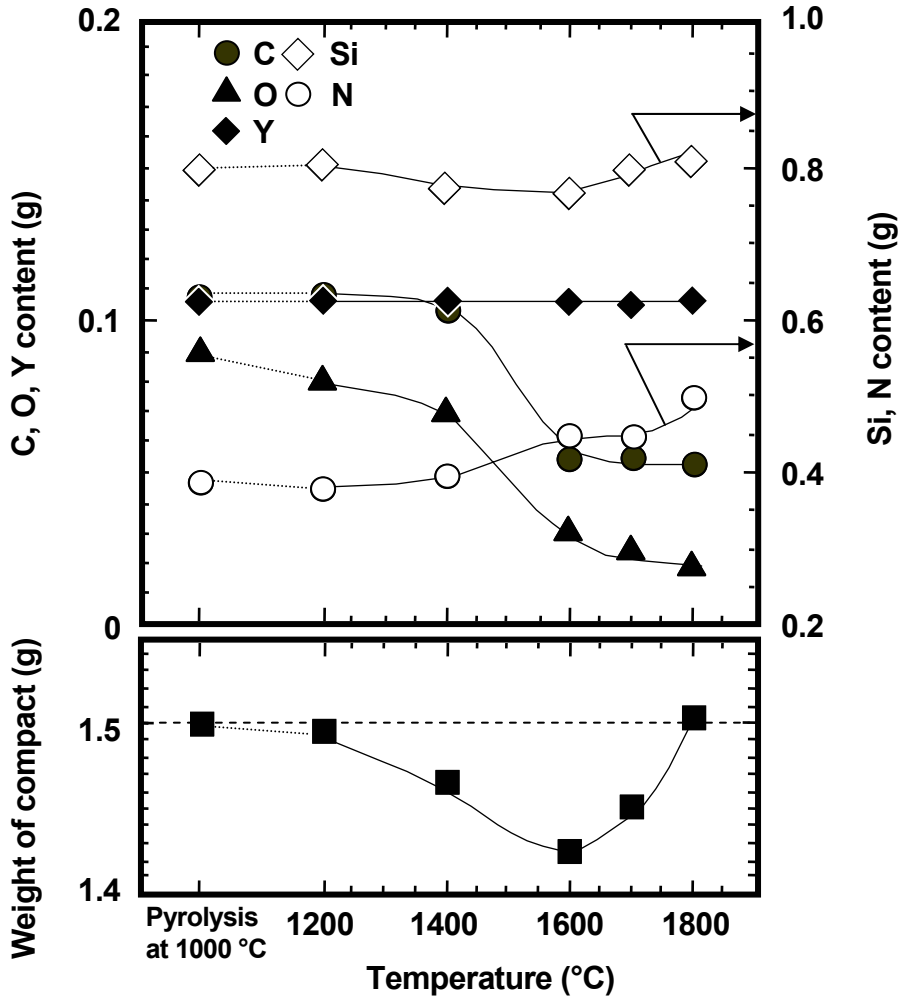

Fig. 2-10. Chemical composition change and weight change of [Si-Y-O-C-N] amorphous powder compact during heat treatment up to 1800 °C.

There are three possible reactions for Si_3N_4 formation associated with gases from the amorphous [Si-Y-O-C-N] powders.

$$3SiO\ (g) + 3C\ (s) + 2N_2\ (g) = \beta\text{-}Si_3N_4\ (s) + 3CO\ (g) \quad (2.4)$$

$\Delta G^{02\text{-}4} = -760.61 + 0.324T$, kJ•mol^{-1} of β-Si_3N_4

$$3SiO(g) + 3CO(g) + 2N_2\ (g) = \beta\text{-}Si_3N_4\ (s) + 3CO_2\ (g) \quad (2.5)$$

$\Delta G^{02\text{-}5} = -1288.13 + 0.846T$, kJ•mol^{-1} of β-Si_3N_4

$$3SiO(g) + 2N_2\ (g) = \beta\text{-}Si_3N_4\ (s) + 3/2O_2\ (g) \quad (2.6)$$

$\Delta G^{02\text{-}6} = -434.37 + 0.585T$, kJ•mol^{-1} of β-Si_3N_4

In this calculation, all of the standard free energies were obtained from JANAF Tables [24] except that of β-Si_3N_4, which was referred from another literature [25]. At 1600 °C (1873 K), the changes of free energy based on the Eqs. 2.4, 2.5 and 2.6 are -163.8, 296.4 and 661.3 kJ•mol^{-1}, respectively. Accordingly, a possible reaction for the Si_3N_4 formation is Eq. 2.4. However, in this case, the nucleation site is limited on solid carbon, while carbon content of the amorphous [Si-Y-O-C-N] powder compact remarkably decreased before whisker growth occurred, as shown in Fig 2-9. Therefore, the Eq. 2-4 is not acceptable in this case. Based on the thermodynamic calculation results, it is difficult to explain the fibrous microstructure development by gas phase reactions.

Figure 2-11 shows the densification behavior of the [Si-Y-O-C-N] powder compact. The density slightly increases up to 1600 °C, then, increases rapidly above this temperature. However, even at 1800 °C, the relative density is as low as 61%. During heat treatment, the densification of the compact was hampered by the volatilization of gases such as CO and SiO. Thus, the fine Si_3N_4 crystallites were able to grow up without steric hindrance [26]. Consequently, the [Si-Y-O-C-N] powders yielded a unique fibrous microstructure.

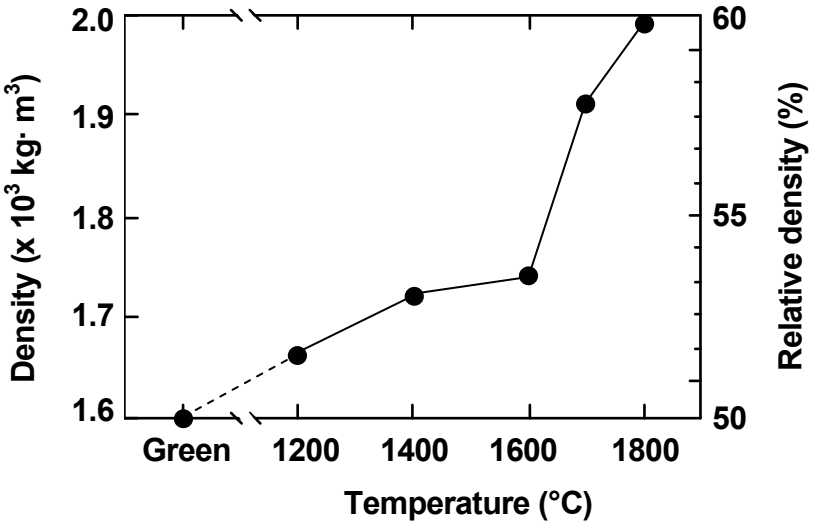

Fig. 2-11. Densification behavior of [Si-Y-O-C-N] amorphous powder compact during heat treatment up to 1800 °C.

Figure 2-12 shows a typical TEM image of the polycrystalline existed at the root of the whiskers. The polycrystalline consists of submicron β-Si_3N_4 grains, [Si-Y-O-N] glassy phases and some nanometer particles within the β-Si_3N_4 grains, which are thought to be β-SiC detected by XRD above 1700 °C as a minor phase. The observation result suggests that the polymeric precursor-derived amorphous [Si-Y-O-C-N] powders have a potential to synthesize β-SiC nano-particle dispersed Si_3N_4-Y_2O_3 ceramics.

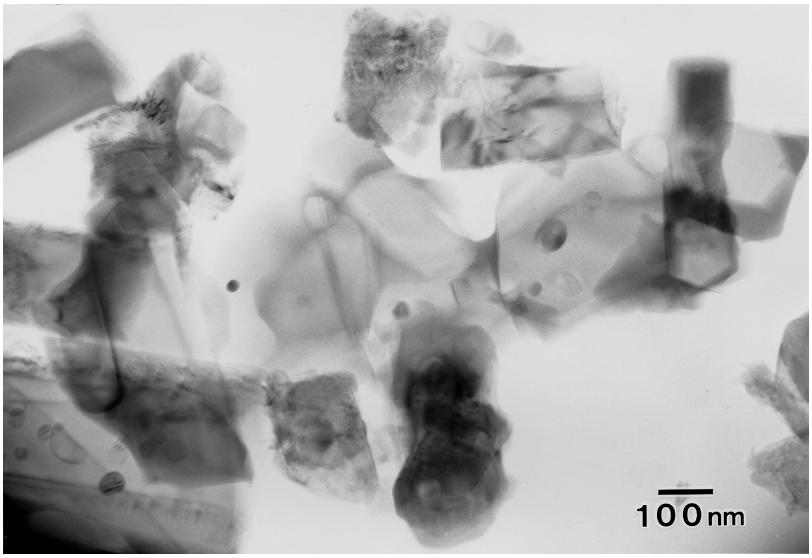

Fig. 2-12. The typical TEM micrograph of the polycrystalline existed at the root of the whiskers.

2.4. Conclusions

Polymeric precursor for Si_3N_4-SiC-Y_2O_3 ceramics has been synthesized by chemical modification of commercially available PHPS with $CH_3(CH_2)_9OH$ and $Y(OCH_3)_3$. FT-IR and ^{1}H-NMR spectroscopic analyses of the synthesized precursor revealed that $CH_3(CH_2)_9OH$ reacted mainly with SiH_2N_2 groups in PHPS to yield $CH_3(CH_2)_9O$-$Si(H)N_2$ groups, while $Y(OCH_3)_3$ reacted with N-H groups of PHPS to yield N-$Y(OCH_3)_{3-x}$ (x=1, 2) groups.

Amorphous [Si-Y-O-C-N] multicomponent powders were successfully synthesized by pyrolysis of the precursor at 1000 °C in N_2. The amorphous [Si-Y-O-C-N] powders yielded Si_3N_4-SiC-Y_2O_3 ceramics by heat treatment at 1800 °C in N_2. The microstructure was composed of β-Si_3N_4 whiskers with submicron in diameter and more than 10 μm in length. The unique

microstructure development was explained by the slow densification cased by the volatilization of gases such as CO and SiO, which lead to the Si_3N_4 grain growth without steric hindrance. The TEM observation result of the 1800 °C heat treated-sample revealed that the polymeric precursor-derived amorphous [Si-Y-O-C-N] powders had a potential to synthesize β-SiC nano/micro-particle dispersed Si_3N_4-Y_2O_3 ceramics.

References

[1] K. Niihara, K. Izaki and T. Kawakami, J. Mater. Sci. Lett., **10**, 112-114 (1990).

[2] G. Sasaki, H. Nakase, K. Suganuma, T. Fujita and K. Niihara, J. Ceram. Soc. Japan, **100**, 536-40 (1992).

[3] Y. Ukyo, T. Kandori and S. Wada, J. Ceram. Soc.Japan, **101**, 536-40 (1992).

[4] M. Herrmann, C. Scuber, A. Rendel and H. Hubner, J. Am. Ceram. Soc., **81**, 1095-1108 (1998).

[5] K. J. Wynne and R. W. Rice, Annu. Rev. Mater. Sci., **14**, 297-334 (1984).

[6] D. Seyferth and G. H. Wiseman, pp. 2656-71 in Ultrastructure Processing of Ceramics, Glasses and Composites, edited by L. L. Hench and D. R. Ulrich (Willey-Interscience, New York), 1984.

[7] K. B. Schwartz, D. J. Rowcliffe, Y. D. Blum and R. M. Raine, pp. 265-71 in Better Ceramic Through Chemistry II, edited by C. Brinker, D. Clark and D. Ulrich (Mat. Res. Soc. Symp. Proc. **73**, Materials Research Society, Pittsburgh, PA), 1986.

[8] W. R. Schmit, V. Sukumar, W. J. Hurley, Jr., R. Garcia, R. H. Doremus and L. V. Interrante, J. Am. Ceram. Soc., **73**, 2412-18 (1990).

[9] O. Funayama, M. Arai, Y. Tashiro, H. Aoki, T. Suzuki, K. Tamura, H. Kaya, H. Nishii and T. Isoda, J. Ceram. Soc. Japan, **98**, 104-107 (1990).

[10] D. Seyferth, G. Brodt and B. Boury, J. Am. Ceram. Soc., **73**, 2131-33 (1990).

[11] W. R. Schmit, W. J. Hurley, Jr., R. H. Doremus, L. V. Interrante and P. S. Marchetti, pp. 19-25 in Advanced Composite Materals, edited by M. D. Sacks (Ceram. Trans. **19**, The American Ceramic Society, Westerville, OH), 1991.

[12] D. Seyferth and H. Plenio, J. Mater. Sci. Lett., **15**, 348-349 (1996).

[13] J. Bill, M. Friess, F. Aldinger and R. Riedel, pp. 605-615 in Better Ceramics Through Chemistry VI, edited by A. K. Cheetham, C. J. Brinker, M. L. Mecartney and C. Sanchez (Mat. Res. Soc. Symp. Proc. **346**, Materials Research Society, Pittsburgh, PA), 1994.

[14] J. Bill and F. Aldinger, Adv. Mater., **7**[9], 775-787 (1995).

[15] R. Riedel and W. Dressler, Ceram.Int., **22**, 233-239 (1996).

[16] O. Funayama, T. Kato, Y. Tashiro and T. Isoda, J. Am. Ceram. Soc., **76**, 717-723 (1993).

[17] O. Funayama, Y.Tashiro, T. Aoki and T. Isoda, J. Ceram. Soc. Japan, **102**, 908-912 (1994).

[18] O. Funayama, T. Aoki and T. Isoda, J. Ceram. Soc. Japan, **104**, 355-360 (1996).

[19] D. Seyferth, G. Wiseman and C. Prud'homme, J. Am. Ceram. Soc., **66**, C-13-C-14 (1983).

[20] R. M. Silverstein, G. C. Bassler and T. C. Morrill, "Spectrometric Identification of Organic Compounds," 5th Edition, John Wiley & Sons, Inc., 1991.

[21] W. J. Evans and M.S. Solleberger, J. Am. Chem. Soc., **108**, 6095-96 (1986).

[22] C. R. Blanchar and S. T. Schwab, J. Am. Ceram. Soc., **77**, 1729-39 (1994).

[23] R. S. Wagner and W. C. Ellis, Trans. AIME, **243**, 1053-64 (1965).

[24] JANAF Thermodynamical Table, 3rd Edition, US National Bureau of Standards, Washington D. C., 1986.

[25] A. H. Heuer and V. L. K. Lou, J. Am. Ceram. Soc., **73**, 2785-3128(1990).

[26] M. J. Hoffman and G. Petzow, pp.3-15 in Silicon Nitride Ceramics-Scientific and Technological Advances, edited by I. W. Chen, P.F. Becher, M. Mitomo, G. Petzow, and T-S. Yen (Mater. Res. Soc. Symp. Proc. **287**, Pittsburgh, PA), 1993.

Chapter 3

Microstructure development of SiC nano/micro-particle dispersed Si_3N_4-Y_2O_3 ceramics from chemically modified PHPSs

3.1. Introduction

As investigated in the previous chapter, the Y-DEOPHPS synthesized by chemical modification of PHPS with $CH_3(CH_2)_9OH$ and $Y(OCH_3)_3$ was found to have a potential for the fabrication of [Si-Y-O-C-N] multiconponent ceramics such as SiC nano/micro-particle dispersed Si_3N_4-Y_2O_3 ceramics [1]. In this chemical modification route, the polymeric precursor-derived multicomponent amorphous ceramics can be processed into polycrystalline ceramics by heat treatment. During this crystallization process, the metastable multicomponent ceramics are partitioned into thermodynamically stable phases, and it is expected to control the resulting composite microstructure of polycrystalline ceramics by controlling chemical structure of polymeric precursors. However, such investigations have been only performed and discussed on the polycrystalline powder syntheses [2,3], or other studies reported only a tendency of the microstructure homogeneity and refinement of polymeric precursor-derived SiAlON [4,5] and Si_3N_4 ceramics [6] compared to those fabricated by the conventional powder processing.

In this chapter, another novel polymeric precursor for Si_3N_4-SiC-Y_2O_3 ceramics, Y-PCSOPHPS has been designed and synthesized as shown in Fig. 3-1. Hydroxy-polycarobosilane (PCS-OH) has been synthesized from commercially available PCS, which is a typical polymeric precursor for SiC ceramics [7-10]. The PCS-OH has been combined with PHPS instead of molecular carbon source, $CH_3(CH_2)_9OH$ by block copolymerization. The block copolymer of PCSOPHPS has been further modified with $Y(OCH_3)_3$ to yield Y-PCSOPHPS.

The chemical structure of the Y-PCSOPHPS is characterized by FT-IR, ^1H- and ^{29}Si-NMR spectroscopic analyses. Fully dense Si_3N_4-SiC-Y_2O_3 ceramics are successfully synthesized from the polymeric precursors, Y-PCSOPHPS and Y-DEOPHPS. The effect of chemical structure of the polymeric precursors on the microstructure development of Si_3N_4-SiC-Y_2O_3 ceramics is discussed from a viewpoint of microstructure control through polymeric precursor route.

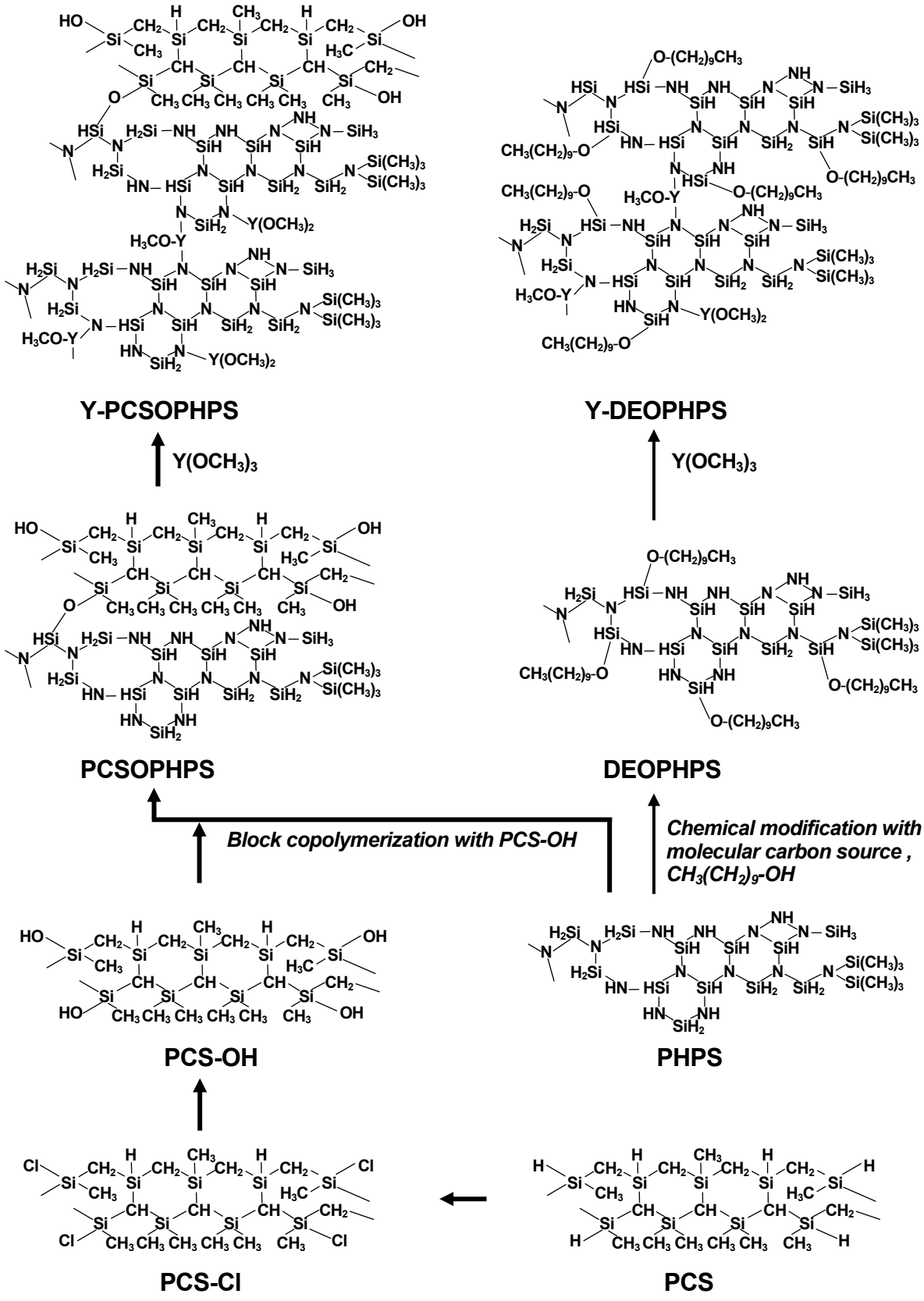

Fig. 3-1. Synthesis route for yttrium modified block copolymer of PHPS and PCS-OH (Y-PCSOPHPS) in comparison with that for the Y-DEOPHPS studied in the section 2.1.

3.2. Experimental procedure

3.2.1. Synthesis of yttrium modified block copolymers of PHPS and PCS-OH

Commercially available PHPS (Tonen Co. N-N 410, Tokyo, Japan), PCS (Nippon Carbon Co. Ltd., Type S, Tokyo, Japan) and $Y(OCH_3)_3$ (Kojundo Chemical Laboratory Co., Saitama, Japan) were used for the polymeric precursor synthesis. Carbon tetrachloride (CCl_4), xylene and pyridine (Nakarai chemical, reagent grade, Tokyo, Japan) were distilled and dried before use. The chemical modification reactions of PHPS were carried out under N_2 atmosphere, and the yield was evaluated by wt% based on the total amount of PHPS and the reagent used in each chemical modification reaction.

(1) Synthesis of PCS-OH

As-received PCS (5 g) was dissolved into 50 ml of dry CCl_4, followed by refluxing for 24h in the presence of catalytic amount of benzoyl peroxide (BPO, Nakarai chemical, reagent grade, Tokyo, Japan). After cooling down to room temperature, the reaction mixture was concentrated in a rotary evaporator. The residue of chlorinated PCS (PCS-Cl) was dissolved into 100 ml of tetrahydrofuran (THF, Nakarai chemical, reagent grade, Tokyo, Japan) and cooled to 0 °C. To this solution, 5 % aqueous ammonia (NH_4OH, 30 ml) was added. Then, the reaction mixture was warmed to room temperature, and stirred at room temperature for 24h in order to hydrolyze Si-Cl bonds in PCS-Cl. The reaction mixture was neutralized by diluted aqueous HCl, followed by concentrating in a rotary evaporator. The residue was suspended in water and extracted with toluene. The organic extracts were washed with water, saturated aqueous sodium chloride, dried over anhydrous magnesium sulfate, and concentrated in a rotary evaporator, then the residue was dried under vacuum to give PCS-OH (5.7 g) as a white solid.

(2) Synthesis of block copolymers of PHPS and PCS-OH

As-received PHPS (7.30 g: Si, 57.7; N, 23.9; O, 0.8; C, 4.1 wt.%, Si=150 mmol, C=25 mmol) and PCS-OH (1.86 g: Si, 46.4; N, 0.7; O, 3.4; C, 41.6 wt.%, Si=31 mmol, C=65 mmol, hence a total atomic ratio of Si/C=2, PCS-OH/PHPS=0.25) were dissolved into 30 ml of dry xylene. Then, the solution was heated at 140 °C for 2h in the presence of catalytic amount of dry pyridine. After cooling down to room temperature, the reaction mixture was concentrated in a rotary evaporator. The residue was dried under vacuum to give a block copolymer of PHPS and PCS-OH [PCSOPHPS (PCS-OH/PHPS=0.25)] as a viscous liquid (9.0 g, 98%). To study the chemical structure of the PCSOPHPS, as-received PHPS (0.5 g) was also reacted with PCS-OH (0.25 g) to

give a block copolymer of PCSOPHPS (PCS-OH/PHPS=0.5) as a viscous liquid (0,72 g, 96%).

(3) Chemical modification of PCSOPHPS with $Y(OCH_3)_3$

The PCSOPHPS (PCS-OH/PHPS=0.25) was chemically modified with $Y(OCH_3)_3$ (1.2 g, 6.6 mmol, hence an atomic ratio of Si/Y=27) using dry pyridine (150 ml) under the condition as described in the section 2.2.1 to give a yttrium modified PCSOPHPS (Y-PCSOPHPS) as a pale yellow solid (9.7 g, 95%). This polymer was found to be almost insoluble in organic solvents such as toluene, ether and $CHCl_3$.

3.2.2. Pyrolysis and hot pressing

Pyrolysis of precursors was performed as described in the section 2.2.2. The pyrolysis product was ground to a fine powder using a mortar and pestle, then sieved through a 250 μm screen before forming by uniaxial pressing at 150 MPa (10 x 30 mm, thickness of about 10 mm, 3.5 g). The green compact was placed in a BN coated graphite die and hot pressed at 1800 °C for 1h at a stress of 40 MPa under a nitrogen pressure of 392 kPa. The hot pressing was carried out in a graphite resistance-heated furnace (Model High Multi 10000, Fujidempa Kogyo, Osaka, Japan).

To study the effect of chemical structure of polymeric precursors on the microstructure of Si_3N_4-SiC-Y_2O_3 ceramics, another [Si-Y-O-C-N] amorphous powder derived from Y-DEOPHPS investigated in the chapter 2 was also hot pressed under the same condition as mentioned above.

3.2.3. Characterization

FT-IR spectrum of the polymer samples was recorded as described in the section 2.2.3. ^{1}H- and ^{29}Si-NMR spectra were recorded for the polymer samples in $CDCl_3$ solution at room temperature (Model UNITYINOVA 300, Varian Japan Ltd., Tokyo, Japan). All the chemical shifts were quoted relative to the signal of TMS.

Molecular weight distributions of the polymer samples were measured with a gel permeation chromatography (GPC, Model GPC-244, Waters, Tokyo, Japan) system using $CHCl_3$ as solvent. Molecular weights quoted were based on polystyrene standards.

TGA of the polymer samples, elemental analyses and XRD measurements of the pyrolyzed- and hot pressed-samples were performed as described in section 2.2.3.

Apparent density of the hot pressed specimens was measured by the Archimedes method. Relative density (RD) of the hot pressed samples was evaluated using the theoretical density (3.219 x 10^3 kg/m^3 for the Y-PCSOPHPS, 3.310 x 10^3 kg/m^3 for the Y-DEOPHPS) calculated from the composition of the polymeric precursor-derived amorphous powders.

Microstructure of the hot pressed-sample was characterized using SEM (Model S-800, Hitachi, Tokyo, Japan), TEM (Model EM-002B, Topcon Co., Tokyo, Japan, operating at 200 kV), and focused ion beam (FIB) equipment (Model FIB 200, FEI Company, OR, USA). Secondary ion mass spectrometry (SIMS) mapping analysis of the hot pressed samples was performed by SIMSmap^{TM} III (FEI Company) mounted on the FIB equipment.

3.3. Results and discussion

3.3.1. Characterization of polymeric precursors

Figure 3-2 shows the FT-IR spectra of polymer samples. As-received PCS (Fig. 3-2 (a)) presents absorptions at 2900, 2950 cm^{-1} (C-H), 2100 cm^{-1} (Si-H), 1350-1450 cm^{-1} (C-H), 1250 cm^{-1} (Si-CH_3), 1020 cm^{-1} (Si-CH_2-Si) and 840 cm^{-1} (Si-C). The spectrum of PCS-Cl shows a remarkable decrease in absorption intensity at 2100 cm^{-1} (Si-H) and a new absorption band at 490 cm^{-1} assigned to Si-Cl bond [11] (Fig. 3-2 (b)). In the IR spectrum of PCS-OH (Fig. 3-2 (c)), the absorption band at 490 cm^{-1} almost disappears and a new absorption band appears at 3480 cm^{-1} assigned to Si-OH groups.

Figure 3-3 shows the ^{1}H-NMR spectra of polymer samples. As-received PCS presents two broad peaks at 0.18 ppm with two shoulders at -0.08 and -0.6 ppm (Si-CH_2/Si-CH_3/Si-CH-Si : C-H), and 4.3 ppm (Si-H).

The ratio between C-H and Si-H is 1 : 0.08 (Fig. 3-3 (a)), while that of PCS-Cl is 1 : 0.04, which indicates the decrease in number of Si-H bonds (Fig. 3-3 (b)). In the spectrum of PCS-OH (Fig. 3-3 (c)), an additional broad peak is observed at 1.78 ppm assigned to Si-OH groups. The ratio of C-H : Si-H : Si-OH is 1 : 0.04 : 0.03. The value of Si-OH (0.03) is slightly smaller than the calculated value of 0.04. According to these spectroscopic analyses, a small amount of Si-Cl bonds exists in the synthesized PCS-OH. However, about 37% of Si-H groups in as-received PCS have been successfully converted to Si-OH groups.

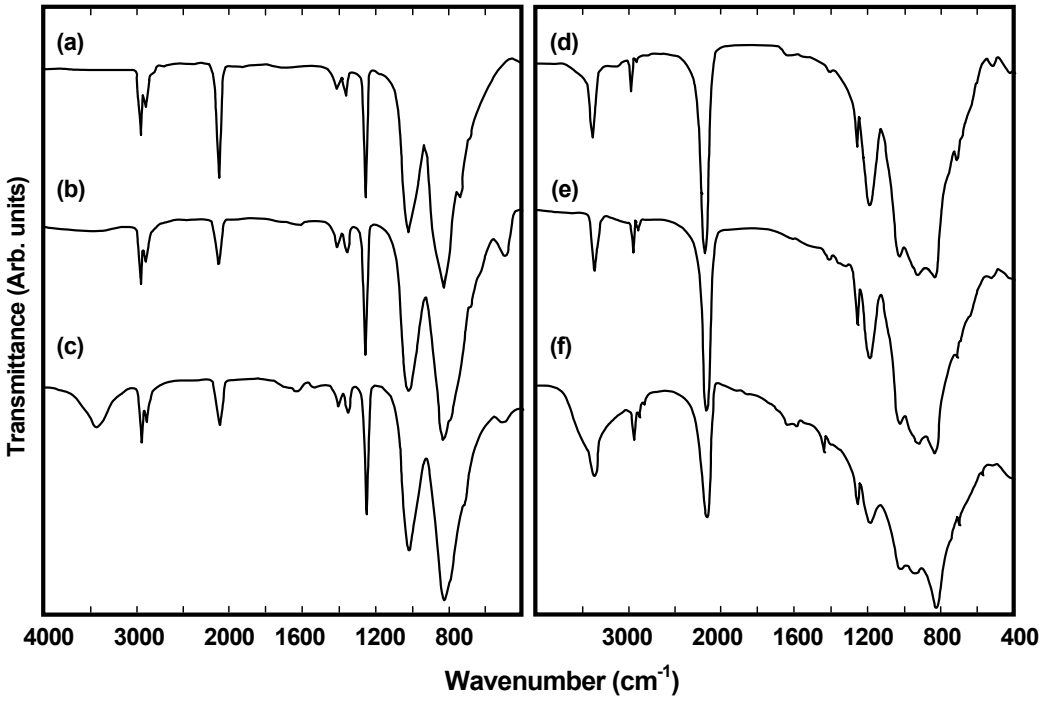

Fig. 3-2. FT-IR spectra of (a) as-received PCS, (b) PCS-Cl, (c) PCS-OH, (d) as-received PHPS, (e) PCSOPHPS (PCS-OH/PHPS=0.25) and (f) yttrium modified PCSOPHPS.

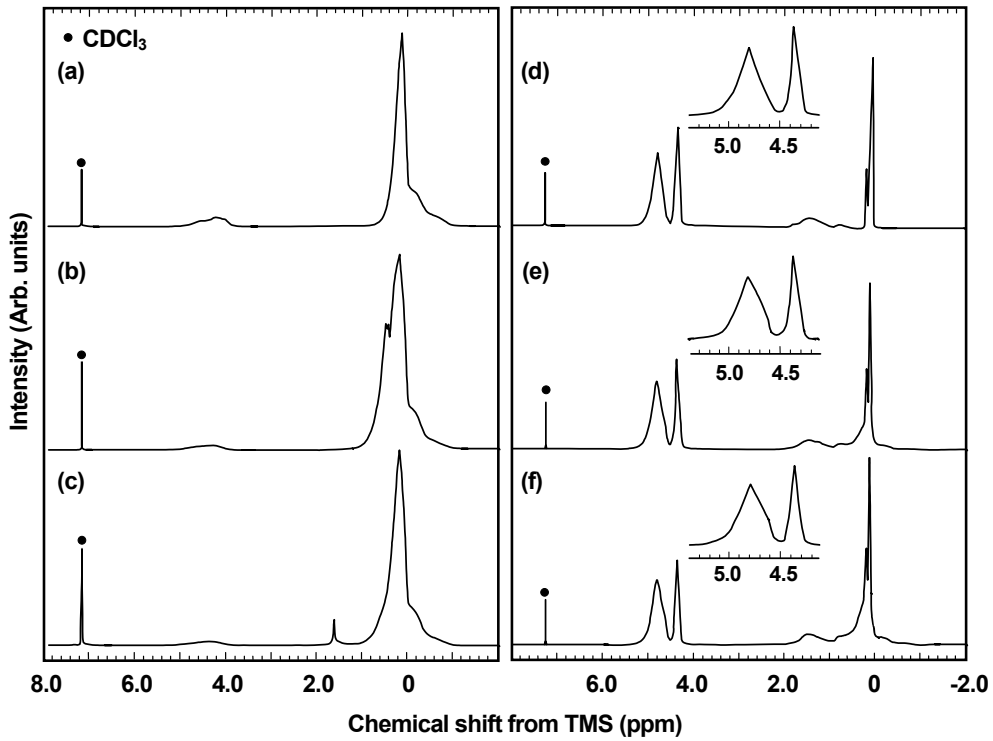

Fig. 3-3. ^{1}H-NMR spectra of (a) as-received PCS, (b) PCS-Cl, (c) PCS-OH, (d) as-received PHPS, (e) PCSOPHPS (PCS-OH/PHPS=0.25) and (f) PCSOPHPS (PCS-OH/PHPS=0.5).

In the IR spectrum of as-received PHPS (Fig. 3-2 (d)), absorptions are observed at 3400 cm^{-1} (N-H), 2950-2900 cm^{-1} (C-H), 2150 cm^{-1} (Si-H), 1250 cm^{-1} ($Si-CH_3$), 1180 cm^{-1} (N-H) and 840-1020 cm^{-1} (Si-N-Si). The IR spectrum of PCSOPHPS (PCS-OH/PHPS=0.25) consists of the absorption bands derived from as-received PHPS and PCS-OH (Fig. 3-2 (e)). Even when the ratio of PCS-OH/PHPS was increased from 0.25 to 0.5, it was difficult to confirm certain chemical bondings between PHPS and PCS-OH by FT-IR spectroscopy.

^{1}H-NMR spectrum of as-received PHPS presents four peaks at 4.8, 4.3, 1.4 (broad) and 0.1-0.2 ppm assigned to SiH/SiH_2, SiH_3, NH and $SiCH_3$, respectively (Fig. 3-3 (d)). In the spectrum of PCSOPHPS (PCS-OH/PHPS=0.25), the peak at 4.8 ppm is slightly asymmetric (Fig. 3-3 (e)). The asymmetric feature becomes more remarkable when the ratio of PCS-OH/PHPS is increased from 0.25 to 0.5 (Fig. 3-3 (f)), which suggests the existence of some $SiHN_2O$ units in the PCSOPHPS.

To study the reaction of PHPS and PCS-OH in more detail, chemical structure of the polymer samples were further studied by ^{29}Si-NMR spectroscopy, and the results are summarized in Fig. 3-4. As-received PHPS (Fig. 3-4 (a)) presents three peaks at 3.7, -35.4 and -50.6 ppm assigned to SiC_3N ($N-Si(CH_3)_3$), $SiHN_3/SiH_2N_2$ and SiH_3N units, respectively. PCS-OH (Fig. 3-4 (b)) presents three peaks at 11.3, -0.8 and -18.7 ppm assigned to SiC_3O, SiC_4 and SiC_3H units, respectively. A small broad peak observed at around 26 ppm is considered to be due to the SiC_3Cl units existed in this sample as mentioned above. In addition to the peaks of PHPS and PCS-OH, PCSOPHPS (PCS-OH/PHPS=0.25) presents a new peak at -45 ppm assigned to $SiHN_2O$ units [12] (Fig. 3-4 (c)). The relative peak intensity of the new peak increases with increasing the ratio of PCS-OH/PHPS from 0.25 to 0.5 (Fig. 3-4 (d)). The existence of $SiHN_2O$ units is in consistence with the ^{1}H-NMR spectra.

As discussed in the section 2.3.1, $CH_3(CH_2)_9$-OH reacted mainly with SiH_2 groups in PHPS to form Si-O-C bonds [1]. Based on the previous result and these spectroscopic analyses results, the PCS-OH was also found to react mainly with SiH_2 groups in PHPS, and a block copolymer of PCSOPHPS has been successfully synthesized through Si-O-Si bond formation as shown in Fig. 3-1.

Figure 3-5 shows molecular weight distribution curves of the polymer samples. The mean molecular weight ($\overline{Mw}$) of the each polymer sample is also shown in Fig. 3-5. As-received PHPS shows the molecular weight fraction from 140 to 1 x 10^4, and the $\overline{Mw}$ of 815, while as-synthesized PCS-OH shows the molecular weight fraction from 140 to 3 x 10^4, and the $\overline{Mw}$ of 2930 (Fig. 3-5 (a)).

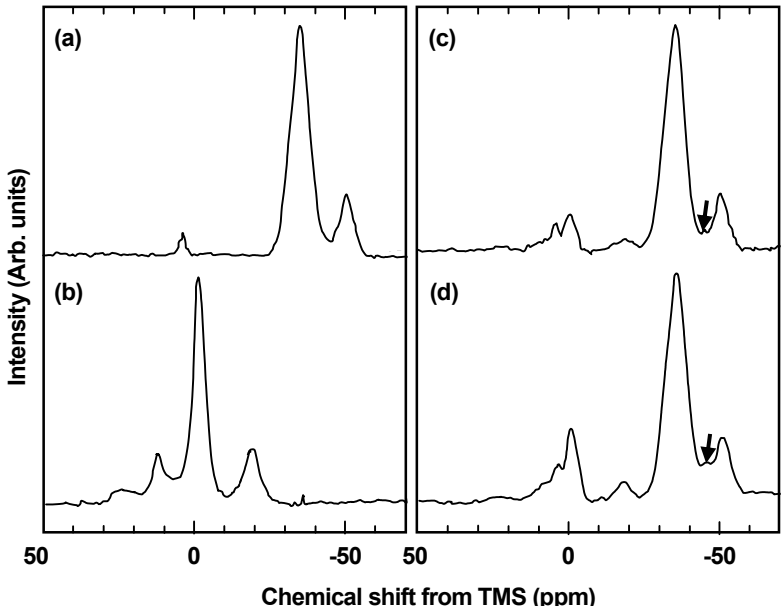

Fig. 3-4. ^{29}Si-NMR spectra of (a) as-received PHPS, (b) PCS-OH, (c) PCSOPHPS (PCS-OH/PHPS=0.25) and (d) PCSOPHPS (PCS-OH/PHPS=0.5).

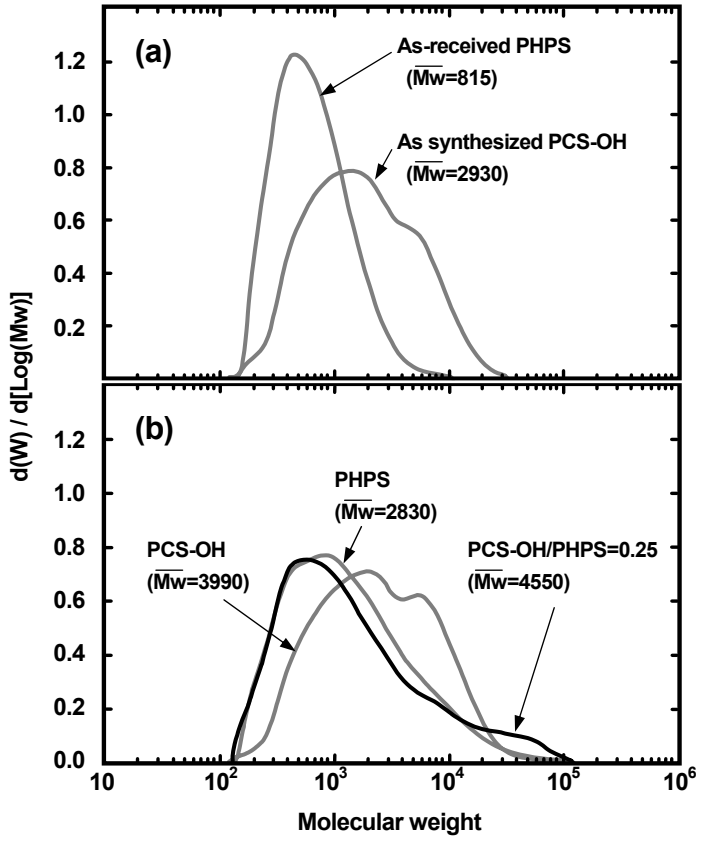

Fig. 3-5. Molecular weight distribution curves of (a) as-received PHPS and as-synthesized PCS-OH, (b) PHPS, PCS-OH and PCS-OH/PHPS=0.25 after heat treatment in xylene at 140 °C for 2 h with catalytic amount of pyridine.

To examine the self-condensation behavior of the each starting polymer, as-received PHPS and as-synthesized PCS-OH were also heat-treated in dry xylene with catalytic amount of dry pyridine, respectively, and the heat-treated samples were analyzed by GPC system together with the reaction product of PCSOPHPS (PCS-OH/PHPS=0.25). After heat treatment (Fig. 3-5 (b)), PHPS shows a decrease in lower molecular weight fraction below 1 x 10^3, and a broader molecular weight distribution curve with the highest molecular weight fraction of 1 x 10^5. The $\overline{Mw}$ of PHPS increases up to 2830. The heat-treated PCS-OH also shows a slightly broader curve with the highest molecular weight fraction of 6 x 10^5, and the $\overline{Mw}$ of 3990. Compared with the heat-treated PHPS and PCS-OH, the reaction product of the PCSOPHPS shows a remarkable increase in higher molecular weight fraction above 4 x 10^4, and the $\overline{Mw}$ of the PCSOPHPS increases up to 4550.

During the reaction of PHPS with PCS-OH, pyridine was considered to behave as a basic catalyst for dehydrogenation of PHPS [12,13], and for dehydration or dehydrogenation of PCS-OH [14]. Thus, self-condensation of the each polymer could be occurred to some extent. However, the increased higher molecular weight fraction above 4 x 10^4 in the PCSOPHPS is due to the block copolymerization of PHPS and PCS-OH.

The PCSOPHPS (PCS-OH/PHPS=0.25) was further modified with $Y(OCH_3)_3$. As mentioned in the experimental section, the reaction product of Y-PCSOPHPS was almost insoluble in organic solvents, and the chemical structure was studied by FT-IR spectroscopy (Fig. 3-2 (f)). Compared with the spectrum of the PCSOPHPS (Fig. 3-2 (d)), the Y-PCSOPHPS shows a remarkable decrease in absorption intensity at 2150 cm^{-1} (Si-H) and 1180 cm^{-1} (N-H). These changes in the FT-IR spectrum suggest that $Y(OCH_3)_3$ reacted mainly with N-H and Si-H bonds of PHPS moieties in the PCSOPHPS as previously discussed in the section 2.3.1 [1], and further cross-linking of PHPS moieties in the Y-PCSOPHPS is considered to occur via functional groups such as $NY(OCH_3)N$ as shown in Fig. 3-1.

3.3.2. Conversion of polymeric precursors into Si_3N_4-SiC-Y_2O_3 ceramics

The TGA curves of the polymer samples are shown in Fig. 3-6. The data of as-received PHPS and Y-DEOPHPS are also plotted in the figure. The weight loss of these samples starts at around 80 °C and completed at around 600 °C in N_2. The PCSOPHPS shows a continuous weight loss from 100 to 600 °C, and the total weight loss is suppressed in comparison with that of as-received PHPS. The weight loss of the Y-PCSOPHPS is mainly observed below 200 °C, then, rather stable up to 300 °C. Finally at 1000 °C, the total weight loss of the Y-PCSOPHPS is further suppressed in comparison with those of the PCSOPHPS and the Y-DEOPHPS.

As shown in Fig. 3-5, the $\overline{Mw}$ of the PCSOPHPS is much larger than that of as-received PHPS, which leads to suppress the total weight loss of the PCSOPHPS. The weight loss observed below 200 °C of the Y-PCSOPHPS is thought be caused by the residual pyridine used in the chemical modification reaction of the PCSOPHPS with $Y(OCH_3)_3$. The total weight loss is thought to be further suppressed by the highly cross-linked structure via Si-O-Si bonds and $NY(OCH_3)N$ functional groups.

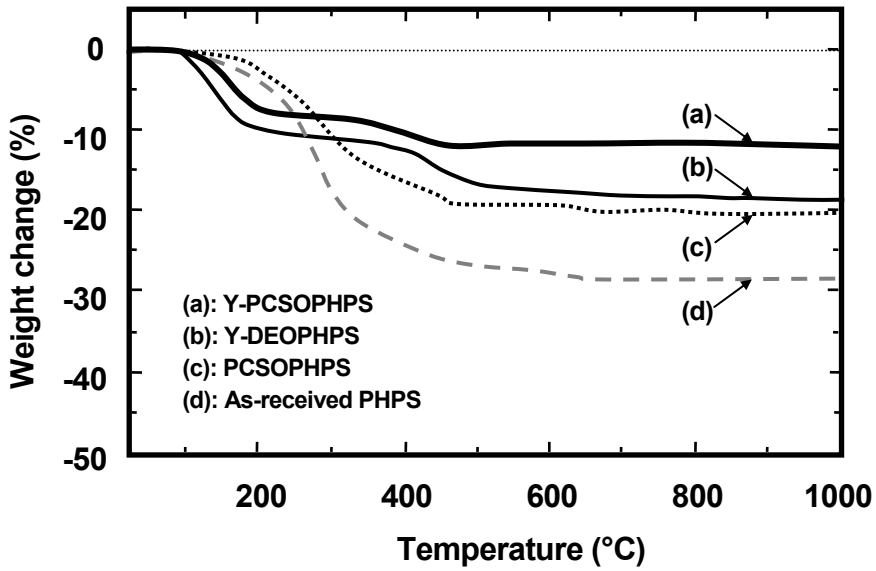

Fig. 3-6. TGA of polymer samples from room temperature to 1000 °C at a heating rate of 10 °C/min under a nitrogen flow of 100 ml/min.

The pyrolysis of the Y-PCSOPHPS in larger scale using the alumina tube furnace resulted in almost the same ceramic yield (above 85 %). The chemical compositions of the pyrolyzed samples are shown in Table 3-1. The data of Y-DEOPHPS is also listed in the table. Compared with as-received PHPS, both carbon and yttrium have been successfully doped in the pyrolyzed Y-PCSOPHPS. The Si/Y atomic ratio of the pyrolyzed Y-PCSOPHPS is 25, which is the same value of the pyrolyzed Y-DEOPHPS. The Si/C atomic ratio is 2.9, and the carbon content is a slight larger than that of the pyolyzed Y-DEOPHPS. Based on this chemical composition analysis, the theoretical amounts of Y_2O_3 and SiC in the pyrolyzed Y-PCSOPHPS are 8.4 wt% and 27 wt%, respectively, while those in the pyrolyzed Y-DEOPHPS are 9.6 wt% and 21 wt%, respectively.

Table 3-1. Chemical composition of 1000 °C pyrolyzed-samples.

Precursor	Composition (wt%)					Atomic ratio
	Si	Y	O	C	N	
Y-PCSOPHPS	57.6	6.7	7.4	8.2	19.6	$Si_{1.0}Y_{0.04}O_{0.23}C_{0.34}N_{0.69}$
Y-DEOPHPS	52.8	6.0	7.1	7.2	25.9	$Si_{1.0}Y_{0.04}O_{0.24}C_{0.27}N_{0.98}$
PHPS	73.9	--	0.4	3.1	21.6	$Si_{1.0}Y_{0.00}O_{0.01}C_{0.09}N_{0.56}$

As shown in Fig. 3-7 (a), the pyrolyzed Y-PCSOPHPS presents broad peaks at 2θ (degrees) of 29.3, 29.6, 31.0, 32.5, 33.6 and 48.7, which suggests that the crystallization of Y_2SiO_5 started during pyrolysis (based on JCPDS card No. 41-0004). After hot pressing up to 1800 °C, the polymeric precursor-derived powders are well crystallized and the resulting ceramics present desired phases of β-Si_3N_4 and β-SiC, and a grain boundary phase of $Y_5(SiO_4)_3N$ (Figs. 3-7 (a) and (b)). The densities of the hot pressed sample derived from the Y-PCSOPHPS and Y-DEOPHPS reached 99.8 and 99.7 % RD, respectively.

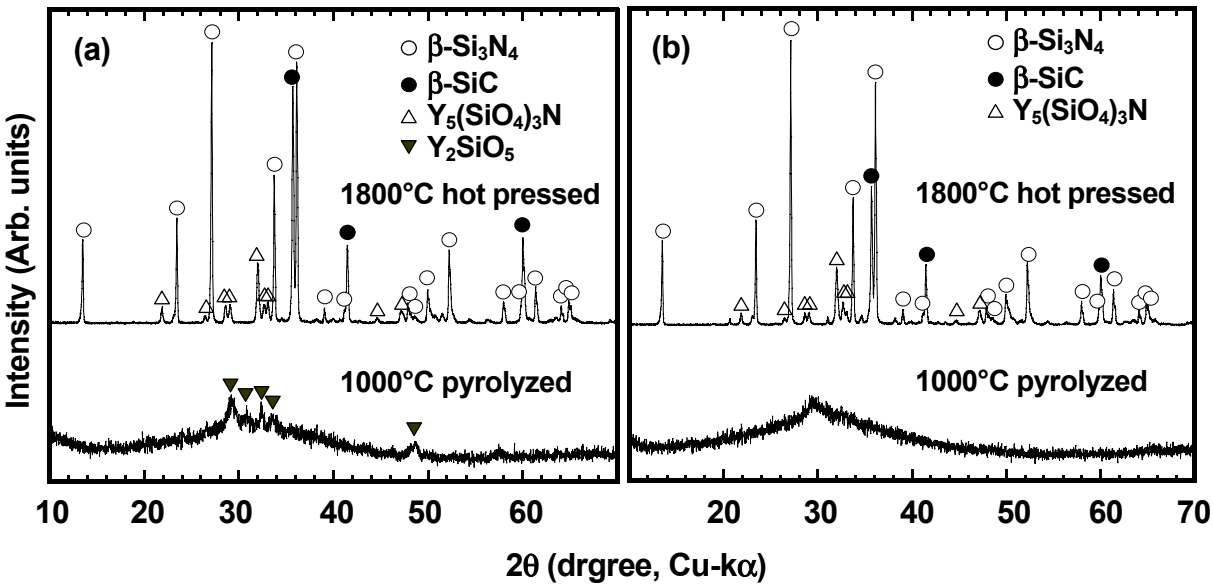

Fig. 3-7. XRD patterns of ceramics derived from (a)Y-PCSOPHPS and (b) Y-DEOPHPS.

3.3.3. Effect of chemical structure of polymeric precursors on microstructure development of Si_3N_4-SiC-Y_2O_3 ceramics

Figure 3-8 shows SEM images on polished and chemically etched section of the hot-pressed samples. The microstructure of these samples is composed of large rod-like grains of about 3 μm in length, fine rod-like grains of less than 1.5 μm in length and submicron equiaxed grains. Figure 3-9 shows typical TEM images of the hot pressed sample derived from Y-PCSOPHPS. As shown in Fig. 3-9 (a), β-Si_3N_4 matrix grains are in a size range of about 200 to 450 nm, and fine particles are dispersed within the β-Si_3N_4 matrix grains. The fine particles are in a size range of about 10 to 40 nm, while a large particle with diameter of about 150 nm is located at the β-Si_3N_4 matrix grain boundary (marked by four arrows in Fig. 3-9 (a)). Furthermore, a large particle with a diameter of about 600 nm, which can be easily distinguished from the β-Si_3N_4 matrix grains, is observed (Fig. 3-9 (b), marked by an arrow). The selected area diffraction pattern (SADP) obtained from the marked particle is indexed as [$0\bar{1}1$] 3C polytype of β-SiC (inset in Fig. 3-9 (b)). These observation results indicate that β-SiC is dispersed as particles having a size range of about 10 to 600 nm, and the β-Si_3N_4 matrix grain growth is thought to be suppressed by the large β-SiC particles located at the β-Si_3N_4 matrix grain boundaries. However, in addition to these microstructural features, the β-Si_3N_4 matrix grain growth is also observed as shown in Fig. 3-9 (c), and only several nanometer particles are included within the elongated β-Si_3N_4 matrix grains. Accordingly, the microstructure shown in Fig. 3-8 (a) seems to be formed by the heterogeneous dispersion of β-SiC particles.

Figure 3-10 (a) shows a secondary electron (SE) image of polished and Ga^+ ion-implanted section of the Y-PCSOPHPS-derived ceramics obtained by FIB equipment. The SE image is composed of bright grain boundary areas, gray grains and dark particles. The gray grains are in a size range of about 0.2 to 3 μm. The dark particles are in a size range of several nanometers to submicron. The dark nanosized particles are located within the gray grains and also at the grain boundaries, while the dark submicrion particles are segregated at the grain boundaries.

Secondary ion mass spectrometry (SIMS) mapping analyses of the same field of Fig. 3-10 (a) resulted in detection of positive ion SIMS mass species of Si^+ mass 28, Y^+ mass 89 and YO^+ mass 105, and negative ion SIMS mass species of O^- mass 16, C_2^- mass 24, CN^- (or $C_2H_2^-$) mass 26 and SiN^- mass 42. The SIMS mapping analyses of the Y^+ and the O^- signals resulted in good correlation with the bright grain boundary areas in Fig. 3-10 (a), and as shown in Fig. 3-10 (b), the Si^+ signal is strongest in the gray grains, but also existed in the dark submicron particles. The SiN^- (Fig. 3-10 (c)) and the C_2^- (Fig. 3-10 (d)) signals are well correlated with the gray grains and the dark particles in Fig. 3-10 (a), respectively. Thus, the gray grains and the dark particles in the SE image of Fig. 3-10 (a) can be assigned to β-Si_3N_4 and β-SiC, respectively.

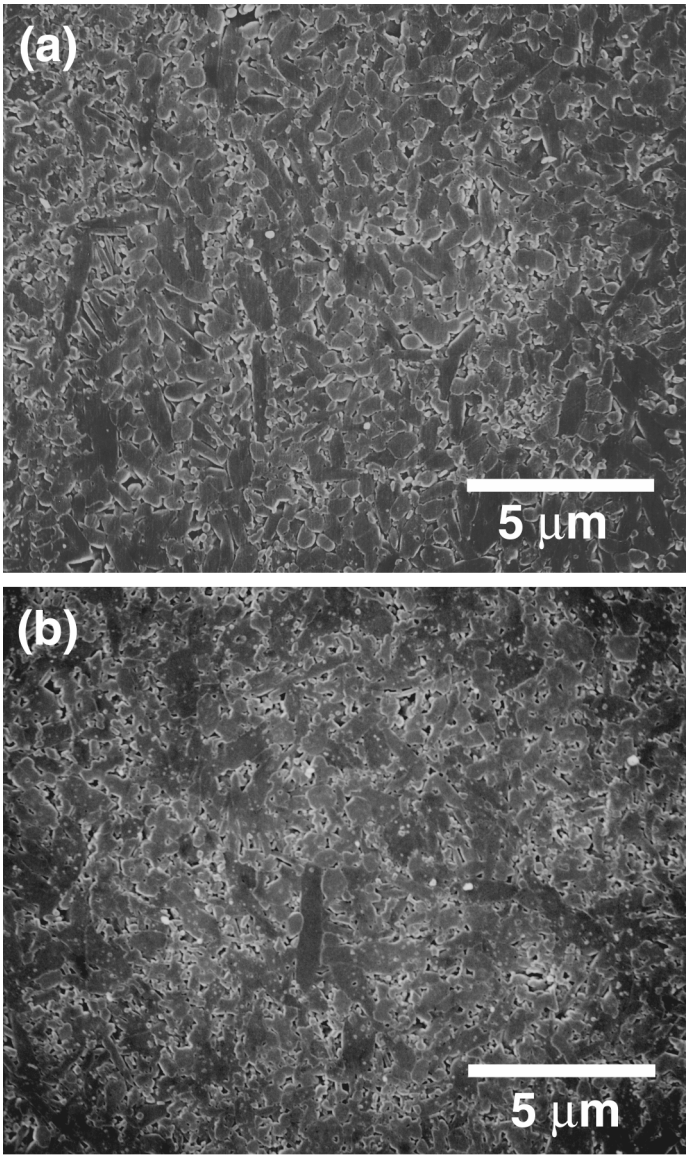

Fig. 3-8. SEM images of polished and chemically etched section of hot pressed sample derived from (a) Y-PCSOPHPS and (b) Y-DEOPHPS.

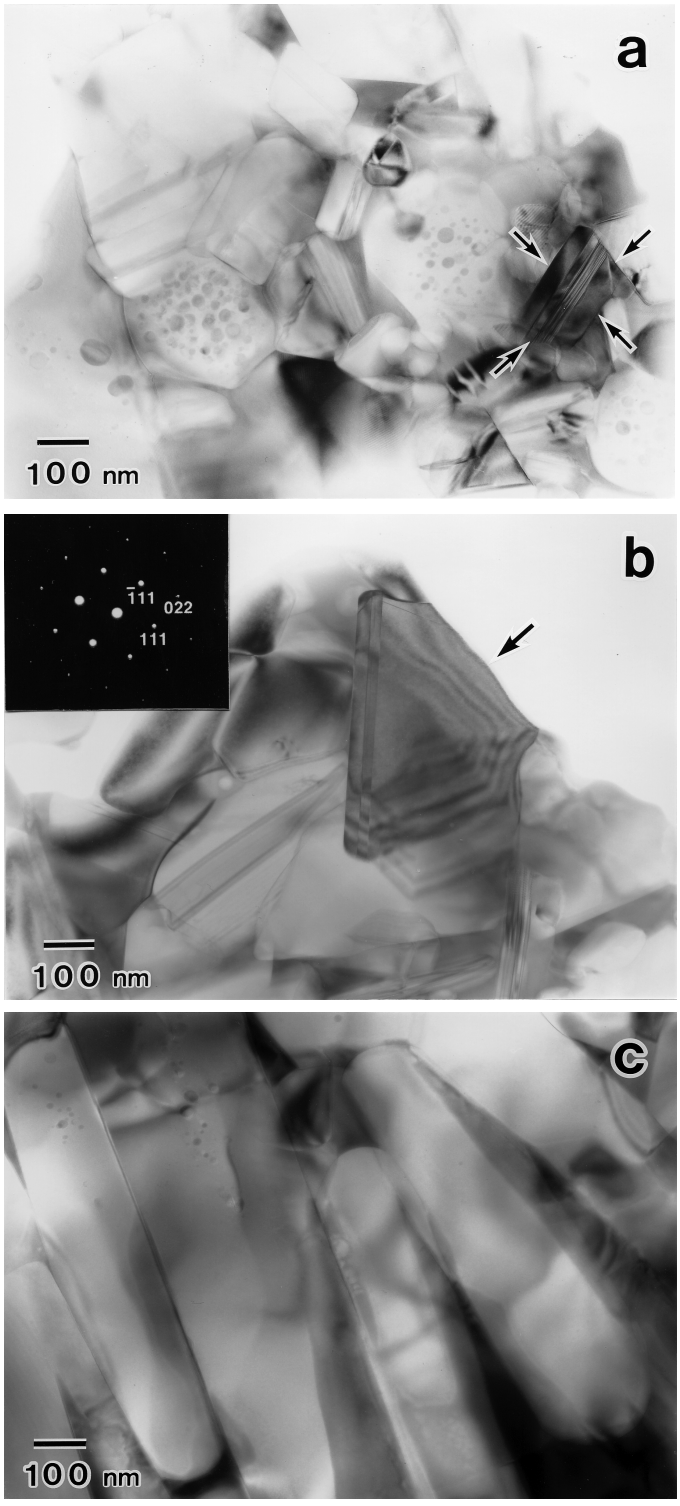

Fig. 3-9. TEM micrograph showing (a) fine particles located within β-Si_3N_4 matrix grains and a large particle (marked by four arrows) located at β-Si_3N_4 matrix grain boundary, (b) a submicrion particle (marked by an arrow) and SADP indexed as [$0\bar{1}1$] 3C polytype of β-SiC (obtained from the marked particle) and (c) β-Si_3N_4 matrix grain growth without β-SiC submicron particles.

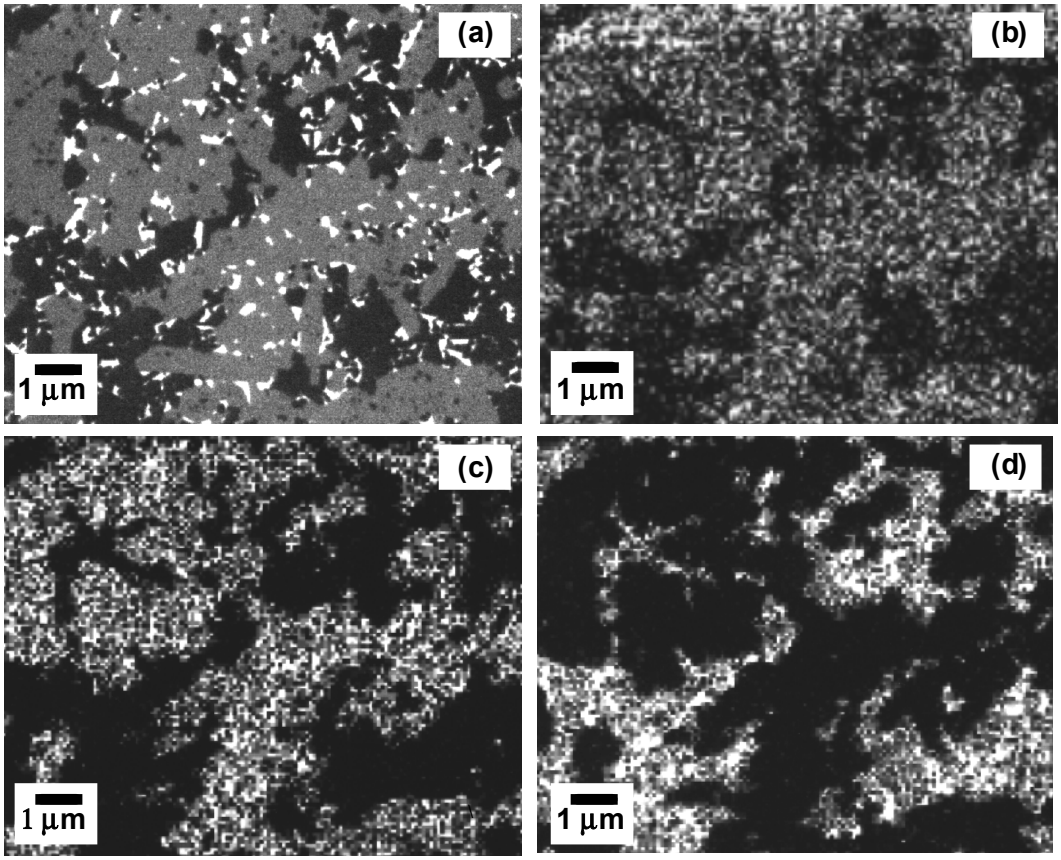

Fig. 3-10. FIB-induced SE image and SIMS mapping analyses of hot pressed-sample derived from Y-PCSOPHPS. (a) SE image, and SIMS mapping analyses of the same field as shown in (a): (b) Si^+ mass 28, (c) SiN^- mass 42 and (d) C_2^- mass 24.

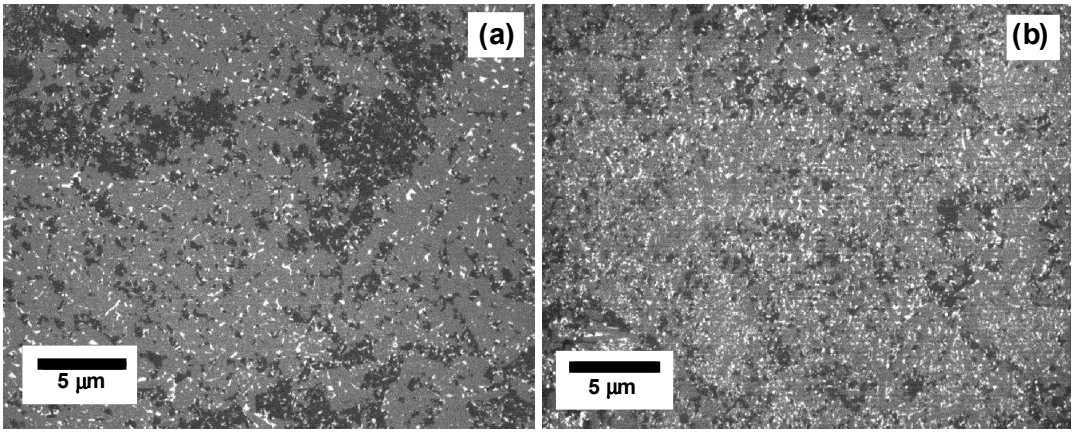

Fig. 3-11. Typical FIB-induced SE images of hot pressed-samples derived from (a) Y- PCSOPHPS and (b) Y-DEOPHPS.

These results indicate that a large amount of β-SiC submicron particles are segregated at the β-Si_3N_4 matrix grain boundaries, and as shown in Fig. 3-11 (a), the segregations are observed at a region range of about 3 to 35 μm^2.

Figure 3-11 (b) shows a typical FIB-induced SE image of the hot pressed sample derived from the Y-DEOPHPS. TEM observation of this sample confirmed that β-SiC was dispersed as particles having a size range of about 10 to 650 nm and the β-SiC submicron particles were located at the β-Si_3N_4 matrix grain boundaries. As shown in Fig. 3-11 (b), the β-SiC submicron particles are uniformly dispersed in comparison with those in Fig. 3-11 (a). It turns out from this microstructure comparison in Fig. 3-11 that the β-SiC dispersibility is strongly influenced by the chemical structure of the polymeric precursors: As shown in Fig. 3-11, when the molecular carbon source was introduced to PHPS followed by chemical modification with $Y(OCH_3)_3$, the polymeric precursor yields a uniform microstructure of β-SiC nano/micro particle-dispersed β-Si_3N_4-Y_2O_3 ceramics, while the yttrium modified block copolymer of PHPS and PCS-OH yields rather unique binary ceramics composed of β-SiC-Y_2O_3 and β-SiC nano/micro particle-dispersed β-Si_3N_4-Y_2O_3 ceramics.

3. 4. Conclusions

A novel polymeric precursor for Si_3N_4-SiC-Y_2O_3 ceramics was synthesized by block copolymerization of PHPS with PCS-OH, followed by chemical modification with $Y(OCH_3)_3$. FT-IR, and ^1H-, ^{29}Si-NMR spectroscopic analyses of the synthesized precursor revealed that the block copolymerization reaction between PHPS and PCS-OH yielded Si-O-Si bonds, while $Y(OCH_3)_3$ reacted mainly with PHPS moieties of the PCSOPHPS to yield N-$Y(OCH_3)_{3-x}$ (x=1, 2) groups.

Fully dense Si_3N_4-SiC-Y_2O_3 ceramics were successfully synthesized by pyrolysis of the synthesized polymeric precursor at 1000 °C, followed by hot pressing at 1800°C in N_2. The resulting ceramics revealed that β-SiC particles were dispersed in a size range of about 10 to 600 nm, and a large amount of β-SiC submicrion particles were segregated at the β-Si_3N_4 matrix grain boundaries.

The microstructure comparison of the fully dense Si_3N_4-SiC-Y_2O_3 ceramics derived from Y-PCSOPHS and Y-DEOPHPS revealed that the β-SiC dispersibility was strongly influenced by the chemical structure of the polymeric precursors: when the molecular carbon source was introduced to PHPS followed by chemical modification with $Y(OCH_3)_3$, the polymeric precursor yielded a uniform microstructure of β-SiC nano/micro particle-dispersed β-Si_3N_4-Y_2O_3 ceramics, while the yttrium modified block copolymer of PHPS and PCS-OH yielded rather unique binary

ceramics composed of β-SiC-Y_2O_3 and β-SiC nano/micro particle-dispersed β-Si_3N_4-Y_2O_3 ceramics. Theses results indicated that the β-SiC dispersibility could be in-situ controlled at nano/micro size level by controlling the chemical structure of polymeric precursors at molecular level.

References

[1] Y. Iwamoto, K. Kikuta and S. Hirano, J. Mater. Res., **13**, 353-361 (1998).

[2] J. Bill, J. Seitz, G. Thurn, J. Dürr, J. Canel, B. Z. Janos, A. Jalowiecki, A. Sauter, S. Schempp, H. P. Lamparter, J. Mayer and F. Aldinger, Phys. Stat. Solidi (a), **166**, 269-296 (1998).

[3] J. Bill and F. Aldinger, Adv. Mater., **7**, 775-87 (1995).

[4] G. D. Sorarú, A. Ravagni, R. D. Maschio and G. Arturan, J. Am. Ceram. Soc., **74**, 2220-23 (1991).

[5] O. Funayama, Y. Tashiro, T. Aoki and T. Isoda, J. Ceram. Soc. Japan, **102**, 908-912 (1994).

[6] Y. Iwamoto, H. Matsubara and R. J. Brook, "Microstructural Development of Si_3N_4-Y_2O_3 Ceramics derived from Polymer Precursors", pp.193-197 in Ceramic Transactions, Vol. 51, Ceramic Processing Science and Technology, edited by H. Hausner, G. L. Messing and S. Hirano (The American Ceramic Society, Westerville, OH), 1995.

[7] S. Yajima, K. Okamura, J. Hayashi and M. Omori, Chem. Lett., No.9, 931-934 (1975).

[8] S. Yajima, J. Hayashi and M. Omori, J. Am. Ceram. Soc., **59**, 324-327 (1976).

[9] R. West, pp. 235-44 in Ultrastructure Processing of Ceramics, Glasses and Composites, edited by L. L. Hench and D. R. Ulrich (Willey-Interscience, New York), 1984.

[10] R. T. Paine and C. K. Narula, Chem. Mater., **5**, 269-79 (1993).

[11] D. Seyferth, G. Wiseman and C. Prud'homme, J. Am. Ceram. Soc., **66**, C-13-C-14 (1983).

[12] O. Funayama, T. Kato, Y. Tashiro and T. Isoda, J. Am. Ceram. Soc., **76**, 717-723 (1993).

[13] E. Kroke, Y-L. Li, C. Konetschny, E. Lecomte, C. Fasel, and R. Riedel, Mater. Sci. Eng., **R26**, 97-199 (2000).

[14] D. Bahloul, M. Pereira, P. Goursat, N. S. Choong, K. Yive and R. J. P. Corriu, J. Am. Ceram. Soc., **76**, 1156-62 (1993).

Chapter 4

Synthesis of poly-titanosilazanes and conversion into Si_3N_4-based ceramics

4.1. Introduction

Recently, ceramic particle-reinforced Si_3N_4 composite has drawn considerable attention because of substantial enhancement of the mechanical properties of Si_3N_4 ceramics [1-4]. Among the ceramic reinforcements, titanium nitride (TiN) and titanium carbonitride (Ti(C,N)) have been reported as a useful nano/micro particle-reinforcement for Si_3N_4 ceramics [5-8].

The fabrication of particle-reinforced ceramic composites by conventional powder processing often generates agglomerates of the particle-reinforcement and the degree of microstructural homogeneity is limited, which strongly influences the enhancement of mechanical properties of composites. As one of the possible ways to overcome this problem, a new fabrication method, in-situ compositing method, has been suggested. This method uses metal-organic precursor which can be homogeneously distributed within the ceramic matrix green body and transformed to a particle-reinforcement by reaction and precipitation during sintering. C. M. Wang reported that Si_3N_4-TiN nanocomposite has been prepared using Si_3N_4 powder and titanium n-butoxide ($Ti(O(CH_2)_3CH_3)_4$) as an in-situ source of TiN nano-particles [9]. C. K. Narula *et al.* also reported that (trimethylsilyl) amino titanium trichloride ($(H_3C)_3SiNHTiCl_3$) is a useful in-situ TiN source for Si_3N_4-TiN composite [10].

As investigated in chapter 3, the PHPSs chemically modified with alcohol derivatives and $Y(OCH_3)_3$ are useful for synthesizing [Si-Y-O-C-N] multicomponent ceramics of SiC nano/micro particle-dispersed Si_3N_4-based ceramics [11,12]. In this polymeric precursor route, desired elements for reinforcement and sintering aids can be introduced to PHPS. The microstructure of the resulting Si-based multicomponent ceramic systems can be regulated at nano/micro size level, which is expected to produce new types of high-performance Si_3N_4-based composites.

In this chapter, poly-titanosilazanes are designed and synthesized for [Si-Ti-(C)-N] multicomponent ceramic system such as TiN or Ti(C,N) nano/micro particle-dispersed Si_3N_4 based-ceramics. As a molecular titanium source, titanium alkoxide ($Ti(OR)_4$) is one of the candidates for the chemical modification of PHPS. However, as discussed in the section 2.3.1, a disadvantage is the weight % order of oxygen impurity in the resulting multicomponent ceramics due to the reactions between the alkoxide-derived R-OH and PHPS. To overcome this problem, the following two different synthetic strategies can be proposed for the poly-titanosilazane syntheses as shown in Fig. 4-1:

(1) Path A

Chemical modification of PHPS with an oxygen-free molecular titanium source, tetrakis (dimethylamino) titanium ($Ti(N(CH_3)_2)_4$) or titanium tetrachloride ($TiCl_4$).

(2) Path B

If PHPS is chemically modified with titanium tetra-isopropoxide ($Ti(OCH(CH_3)_2)_4$) in the presence of silylamine monomers such as tetramethyldisilazane (TMDS, $HN(SiH(CH_3)_2)_2$), TMDS is expected to react with $(CH_3)_2CHOH$. The product, $(H_3C)_2HSi\text{-}NH\text{-}SiOCH(CH_3)_2$, can be easily evaporated during pyrolysis, which is expected to reduce the oxygen impurity in the ceramics.

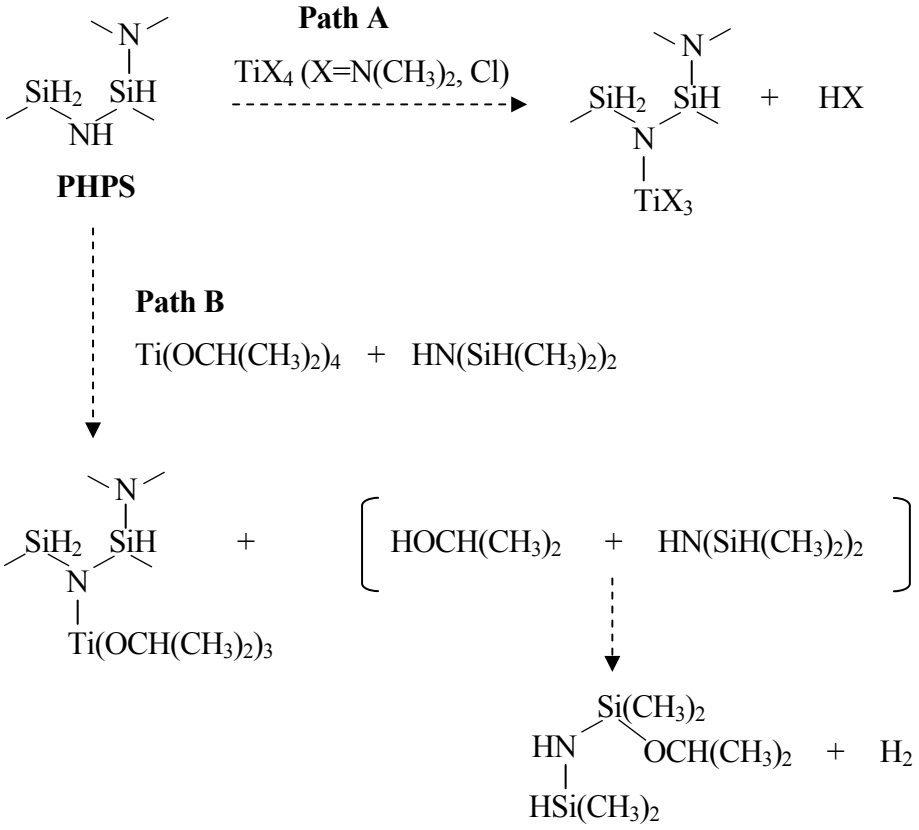

Fig. 4-1. Synthesis strategies of poly-titanosilazanes by chemical modification of PHPS with molecular titanium source.

In this chapter, the chemical modification reactions of PHPS with TiX_4 ($X=N(CH_3)_2$, Cl, $OCH(CH_3)_2$) are investigated by FT-IR, ^1H- and ^{29}Si-NMR spectroscopic analyses to examine the synthesis strategies shown in Fig. 4-1. Then, crystallization and microstructure development of the poly-titanosilazane-derived multicomponent amorphous ceramics are studied by XRD and TEM analyses.

4.2. Experimental procedure

4.2.1. Precursor synthesis

Commercially available perhydropolysilazane (PHPS, Tonen Co. Tokyo, Japan, N-N610, mean molecular weight of 5156) was used as a starting polymer. Reagents of $Ti(N(CH_3)_2)_4$ (Torichemical Co., Yamanashi, Japan), $TiCl_4$ (Wako Pure Chemical Industries, Ltd., Osaka, Japan) and $Ti(OCH(CH_3)_2)_4$ (Kojundo Chemical Laboratory Co., Saitama, Japan)) were used for the chemical modification of PHPS. The chemical modification reactions of PHPS were carried out under N_2 atmosphere, and the yield was evaluated by wt% based on the total amount of PHPS and the reagent used in each chemical modification reaction.

(1) Chemical modification of PHPS with $Ti(N(CH_3)_2)_4$

As-received PHPS (6.65 g: Si, 63.5; N, 24.8; O, 0.7; C, 2.4 wt %, hence Si=150 mmol) was dissolved into dry xylene (100 ml) with stirring, then cooled to 0 °C. To this solution, $Ti(N(CH_3)_2)_4$ (3.36 g, 15 mmol, Ti/Si atomic ratio of 0.10) in dry xylene (5 ml) was slowly added by syringe with stirring. After the addition was completed, the reaction mixture was warmed to room temperature, then maintained for 2h with stirring. The reaction mixture was concentrated in a rotary evaporator. The residue was dried under vacuum to give a brown powder (TNPHPS, 9.51 g, 95%).

(2) Chemical modification of PHPS with $TiCl_4$

As-received PHPS (6.65 g, Si=150 mmol) was dissolved into dry xylene (200 ml) with stirring at room temperature, then cooled to 0 °C. To this solution, $TiCl_4$ (2.85 g, 15 mmol, Ti/Si atomic ratio of 0.10) in dry xylene (10 ml) was slowly added while stirring. After the addition was completed, the reaction mixture was warmed to room temperature, then refluxed at 145 °C for 2h with stirring. After cooling down to room temperature, the reaction mixture was concentrated in a rotary evaporator. The residue was dried under vacuum to give a light green powder (TClPHPS, 9.12 g, 96 %).

(3) Chemical modification of PHPS with $Ti(OCH(CH_3)_2)_4$

As-received PHPS (6.65 g) was chemically modified with $Ti(OCH(CH_3)_2)_4$ (3.43 g, 15 mmol, Ti/Si atomic ratio of 0.10) under the same manner as TNPHPS to give a light green powder (TOPHPS, 9.87 g, 98%).

4.2.2. Pyrolysis

Pyrolysis of precursors was performed in a quartz tube furnace (Motoyama, Osaka, Japan) under flowing ammonia (NH_3, 500 ml/min.). The precursor sample was ground to a fine powder using a mortar and pestle in a glove box under N_2 atmosphere. The powdered-precursor was pyrolyzed at 1000 °C for 3h with heating rate of 200 °C/h followed by cooling down with the same rate to room temperature.

The ceramic yields of the TNPHPS, TClPHPS and TOPHPS were 75, 65 and 73 %, respectively. As-received PHPS was also pyrolyzed under the same condition as mentioned above to give a [Si-N] amorphous product as pale brown solid (76 %).

4.2.3. Heat treatment

The pyrolyzed sample was ground to a fine powder using a mortar and pestle, then sieved through a 250 μm screen before forming by uniaxial pressing at 150 MPa (10 mm diameter, 1.0 g). The green compacts were placed on a BN plate within a BN crucible and heat treated in a graphite resistance-heated furnace (Model High Multi 10000, Fujidempa Kogyo, Osaka, Japan) at temperatures of 1200 °C, 1400 °C, 1600 °C and 1800 °C. The N_2 pressures applied in this heat treatment procedure were 196 kPa at 1200 °C, 392 kPa at 1400 °C and 980 kPa at 1600 to 1800 °C.

4.2.4. Characterization

FT-IR, ^{1}H- and ^{29}Si-NMR spectra of the polymer samples were recorded as described in the section 3.2.3. To study the reaction of PHPS and $Ti(OCH(CH_3)_2)_4$, ^{1}H-NMR spectra were also recorded for $Si(OCH(CH_3)_2)_4$ (Kojundo Chemical Laboratory Co., Saitama, Japan) and $HOCH(CH_3)_2$ (Nakarai Chemical, reagent grade, Tokyo, Japan) as reference data.

Elemental analyses were performed on the pyrolyzed and heat treated-samples for Si and Ti (ICP spectrometry), C (high-temperature combustion method), N and O (inert gas fusion method) as described in the section 2.2.3. XRD measurements of the pyrolyzed- and heat treated-samples were performed as described in the section 2.2.3. The lattice parameter of TiN was measured using Si as internal standard, and the amount of carbon in the solid solution of $Ti(C_x, N_{1-x})$ was determined by the Vegard's low using the values of TiN (c=0.4242 nm, JCPDS Card No. 38-1420) and $Ti(C_{0.3}, N_{0.7})$ (c=0.4264 nm, JCPDS Card No. 42-1488).

Microstructure of heat treated-samples was studied using a transmission electron microscopy (TEM, Model EM-002B, Topcon Co., Tokyo, Japan, operating at 200 kV). Analytical TEM-analysis was performed on the heat treated-samples using GATAN IMAGING FILTER mounted on the TEM.

4.3. Results and discussion

4.3.1. Chemical modification reaction of PHPS with TiX_4

Figure 4-2 shows the FT-IR spectra of polymer samples. Compared with as-received PHPS (Fig. 4-2 (a)), TNPHPS (Ti/Si=0.10) shows a remarkable decrease in absorption intensity at 1180 cm^{-1} (N-H) (Fig. 4-2 (b)). In the spectrum of TClPHPS (Fig. 4-2 (c)), the intensity of Si-CH_3 at 1250 cm^{-1} and N-H at 1180 cm^{-1} decreases. New absorption bands also appears at 3150-3050 and 1400 cm^{-1}. In the spectrum of TOPHPS (Fig. 4-2(d)), the absorption intensity of C-H (2950-2900 cm^{-1}) increases, while those of Si-H (2150 cm^{-1}) and N-H (1180 cm^{-1}) decrease, and new absorption bands appear at 1370, 1340 cm^{-1} and 1160, 1130 cm^{-1} assigned to $CH(CH_3)_2$ and C-O, respectively [13]. These FT-IR spectroscopic changes suggest that $Ti(N(CH_3)_2)_4$ reacted with N-H groups in PHPS, while $TiCl_4$ reacted with N-H and $N(Si(CH_3)_3)_2$ groups in PHPS. The new absorption bands observed in Fig. 4-2 (c) are considered to be due to OH groups in Ti-OH generated by hydrolysis of the residual Ti-Cl bonds during the sample loading and transfer step for FT-IR analysis

The FT-IR spectroscopic analysis of TOPHPS suggests that $Ti(OCH(CH_3)_2)_4$ reacted with PHPS as analogously as $Y(OCH_3)_3$, and the chemical bond formation of N-Ti and Si-O seems to proceed as discussed in the section 2.3.1.

The chemical structures of poly-tinaosilazanes were further studied by ^{1}H-NMR spectroscopy. However, these samples were found almost insoluble in organic solvents such as xylene and chloroform. Then, the PHPS was reacted with $Ti(N(CH_3)_2)_4$ (Ti/Si=0.02), and soluble fractions of the reaction products of TNPHPS (Ti/Si=0.02) was studied. The results are shown in Fig. 4-3. As-received PHPS presents four peaks at 4.80, 4.34, 2.3-0.5 (broad) and 0.1-0.2 ppm assigned to N_3SiH/N_2SiH_2, $NSiH_3$, Si_2NH and $NSi(CH_3)_3$, respectively (Fig. 4-3 (a)). The relative peak intensities to $NSi(CH_3)_3$ of N_3SiH/N_2SiH_2, $NSiH_3$ and Si_2NH are 5.9, 1.8 and 1.2, respectively. In the spectrum of TNPHPS (Ti/Si=0.02), an additional broad peak is observed at 2.53 ppm assigned to N-CH_3 groups [13] (Fig. 4-3 (b)). The relative peak intensities to $NSi(CH_3)_3$ of N_3SiH/N_2SiH_2 and $NSiH_3$ are 5.9 and 1.7, respectively, while that of Si_2NH is remarkably decreased to 0.87. Accordingly, about 28 % of N-H groups in PHPS reacted with $Ti(N(CH_3)_2)_4$.

The FT-IR and ^{1}H-NMR spectroscopic analyses indicate that $Ti(N(CH_3)_2)_4$ reacted with N-H groups in PHPS to form N-Ti bonds as shown in Eq. 4.1.

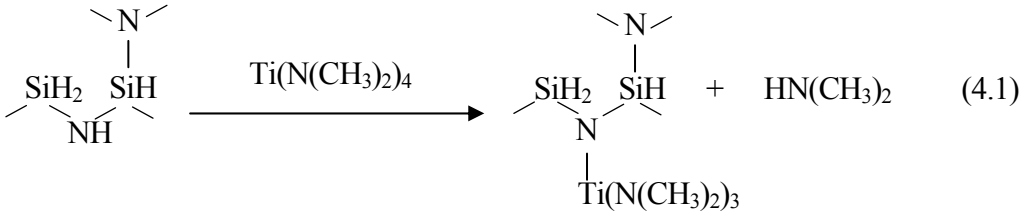

(4.1)

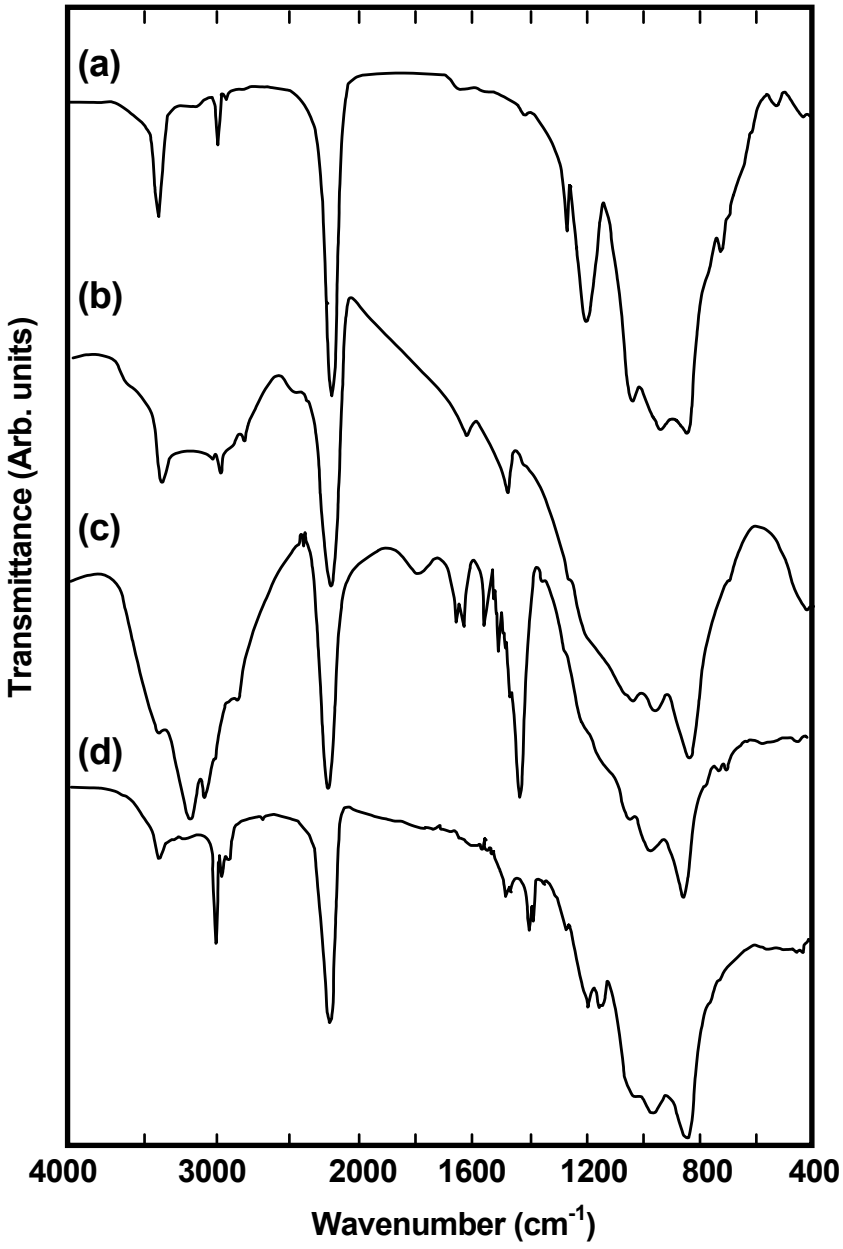

Fig. 4-2. FT-IR spectra of (a) as-received PHPS, (b) TNPHPS (Ti/Si=0.10), (c) TClPHPS (Ti/Si=0.10) and (d) TOPHPS (Ti/Si=0.10).

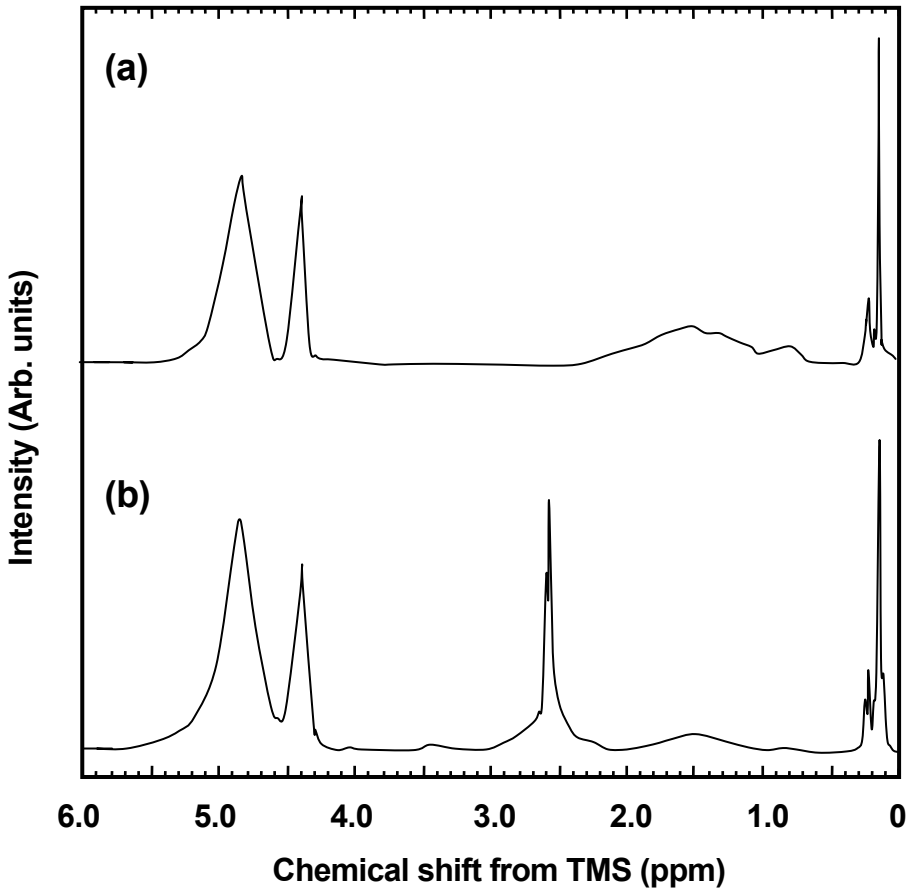

Fig. 4-3. ^{1}H-NMR spectra of (a) as-received PHPS and (b) TNPHPS (Ti/Si=0.02).

Since the FT-IR spectrum of the TClPHPS showed the decrease amount of N-H groups, $TiCl_4$ reacted with N-H groups of PHPS as analogously as $Ti(N(CH_3)_2)_4$. However, the different type of reaction between $TiCl_4$ and $N(Si(CH_3)_3)_2$ group was also suggested. To study this reaction in more detail, another grade of commercial PHPS, N-N 410 (Tonen Co., average molecular weight of 800) was used. As shown in the section 2.2.1, this polymer consists of the same structural units as N-N 610, and contains higher amount of the $N(Si(CH_3)_3)_2$ groups compared with N-N 610. $TiCl_4$ was reacted with PHPS (N-N 410) in $CDCl_3$ (Ti/Si=0.1), then the soluble fraction of the reaction mixture was analyzed by NMR spectroscopy.

The ^{1}H-NMR spectra of as-received PHPS (N-N 410), and the reaction mixture of PHPS and $TiCl_4$ are shown in Fig. 4-4. In the spectrum of as-received PHPS, the relative peak intensities to N_3SiH/N_2SiH_2 of $NSiH_3$, Si_2NH and $NSi(CH_3)_3$ are 0.49, 0.32 and 0.48, respectively (Fig. 4-4 (a)). The spectrum of the reaction mixture (Fig. 4-4 (b)) shows that the peaks of some N_3SiH/N_2SiH_2 groups and $NSi(CH_3)_3$ groups are shifted to lower fields of 6.2-5.2 ppm and 0.39-0.18 ppm, respectively. The relative peak intensity to N_3SiH/N_2SiH_2 (total broad peaks from 6.2 to 4.7 ppm) of $NSiH_3$ is 0.45, while those of Si_2NH (total broad peaks from 2.3 to 0.6 ppm) and $NSi(CH_3)_3$ are remarkably decreased to 0.19 and 0.24, respectively. The spectrum also presents a new peak at 0.42 ppm assigned to Si-CH_3 groups of $ClSi(CH_3)_3$ [13]. Accordingly, about 41 % of Si_2NH groups and almost all of the $N(Si(CH_3)_3)_2$ groups in PHPS reacted with $TiCl_4$.

^{29}Si-NMR spectrum of as-received PHPS presents three peaks at 3.8, -35.4 and -50.6 ppm assigned to SiC_3N ($N(Si(CH_3)_3)_2$), $SiHN_3/SiH_2N_2$ and SiH_3N units, respectively [12,14] (Fig. 4-5 (a)). In the spectrum of the reaction mixture (Fig. 4-5(b)), the peak of SiC_3N units almost disappears, and a new peak appears at 30.2 ppm assigned to $ClSiC_3$ unit [15], which is in consistence with the ^{1}H-NMR spectrum of Fig. 4-4 (b).

C. K. Narula *et al.* reported that hexamethyldisilazane ($HN(Si(CH_3)_3)_2$) reacted with $TiCl_4$ yielding $(H_3C)_3SiNHTiCl_3$ by the simultaneous loss of $ClSi(CH_3)_3$ [10]. Our NMR spectroscopic data indicate that the same type of reaction occurred between $TiCl_4$ and $N(Si(CH_3)_3)_2$ groups in PHPS as shown in Eq. 4.2.

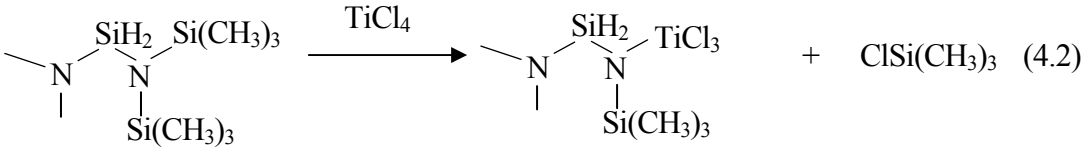

(4.2)

Based on the results obtained by these spectroscopic analyses, TCl_4 is found to react with N-H and $N(Si(CH_3)_3)_2$ groups in PHPS to form N-Ti bonds.

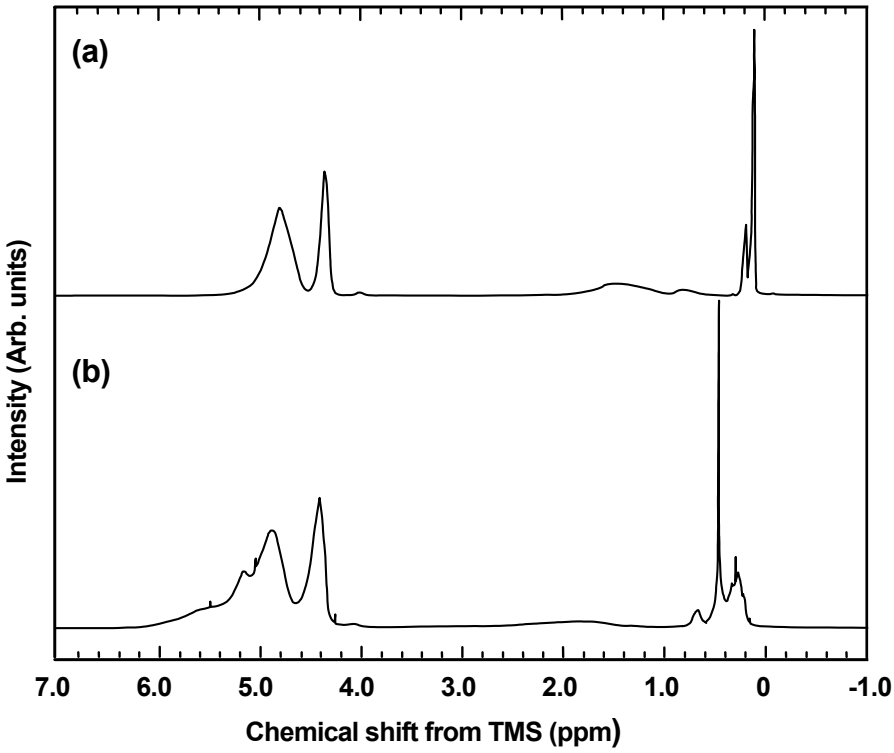

Fig. 4-4. ^{1}H-NMR spectra of (a) as-received PHPS (N-N 410) and (b) reaction mixture of PHPS and $TiCl_4$ (Ti/Si=0.1).

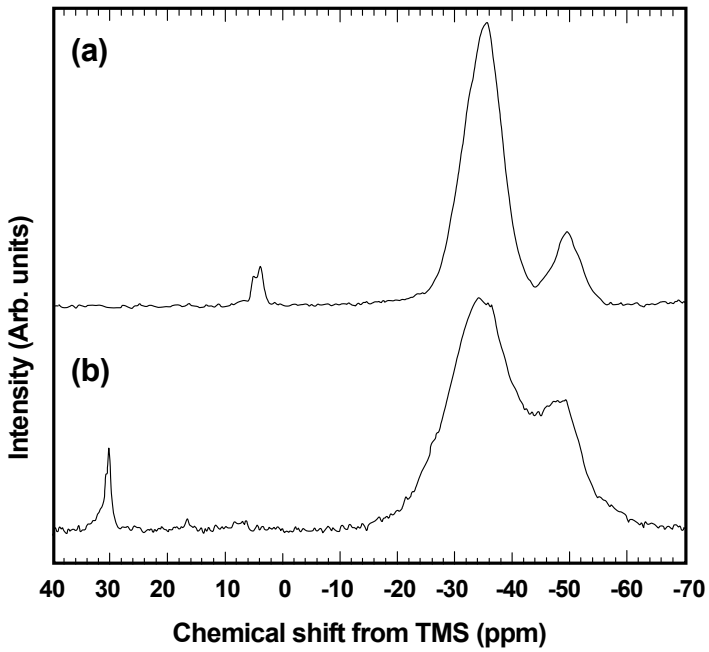

Fig. 4-5. ^{29}Si-NMR spectra of (a) as-received PHPS (N-N 410) and (b) reaction mixture of PHPS and $TiCl_4$ (Ti/Si=0.1).

To examine the possibility to reduce the oxygen impurity in the resulting multicomponent ceramics, the reaction at room temperature of the PHPS with $Ti(OCH(CH_3)_2)_4$ in $CDCl_3$ (Ti/Si=0.1) was monitored by ^{1}H-NMR spectroscopy. The results are shown in Fig. 4-6. After 2h (Fig. 4-6 (a)), the spectrum presents the peaks of PHPS-derived N_3SiH/N_2SiH_2 and $NSiH_3$, $Ti(OCH(CH_3)_2)_4$-derived CH (4.48 ppm, sept), and new peaks at 4.24 and 4.60 ppm. After 24 h (Fig. 4-6 (b)), the peak of $Ti(OCH(CH_3)_2)_4$-derived CH disappears. The peak intensity of $NSiH_3$ also decreases compared with as-received PHPS (Fig. 4-6 (c)), while those of the new peaks increase. At 4.70 ppm, a small shoulder is observed on the peak of N_3SiH/N_2SiH_2, which indicates the existence of $HSiON_2$ unit [14]. The chemical shift of the new peak (4.24 ppm) is close to that of CH group in $Si(OCH(CH_3)_2)_4$ (4.27 ppm, (sept)). According to these results, the new peak at 4.24 ppm is assigned to CH of Si-$OCH(CH_3)_2$ group.

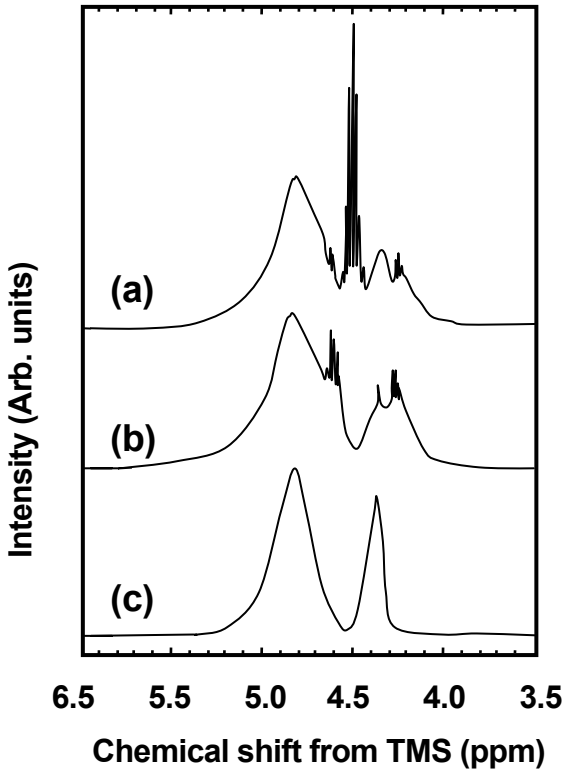

Fig. 4-6. ^{1}H-NMR spectrum showing a reaction mixture of PHPS and $Ti(OCH(CH_3)_2)_4$ (Ti/Si=0.10) maintained at room temperature for (a) 2 h, (b) 24 h and (c) a starting polymer of as-received PHPS.

Based on the spectroscopic analyses results, the proposed reactions between $Ti(OCH(CH_3)_2)_4$ and PHPS are shown in Fig. 4-7. As discussed in the section 2.3.1, $Ti(OCH(CH_3)_2)_4$ reacted with N-H groups in PHPS to form Ti-N bonds (Path A). Then, the produced $HO\text{-}CH(CH_3)_2$ reacted with N_2SiH_2 in PHPS to form $N_2SiH\text{-}OCH(CH_3)_2$ groups, and Si-N bond cleavage also occurred to some extent [11, 14], which caused the decrease amount of $NSiH_3$. The new peak observed at 4.60 ppm is considered to be due to the Si-H groups of the released oligomers and a monomer such as $H_2Si\text{-}OCH(CH_3)_2$.

However, as shown in Fig. 4-6 (a), CH peak of $HO\text{-}CH(CH_3)_2$ (4.05 ppm (sept)) was not detected, these reactions could not proceed stepwise but simultaneously. As another possible reaction for the simultaneous Ti-N and Si-O bond formations, $Ti(OCH(CH_3)_2)_4$ coordinated to PHPS to form a six membered-ring intermediate structure, then the reaction proceeded through the Ti-N and Si-O bond formations with Si-N bond cleavage (Path B). Accordingly, it is concluded that there is less possibility to minimize the oxygen content by trapping the $HO\text{-}CH(CH_3)_2$ with silylamine monomers as shown in Fig. 4.1 (Path B).

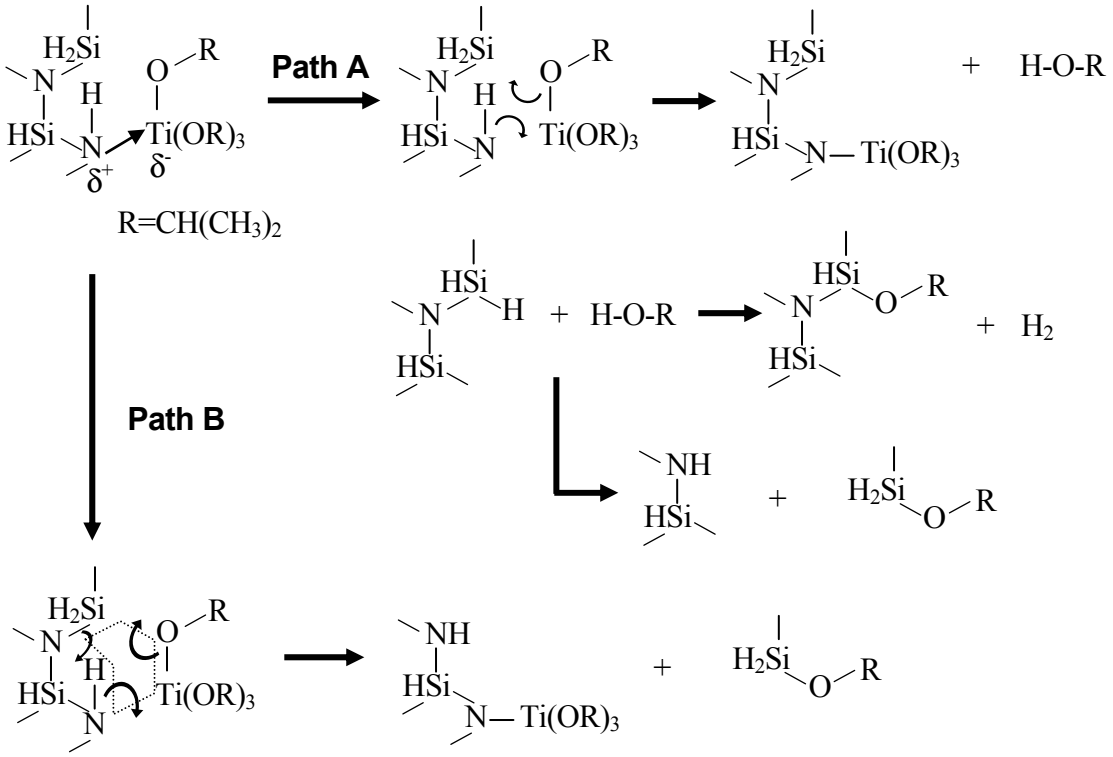

Fig. 4-7. Proposed reactions of PHPS with $Ti(OCH(CH_3)_2)_4$ based on FT-IR and ^{1}H-NMR spectroscopic analyses.

4.3.2. Conversion of polymeric precursors into Si_3N_4-based ceramics

The chemical composition of the pyrolyzed samples is shown in Table 4-1. The Ti/Si atomic ratios of the pyrolyzed polytinano-silazanes are 0.10, and titanium is successfully doped. The carbon content of the pyrolyzed TNPHPS is increased in comparison with that of the pyrolyzed as-received PHPS. To eliminate carbon completely, the pyrolysis condition (heating rate, keeping time and the NH_3 flow rate) was examined. However, it was difficult to eliminate the residual carbon completely up to 1000 °C in NH_3 flow.

Table 4-1. Chemical composition of 1000 °C pyrolyzed-samples.

	Composition (wt%)					
Precursor	Si	Ti	O	C	N	Atomic ratio
PHPS	69.0	0.0	0.3	0.1	29.6	$Si_{1.0}N_{0.86}$
TNPHPS	51.5	8.5	6.0	3.4	30.1	$Si_{1.0}Ti_{0.10}O_{0.21}C_{0.16}N_{1.18}$
TClPHPS	53.0	9.2	11.9	0.1	24.8	$Si_{1.0}Ti_{0.10}O_{0.39}C_{0.00}N_{0.93}$
TOPHPS	52.6	8.6	12.2	0.5	25.1	$Si_{1.0}Ti_{0.10}O_{0.41}C_{0.02}N_{0.96}$

Compared with the pyrolyzed as-received PHPS, oxygen content of the pyrolyzed TNPHPS and TClPHPS is also increased. Especially, the oxygen content of the pyrolyzed TClPHPS is as high as 11.9 wt%. This content is almost the same as that of the pyrolyzed TOPHPS (12.2 wt%). These polymeric precursors and the pyrolyzed samples may be highly reactive towards ambient moisture, which lead to the increase of oxygen content. In the case of TClPHPS, the FT-IR spectrum exhibited strong absorption band of OH groups as shown in Fig. 4-2(c). The higher amount of oxygen in the pyrolyzed TClPHPS is mainly caused by the hydrolysis of the residual Ti-Cl bonds during the sample loading and transfer step for pyrolysis.

Since the chemical composition of the pyrolyzed TClPHPS was almost the same as that of the pyrolyzed TOPHPS, crystallization behavior was studied on the three samples derived from as-received PHPS, TNPHPS and TOPHPS. The results are summarized and shown in Fig. 4-8. The polymeric precursor-derived amorphous ceramics are well crystallized by heat treatment up to 1800 °C in N_2. However, the crystallization behavior is much different in each sample. As-received PHPS-derived amorphous [Si-N] crystallizes at 1200 °C, and leads to the formation of both α- and β-Si_3N_4, and Si as a minor phase. Above 1400 °C, Si_3N_4 peaks continue to increase in intensity, while Si peaks decrease in relation (Fig. 4-8 (a)). The pyrolyzed TNPHPS exhibits only broad peaks at around 2θ (degrees) of 36.5, 42.5 and 61.7 up to 1400 °C, then exhibits both α- and β-Si_3N_4 peaks at 1600 °C (Fig. 4-8 (b)). Accordingly, the amorphous Si_3N_4 in the pyrolyzed TNPHPS is rather stable up to 1400 °C, and titanium is found to suppress crystallization of Si_3N_4.

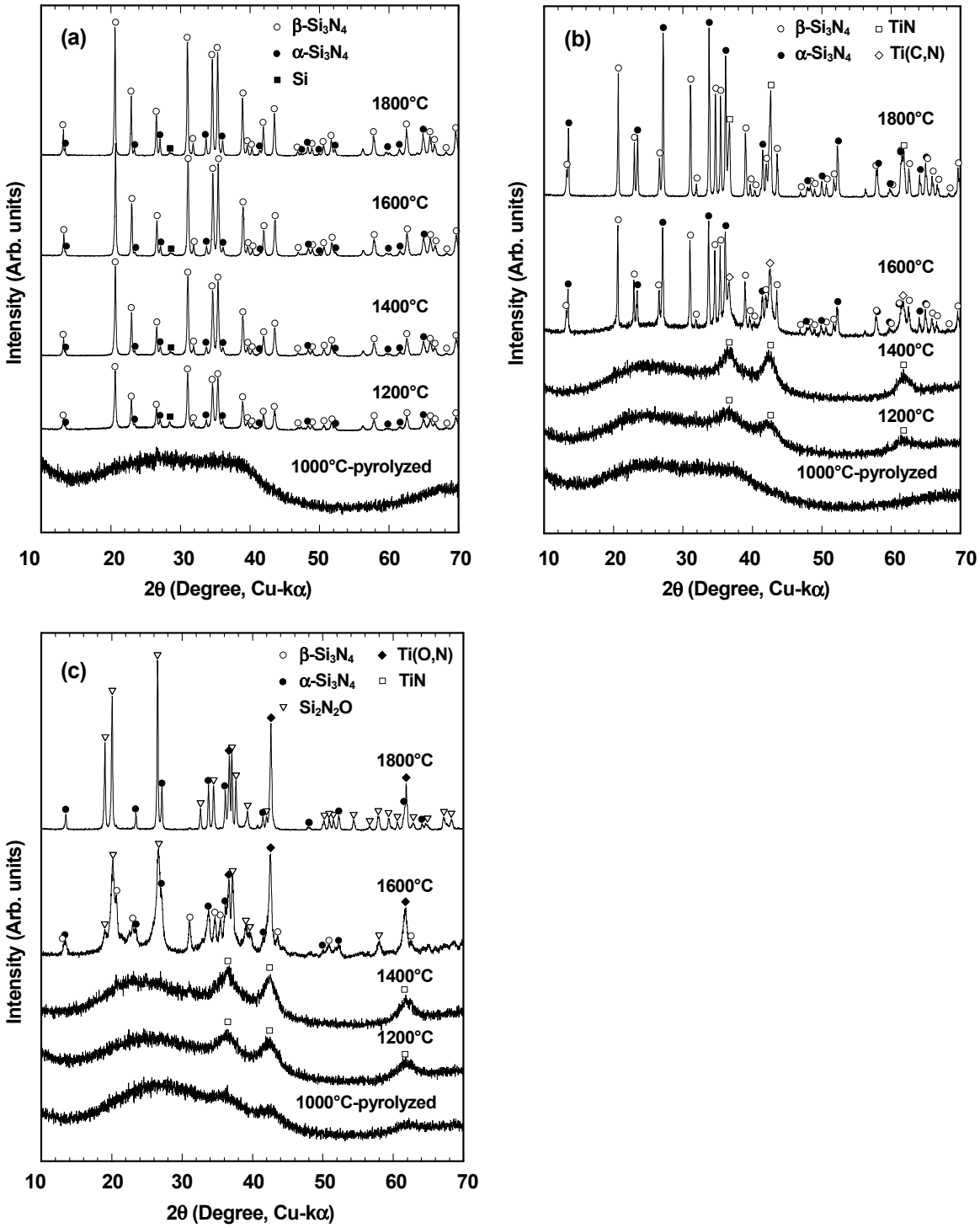

Fig. 4-8. Crystallization behavior of polymeric precursor-derived ceramics during heat treatment up to 1800 °C in N_2. (a) as-received PHPS, (b) TNPHPS (Ti/Si=0.10) and (c) TOPHPS (Ti/Si=0.10).

Figure 4-9 shows typical TEM micrographs of the 1200 °C heat treated-TNPHPS. Fine crystallites having a size range of about 10 to 20 nm are dispersed within a large amorphous powder (Figs. 4-9 (a) and (b)), and the selected area electron diffraction pattern (Fig. 4-9 (c)) is identical to TiN (based on JCPDS Card No. 38-1420). Upon heating to 1800 °C, the TiN peaks become sharp. However, at 1600 °C, these peaks are slightly shifted to lower angles, which indicates the solid solution formation of titanium carbonitride ($Ti(C_x, N_{1-x})$). The lattice parameter of $Ti(C_x, N_{1-x})$ in the 1600 °C heat treated-TNPHPS is 0.4249 nm, and the composition of the $Ti(C_x, N_{1-x})$ can be determined following the Vegard's low as $Ti(C_{0.1}, N_{0.9})$. Then, these peaks are shifted to higher angles, and the lattice parameter of this phase in the 1800 °C heat treated-TNPHPS is 0.4243 nm. This value is close to that of TiN (0.4242 nm, JCPDS Card No. 38-1420).

As shown in Fig. 4-8 (c), the crystallization behavior below 1400 °C of the pyrolyzed TOPHPS is similar to that of the pyrolyzed TNPHPS. However TOPHPS exhibits Si_2N_2O, α- and β-Si_3N_4 peaks at 1600 °C, then Si_2N_2O peaks are observed as a major phase at 1800 °C. Upon heating to 1800 °C, the broad peaks observed below 1400 °C are sharp and shifted to higher angles. The lattice parameter of this phase in the 1800 °C heat treated-TOPHPS is 0.4240 nm, and found to be intermediate between those of TiN (0.4.242 nm) and TiO (0.4178 nm) [16]. These peaks can be indexed as another solid solution of titanium oxynitride (Ti(N,O)).

The chemical compositions of the pyrolyzed- and heat treated-samples are listed in Table 4-2. The N/Si atomic ratio of pyrolyzed PHPS was 0.86, and excess Si relating to the composition of Si_3N_4 (N/Si=1.33) existed in the amorphous powders. Thus Si crystallized at 1200 °C. The crystallized Si could be nitriding to form Si_3N_4 above the melting point of Si at 1410 °C [17]. Finally at 1800 °C, the N/Si atomic ratio reached to 1.25.

The crystallization temperature of both α- and β-Si_3N_4 was as low as 1200 °C. This crystallization temperature is in consistence with those previously reported for silicon-rich amorphous Si_3N_4 derived from PHPS [17] or the vapor phase reaction of silane and NH_3 [18].

Table 4-2. Chemical composition of polymeric precursor-derived ceramics.

Precursor	Sample	Composition (wt%)					Atomic ratio
		Si	Ti	O	C	N	
PHPS	1000 °C-Pyrolyzed in NH_3 flow	69.0	0.0	0.3	0.1	29.6	$Si_{1.0}N_{0.86}$
	1600 °C-Heated in N_2 (980 kPa)	62.8	0.0	0.2	0.0	36.0	$Si_{1.0}N_{1.15}$
	1800 °C-Heated in N_2 (980 kPa)	60.8	0.0	0.3	0.0	37.9	$Si_{1.0}N_{1.25}$
TNPHPS	1000 °C-Pyrolyzed in NH_3 flow	51.5	8.5	6.0	3.4	30.1	$Si_{1.0}Ti_{0.10}O_{0.21}C_{0.16}N_{1.18}$
	1600 °C-Heated in N_2 (980 kPa)	49.8	9.0	5.5	2.7	32.0	$Si_{1.0}Ti_{0.11}O_{0.19}C_{0.13}N_{1.29}$
	1800 °C-Heated in N_2 (980 kPa)	51.2	10.8	1.9	0.6	34.6	$Si_{1.0}Ti_{0.10}O_{0.21}C_{0.16}N_{1.18}$
TOPHPS	1000 °C-Pyrolyzed in NH_3 flow	52.6	8.6	12.2	0.5	25.1	$Si_{1.0}Ti_{0.10}O_{0.41}C_{0.02}N_{0.96}$
	1600 °C-Heated in N_2 (980 kPa)	51.9	9.0	11.8	0.3	26.0	$Si_{1.0}Ti_{0.10}O_{0.40}C_{0.01}N_{1.00}$
	1800 °C-Heated in N_2 (980 kPa)	47.1	13.6	10.5	0.1	27.7	$Si_{1.0}Ti_{0.17}O_{0.37}C_{0.01}N_{1.20}$

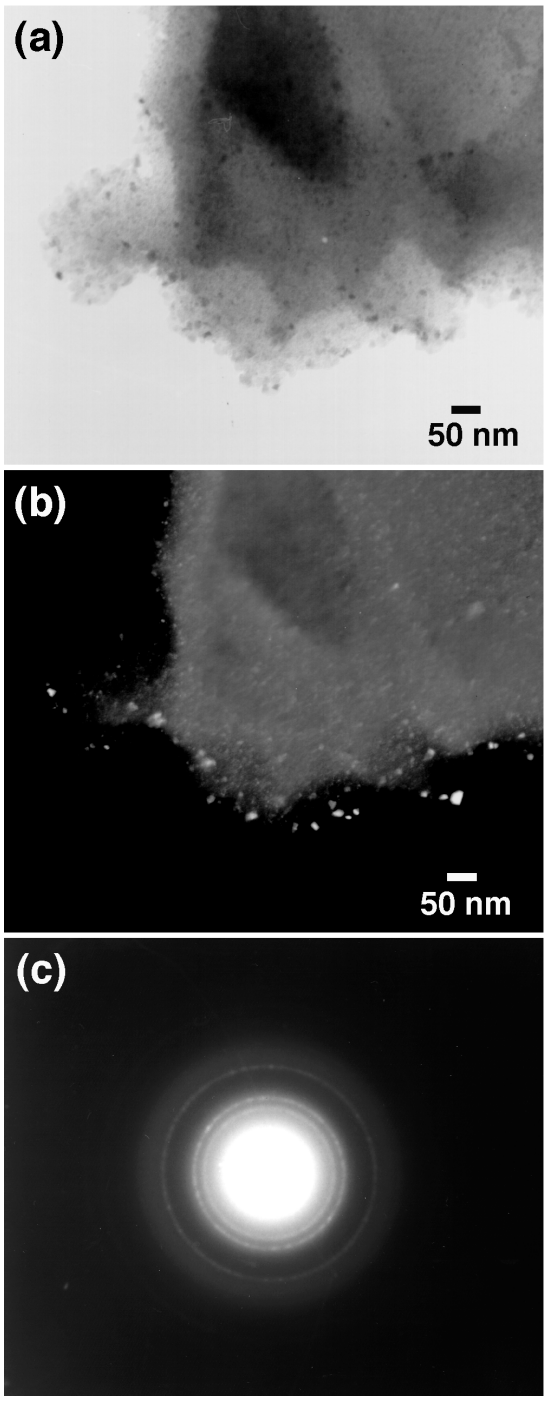

Fig. 4-9. TEM observation of 1200 °C heat treated-TNPHPS. (a) bright-field TEM image, (b) dark-field TEM image and (c) selected-area electron diffraction pattern.

Figure 4-10 shows the ellingham diagram for Si-Ti-C-N_2 system. N_2 pressures applied in this study are also plotted in Fig. 4-10. Values of the thermodynamic equations were taken from literature [19]. As shown in Fig. 4-10, N_2 pressures applied below 1600 °C are higher than the equilibrium pressure for the equation of $3/2SiC + N_2 = Si_3N_4 + 3/2C$. Under this condition, a possible reaction for the solid solution formation of $Ti(C_x, N_{1-x})$ is Eq. 4.3, and the amount of TiC in the solid solution can be determined by its own stability [6].

$$TiN + xC(s) \rightarrow Ti(C_x, N_{1-x}) + x/2N_2 \quad (4.3)$$

Above 1600 °C, SiC and N_2 are thermodynamically stable, and there is another possible reaction for the formation of $Ti(C_x, N_{1-x})$ as shown in Eq. 4.4 [6, 20].

$$(1-x)Si_3N_4 + 3TiC \rightarrow 3(1-x)SiC + 3Ti(C_x, N_{1-x}) + (1-x)/2N_2 \quad (4.4)$$

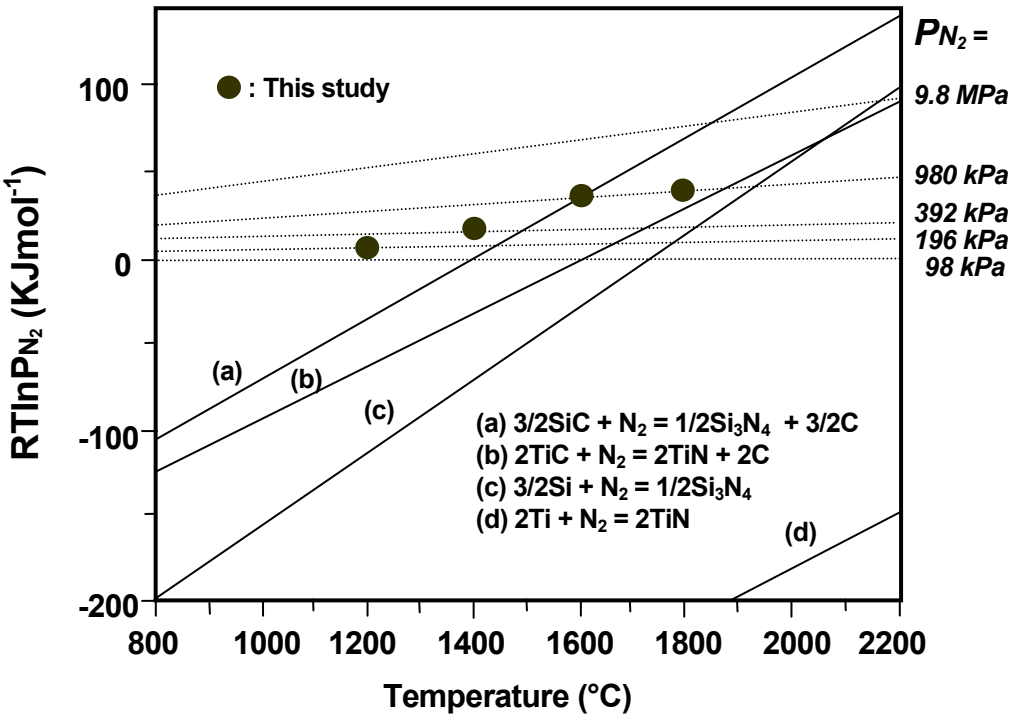

Fig. 4-10. The Ellingham diagram for Si-Ti-C-N_2 system.

However, as shown in Table 4-2, the pyrolyzed TNPHPS was the [Si-Ti-O-C-N] multicomponent amorphous phase. During heat treatment, carbon in the amorphous phase was spent for reactions such as carbothermal nitridation of SiO_2. The multicomponent amorphous phase was thermodynamically metastable and was able to give off gases such as CO and SiO. This lead to the reduction of the amount of TiC in $Ti(C_x, N_{1-x})$. Finally, at 1800 °C, carbon in the amorphous phase was almost spent out (Table 4-2). Consequently, β-Si_3N_4 and $Ti(C_x, N_{1-x})$ ($x = \sim 0.01$) could be detected by XRD.

The formation of Si_2N_2O and Ti(O,N) above 1600 °C of the TOPHPS-derived sample is due to the excess oxygen introduced from $Ti(OCH(CH_3)_2)_4$. As shown in Table 4-2, the Ti/Si atomic ratio of the 1800 °C heat treated-TOPHPS is increased to 0.17, which is considered to be mainly due to the decomposition above 1600 °C of Si_2N_2O with simultaneous loss of SiO and O_2 (Eq. 4.5) [11].

$$2Si_2N_2O \rightarrow Si_3N_4 + SiO\uparrow + 1/2O_2\uparrow \qquad (4.5)$$

Figure 4-11 shows the typical microstructure observation results of the TNPHPS-derived ceramics. At 1400 °C, several particles with diameter of smaller than 30 nm are observed (Fig. 4-11 (a)), and these particles are identified as TiN by the elemental ratio map shown in Fig. 4-11 (b). At 1600 °C to 1800 °C, the nano particles are increased in size and partially sintered. However, even at 1800 °C, the particle size is smaller than 100 nm (Figs. 4-11 (c) and (d)). These observation results indicate that the TNPHPS derived from PHPS and $Ti(N(CH_3)_2)_4$ is suitable for the synthesis of TiN or Ti(C,N) nano/micro particle-dispersed Si_3N_4-based ceramics.

4.4. Conclusions

Poly-titanosilazanes were synthesized by chemical modification of PHPS with TiX_4 ($X=N(CH_3)_2$, Cl, $OCH(CH_3)_2$). The chemical modification reactions were studied using FT-IR, ^1H- and ^{29}Si-NMR techniques, and the poly-titanosilazanes were found to contain some N-Ti bonds.

[Si-Ti-O-C-N] multicomponent amorphous ceramics were synthesized by pyrolysis of the poly-titanosilazanes at 1000 °C in NH_3. The oxygen impurity in the multicomponent amorphous ceramics could be minimized by use of $Ti(N(CH_3)_2)_4$ as a molecular titanium source for the synthesis of the poly-titanosilazane.

The amorphous silicon nitride derived from as-received PHPS crystallized at 1200 °C, while poly-titanosilazane derived from PHPS and $Ti(N(CH_3)_2)_4$ (TNPHPS) yielded TiN nanoparticle-dispersed amorphous [Si-Ti-O-C-N] ceramics up to 1400 °C in N_2, and titanium was

found to suppress crystallization of Si_3N_4.

At 1600 to 1800 °C, the TNPHPS yielded Si_3N_4-Ti(C,N) ceramics. Ti(C,N) was observed as particles with diameter of smaller than 100 nm, and the TNPHPS was found to be suitable for the synthesis of TiN or Ti(C,N) nano/micro particle-dispersed Si_3N_4-based ceramics.

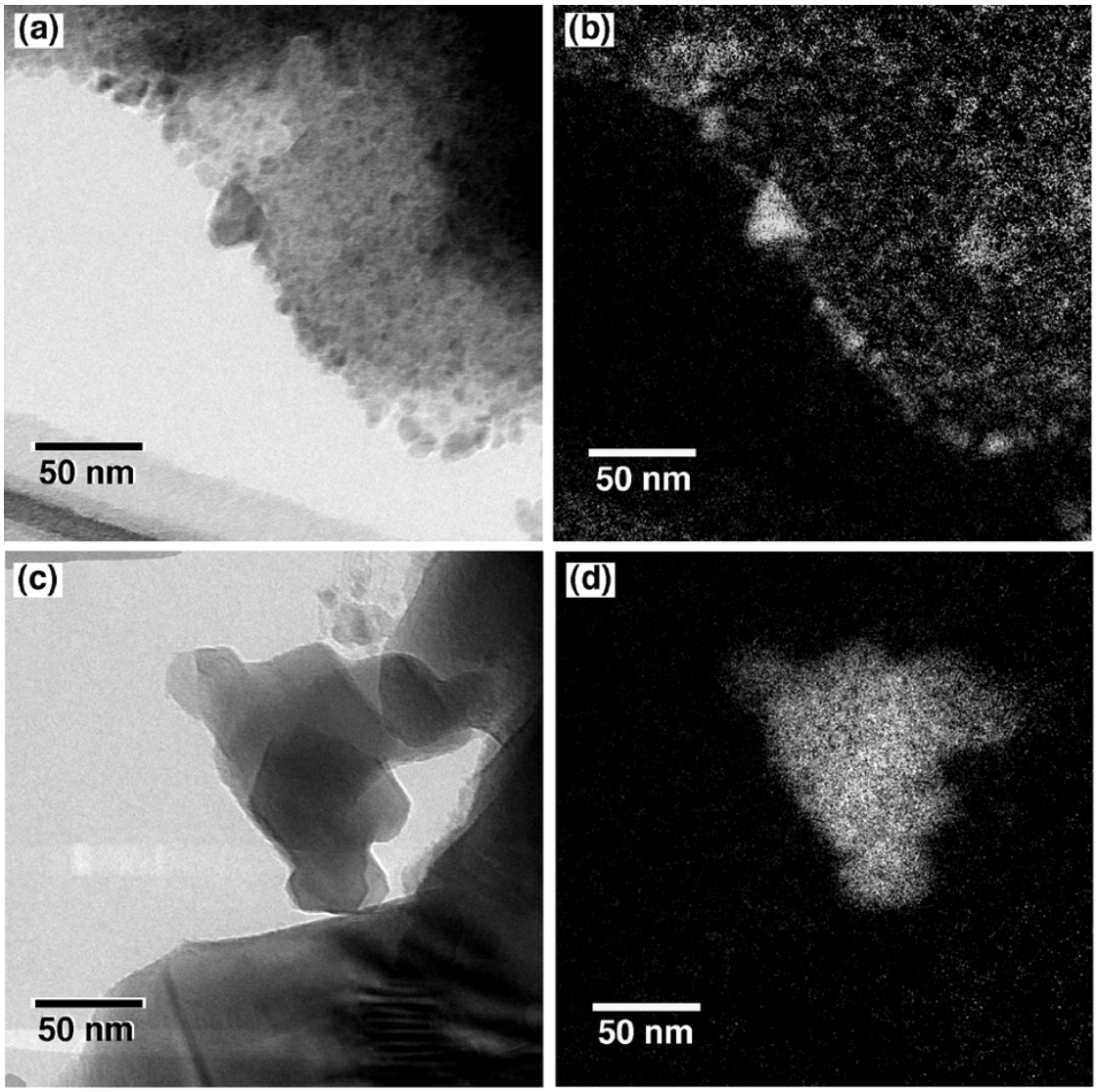

Fig. 4-11. TEM images and elemental ratio maps of TNPHPS-derived ceramics. (a) bright-field TEM image of 1400 °C heat treated-TNPHPS, (b) elemental Ti-L ratio map of titanium from the same field as shown in (a), (c) bright-field TEM image of 1800 °C heat treated-TNPHPS, (d) elemental Ti-L ratio map of titanium from the same field as shown in (c).

References

[1] M. Mitomo and S. Uenosono, J. Am. Ceram. Soc., **75**, 103-108 (1992).

[2] C. H. Li, D. J. Lee and S. C. Lui, J. Am. Ceram. Soc., **75**, 1777-85 (1992).

[3] P. F. Becher, H. T. Lin, and S. L. Huang, pp. 147-158 in Silicon Nitride Ceramics, -Scientific and Technological Advances-, edited by I-W. Chen, P. F. Becher, M. Mitomo, G. Petzow and T-S. Yen (Mat. Res. Soc. Symp. Proc. **287**, Materials Research Society, Pittsburgh, PA), 1993.

[4] Y. G. Gogotsi, J. Mater. Sci., **29**, 2541-56 (1994).

[5] A. Bellosi, S. Guicciardi and A. Tampieri, J. Europ. Ceram. Soc., **9**, 83-97 (1992).

[6] M. Herrmann, B. Balzer, Chr. Schbert and W. Hermel, J Europ. Ceram. Soc., **12**, 287-296 (1993).

[7] J. L. Huahg, M. T. Lee, H. H. Lu and D. F. Lii., Mater. Chem. Phys., **45**, 203-210 (1996).

[8] M. Miyata, Y. Yasutomi, Y. Sawai and T. Kanai, J. Ceram. Soc. Japan., **105**, 761-777 (1997).

[9] C. M. Wang, J. Mater. Sci., **30**, 3222-30 (1995).

[10] C. K. Narula, B. G. Demczyk, P. Czubarow and D. Seyferth, J. Am. Ceram. Soc., **78**, 1247-51 (1995).

[11] Y. Iwamoto, K. Kikuta and S. Hirano, J. Mater. Res., **13**, 353-361 (1998).

[12] Y. Iwamoto, K. Kikuta and S. Hirano, J. Mater. Res., **14**, 1886-95 (1999).

[13] R. M. Silverstein, G. C. Bassler and T. C. Morrill, Chaps. 3-4 in Spectrometric Identification of Organic Compounds, 5th Edition (John Wiley & Sons, Inc., New York), 1991.

[14] O. Funayama, T. Kato, Y. Tashiro and T. Isoda, J. Am. Ceram. Soc., **76**, 717-723 (1993).

[15] R. Riedel, E. Kroke, A. Greiner, A. O. Gabriel, L. Ruwish and J. Nicolich, Chem. Mater., **10**, 2964-79 (1998).

[16] S. Koyama, D. Iizuka, Y. Sugahara and K .Kuroda, Appl. Organometal. Chem., **12**, 787-792 (1998).

[17] C. R. Blanchar and S. T. Schwab., J. Am. Ceram. Soc., **77**, 1729-39 (1994).

[18] S. Prochazka and C. Greskovich., J. Am. Ceram. Soc., **57**, 578-86 (1978).

[19] JANAF Thermodynamical Table, 3rd Edition, US National Bureau of Standards, Washington D. C., 1986.

[20] S. T. Buljan and G. Zilberstein, J. Mater. Sci. Res., **20**, 305-316 (1985).

Chapter 5

Crystallization and microstructure development of Ti(C,N) nano/micro particle-dispersed Si_3N_4-Y_2O_3 ceramics derived from chemically modified PHPS

5.1. Introduction

Incorporation of hetero elements into binary Si-N [1-3] or ternary Si-C-N system [4,5] strongly influences the crystallization behavior of amorphous materials to Si_3N_4-based composite materials derived from polymeric precursors. Bill *et al*. studied the crystallization behaviors of amorphous Si-(M)-C-N systems (M=B, P) derived from chemically modified polysilazanes [4,5]. It was found that B element stabilized the amorphous state of Si-N, while P element accelerated crystallization of Si_3N_4, and it was suggested that the difference in the crystallization behavior can offer an opportunity to control the microstructure development of the Si_3N_4/SiC composite materials at nano-/ micro-meter scale level.

As investigated in the previous chapter, the poly-titanosilazane derived from PHPS and $Ti(N(CH_3)_2)_4$ has a potential to synthesize TiN or Ti(C,N) nano/micro particle dispersed Si_3N_4-based ceramics. Additionally, Ti element has been found to suppress crystallization of Si_3N_4 [6]. From a view point of development of a novel microstructure control technology through polymeric precursor route, it is quite interesting to study on the microstructure development of the poly-titanosilazane derived Si_3N_4-Ti(C,N) composites through liquid phase sintering.

As additives for liquid phase sintering of Si_3N_4 ceramics, MgO, Y_2O_3 or Y_2O_3-Al_2O_3 are frequently used [7,8], and Si_3N_4-TiN or Ti(C,N) composites have been successfully fabricated using Y_2O_3-Al_2O_3 [9-12] and MgO-Y_2O_3-Al_2O_3 [13]. However, Si_3N_4 and Al_2O_3 can form solid solutions of SiAlONs [14,15], which also influences on the microstructure development of Si_3N_4 matrix [16].

In this chapter, Si_3N_4-Ti(C,N)-Y_2O_3 ceramic system has been selected for the study on the microstructure development. Poly-tinanosilazanes with different Ti content are prepared, then further modified with yttrium tri-isopropoxide ($Y(OCH(CH_3)_2)_3$). [Si-Y-Ti-O-C-N] multicomponent amorphous powders are synthesized by pyrolysis of the polymeric precursors. The crystallization and microstructure development of Si_3N_4-Ti(C,N)-Y_2O_3 ceramics from the polymeric precursor-derived [Si-Y-Ti-O-C-N] multicomponent powders are studied by comparison with [Si-Y-O-C-N] amorphous powders derived from PHPS chemically modified with $Y(OCH(CH_3)_2)_3$. The effect of titanium element on the crystallization and microstructure development of Si_3N_4-Ti(C,N)-Y_2O_3 ceramics is discussed from a view point of microstructure control of Si_3N_4-Ti(C,N)-Y_2O_3 ceramics through polymeric precursor route.

5.2. Experimental procedure

5.2.1. Precursor synthesis

Figure 5-1 shows synthesis routes for polymeric precursors investigated in this section. Commercially available PHPS (Tonen Co. N-N610 average molecular weight of 5156, Tokyo, Japan) was used as a starting polymer. Reagents of $Y(OCH(CH_3)_2)_3$ (Kojundo Chemical Laboratory Co., Saitama, Japan) and $Ti(N(CH_3)_2)_4$ (Torichemical Co., Yamanashi, Japan) were used for the chemical modification of PHPS.

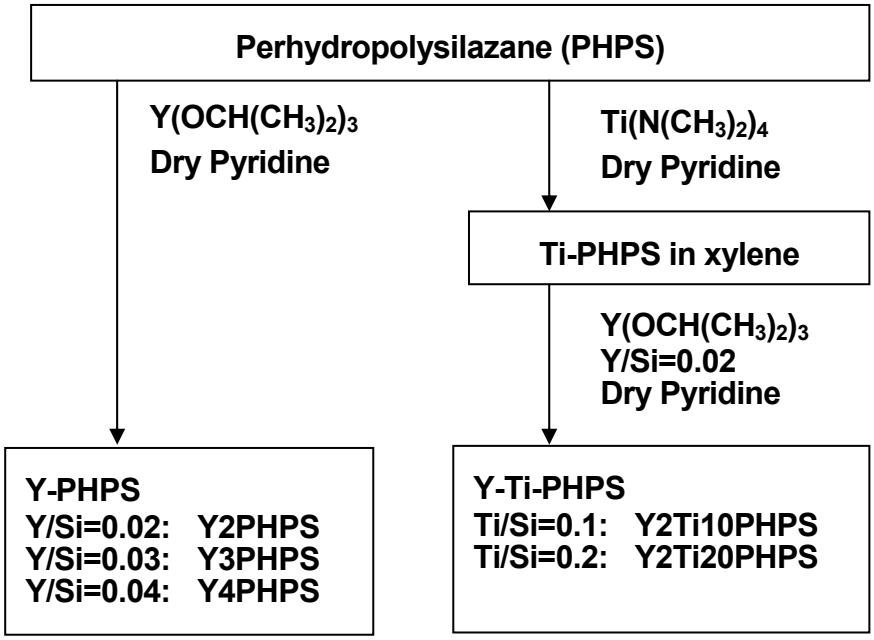

Fig. 5-1. Synthesis routes for polymeric precursors.

Yttrium modified PHPS (Y-PHPS) was synthesized by following the procedure described in the section 2.2.1 [17]. As-received PHPS (6.65 g: Si, 63.5; N, 24.8; O, 0.7; C, 2.4 wt%, hence Si=150 mmol) and $Y(OCH(CH_3)_2)_3$ in given Y/Si atomic ratios of 0.02 (Y2PHPS), 0.03 (Y3PHSPS) and 0.04 (Y4PHPS) were mixed with dry pyridine (500 ml). The mixture was refluxed for 2h with stirring. After cooling down to room temperature, the reaction mixture was concentrated in a rotary evaporator to give a reaction product. Since the product contained large amount of pyridine, dry xylene was added to the product and the mixture was again concentrated in a rotary evaporator to get rid of the residual pyridine, then the residue was dried in vacuum to give Y-PHPS as a pale yellow powder.

Xylene solution of titanium modified PHPS (Ti-PHPS) was prepared by the procedure described in the section 4.2.1 [6]. PHPS (6.65 g, Si=150 mmol) was dissolved into dry xylene (100ml) with stirring, then cooled to 0 °C. To this solution, $Ti(N(CH_3)_2)_4$ (Ti/Si atomic ratio of 0.10 for Y2Ti10PHPS, and 0.20 for Y2Ti20PHPS) in dry xylene (15 ml) was slowly added by syringe with stirring. After the addition was completed, the reaction mixture was warmed to room temperature, then maintained for 2h with stirring. To this solution, $Y(OCH(CH_3)_2)_3$ (0.8 g, 3 mmol, Y/Si =0.02) and dry pyridine (20 ml) were added. The mixture was refluxed at 145 °C for 4h. After cooling down to room temperature, the reaction mixture was concentrated in a rotary evaporator. The residue was dried in vacuum to give yttrium and titanium modified PHPS (Y-Ti-PHPS) as a brown powder.

5.2.2. Pyrolysis

Pyrolysis of precursors was performed as described in the section 4.2.2. Ceramic yields of Y2PHPS, Y3PHPS, Y4PHPS, Y2Ti10PHPS and 2YTi20PHPS were 89, 87, 84, 70 and 68 %, respectively.

5.2.3. Heat treatment and hot pressing

The amorphous powder was ground to a fine powder using a mortar and pestle, then sieved through a 250 μm screen before forming by uniaxial pressing at 150 MPa (10 mm x 10 mm, 1.5 g). The green compacts were heat treated as described in the section 4.2.3. Hot-pressing was carried out in a graphite resistance-heated furnace (Model High Multi 10000, Fujidempa Kogyo, Osaka, Japan). The green compacts (10 mm x 10 mm, 1.5 g) were placed in a BN coated graphite die and hot-pressed at 1800 °C for 1h at a stress of 40 MPa under a nitrogen pressure of 980 kPa.

5.2.4. Characterization

Elemental analyses were performed on the pyrolyzed and 1800 °C heat treated-powders for Si, Y and Ti (ICP spectrometry), C (high-temperature combustion method), N and O (inert gas fusion method) as described in the section 2.2.3. Molar ratio compositions of the 1800 °C heat treated-samples were calculated assigning all Y to O as Y_2O_3; all O to Si as SiO_2; all Ti to N and C as $Ti(C_x, N_{1-x})$; all N to Si as Si_3N_4. Then, excess C was assigned to be in the elemental state. Based on the molar ratio composition, the total amount of sintering additives was calculated by Eq. 5.1 using the volume (V) contents of Si_3N_4, Y_2O_3 and SiO_2.

$$(V_{Y_2O_3} + V_{SiO_2}) / (V_{Si_3N_4} + V_{Y_2O_3} + V_{SiO_2}) \quad (5.1)$$

XRD measurements of the precursor-derived ceramics were performed as described in the section 2.2.3.

The relative amount of α- and β-Si_3N_4 in the heat treated-samples were calculated using the method reported by C. P. Gazzara and D. R. Messier [18]. The β / (β + α) phase ratio of Si_3N_4 was determined by Eq. 5.2 using the corrected values for peak intensity of β-Si_3N_4 (210) and α-Si_3N_4 (210) [18,19].

$$I_{\beta(210)c} / (I_{\beta(210)c} + I_{\alpha(210)c}) \quad (5.2)$$

The amount of carbon in the $Ti(C_x,N_{1-x})$ of the precursor derived ceramics was determined by the method described in the section 4.2.4.

Apparent densities of the hot pressed-samples were measured by the Archimedes method. Relative densities of the hot pressed-samples were evaluated using theoretical densities (3.242 x 10^3 kg/m^3 for Y2PHPS, 3.400 x 10^3 kg/m^3 for Y2Ti10PHPS and 3.292 x 10^3 kg/m^3 for Y2Ti20PHPS) calculated from the molar ratio compositions of the 1800 °C heat treated-samples.

The hot pressed-samples were polished with diamond powder (0.5 μm), and plasma etched using CF_4 for 3 min. Then, the samples were carbon coated and the microstructures were observed using a scanning electron microscopy (SEM, Model S-800, Hitachi, Tokyo, Japan), and characterized by measuring diameters and lengths of 1000 to 1200 β-Si_3N_4 matrix grains. Microstructures were also studied using a transmission electron microscopy (TEM, Model EM-002B, Topcon Co., Tokyo, Japan). Analytical TEM-analysis was performed on the hot-pressed samples using GATAN IMAGING FILTER mounted on the TEM.

5.3. Results and discussion

5.3.1. Polymeric precursor-derived multicomponent powders

Chemical compositions of polymeric precursor-derived multicomonent powders are listed in Table 5-1. The Y/Si atomic ratios of these ceramics are well consistent with the calculated ratios for the chemical modification reactions of PHPS. The Ti/Si atomic ratios of Y2Ti10PHPS and Y2Ti20PHPS are 0.11 and 0.24, respectively. Although, these values are slight larger than the calculated values, yttrium and titanium were successfully doped in the multicomponent powders by two-step chemical modification reaction of PHPS.

Table 5-1. Chemical composition of polymeric precursor-derived multicomponent powders.

Precursor	Composition (wt%)						Atomic ratio
	Si	Y	Ti	O	C	N	
Y2PHPS	60.4	4.1	0.0	3.5	1.8	29.2	$Si_{1.0}Y_{0.02}Ti_{0.00}O_{0.10}C_{0.07}N_{0.97}$
Y3PHPS	60.2	5.7	0.0	4.4	1.2	27.5	$Si_{1.0}Y_{0.03}Ti_{0.00}O_{0.14}C_{0.05}N_{0.92}$
Y4PHPS	57.1	7.8	0.0	6.8	1.0	27.2	$Si_{1.0}Y_{0.04}Ti_{0.00}O_{0.21}C_{0.04}N_{0.95}$
Y2Ti10PHPS	47.8	2.9	8.7	8.2	4.2	29.2	$Si_{1.0}Y_{0.02}Ti_{0.11}O_{0.31}C_{0.21}N_{1.28}$
Y2Ti20PHPS	40.7	2.8	16.7	8.3	3.9	26.6	$Si_{1.0}Y_{0.02}Ti_{0.24}O_{0.36}C_{0.22}N_{1.31}$

XRD measurements were performed on the multicomponent powders. Y2PHPS and Y2Ti10PHPS exhibit broad amorphous diffraction lines (Figs. 5-2 (a) and (b)). Y2Ti20PHPS presents broad peaks at around 2θ (°) of 36.5, 42.5 and 61.7 (Fig. 5-2 (c)). Figure 5-3 shows typical TEM images of the Y2Ti20PHPS-derived powders. Fine crystallites having a size range of about 10 to 40 nm are dispersed within a large amorphous powder (Figs. 5-3 (a) and (b)). The selected area electron diffraction pattern (Fig. 5-3 (c)) is identical to TiN (based on JCPDS Card No. 38-1420).

5.3.2. Crystallization behavior

Further crystallization behaviors of the multicomponent powders are summarized and shown in Fig. 5-2. Y2PHPS presents both α- and β-Si_3N_4 peaks at 1400 °C, then the α-/β-Si_3N_4 phase transformation is completed at 1800 °C (Fig. 5-2 (a)). According to the XRD analyses, Y3PHPS and Y4PHPS also presented both α- and β-Si_3N_4 peaks at 1400 °C. Then, these powders presented only β-Si_3N_4 peaks at 1800 °C.

Y2Ti10PHPS (Fig. 5-2 (b)) presents TiN broad peaks at 1200 °C, then presents Si_2N_2O broad peaks at 1400 °C. At 1600 °C, Y2Ti10PHPS presents both α- and β- Si_3N_4 peaks. The Si_2N_2O peaks disappear and the α-/β-Si_3N_4 phase transformation is completed at 1800 °C. Upon heating to 1800 °C, the TiN peaks become sharp. However, these peaks are slightly shifted to lower angles, which indicates the solid solution formation of titanium carbonitride ($Ti(C_x, N_{1-x})$). The lattice parameter of $Ti(C_x, N_{1-x})$ in the 1800 °C heat treated-Y2Ti10PHPS is 0.4249 nm and the composition can be determined following the Vegard's law as $Ti(C_{0.1}, N_{0.9})$.

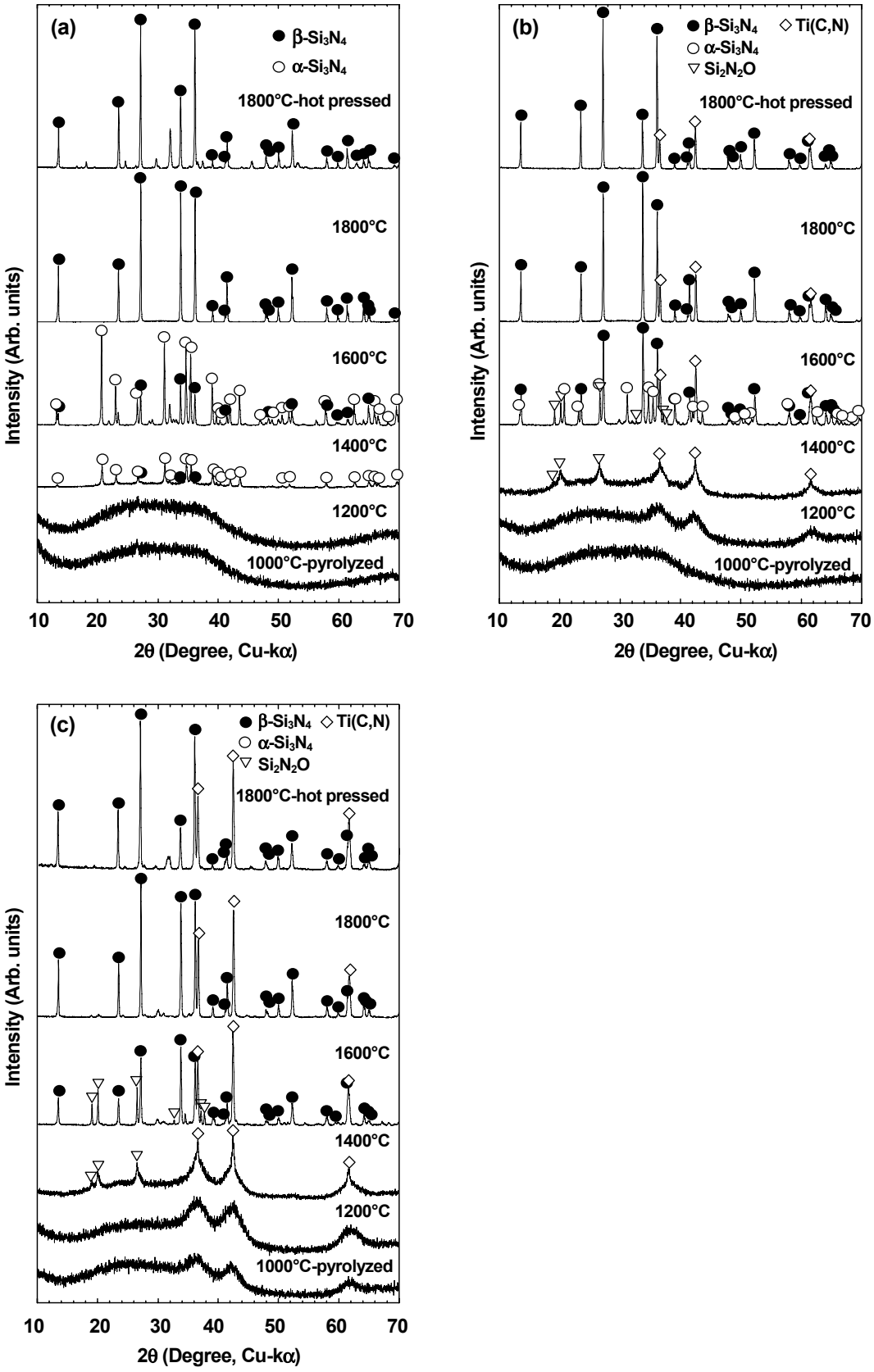

Fig. 5-2. XRD patterns of polymeric precursor-derived ceramics.
(a) Y2PHPS, (b) Y2Ti10PHPS and (c) Y2Ti20PHPS.

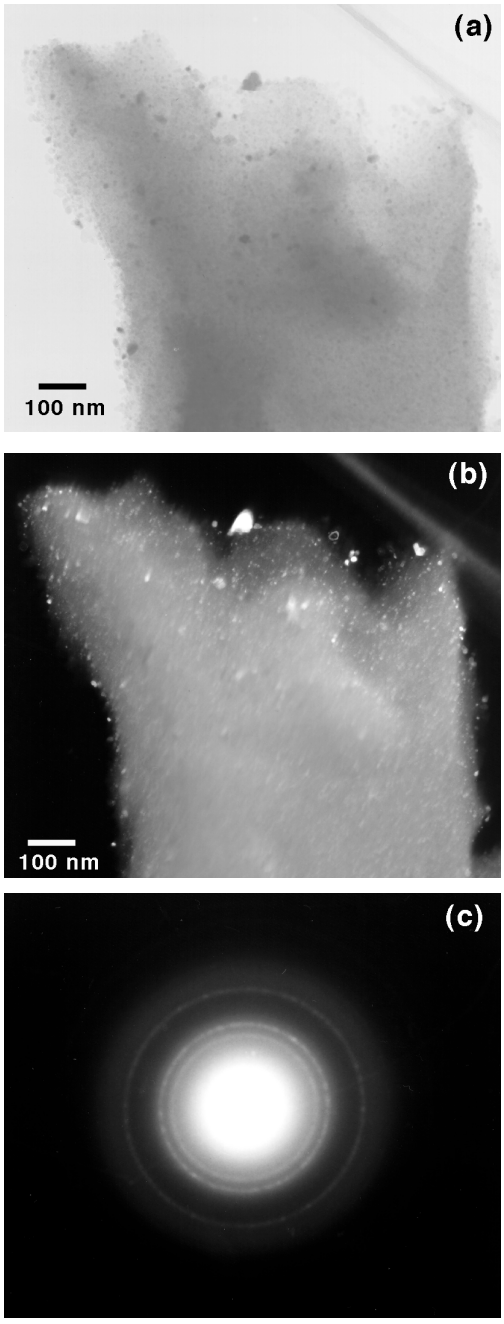

Fig. 5-3. TEM observation of 1000 °C-pyrolyzed Y2Ti20PHPS. (a) bright-field TEM image, (b) dark-field TEM image and (c) selected-area electron diffraction pattern.

The crystallization behavior of Y2Ti20PHPS is similar to that of Y2Ti10PHPS. Finally at 1800 °C, Y2Ti20PHPS presents β-Si_3N_4 and Ti($C_{0.11}$, $N_{0.89}$) peaks (Fig. 5-2(c)). The relative peak intensity to β-Si_3N_4 of Ti(C_x, N_{1-x}) is higher than that of 1800 °C heat treated-2YTi10PHPS (Fig. 5-2(b)), which is well consistent with the difference in Ti content of these powders as shown in Table 5-1.

The formation of Si_2N_2O from 1400 to 1600 °C in the Y-Ti-PHPS-derived powders is due to the large amount oxygen introduced together with yttrium and titanium (Table 5-1). During heat treatment above 1600 °C, Si_2N_2O decomposed to Si_3N_4 with volatile SiO and O_2 as discussed in the section 4.3.2.

Chemical compositions and calculated molar ratio compositions of the 1800 °C heat treated-powders are listed in Table 5-2. Compared with the initial compositions (Table 5-1), Y-PHPS-derived [Si-Y-O-C-N] powders show decrease in carbon and oxygen contents, and increase in nitrogen content. These chemical composition changes are due to some reactions such as carbothermal nitridation of SiO_2 (Eq. 5.3) [7], and the carbon in these powders was almost spent out for the reactions.

$$3SiO_2 + 6C + 2N_2 \rightarrow Si_3N_4 + 6CO\uparrow \qquad (5.3)$$

Y-Ti-PHPS-derived [Si-Y-Ti-O-C-N] powders also show the same changes in chemical composition. However, the carbon contents of Y2Ti10PHPS and Y2Ti20PHPS are 0.3 and 0.6 %, respectively (Table 5-2). These carbon contents are due to the Ti(C_x, N_{1-x}) solid solution formation between TiN and carbon in the [Si-Y-Ti-O-C-N] powders, and the rest of free carbon in the Ti-Y-PHPS-derived powders is almost the same level as that in the Y-PHPS-derived powders.

Table 5-2. Chemical composition of 1800 °C heat treated-powders.

	Composition (wt%)						Calculated molar ratio				
Precursor	Si	Y	Ti	O	C	N	Si_3N_4	Y_2O_3	SiO_2	Ti(C_x,N_{1-x})[x]	Free C
Y2PHPS	56.5	4.1	0.0	2.2	0.04	37.2	1.0	0.035	0.054	0.0	0.005
Y3PHPS	54.4	6.4	0.0	3.6	0.02	35.6	1.0	0.057	0.093	0.0	0.003
Y4PHPS	52.9	8.7	0.0	4.6	0.01	33.8	1.0	0.080	0.118	0.0	0.001
Y2Ti10PHPS	49.2	3.4	10.1	2.8	0.30	34.3	1.0	0.034	0.101	0.374[0.10]	0.007
Y2Ti20PHPS	41.8	3.1	19.6	3.0	0.61	31.6	1.0	0.036	0.141	0.856[0.11]	0.005

Figure 5-4 shows the change of $\beta/(\beta+\alpha)$ phase ratio of Si_3N_4 in the polymeric precursor-derived powders during heat treatment up to 1800 °C. As reference data, the ratios of as-received PHPS-derived amorphous [Si-N] powder investigated in the chapter 4 are also plotted in Fig. 5-4. Both α- and β-Si_3N_4 crystallization of the [Si-N] powder started at 1200 °C. Then, the β-Si_3N_4 contents are below 15 % at temperatures from 1400 to 1800 °C.

Amorphous Si_3N_4 in the multicomponent powders investigated in this study is rather stable up to 1200 °C. After Si_3N_4 crystallization started above 1400 °C, the β-Si_3N_4 content increases consistently with heat treatment temperature. Then, the transformation is completed at 1800 °C, and the β-Si_3N_4 content at 1600 °C is much different in each powder.

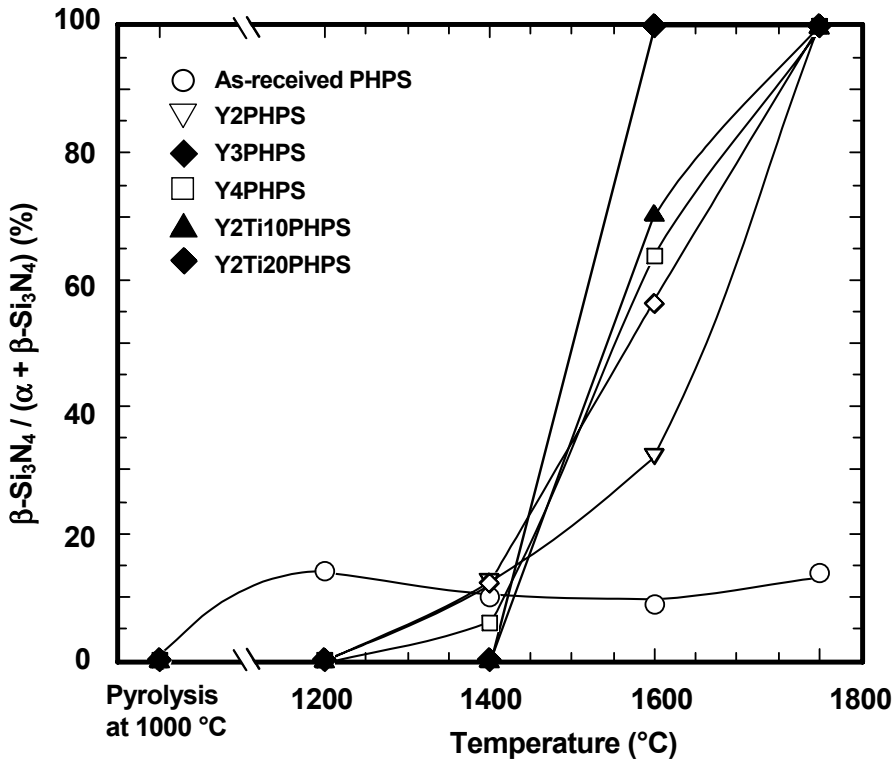

Fig. 5-4. $\beta/(\beta+\alpha)$ phase ratio of Si_3N_4 in polymeric precursor-derived powders as a function of heat treatment temperature in N_2.

Figure 5-5 shows the relation between total amount of sintering additives and β / (β + α) Si_3N_4 phase ratio after heat treatment at 1600 °C. Y-PHPS-derived powders show that the β-Si_3N_4 content increases with increasing total amount of sintering additives and the ratio reaches 63.9 % at 12.8 vol % (Y4PHPS). Although the total amount of sintering additives in the Y-Ti-PHPS-derived powders is below 11 vol %, the ratios of Y2Ti10PHPS and Y2Ti20PHPS reach 70.5 and 100 %, respectively.

As investigated in chapter 2, polymeric precursor-derived [Si-Y-O-C-N] multicomponent powders produced Si-Y-O-N liquid phase at 1600 °C [6]. Thus, the Si-Y-O-N liquid phase could promote the α-/β-Si_3N_4 phase transformation above 1600 °C of Y-PHPS-derived powders, and the transformation was enhanced consistently with amount of liquid phase.

The rapid α-/β-Si_3N_4 phase transformation observed in the Y-Ti-PHPS-derived powders is due to the existence of Ti. The Si-Ti-O system can produce a liquid phase above 1550 °C [20] and the amount of the liquid phase increases with increasing Ti content. Accordingly, the formation of Si-Ti-Y-O-N liquid phase accelerated the α-/β-Si_3N_4 phase transformation, and the transformation was accelerated consistently with Ti content in the Y-Ti-PHPS-derived powders.

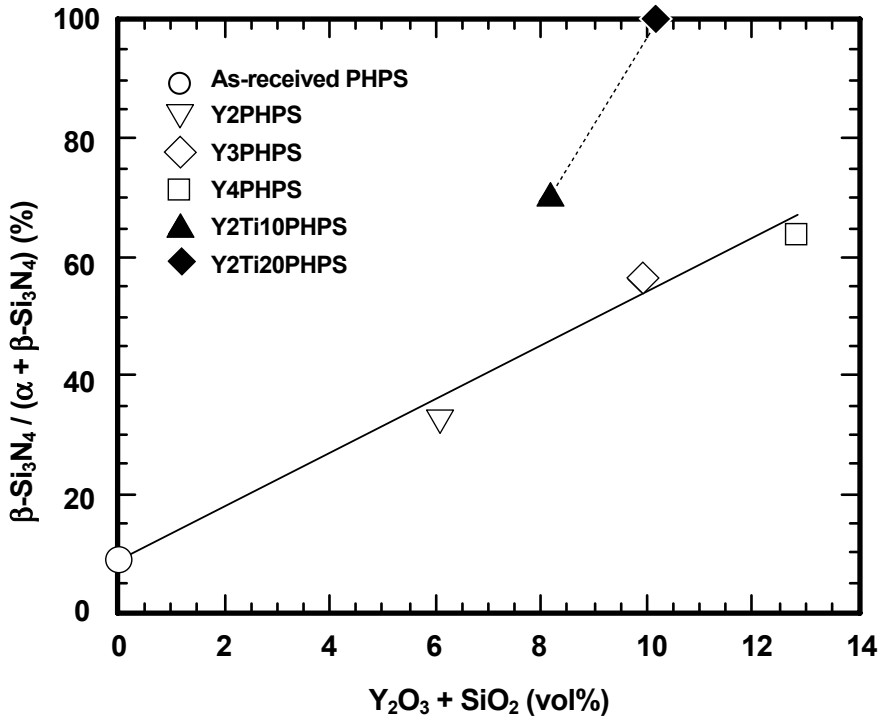

Fig. 5-5. Relation between total amount of sintering additives and β / (β + α) phase ratio of Si_3N_4 after heat treatment at 1600 °C.

5.3.3. Microstructure of hot-pressed samples

The polymeric precursor-derived powders were also fully crystallized during hot pressing up to 1800 °C for 1h (Fig. 5-2), and relative densities of Y2PHPS-, Y2Ti10PHPS- and Y2Ti20PHPS-derived ceramics reached 99.0, 99.5 and 99.2 %, respectively. Figure 5-6 shows polished and plasma etched sections of the hot pressed-samples, and the β-Si_3N_4 matrix grain size distributions of these samples are shown in Fig. 5-7. Y2PHPS yielded an extremely bimodal microstructure composed of large rod-like grains and fine needle-like grains (Fig. 5-6 (a)). The large rod-like grains are in a size range of about 2 to 4 μm in diameter and 4 to 20 μm in length. The fine needle-like grains are submicron in diameter and smaller than 3.5 μm in length (Fig. 5-7 (a)). Compared with Y2PHPS, Y2Ti10PHPS yielded a uniform microstructure composed of fine rod-like β-Si_3N_4 matrix grains of submicron in diameter and smaller than 3.5 μm in length (Figs. 5-6 (b) and 5-7 (b)). Y2Ti20PHPS yielded a uniform and extremely fine microstructure composed of β-Si_3N_4 matrix grains of submicron in diameter and smaller than 2.5 μm in length (Figs. 5-6 (c) and 5-7 (c)).

The bimodal microstructure development observed in the Y2PHPS-derived ceramics can be explained by relating to the slow α-/β-Si_3N_4 phase transformation as shown in Figs. 5-4 and 5-5. As formerly discussed, the α-/β-Si_3N_4 phase transformation through liquid phase involved the dissolution of α-Si_3N_4 into liquid phase, saturation of the liquid phase with dissolved Si and N atoms/ions and the nucleation of β-Si_3N_4 on the nucleation site. As nucleation sites, preexisting β-Si_3N_4 in the starting Si_3N_4 powder and liquid matrix were first suggested [21]. Recently, core structures of small β-Si_3N_4 grains within β-SiAlON and small α-Si_3N_4 grains within α- or β-SiAlON were also reported as nucleating sites [22-24]. As shown in Fig. 5-3(a), Y2PHPS-derived amorphous powders were free from preexisting β-Si_3N_4. Among other possible nucleation sites, in-situ produced β-Si_3N_4 in the Y2PHPS-derived powders is thought to be the most favorable one due to its same crystal structure. The β-Si_3N_4 content at 1400 °C of Y2PHPS-derived powders was 12.5 %. Even at 1600 °C, the content was as low as 32.2 %. During hot pressing from 1400 to 1800 °C, the small amount of β-Si_3N_4 could act as selected nucleation sites to grow as large rod-like grains with consumption of α-Si_3N_4. Consequently, Y2PHPS yielded the extremely bimodal microstructure.

On the other hand, the β-Si_3N_4 contents at 1600 °C of Y-Ti-PHPS-derived powders were above 70 %. Accordingly, higher number of β-Si_3N_4 grains could grow through Ostwald ripening during hot pressing from 1600 to 1800 °C, which lead to the microstructure uniformity observed in the Y-Ti-PHPS-derived ceramics.

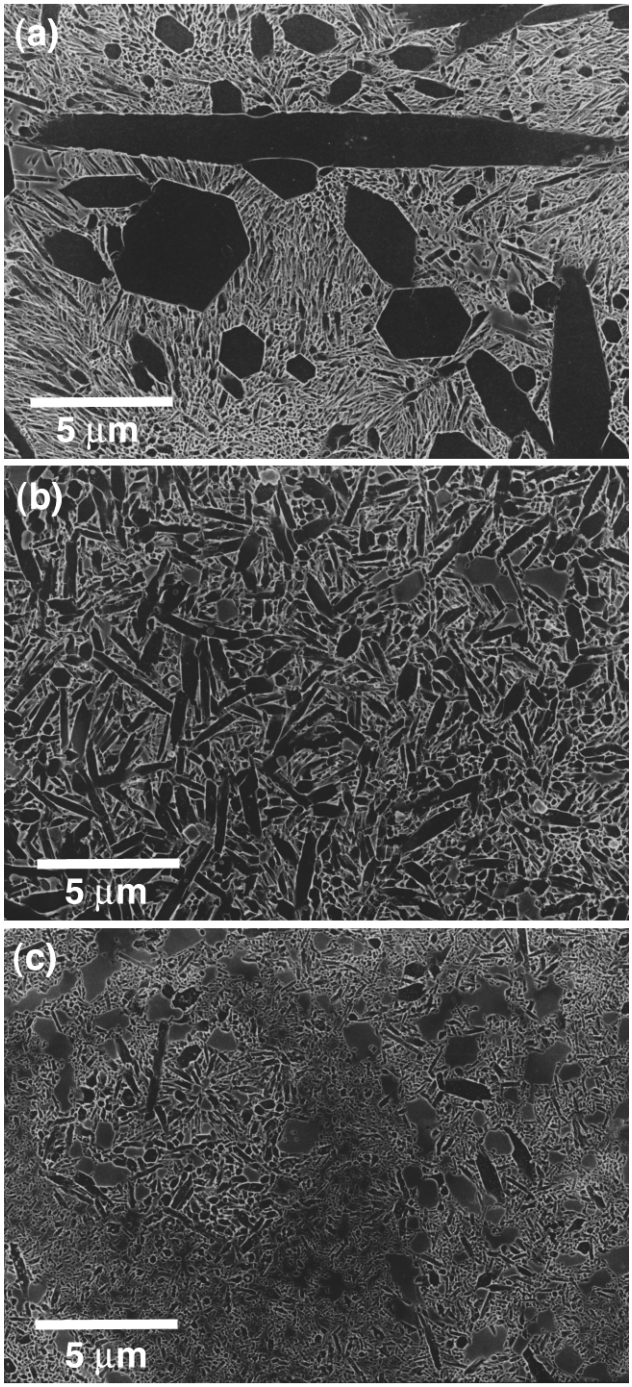

Fig. 5-6. Polished and plasma etched sections of hot-pressed samples. (a) Y2PHPS, (b) Y2Ti10PHPS and (c) Y2Ti20PHPS.

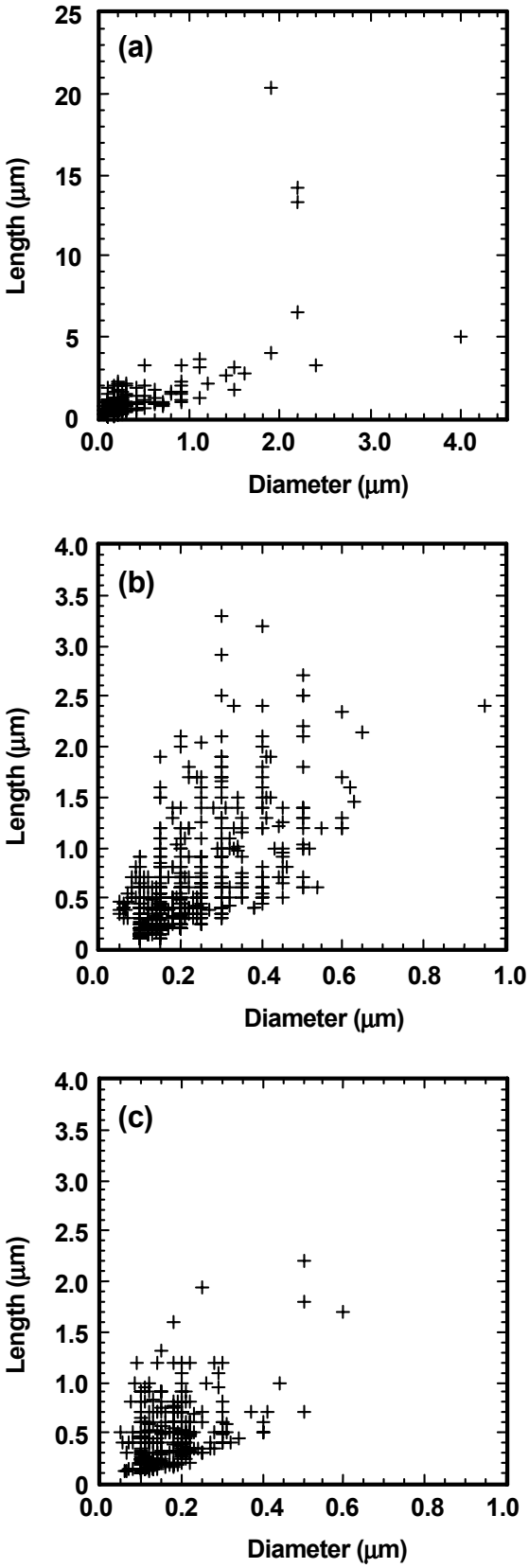

Fig. 5-7. β-Si_3N_4 matrix grain size distributions of hot-pressed samples. (a) Y2PHPS, (b) Y2Ti10PHPS and (c) Y2Ti20PHPS.

To study the dispersion behavior of Ti(C,N) phase, microstructures of Y-Ti-PHPS-derived ceramics were observed by TEM. As typical observation results, TEM images of Y2Ti10PHPS-derived ceramics are shown in Fig. 5-8. Fine particles with diameters of about 10-100 nm are observed within a β-Si_3N_4 matrix grain (Fig. 5-8 (a)). These particles are identified as Ti(C,N) phase by the elemental ratio map shown in Fig. 5-9. A large particle with a diameter of about 0.6 μm, which can be easily distinguished from β-Si_3N_4 matrix grains, is also observed (Fig. 5-8 (b), marked by an arrow). The large particle can be assigned as Ti(C,N) by the EDS analysis (Fig. 5-8 (c)). Further TEM observation confirmed that Ti(C,N) phase was dispersed as particles having a size range of about 10 nm to 1.6 μm and the Ti(C,N) particles with diameters larger than 0.5 μm were located at β-Si_3N_4 matrix grain boundaries.

The large Ti(C,N) particles located at β-Si_3N_4 matrix grain boundaries were thought to suppress β-Si_3N_4 matrix grain growth in the Y-Ti-PHPS-derived ceramics, which could especially contribute the microstructure refinement observed in the Y2Ti20PHPS-derived ceramics.

5.4. Conclusions

[Si-Yi-Ti-O-C-N] multicomponent amorphous powders were synthesized by pyrolysis at 1000 °C, in NH_3 flow, of chemically modified PHPS using $Y(OCH(CH_3)_2)_3$ and $Ti(N(CH_3)_2)_4$. The crystallization and microstructure development were studied by comparison with [Si-Y-O-C-N] amorphous powders derived from PHPS chemically modified with $Y(OCH(CH_3)_2)_3$.

Amorphous Si_3N_4 in the [Si-Y-Ti-O-C-N] powders was rather stable below 1400 °C in N_2. Above 1600 °C, Si-Y-Ti-O-N liquid phase accelerated the α-/β- phase transformation of Si_3N_4 and the [Si-Y-Ti-O-C-N] powders yielded β-Si_3N_4-Ti(C,N)-Y_2O_3 ceramics at 1800 °C. Fully dense β-Si_3N_4-Ti(C,N)-Y_2O_3 ceramics were successfully synthesized by hot pressing at 1800 °C in N_2. The resulting ceramics exhibited a uniform and fine-grained microstructure. Ti(C,N) phase was dispersed as particles having a size range of 10 nm to 1.6 μm and the large Ti(C,N) particles with diameters larger than 0.5 μm were located at the β-Si_3N_4 matrix boundaries. Titanium element in the [Si-Y-Ti-O-C-N] powders could act as a catalyst to accelerate α-/β-Si_3N_4 phase transformation as well as an in-situ source for nano/micro Ti(C,N) particles, which lead to the microstructure uniformity and refinement of Ti(C,N) nano/micro particle-dispersed Si_3N_4-Y_2O_3 ceramics.

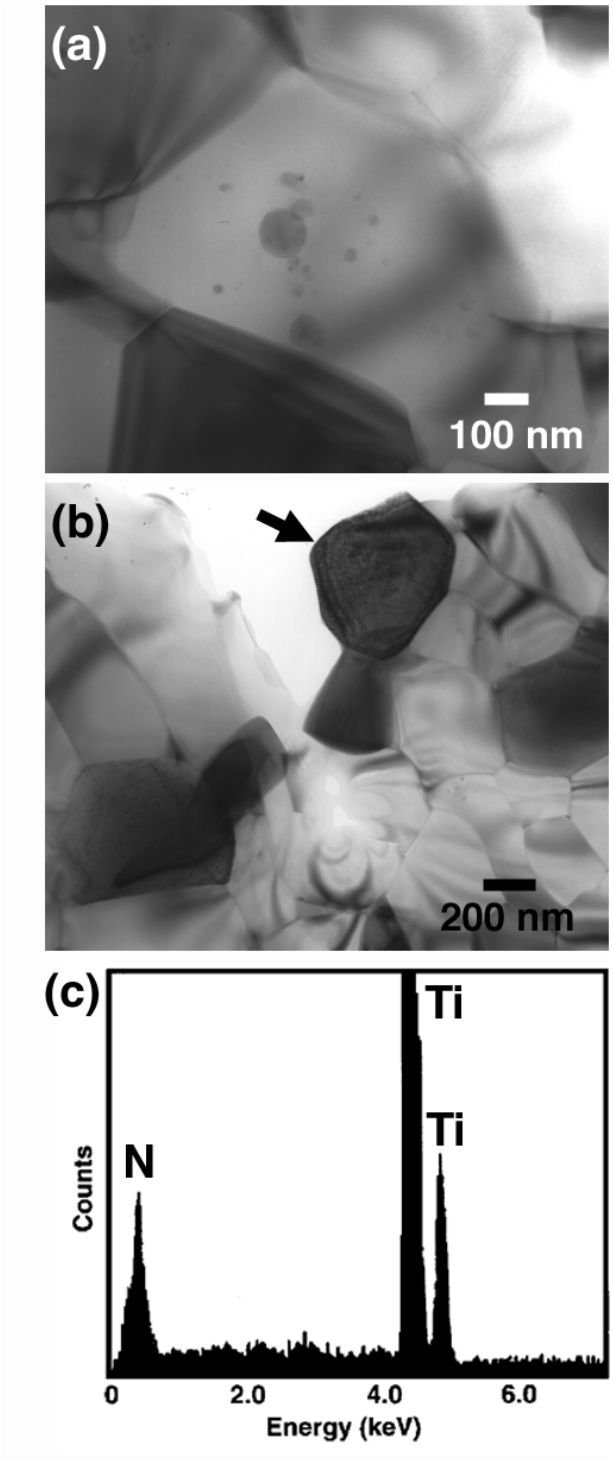

Fig. 5-8. TEM images of Y2Ti10PHPS-derived ceramics showing (a) fine particles located within a β-Si_3N_4 matrix grain and (b) a submicron particle (marked by an arrow), (c) EDS spectrum obtained from the particle marked by the arrow.

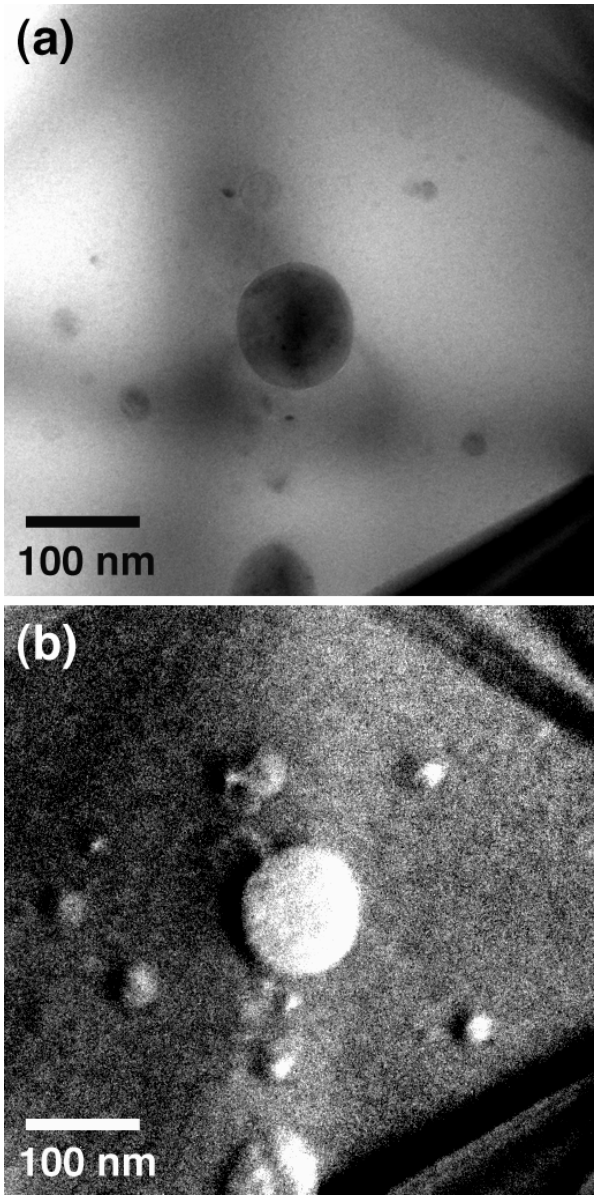

Fig. 5-9. TEM image and elemental ratio map of Y2Ti10PHPS-derived ceramics. (a) bright-field TEM image and (b) elemental Ti-L ratio map of titanium from the same field as shown in (a).

References

[1] H.-P. Baldus, M. Jansen and O. Wagner, "New Materials in the system Si-(N,C)-B and their characterization", pp. 75-80 in Silicon Nitride '93, Key Engineering materials Vol. 89-91, edited by M. J. Hoffmann, P. F. Becher and G. Petzow (Trans Tech Publications, Aedermannsdorf, Switzerland), 1994.

[2] O. Funayama, T. Kato, Y. Tashiro and T.Isoda, J. Am. Cerm. Soc., **76**, 717-723 (1993).

[3] O. Funayama, Y. Tashiro, T. Aoki and T. Isoda, J. Ceram. Soc. Japan, **102**, 908-912 (1994).

[4] J. Bill, J. Seitz, G. Thurn, J. Dürr, J. Canel, B. Z. Janos, A. Jalowiecki, A. Sauter, S. Schempp, H. P. Lamparter, J. Mayer and F. Aldinger, Phys. Stat. Solidi (a), **166**, 269-296 (1998).

[5] J. Bill and F. Aldinger, Adv. Mater., **7**, 775-87 (1995).

[6] Y. Iwamoto, K. Kikuta and S. Hirano, J. Ceram. Soc. Japan, **108**, 350-356 (2000).

[7] G. Ziegler, J. Heinrich and G. Wötting, J. Mater. Sci., **22**, 3041-86 (1987).

[8] M. Mitomo, "Microstructural Development During Liquid Phase Sintering of Silicon Nitride", pp. 93-108 in Silicon nitride ceramics 2, edited by M. Mitomo and S. Somiya (Uchida Rokakuho, Tokyo, Japan), 1990.

[9] A. Bellosi, S. Guicciardi and A. Tampieri, J. Europ. Ceram. Soc., **9**, 83-97 (1992).

[10] M. Herrmann, B. Balzer, Chr. Schbert and W. Hermel, J Europ. Ceram. Soc., **12**, 287-296 (1993).

[11] J. L. Huahg, Y. L.Chang and H. H. Lu, J. Mater. Res., **12**, 2337-44 (1997).

[12] M. Miyata, Y. Yasutomi, Y. Sawai and T. Kanai, J. Ceram. Soc. Japan, **105**, 761-777 (1997).

[13] T. Nagaoka, M. Yasuoka, K. Hirao and S. Kanzaki, J. Ceram. Soc. Japan, **100**, 617-620 (1992).

[14] T. Oyama, J. J. Appl. Phys., **11**, 760-761 (1972).

[15] K. H. Jack, J. Mater. Sci., **11**, 1135-58 (1976).

[16] M. Umebayashi and K. Kishi, "Sintering of β-Sialon", pp. 109-116 in Silicon nitride ceramics 2, edited by M. Mitomo and S. Somiya (Uchida Rokakuho, Tokyo, Japan), 1990.

[17] Y. Iwamoto, K. Kikuta and S. Hirano, J. Mater. Res., **13**, 353-361 (1998).

[18] C. P. Gazzara and D. R. Messier, Am. Ceram. Soc. Bull., **56**, 777-780 (1977).

[19] C. R. Blanchar and S. T. Schwab, J. Am. Ceram. Soc., **77**, 1729-39 (1994).

[20] R. C. DeVries, R. Roy and E. F. Osborn, Trans. Brit. Ceram. Soc., **53**, 525-540 (1954).

[21] J. Wess and W. A. Kaysser, p. 169 in Progress in Nitrogen Ceramics, edited by F. L. Riley (Martinus Nijhoff Publisher, The Hauge), 1983.

[22] M. Kramer, M. J. Hoffman and G. Petzow, J. Am. Ceram. Soc., **76**, 2778- 84 (1993).

[23] S-L. Hwang and I-W. Chen, J. Am. Ceram. Soc., **77**, 1711-18 (1994).

[24] S-L. Hwang and I-W. Chen, J. Am. Ceram. Soc., **77**, 1719-28 (1994).

Chapter 6

Design and synthesis of a novel "self-binder" for SiC ceramics, chemically modified polycarbosilane containing fluoroalkoxy groups

6.1. Introduction

SiC ceramics are well known for their high thermal and chemical stability, high strength, hardness and thermal conductivity. However, the strength of the SiC ceramics is sensitive to the size of defects due to their low fracture toughness. These features in the properties are originated from the strong covalent nature of SiC.

The microstructure control is one of the ways to improve the mechanical properties of ceramics. Strengthening leads to high allowable stress. Toughening leads to enhance the fracture strength when the increase in the size of fracture origin is prevented. As mentioned in the section 3.1, the enhancement in the mechanical properties has been achieved in ceramic composites. It is, however, difficult to toughen the monolithic ceramics without any reinforcements. The fracture strength often decreases due to the increase in defect size [1,2]. Thus, it is effective to decrease total amount of defects and the defect size for improving the reliability of the monolithic ceramics. Basically, an important method to decrease the size of defects in ceramics is to fabricate well-densified powder compacts as well as the microstructure control.

Recently, the development of SiC ceramics has become active by pyrolysis of silicon-based polymeric precursors [3-5]. This polymeric precursor route has some important advantages with respect to conventional powder metallurgy techniques: (1) the solubility and fluidity of the polymeric precursors afford potential routes for the preparation of SiC fibers [6-10] and coatings [11], and (2) design of ceramics with specific properties by using the polymeric precursors as a binder for green body forming in the conventional powder metallurgy route [12-14].

As mentioned in chapter 3, polycarbosilane (PCS) is the most typical polymeric precursor for SiC ceramics, and PCS can be chemically modified to yield binary systems such as SiC-TiC [15,16], SiC-ZrC [17,18] and SiC-Al_2O_3 [19,20]. If a polymeric SiC precursor is applied for the conventional powder metallurgy route of the monolithic SiC ceramics, the polymeric precursor can act both a compaction binder during forming and an in-situ source for microstructure control during sintering, which is expected to develop high quality monolithic SiC ceramics. Such a novel "self-binder" [21] can be flexibly designed and synthesized by chemical modification of PCS. In this chapter, chemically modified PCS containing fluoroalkoxy groups (PCSOCF1) has been designed and synthesized to improve the fluidity of PCS. This is expected to be essential for improving green density of SiC powder compacts when combined with SiC powders. The

chemical structure of the PCSOCF1 is studied using FT-IR. The effect of PCSOCF1 coating on green density of SiC powder compacts and pyrolysis behavior of PCSOCF1 on SiC powder surfaces are investigated to evaluate the PCSOCF1 as a "self-binder" for SiC ceramics.

6.2. Experimental procedure

6.2.1. Synthesis of PCSOCF1

Figure 6-1 shows a synthesis route for PCSOCF1. Commercially available PCS (Nippon Carbon Co. Ltd., Type L, mean molecular weight of 800, Tokyo, Japan) was selected as a starting polymer. This polymer consists of the same structural units as those of the PCS (Type S) used in chapter 3. Tetrahydrofuran (THF) and n-hexane were distilled and dried before use. 1H,1H,5H-octafluoro-1-pentanol ($CF_2H(CF_2)_3CH_2OH$, PCR Incorporated, reagent grade, Gainesville, FL, USA) was purified by distillation. Sodium hydride (NaH, Nakarai chemical, reagent grade, Tokyo, Japan) was washed with dry n-hexane before use. Chemical modification reaction of PCS was carried out under N_2 atmosphere.

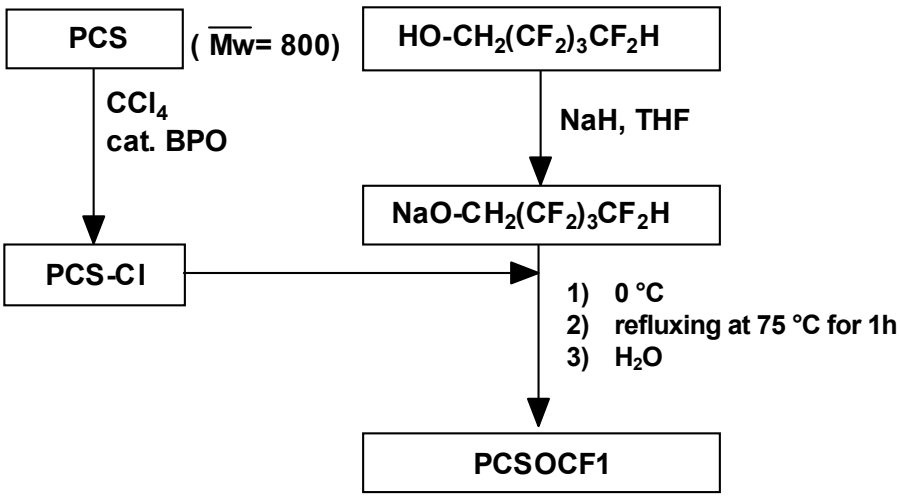

Fig. 6-1. Synthesis route for chemically modified PCS with $CHF_2(CF_2)_3CH_2OH$ (PCSOCF1).

The PCS was converted to PCS-Cl by the same procedure as described in the section 3.2.1 [22]. Sodium fluoroalkyl alkoxide ($CF_2H(CF_2)_3CH_2ONa$) was in-situ prepared from $CF_2H(CF_2)_3CH_2OH$ and NaH as follows: $CF_2H(CF_2)_3CH_2OH$ (4.98 g, 22 mmol) was added dropwise to a suspension of NaH (0.64 g, 26.6 mmol) in dry THF (100 ml) at 0 °C, then the mixture was stirred for 30 min at room temperature to give a suspension of $CF_2H(CF_2)_3CH_2ONa$ in THF. To this suspension, a solution of PCS-Cl (5 g) in dry THF (20 ml) was added dropwise at 0 °C, then the reaction mixture was refluxed at 75 °C for 3 h. After addition of ice-water, the mixture was stirred at room temperature for 1h in order to neutralize excess NaH and hydrolyze Si-Cl bonds which didn't react with $CF_2H(CF_2)_3CH_2ONa$, followed by concentrating in a rotary evaporator. The residue was suspended in water and extracted with toluene. The organic extracts were washed with water, saturated aqueous sodium chloride, dried over anhydrous magnesium sulfate, and concentrated in a rotary evaporator to give PCSOCF1 (8.6 g).

6.2.2. Preparation of PCSOCF1 coated-SiC powder compact

The synthesized PCSOCF1 was dissolved in acetone, and α-SiC powders (d_{50}=0.45 μm, DU-A1, Showa-Denko, Tokyo, Japan) were soaked in the solution for 24 h at room temperature. The amount of PCSOCF1 was 5 wt% of the total weight of the mixture with SiC powders. The suspension was dried, sieved and uniaxially pressed at 64 MPa into pellets of 14 mm diameter.

6.2.3. Characterization

The green densities were calculated by measuring the weight and volume of the green pellets. Relative density (RD) was calculated using the theoretical density of SiC (3.21 x 10^3 kg/m^3) and that of as-received PCS or PCSOCF1 (1.1 x 10^3 kg/m^3).

FT-IR spectra were recorded on KBr pellets containing samples as described in the section 2.2.3. TGA was performed on PCSOCF1 coated-SiC powders up to 1000 °C at a heating rate of 10 °C/min under helium (He) flow (Model Thermoflex TAS 300, Rigaku, Tokyo, Japan). Mass analysis of PCSOCF1 during pyrolysis was recorded using a gas chromatograph mass spectrometer (Model PARVUM QP-500, Shimadzu Co., Tokyo, Japan). Elemental analyses of oxygen and fluorine were performed on the PCSOCF1-coated powders. After pyrolysis at 1000 °C, the crystallization behavior of PCSOCF1 was observed by TEM (Model JEM-100CX, JEOL, Tokyo, Japan). The sample was prepared from fine powders mixed with acetone on a micromesh screen.

6.3. Results and discussion

6.3.1. Characterization of PCSOCF1

Figure 6-2 shows FT-IR spectra of polymer samples and $CF_2H(CF_2)_3CH_2OH$. In the FT-IR spectrum of as-received PCS (Fig. 6-2 (a)), absorptions are observed at 2900, 2950 cm^{-1} (C-H), 2100 cm^{-1} (Si-H), 1350-1450 cm^{-1} (C-H), 1250 cm^{-1} ($Si-CH_3$), 1020 cm^{-1} ($Si-CH_2-Si$) and 840 cm^{-1} (Si-C). The spectrum of PCS-Cl shows a remarkable decrease in absorption intensity at 2100 cm^{-1} (Si-H) and a new absorption band at 490 cm^{-1} assigned to Si-Cl bonds (Fig. 6-2 (b)). $CF_2H(CF_2)_3CH_2OH$ has C-F bonds, which show strong absorption bands at 1143 and 1180 cm^{-1} [23] (Fig. 6-2 (c)). Compared with Fig. 6-2(b), in the FT-IR spectrum of PCSOCF1 (Fig. 6-2 (d)), the absorption band at 490 cm^{-1} disappears and new absorption bands are observed at 1143, 1180 cm^{-1} (C-F) and 1100 cm^{-1} (Si-O-C). These changes in Fig. 6-2 (d) reveal that Si-O-C bonds have been successfully formed by the reaction of Si-Cl bonds in PCS-Cl with $CHF_2(CF_2)_3CH_2ONa$.

Another weak and broad absorption band at 3350 cm^{-1} in Fig. 6-2 (d) is assigned to Si-OH groups, which is considered to be formed by hydrolization of unreacted Si-Cl bonds in PCSOCF1 during work-up process as mentioned in the experimental procedures. According to these FT-IR spectroscopic analyses, PCSOCF1 is a chemically modified PCS which has $CHF_2(CF_2)_3CH_2O$ groups as side chains.

6.3.2. Green density of SiC powders coated with PCSOCF1

Table 6-1 shows green density of SiC powder compacts. In the case of as-received SiC powders, the green density is 1.88 x 10^3 kg/m^3 (58.6 % RD). The green density can be improved to 1.94 x 10^3 kg/m^3 (62.6 % RD) by coating with 5wt%-as-received PCS, and further improved to 2.03 x 10^3 kg/m^3 (65.5 % RD) by coating with 5wt%-PCSOCF1. It is apparent that the green density is remarkably improved by coating with PCSOCF1, which is considered to be result in the increased fluidity given to PCS by the fluoroalkoxy groups.

Table 6-1. Green density of SiC powder compact.

SiC powder	Density (x 10^3 kg/m^3)	Relative density (%)
5 wt% PCSOCF1 coated	2.03	65.5
5 wt% PCS coated	1.94	62.6
As-received	1.88	58.6

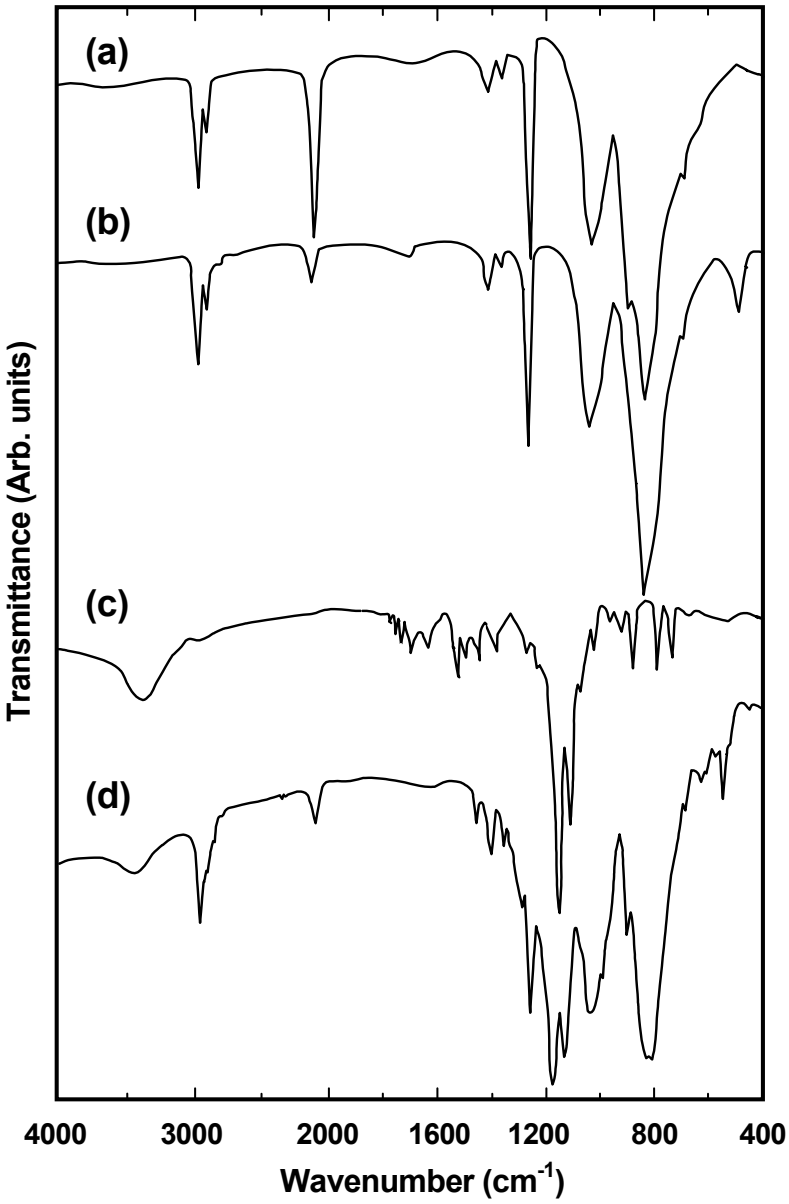

Fig. 6-2. FT-IR spectra of (a) as-received PCS, (b) PCS-Cl, (c) $CHF_2(CF_2)_3CH_2OH$ and (d) PCSOCF1.

6.3.3. Pyrolysis behavior of PCSOCF1 on SiC powders

The TG curve of PCSOCF1-coated SiC powders is shown in Fig. 6-3. Some gases measured by chromatograms with various mass numbers are also shown in Fig. 6-3. The TG curve shows that the weight loss starts at around 100 °C and is almost completed at 800 °C. At 1000 °C, the ceramic yield derived from PCSOCF1 is 24 wt%. It is slightly larger than that of as-received PCS itself (19 wt%). During pyrolysis from 300 °C to 600 °C, some gases measured by chromatograms with mass numbers (m/e) of 44, 51, 69, 77, and 81 were detected.

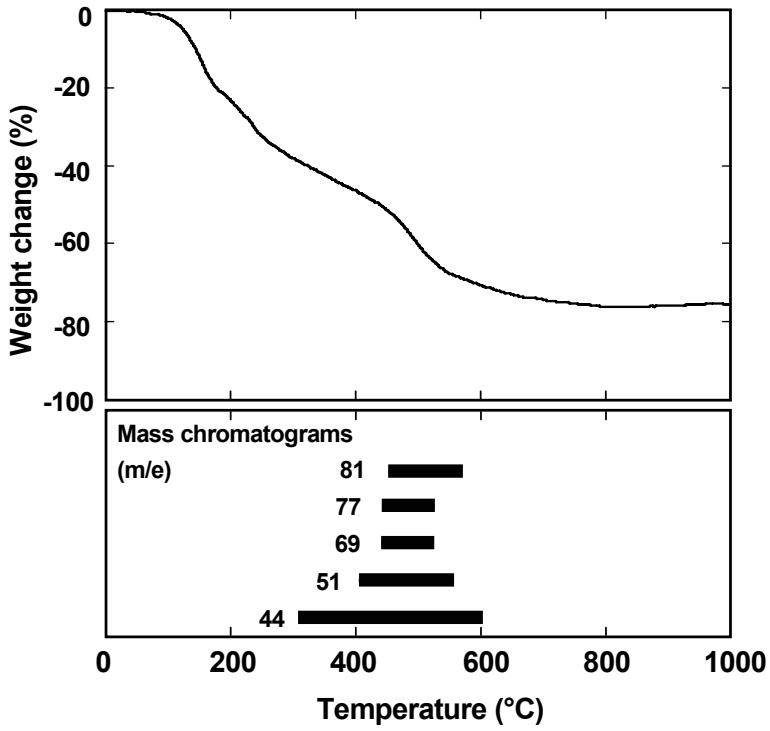

Fig. 6-3. TG curve of PCSOCF1 coated on SiC powders and some gases detected by chromarograms with various m/e (Heating rate :10 °C /min in He flow) .

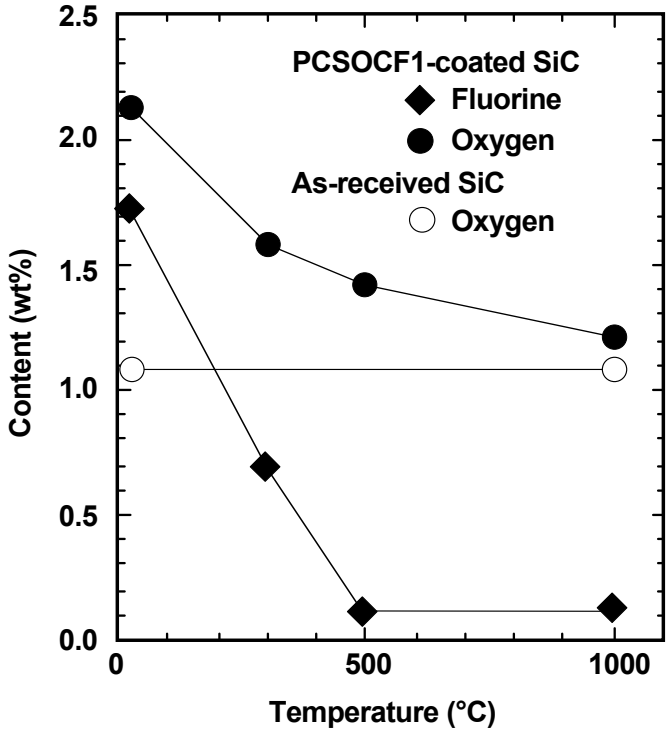

Fig. 6-4. Oxygen and fluorine content in PCSOCF1-coated SiC powders, and oxygen content in as-received SiC powders during pyrolysis.

Figure 6-4 shows oxygen and fluorine content of PCSOCF1-coated SiC powders, and oxygen content of as-received SiC powders. Both oxygen and fluorine in PCSOCF1-coated SiC powders decrease with increasing temperature, especially, a remarkable decrease in fluorine content is observed up to 500 °C and the fluorine content is less than 0.1 wt% above this temperature. The oxygen in as-received SiC powders is 1.1 wt% and constant up to 1000 °C.

The increase in the initial oxygen content of PCSOCF1-coated SiC powders was originated from PCSOCF1, and the oxygen and fluorine originated from PCSOCF1 were almost removed during pyrolysis up to 1000 °C. These chemical composition changes reveal that the side chains of $CHF_2(CF_2)_3CH_2O$ groups in PCSOCF1 were removed during pyrolysis from 300 °C to 500 °C. Some gases detected from 300 to 600 °C were considered as decomposition species of $Si\text{-}OCH_2(CF_2)_3CHF_2$ moieties in PCSOCF1 and their chromatograms with m/e of 44, 51, 69, 77, and 81 were considered as CO_2, CF_2H, CF_3, $Si(CH_3)_2F$ and $Si(CH_3)F_2$, respectively.

The weight loss at T< 300 °C is considered as volatilization of oligomers in PCSOCF1, while that observed at T > 600 °C is due to the decomposition of side chains such as $Si\text{-}CH_3$ groups, which are often observed during pyrolysis of various kinds of PCS [24,25]. The slight increase in ceramic yield after pyrolysis at 1000 °C is probably explained by interaction between PCSOCF1 and SiC powder surfaces, for example, Si-O-Si bond formation between Si-OH groups in PCSOCF1 and Si-OH groups existed on SiC powder surface, and PCSOCF1 yielded microcrystallite β-SiC on SiC powder surfaces after pyrolysis at 1000 °C as shown in Fig. 6-5. These results suggest that PCSOCF1 is useful for fabrication of monolithic SiC ceramics with controlled microstructure.

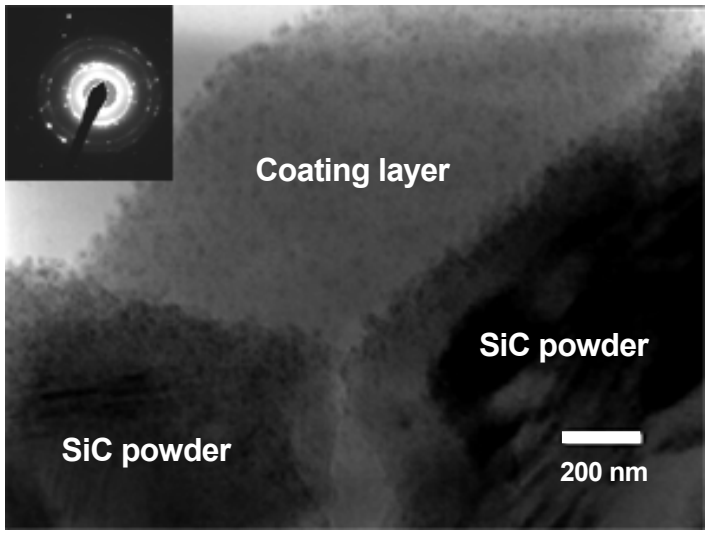

Fig. 6-5. TEM micrograph and selected-area diffraction pattern of PCSOCF1 on SiC powder surfaces after pyrolysis at 1000 °C.

6.4. Conclusions

Chemically modified PCS containing fluoroalkoxy groups as side chains (PCSOCF1) was successfully synthesized from a commercially available PCS and $CF_2H(CF_2)_3CH_2OH$. Coating of PCSOCF1 on SiC powders was found to be effective in increasing the green density of uniaxially pressed SiC powder compact, which was considered to be result in the increased fluidity given to PCS by the fluoroalkoxy groups. The fluoroalkoxy groups in PCSOCF1 were removed during pyrolysis from 300 °C to 500 °C and PCSOCF1 yielded β-SiC microcrystallites at 1000 °C.

These results suggest that PCSOCF1 has a potential as a novel "self-binder" for fabrication of monolithic SiC ceramics with controlled microstructure.

References

[1] K. Hirao, T. Nagaoka, M. E. Brito and S. Kanzaki, J. Am. Ceram. Soc., **77**, 1857-62 (1994).

[2] K. Ueno, Bull. Ceram. Soc. Japan, **18**, 1040-46 (1983).

[3] K. J. Wynne and R. W. Rice, Annu. Rev. Mater. Sci., **14**, 297-334 (1984).

[4] E. Bouillon, F. Langlais, R. Pailler, R. Naslain, F. Cruege, P. V. Huong, J. C. Sarthou, A. Delpuech, C. Laffon, P. Lagarde, M. Monthioux and A. Oberlin, J. Mater. Sci., **26**, 1333-45 (1991).

[5] R. Riedel and W. Dressler, Ceram. Int., **22**, 233-39 (1996).

[6] S. Yajima, J. Hayashi and M. Omori, Chem. Lett., No.9, 931-34 (1975).

[7] S. Yajima, J. Hayashi and M. Omori, J. Am. Ceram. Soc., **59**, 324-327 (1976).

[8] R. M. Laine and F. Babonneau, Chem. Mater., **5**, 260-79 (1993).

[9] M. Sugimoto, T. Shimoo, K. Okamura and T. Seguchi, J. Am. Ceram. Soc., **78**, 1849-52 (1995).

[10] G. Chollon, M. Czerniak, R. Pailler, X. Bourrat, R. Naslain, J. P. Pillot and R. Cannet, J. Mat. Sci., **32**, 893-911(1997).

[11] P. Colombo, T. E. Paulson and C. G. Pantano, J. Am. Ceram. Soc., **80**, 2333-40 (1997).

[12] S. Yajima, T. Shishido and K. Okamura, Ceramic Bulletin, **56**, 1060-63 (1977).

[13] Y. W. Kim and J. G. Lee, J. Mater. Sci., **27**, 4746-50 (1992).

[14] P. Czubarow and D. Seyferth, J. Mater. Sci., **32**, 2121-30 (1997).

[15] S. Yajima, T. Iwai, T. Yamanaka, K. Okamura and Y. Hasegawa, J. Mat. Sci., **16**, 1349-55 (1981).

[16] T. Ishikawa, T. Yamamura and K. Okamura, J. Mat. Sci., **27**, 6627-34 (1992).

[17] G. D. Sorarú, A. Ravagni and R. Campostrini, J. Europ. Ceram. Soc., **8**, 29-34 (1991).

[18] F. Babonneau and G. D. Sorarú, J. Eur. Ceram. Soc., **8**, 29-34 (1991).

[19] F. Babonneau, G. D. Sorarú, K. J. Thorne and J. D. Mackenzie, J. Am. Ceram. Soc., **74**, 1725-28 (1991).

[20] S. Okuzaki, Y. Iwamoto, S. Kondoh, K. Kikuta and S. Hirano, J. Mater. Res., **14**, 189-195 (1999).

[21] S. Hirano, Y. Iwamoto, Y. Sawai and T. Nagaoka, pp. 9-18 in Synergy Ceramics, edited by Fine Ceramics Research Association (Gihoudo, Tokyo, Japan), 2000.

[22] Y. Iwamoto, K. Kikuta and S. Hirano, J. Mater. Res., **14**, 1886-95 (1999).

[23] R. M. Silverstein, G. C. Bassler and T. C. Morrill, "Spectrometric Identification of Organic Compounds," 5th Edition, John Wiley & Sons, Inc., 1991.

[24] Y. Hasegawa, J. Mater. Sci., **24**, 1177-90 (1989).

[25] E. Bouillon, F. Langlais, R. Paller R. Naslain, F. Cruege, P. V. Huong, J. C. Sarthou, A. Delpuech, C. Laffon, P. Lagarde, M. Monthioux and A. Oberlin, J. Mater. Sci., **26**, 1333-45 (1991).

Chapter 7

Processing of SiC ceramics with high reliability using chemically modified PCS as a novel "self-binder"

7.1. Introduction

As investigated in the previous chapter, the chemically modified PCS containing fluoroalkoxy groups, PCSOCF1 was found to be effective in increasing the green density of uniaxially pressed SiC powder compact [1]. However, the ceramic yield of the PCSOCF1 coated on SiC powders limited to be low (24 %). This is due to the volatilization during pyrolysis of the lower molecular weight fraction of PCSOCF1.

It is essentially important for increasing the ceramic yield to form three-dimensional highly cross-linked preceramic network prior to pyrolysis [2,3]. Furthermore, this process provides a means to transform the precursors into infusible materials, which prevents the degradation of their shape by melting during pyrolysis at higher temperature. PCS can be cross-linked by air oxidation [4,5], or electron beam irradiation in a helium atmosphere [6,7]. In the case of PCSOCF1, it was expected to increase the ceramic yield by the same reaction in the air oxidation cross-linking process, Si-O-Si bond formation among the free Si-OH groups in PCSOCF1:

$$2Si{-}O{-}H \rightarrow \equiv Si{-}O{-}Si\equiv + H_2O \qquad (7.1)$$

However, the experimental result of the low ceramic yield showed that another strategy in precursor design must be necessary for the development of a novel "self-binder". In this chapter, another commercially available PCS with higher molecular weight fraction [8] has been selected as a starting polymer for the synthesis of chemically modified PCS with high ceramic yield. Additionally, the organofuluoric side chains have been introduced to the PCS using dimethoxymethyl-1H,1H,2H,2H-perfluorodecylsilane ($(CH_3O)_2Si(CH_3)CH_2CH_2(CF_2)_7CF_3$), which is expected to increase the ceramic yield by the formation of higher molecular weight compounds with ≡SiO-X-OSi≡ bridges ($X=Si(CH_3)CH_2CH_2(CF_2)_7CF_3$) like those in the chemically modified polysilazanes with higher ceramic yield [9-11]. Moreover, $(CH_3O)_2Si(CH_3)CH_2CH_2(CF_2)_7CF_3$ is expected to enhance the water repellency [12] as well as the fluidity of the PCS. Then, the resulting chemically modified PCS (PCSOCF2) has been applied for fabrication of monolithic SiC ceramics as a novel "self-binder". The chemical structure of the PCSOCF2 is characterized by ^{1}H-NMR and GPC analyses. The effects of PCSOCF2 coating on the SiC powder properties, green compacts and the mechanical properties of the sintered compact are studied.

7.2. Experimental Procedure

7.2.1. Synthesis of PCSOCF2

Figure 7-1 shows the synthesis route for PCSOCF2. Commercially available PCS (Nippon Carbon Co. Ltd., Type UH, mean molecular weight of 10700, Tokyo, Japan) was selected as a starting polymer. The PCS (10 g) was converted to PCS-Cl, followed by hydrolysis under the same procedure as described in the section 3.2.1 to give PCS-OH (9.2g). The PCS-OH (5.0g) and $(CH_3O)_2Si(CH_3)CH_2CH_2(CF_2)_7CF_3$ (3.0g, TOSHIBA silicone, TSL-8231,Tokyo, Japan) were dissolved into dry xylene (100ml). The mixture was refluxed at 140 °C for 24h in the presence of a catalytic amount of dry pyridine (1ml, Nakarai chemical, reagent grade,Tokyo, Japan), followed by concentrating in a rotary evaporator. The residue was washed using methanol to remove the excess $(CH_3O)_2Si(CH_3)CH_2CH_2(CF_2)_7CF_3$ and to give PCSOCF2 (5.5g).

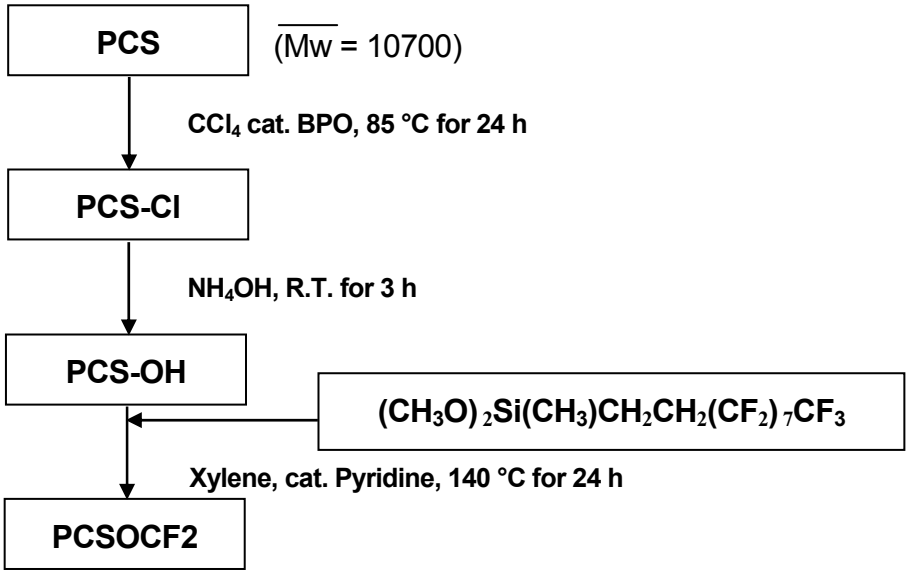

Fig. 7-1. Synthesis route for PCSOCF2.

7.2.2. Preparation of SiC powders and green compacts

The PCSOCF2 coated-SiC powders were prepared as follows: Calculated amount of toluene solution of PCSOCF2 was mixed with α-SiC powder (d_{50}=0.47 μm, DU-A1, Showa-Denko, Tokyo, Japan) and 0.5 wt% of boron (d_{50}=0.85 μm, Mitsuwa pure chemicals,Tokyo, Japan) as a

sintering aid by a glass mortar for 1.5h. The mixed slurry was then dried and sieved through a 250 μm screen. In this way, 1, 3, 5 and 10 wt% PCSOCF2 coated-SiC powders were prepared. On the other hand, one of the typical compaction binders for SiC powder is phenol, and phenol (Mitsubishi Co. Ltd., Novolac, Tokyo, Japan) coated-SiC powder was prepared by the same way as the PCSOCF2 coating using ethanol solvent. As other comparable samples, as-received PCS, polyvinyl alcohol (PVA, Shin-Etsu Chemical Co. Ltd., SMR-10M, Tokyo, Japan) and dextrin (Nippon Starch Chemical Co., Ltd., type 4-C, Tokyo, Japan) were also coated on SiC powders by the same way using ethanol or water solvent. Green compacts of the SiC sample powders were prepared by uniaxial pressing into pellets (15mm in diameter and 3mm in thickness) at a stress of 30MPa.

7.2.3. Hot pressing

The green compacts for hot pressing (40 x 50 x 10 mm) of 1, 3, 5 wt% PCSOCF2 or 3 wt% phenol coated-SiC powders were prepared under the same compaction conditions described above. The green compacts were placed in a graphite die and hot pressed in a graphite resistance-heated furnace (Model High Multi 10000, Fujidempa Kogyo, Osaka, Japan) under Ar atmosphere. The hot pressing condition consists of the following three steps: (1) Heating to 1000 °C at the rate of 100 °C/h for pyrolysis, (2) Heating to 1500 °C at the rate of 600 °C/h and holding at 1500 °C for 1h for the reduction of the surface oxide of SiC powders, and (3) Heating to 2050 °C at the rate of 600 °C/h and holding at 2050 °C for 15min at a hot pressing stress of 30 MPa.

7.2.4. Characterization

^{1}H-NMR and GPC analyses (Model System-21, Shodex Co., Tokyo, Japan) were performed on the polymer samples as described in the section 3.2.3.

TGA was performed on the polymer samples up to 1000 °C at a heating rate of 5 °C/min under Ar flow (Model TG-DTA2000, Mac Science, Tokyo, Japan). To investigate the crystallization behavior above 1000 °C, XRD measurements were performed on the heat treated-PCSOCF2 as described in the section 3.2.3.

Oxidation resistance of PCSOCF2 coated-SiC powders was evaluated as follows: The sample powders were left in a sealed vessel containing liquid water (i.e., in the wet air at room temperature). A comparable sample of the as-received SiC powder was also placed in the same vessel. The oxygen content of each powder sample was measured by the inert gas fusion method as described in the section 2.2.3.

Evaluation of powder fluidity and packing property was performed on the as-received, PCSOCF2 coated- and phenol coated-SiC powders by measuring the angle of repose of the sample powders on a spatula as well as measuring the tap density of the loosely accumulated sample powders. The angle of repose was determined by a restricted-pile method as shown in Fig. 7-2 (a). A spatula (120 x 22 mm) and a sieve of 0.21 mm mesh were used. The powder was passed slowly through the sieve onto the spatula. After the spatula was buried under the powder, the saucer was removed and the limit accumulation angle (θ_1) was measured. Next a small weight (50g) was dropped from the height of 160 mm on to one end of the spatula to knock off the loose surface powder, and the second limit accumulation angle (θ_2) was measured. The tap density was determined using a cup (100 ml) and a sieve of 0.21 mm mesh as shown in Fig. 7-2 (b). The powder was dropped from the height of 220 mm, passed slowly through the sieve into the cup. After the cup was buried under the powder, the loose surface powder was removed, and the weight of the powder in the cup, i.e. 100 ml, was measured. These measurements were carried out four times.

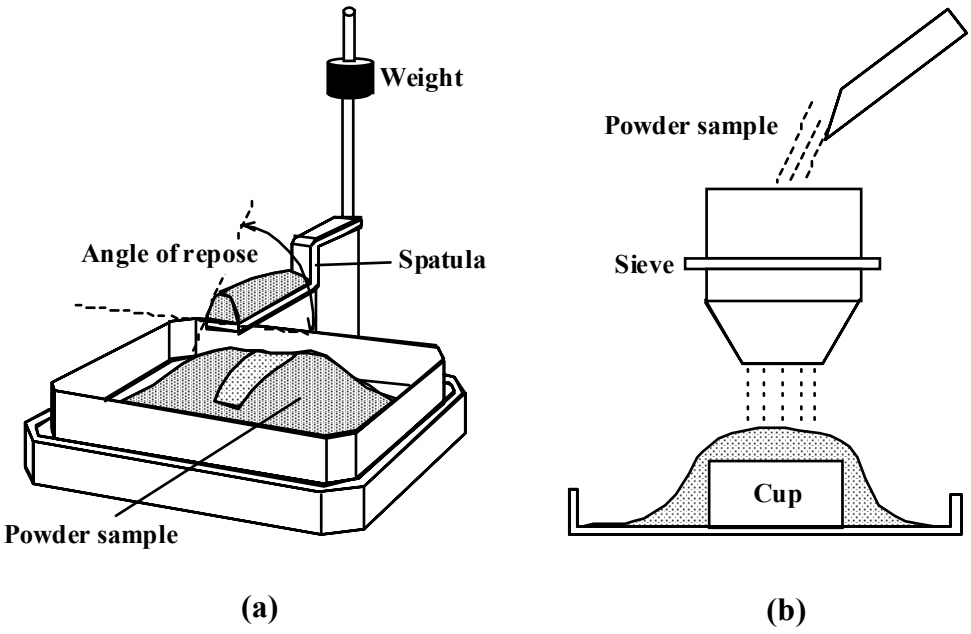

Fig. 7-2. Experimental system to measure (a) the angle of repose and (b) the tap density.

Relative densities of the green compacts were evaluated as a function of binder addition. The green densities were calculated by measuring the volume and the weight of the green compacts. The relative density was calculated using the theoretical density of SiC (3.21 x 10^3 kg/m^3) and that of PCSOCF2 or other binders (1.1 x 10^3 kg/m^3). Pore size distributions of all samples were obtained by a mercury porosimetry (Model Auto Pore 3, Shimadzu Co., Tokyo, Japan), under a pressure up to 413 MPa (6×10^4 psi). A contact angle of 130 ° was used to calculate pore radius.

Apparent density of hot pressed-samples was measured by the Archimedes method. Four point bending strengths were determined using a four point rupture test on 3 x 4 x 40 mm bar samples of which surfaces and edges were polished with diamond powder (0.5 μm). The fracture toughness was determined by the single-edge pre-cracked beam (SEPB) method. The microstructure was observed by SEM (Model S-800, Hitachi, Tokyo, Japan).

7.3. Results and discussion

7.3.1. Characterization of PCSOCF2

Figure 7-3 shows the ^{1}H-NMR spectra of polymer samples and $(CH_3O)_2Si(CH_3)CH_2CH_2(CF_2)_7CF_3$. As-received PCS presents two broad peaks at 0.18 ppm with two shoulders at -0.08 and -0.6 ppm (Si-CH_2/Si-CH_3/Si-CH-Si), and 4.3 ppm (Si-H). The relative peak intensity of Si-H to C-H is 0.09. In the spectrum of PCS-OH, a new broad peak appears at 1.6 ppm assigned to Si-OH groups, and the relative peak intensities to C-H of Si-H and Si-OH are 0.02 and 0.05, respectively. According to these spectroscopic analyses, about 56 % of the Si-H groups in as-received PCS have been successfully converted to Si-OH groups. However, the FT-IR spectrum of PCS-OH indicated that a small amount of Si-Cl bonds remained in PCS-OH.

$(CH_3O)_2Si(CH_3)CH_2CH_2(CF_2)_7CF_3$ presents four peaks at 0.16 ppm (Si-CH_3), 0.82 and 2.10 ppm (CH_2), and 3.54 ppm (O-CH_3) [13]. The spectrum of PCSOCF2 mainly consists of the peaks of PCS-OH and $(CH_3O)_2Si(CH_3)CH_2CH_2(CF_2)_7CF_3$. However, in the spectrum of PCSOCF2, the peak due to O-CH_3 groups at 3.54 ppm disappears and new peaks due to O-CH_3 appear at 3.40 and 3.50 ppm [13]. The peaks of CH_2 groups also become broader in comparison with those of $(CH_3O)_2Si(CH_3)CH_2CH_2(CF_2)_7CF_3$, indicating the influence of the polymer network.

The appearance of the new peaks due to the O-CH_3 group indicates that some of Si-O-CH_3 groups of $(CH_3O)_2Si(CH_3)CH_2CH_2(CF_2)_7CF_3$ are substituted by PCS-OH as shown in Eq. 7.2, and one of the new peaks at 3.40 and 3.50 ppm is possibly due to the O-CH_3 groups in PCS-O-CH_3, which could form from the produced CH_3OH and unreacted PCS-Cl.

$$PSC\text{-}OH + (H_3CO)_2Si(CH_3)R \xrightarrow[-\ HOCH_3]{} PCS\text{-}O\text{-}Si(OCH_3)(CH_3)R \quad (R=CH_2CH_2(CF_2)_7CF_3) \qquad (7.2)$$

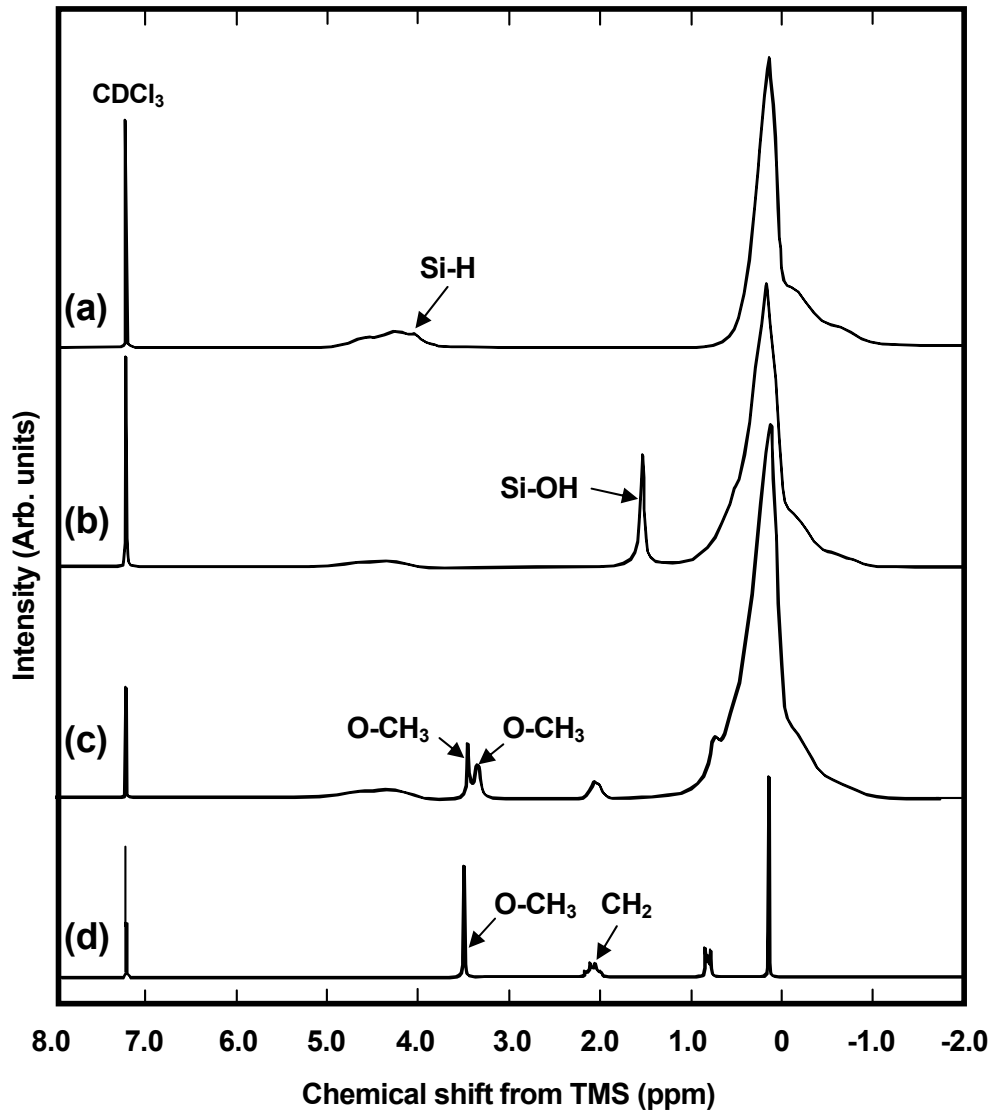

Fig. 7-3. ^{1}H-NMR spectra of (a) PCS, (b) PCS-OH, (c) PCSOCF2 and (d) $(CH_3O)_2Si(CH_3)CH_2CH_2(CF_2)_7CF_3$.

The results of the GPC analyses of PCSOCF2, PCS-OH and as-received PCS are shown in Fig. 7-4. Mean molecular weight ($\overline{Mw}$) of each polymer sample is also given in Fig. 7-4. $\overline{Mw}$ of PCSOCF2 is almost three times larger than that of as-received PCS or PCS-OH. It indicates that two OCH_3 sites of some $(CH_3O)_2Si(CH_3)CH_2CH_2(CF_2)_7CF_3$ are fully substituted by PCS-OH. According to these chemical structural analyses, PCSOCF2 most likely consists of the following functional groups as shown in Eq. 7.3.

$$PCS\text{-}O\text{-}Si(OCH_3)(CH_3)R, \quad (PCS\text{-}O)_2Si(CH_3)R, \quad (R=CH_2CH_2(CF_2)_7CF_3) \qquad (7.3)$$

The TG curves of the as-received PCS, PCS-OH, PCSOCF2 and PCSOCF2 coated on SiC powder are shown in Fig. 7-5. The weight loss of the as-received PCS starts at 100 °C, and a drastic weight loss appears at 550 °C to be completed at 700 °C in Ar. The ceramic yield of the as-received PCS is 85 %. The weight loss of PCSOCF2 starts at 200 °C and is completed at 700 °C in Ar. However, the large weight loss of PCSOCF2 starts at 400 °C, which is a relatively low temperature in comparison with that of the as-received PCS.

As investigated in the section 6.3.3, decomposition of the organofluoric groups in PCSOCF1 during pyrolysis causes the large weight loss at temperatures from 400 °C to 700 °C [1]. The difference in the ceramic yield of PCS-OH and PCSOCF2 indicates that 1g of PCSOCF2 contains 10^{-3} mol of organofluoric side chains.

The TG behavior of PCSOCF2 coated on SiC powder is similar to that of PCSOCF2 itself. Thus, the organofluoric groups of PCSOCF2 in the SiC powder compact may burned out completely at T > 700 °C. The ceramic yield of PCSOCF2 after heat treatment up to 1000 °C is reasonably high, i.e. 75 %. Compared with that of the PCSOCF1 investigated in the previous chapter, the ceramic yield has been successfully improved as designed for PCSOCF2 by use of the PCS (Type UH) with higher molecular weight fraction as a starting polymer as well as the chemical modification using $(CH_3O)_2Si(CH_3)CH_2CH_2(CF_2)_7CF_3$.

The XRD patterns of the PCSOCF2 heat-treated at 1000 °C, 1500 °C and 2050 °C are shown in Fig. 7-6. The heat treated-PCSOCF2 gives an amorphous phase at 1000 °C from which the crystallization into 3C-SiC phase starts at 1500 °C and completes at 2050 °C. Almost all the heat treated-PCSOCF2 converted to 3C-SiC crystallites.

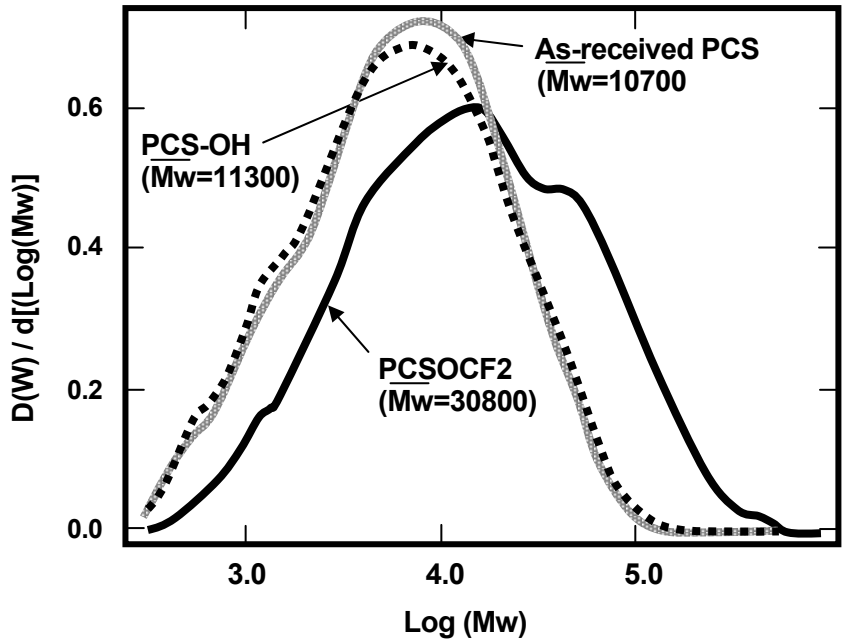

Fig. 7-4. Molecular weight distribution of as-received PCS, PCS-OH and PCSOCF2.

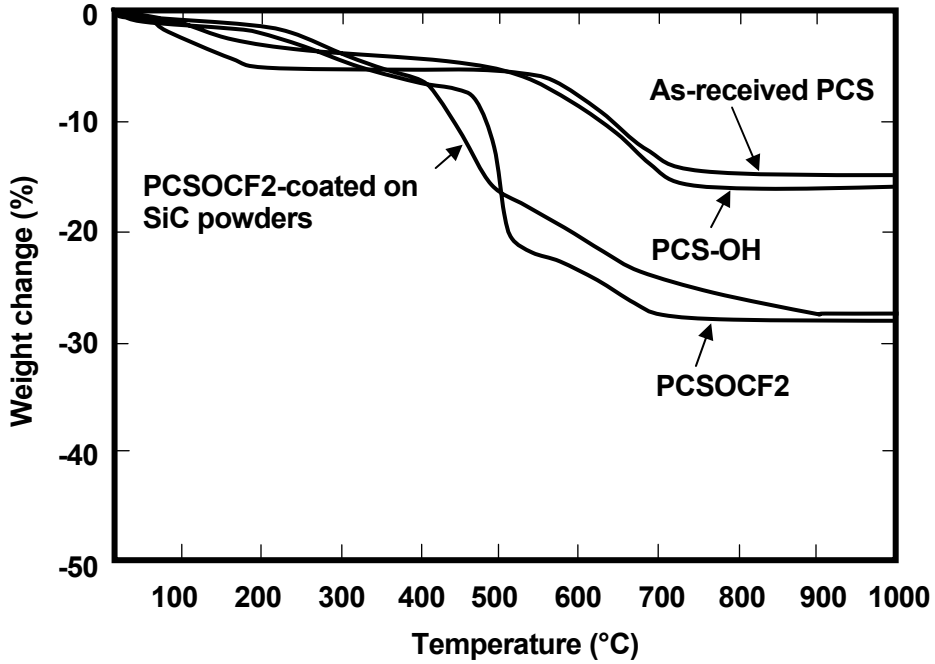

Fig. 7-5. TGA curves of as-received PCS, PCS-OH, PCSOCF2 and PCSOCF2 coated on SiC powders in flowing Ar (heating rae: 5 °C/min).

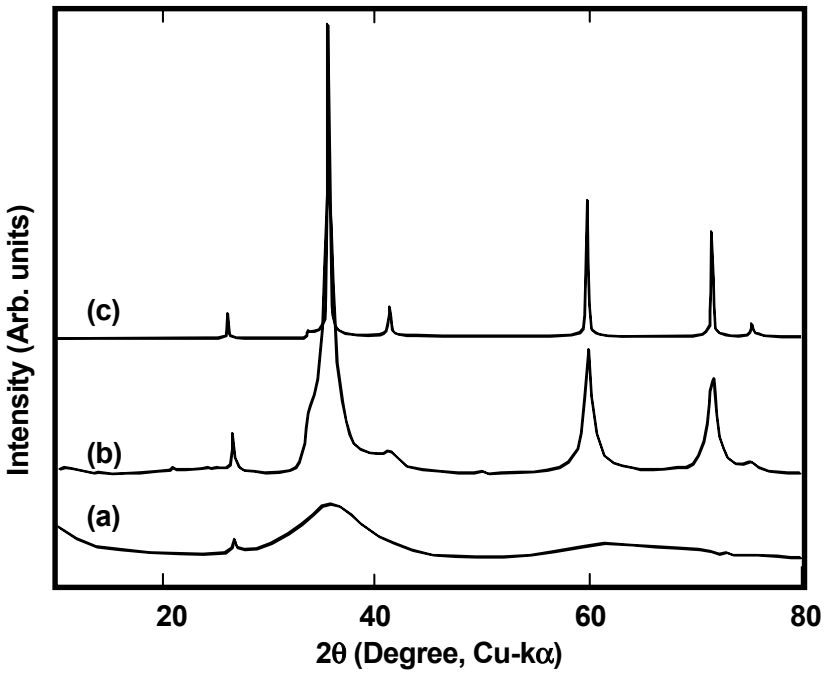

Fig. 7-6. XRD pattern of PCSOCF2 heat-treated at (a) 1000 °C, (b) 1500 °C and (c) 2050 °C in Ar (0.1MPa) .

7.3.2. Properties of PCSOCF2 coated-SiC powders

Figure 7-7 shows the oxygen contents of the PCSOCF2 coated-SiC powders left in wet air as a function of holding time. No significant change in the oxygen content can be observed in each PCSOCF2 coated-SiC powder sample, while the oxygen content of the as-received SiC powder increases to 2.0 wt% in 10 days. This means that the excellent water repellency could be achieved by modifying SiC powder surface with PCSOCF2.

The angles of repose of the powder samples on a spatula θ_1 and θ_2 are summarized in Fig. 7-8 (a). Both θ_1 and θ_2 of the 5 wt% PCSOCF2 coated-SiC powder are smaller than those of the as-received SiC and the 5 wt% phenol coated-SiC powders. The difference (θ_1 - θ_2) of the PCSOCF2 coated-SiC powder is larger than those of the as-received SiC and the phenol coated-SiC powders. The tap densities of the powder samples are summarized in Fig. 7-8 (b). The tap density of the 5 wt% PCSOCF2 coated-SiC powder is higher than that of the as-received SiC and the 5 wt% phenol coated-SiC powders.

These results suggest the improvement of powder fluidity by the PCSOCF2 coating leads to the highly dense accumulation, while the phenol coating conducts no improvement in the powder fluidity.

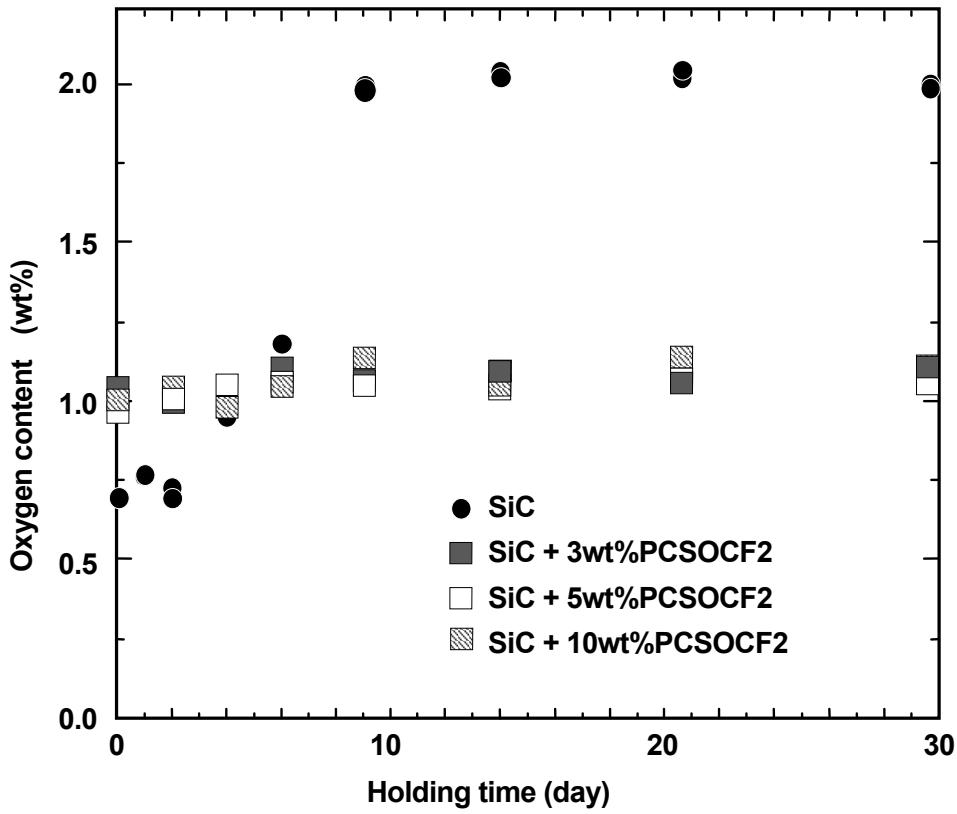

Fig. 7-7. Oxygen content of PCSOCF2 coated-SiC powder left in wet air as a function of holding time.

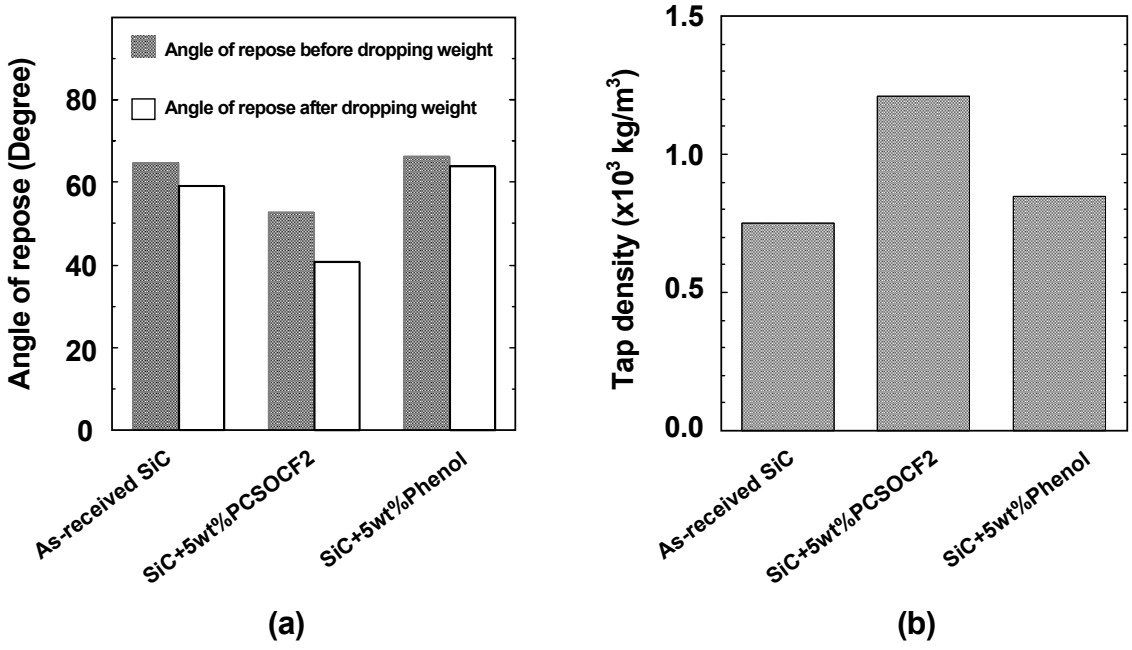

Fig. 7-8. Properties of powder samples. (a) the angles of repose and (b) the tap densities.

7.3.4. Properties of PCSOCF2 coated-SiC powder compacts

Figure 7-9 shows the relationship between the binder content and the relative green densities of the binder coated-SiC powder compacts under the same loading condition of 30 MPa. The relative green density of the PCSOCF2 coated-SiC compact is higher than those of the phenol coated- and other binder coated-SiC powder compacts.

Figure 7-10 (a) shows a comparison of the pore size distributions of the green compacts of the 5 wt% PCSOCF2 coated-SiC powder and the 5 wt% phenol coated-SiC powder. The peak position of pore size distribution of the PCSOCF2 coated-SiC powder compact is observed at about 0.07 μm, which is smaller than that of the phenol coated-SiC powder compact. The pore size distribution of the PCSOCF2 coated-SiC powder compact is sharper than that of the phenol coated-SiC powder compact. These results indicate that the PCSOCF2 coating does lubricate the SiC powders better than phenol, which results in higher compaction under the same loading condition.

Figure 7-10 (b) shows a comparison of the pore size distributions of the compacts after heat treatment at 1000 °C. No significant change in the peak position can be observed for each sample. However, the pore size distribution of the PCSOCF2 coated-SiC powder compact is still sharp, while that of the phenol coated-SiC powder compact becomes slightly broader than that of the green compact.

The properties of the SiC green compacts and the heat treated-compacts are summarized in Table 7-1. The mean pore size of the PCSOCF2 coated-SiC green compact is about the half of that of the phenol coated-SiC compact. The green density of the PCSOCF2 coated-SiC powder compact is larger, i.e. its porosity is smaller, than that of the phenol coated-SiC powder compact. After heat treatment up to 1000 °C, these SiC compacts show the decrease in density and the increase in mean pore size. However, the changes of the PCSOCF2 coated-SiC powder compact are smaller in comparison with those of the phenol coated-SiC powder compact.

Table 7-1. Properties of binder coated-SiC powder compacts.

Property	As-prepared		1000 °C heat-treated	
	5wt%Phenol	5wt%PCSOCF2	5wt%Phenol	5wt%PCSOCF2
Mean pore size (μm)	0.12	0.06	0.15	0.06
Density (10^3kg·m^{-3})	1.85	1.95	1.81	1.86
Porosity (%)	37.3	34.8	39.1	36.0
Relative density (%)	63.2	65.5	--	--

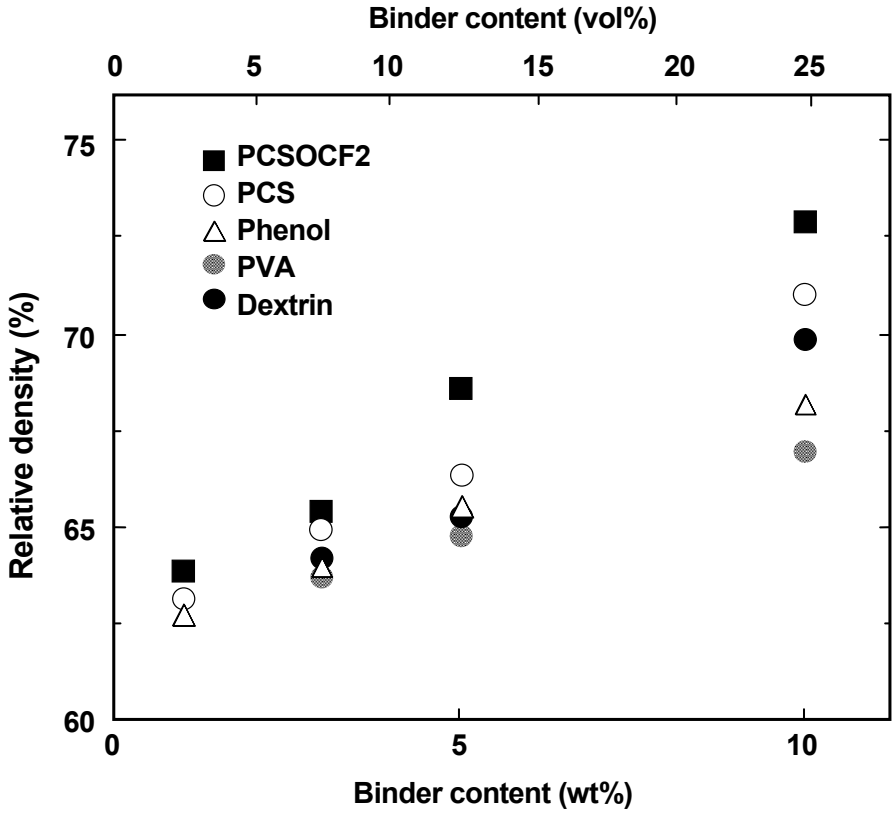

Fig. 7-9. Relationship between binder content and relative green density.

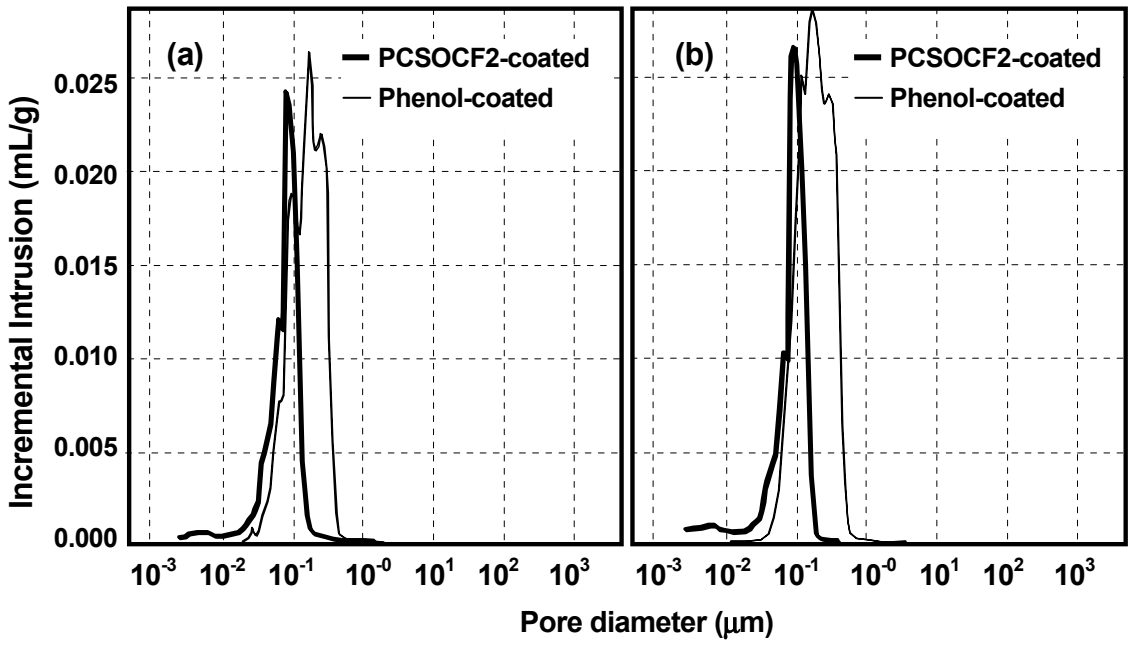

Fig. 7-10. Pore size distributions of SiC powder compacts. (a) as-prepared at room temperature and (b) after heat treatment at 1000 °C for 1h.

Assuming that the SiC particles are uniform spheres with diameter r_0 and are closest packed, the relative density of the compact is 74%, i.e., the volume fraction of binder filling up the gaps is 26 vol% (about 9 wt%), and the gap size is about $0.155r_0$ [14]. As shown in Fig. 7-9, the relative density of 74 %, i.e., near-closest packing is achieved by 10 wt% PCSOCF2 coating, while the relative densities of the green compacts using phenol and the other binders are lower than 70 %. The measured gap size of the PCSOCF2 coated-SiC power compact, i.e., the average pore diameter is 0.06 μm as shown in Table 7-1. The average particle size of the as-received SiC powder is 0.47 μm, and the calculated gap size of the closest packed compact is $0.155r_0$=0.07 μm, which agrees reasonably with the measured average pore diameter of 0.06 μm.

Phenol is commonly used as the compaction binder for SiC powders because it assists powder compaction and supplies carbon to remove the surface oxide of SiC powder. However, the phenol coating conducts no improvement in the powder fluidity and a considerable amount of the phenol could be burned out during heat treatment up to 1000 °C. On the other hand, PCSOCF2 contains free-carbon and can also supply carbon to remove the surface oxide of SiC powder. In addition, the PCSOCF2 coating remarkably improves the powder fluidity and packing, and its high ceramic yield (75 %) is also desirable. Thus, green compacts with high quality can be prepared by the PCSOCF2 coating.

7.3.4. Properties of sintered SiC compacts

Density and four point bending strength of the hot press sintered-samples are shown in Fig. 7-11. Density and bending strength of the sintered body derived from 3 wt% phenol coated-SiC powder (denoted as 3wt%-phenol/SiC) are plotted in the left part of the figure. Small amount of PCSOCF2 coating is effective for increase in density, which reflects the high green density of SiC powders. Coating of 10 wt% of PCSOCF2, however, decreases in density even if the relative density of the green compact is the highest. It may be due to trapping gases from PCSOCF2 during sintering.

Pore concentration variation in the sintered body possibly results from green density variations caused by particle-particle friction during forming, as well as from particle size variations in the starting material. Green density of the PCSOCF2 coated-SiC powder compact was higher than that of the phenol coated-SiC powder compact because of its excellent powder fluidity as shown in Figs. 7-9, so the higher density of the sintered body could be achieved by PCSOCF2 coating.

The bending strength slightly increases by PCSOCF2 coating (<10 wt%), and it takes the maximum (550 MPa) at 3 wt% PCSOCF2 coating. The scatter in strength values of the 3wt%-phenol/SiC is relatively large. However, the scatter was significantly decreased by

PCSOCF2 coating (3 to 5 wt%) and the mean value of the bending strength increased. Bending strength of the sintered compact with 5wt%- PCSOCF2 coating is slightly lower than that of the sintered compact with 3wt%- PCSOCF2 coating.

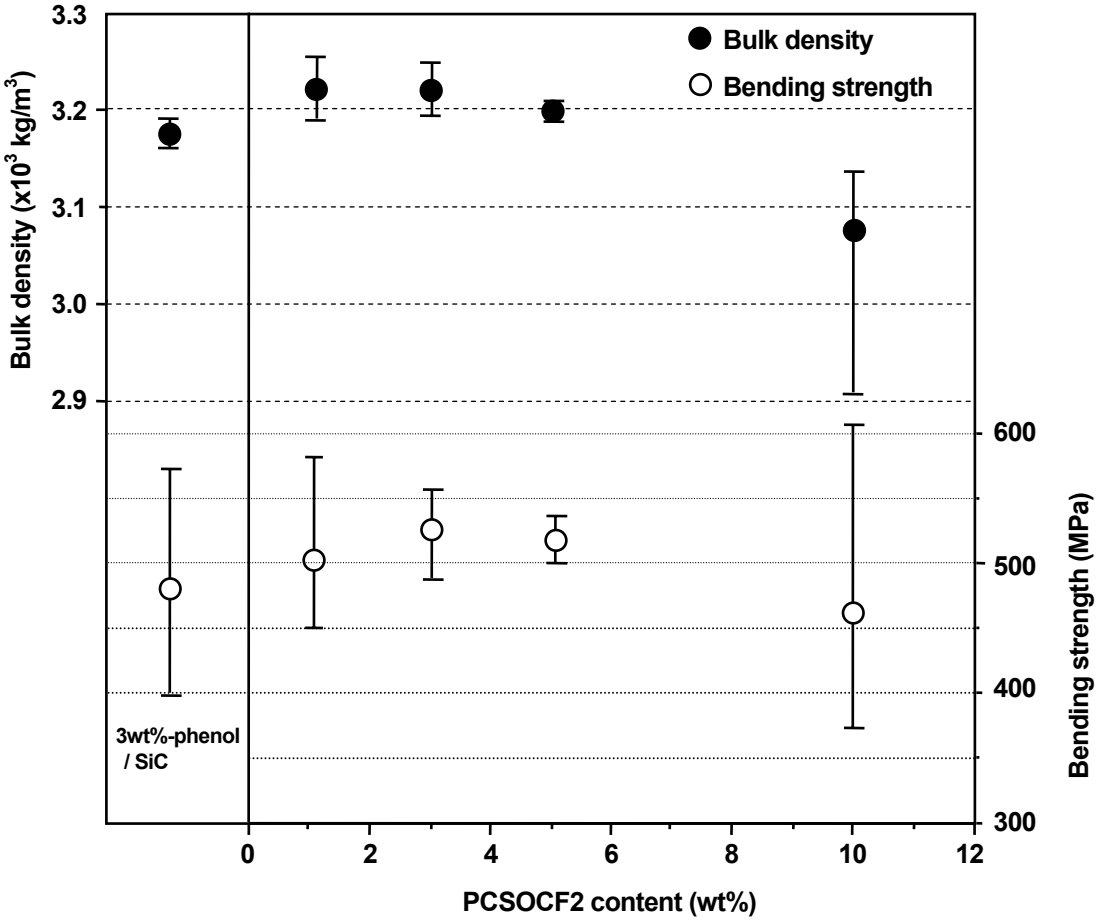

Fig. 7-11. Bulk density and four point bending strength of hot press sintered-SiC powder compacts as a function of PCSOCF2 content.

Figure 7-12 shows the polished and etched surfaces of the sintered compacts with different amount of PCSOCF2 coating (denoted as PCSOCF2/SiC). The 3wt%-PCSOCF2/SiC consists mainly of uniform fine grains (3 to 10 μm) containing a small amount of elongated grains. Constituent grains of the 5wt%-PCSOCF2/SiC are larger in comparison with those of the 3wt%-PCSOCF2/SiC, and the microstructure is very similar to that of the 3wt%-phenol/SiC. Lots of elongated grains can be seen in the 10wt%-PCSOCF2/SiC.

The fracture surface of each test piece was observed by SEM. Numbers of fracture surfaces were observed and the typical fracture surfaces are shown in Fig. 7-13. Both samples show the intra-grain fracture behavior. Some pores smaller than 1 μm can be seen at the fracture surface of the 3wt%-phenol/SiC, while no such pores can be seen at the fracture surface of the 5wt%-PCSOCF2/SiC.

Boron and carbon are used as the sintering aids in this investigation, and sintering of both samples occurs by the solid state process. In such a case, the interface between two solid grains reaches equilibrium by the surface diffusion process and the large pores remain in the sintered body. The critical radius, R, of the pore which is not eliminated during sintering is R=1.4r_0 in the first approximation, where r_0 is the average particle diameter of the starting powder [14]. The phenol coated-SiC powder compact contained pores larger than 1.4r_0 (0.7 μm) as shown in Fig. 7-10. Thus, the phenol/SiC contained pores as shown in Fig. 7-13, and its bending strength varied in wide range. The ceramic yield of the PCSOCF2 was as high as 75 %, and it converted to SiC phase as shown in Fig. 7-6, which fills up the gaps among the matrix grains. Therefore, comparing with the phenol coated-SiC powder compact, pore size distribution of the PCSOCF2 coated-SiC powder compact was sharp and the mean pore diameter was small, thus the sintered body may contain smaller amount of pores, which results in the decrease in scatter of the strength value.

Fracture toughness of all the sintered compacts is almost constant at about 3.0 MPa· $m^{1/2}$. Thus, the bending strength increased and the scatter in strength values decreased by PCSOCF2 coating (<10 wt%) without decreasing the fracture toughness.

It can be concluded that the PCSOCF2 coating is very effective to improve in water repellency, fluidity and packing property of SiC powder and ceramic conversion in high yield, which results in high reliability of the sintered body in terms of the less scatter of the fracture strength. However, too much PCSOCF2 addition (10 wt% or more) enhances the grain growth of SiC, which possibly results in the decrease in the bending strength. Thus, small amount of PCSOCF2 coating (3 to 5 wt%) is effective for increase in the density, increase in the bending strength, and decrease in the scatter in strength values of the SiC sintered body.

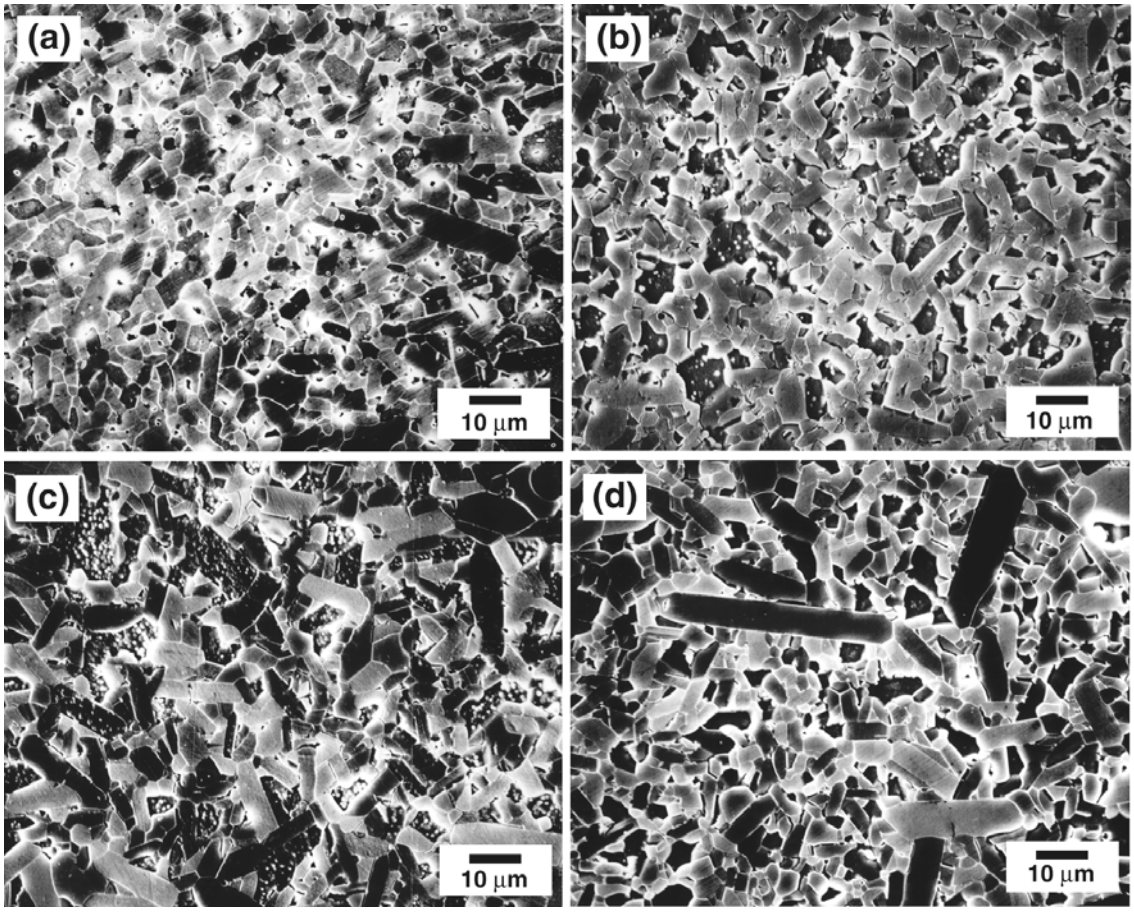

Fig. 7-12. SEM images of polished and chemically etched sections of sintered body of SiC-0.5wt% boron with (a) 3wt%-phenol, (b) 3wt%-PCSOCF2, (c) 5wt%-PCSOCF2 and (d) 10wt%-PCSOCF2.

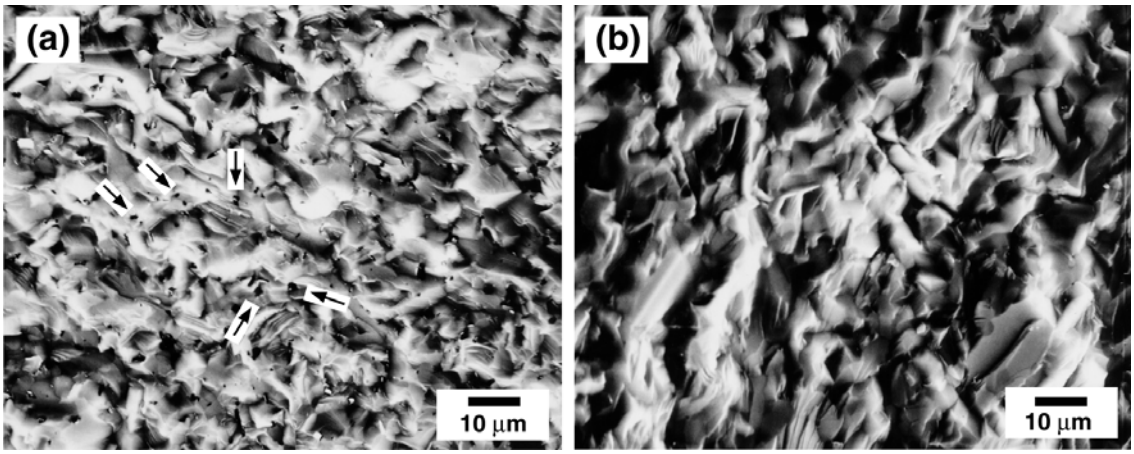

Fig. 7-13. SEM images of the fracture surfaces of SiC-0.5wt%boron with (a) 3wt%-phenol and (b) 5wt%-PCSOCF2.

7.4. Conclusions

Chemically modified PCS containing organofluoric groups as side chains, PCSOCF2, was successfully synthesized from commercially available PCS and $(CH_3O)_2Si(CH_3)CH_2CH_2(CF_2)_7CF_3$. The PCSOCF2 was applied for fabrication of monolithic SiC ceramics as a novel "self-binder". The results are summarized as follows:

(1) Reasonably high ceramic yield of 75 % was achieved in PCSOCF2 by use of commercially available PCS with higher molecular weight fractions as a starting polymer.

(2) PCSOCF2 coated-SiC powders showed excellent oxidation resistance.

PCSOCF2 coated-SiC powder showed improved fluidity and packing properties owing to the organofluoric side chains of the PCSOCF2 as follows:

(3) Angle of repose of the PCSOCF2 coated-SiC powder was lower than that of the phenol coated-SiC powders.

(4) Tap density of the PCSOCF2 coated-SiC powder was higher than that of the phenol coated SiC-powder.

(5) Green densities of the PCSOCF2 coated-SiC powders were higher than that of the phenol- or the other binder coated-SiC powders at 1 wt% to 10 wt% additions.

(6) Average pore diameter of the PCSOCF2 coated-SiC powder compact was smaller than that of the phenol coated-SiC powder compact.

(7) Pore size distribution of the PCSOCF2 coated-SiC powder compact was sharper and its peak pore diameter was smaller than those of the phenol coated-SiC powder compact.

The conclusion (3) to (7) indicated that the PCSOCF2 coating did lubricate the SiC powders better than phenol, which resulted in higher compaction for the same loading conditions. So the PCSOCF2 coated-SiC powder compact contained less large pores. Therefore, mechanical strength of the PCSOCF2/SiC hot press sintered-body was improved as follows:

(8) Four point bending strength was increased by PCSOCF2 coating, and it took the maximum (550 MPa) at 3 wt% PCSOCF2 coating.

(9) The scatter in bending strength values of the hot press sintered SiC significantly decreased by PCSOCF2 coating.

Microstructure study revealed that too much PCSOCF2 addition (10 wt% or more) enhanced the partial grain growth of SiC, which possibly resulted in the decrease in the bending strength. Thus, small amount of PCSOCF2 coating (3 to 5 wt%) was effective for controlling the uniform microstructure, the increase in the density, the increase in the bending strength and the decrease in the scatter of the strength values. These results indicated that the PCSOCF2 is useful as a novel "self-binder" for fabrication of monolithic SiC ceramics with uniform microstructure.

References

[1] Y. Iwamoto, S. Okuzaki, K. Kikuta and S. Hirano, Ceram. Trans., **83**, 77-82 (1998).

[2] Y. D. Blum, K. B. Schwartz and R. M. Laine, J. Mater. Sci., **24**, 1707-11 (1989).

[3] J. Bill and F. Aldinger, Adv. Mater., 7, 775-787 (1995).

[4] Y. Hasegawa, M. Iimura and S. Yajima, J. Mater. Sci., **15**, 720-728 (1980).

[5] K. Okamura, "Continuous silicon carbide fibers", pp.73-88 in "Silicon carbide ceramics", edited by S. Somiya and Y. Inomata (Uchida Rokakuho, Tokyo, Japan), 1988.

[6] M. Takeda, Y. Imai, H. Ichikawa, T. Ishikawa, T. Seguchi and K. Okamura, Ceram. Eng. Sci. Proc., **12**[7-8], 1007-18 (1991).

[7] M. Takeda, Y. Imai, H. Ichikawa, T. Ishikawa, N. Kasai, T. Seguchi and K. Okamura, Ceram. Eng. Sci. Proc., **13**[7-8], 209-217 (1992).

[8] Nippon Carbon Co., LTD, Technical information, Polycarbosilanes "Nipusi®", 19, May, 1995.

[9] J. Bill, M. Friess, F. Aldinger and R. Riedel, "Doped Silicon Carbonitride: Synthesis, Characterization and Properties", pp. 605-615 in Better Ceramics Through Chemistry VI, Mat. Res. Soc. Symp. Proc. Vol. 346, edited by A. K. Cheetham, C. J. Brinker, M. L. Mecartney and C. Sanchez, (Materials Research Society, Pittsburgh, PA), 1994.

[10] O. Funayama, T. Kato, Y. Tashiro and T.Isoda, J. Am. Cerm. Soc., **76**, 717-723 (1993).

[11] O. Funayama, Y. Tashiro, T. Aoki and T. Isoda, J. Ceram. Soc. Japan, **102**, 908-912 (1994).

[12] K. Izumi, H. Tanaka, M. Murakami, T. Deguchi, A. Morita, T. Tohge and T. Minami, J. Non-Cryst. Solids, **121**, 347-358 (1991).

[13] R. M. Silverstein, G. C. Bassler and T. C. Morrill, "Spectrometric Identification of Organic Compounds," 5th Edition, John Wiley & Sons, Inc., 1991.

[14] W. D. Kingery, H. K. Bowen and D. R. Uhlmann, Chapter 10 in Introduction to Ceramics, 2nd Edition (John Wiley & Sons, Inc., USA), 1976.

Chapter 8

Conclusions

8.1. Summary

The design, synthesis and controlled conversion of polymeric precursors into ceramics can serve an opportunity to control the chemical composition, homogeneity of the ceramics at atomic or molecular size level, which is expected to develop novel nano/microstructure control technologies for ceramics through precursor design. However, few papers have reported on the investigation to clarify the relationships between precursor chemistry, conversion process and the microstructure development of the precursor-derived ceramics.

In this study, novel polymeric precursors are designed and synthesized for Si_3N_4- and SiC-based ceramics (Fig. 8-1), then the microstructure development of the resulting ceramics are studied:

(1) Polymeric precursors composed of all the elements for Si_3N_4 matrix, secondary phase as reinforcement, and an additive for liquid phase sintering of Si_3N_4 matrix are designed and synthesized by chemical modification of PHPS. The polymeric precursors are found to be useful for synthesizing nano/micro particle-dispersed Si_3N_4-based composites. Novel nano/micro-structure control technologies for Si_3N_4-based composites are also proposed by controlling the chemical composition and structure of the polymeric precursors.

(2) Chemically modified PCS with fluoro-alkoxy or -alkyl side chains are designed and synthesized to develop a novel "self-binder" for SiC ceramics with controlled microstructure. The precursors are successfully applied for fabrication of SiC ceramics by conventional powder processing, and found to be useful as a novel "self-binder" for fabrication of SiC ceramics with uniform microstructure.

In chapter 1, the polymeric precursor route for Si-based non-oxide ceramics is reviewed from viewpoints of historical backgrounds, precursor chemistry and the strategy to develop novel microstructure control technologies for Si_3N_4- and SiC-based ceramics.

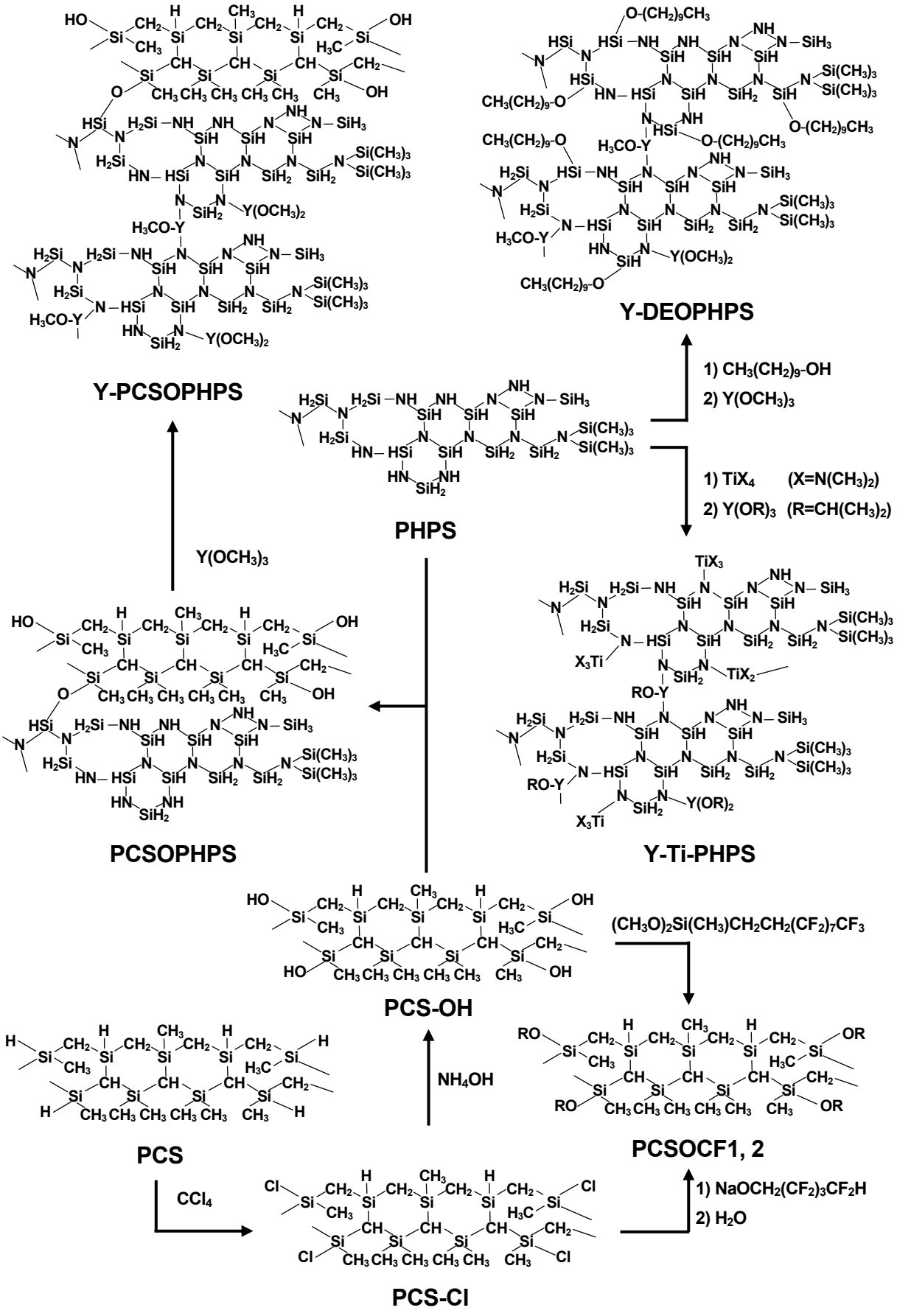

Fig. 8.1. Novel polymeric precursors for Si_3N_4- and SiC-based ceramics investigated in this study.

In chapter 2, a novel polymeric precursor, Y-DEOPHPS was designed and synthesized for SiC nano/micro-particle dispersed Si_3N_4-Y_2O_3 by chemical modification of PHPS with molecular carbon source of $CH_3(CH_2)_9OH$ for SiC nano/micro-particles, and $Y(OCH_3)_3$ as a precursor for sintering additive of Y_2O_3. FT-IR and ^{1}H-NMR spectroscopic analyses of the synthesized precursor revealed that $CH_3(CH_2)_9OH$ reacted mainly with SiH_2N_2 groups in PHPS to yield $CH_3(CH_2)_9O$-$Si(H)N_2$ groups, while $Y(OCH_3)_3$ reacted with N-H groups of PHPS to yield N-$Y(OCH_3)_{3-x}$ (x=1, 2) groups. Amorphous [Si-Y-O-C-N] multicomponent powders were successfully synthesized by pyrolysis of the precursor at 1000 °C in N_2. The amorphous [Si-Y-O-C-N] powders were converted into SiC nanoparticle-dispersed Si_3N_4-Y_2O_3 ceramics by heat treatment at 1800 °C in N_2. The microstructure was composed of β-Si_3N_4 whiskers with submicron in diameter and more than 10 μm in length. The unique microstructure development was explained by the slow densification cased by the volatilization of gases such as CO and SiO, which lead to the Si_3N_4 grain growth without steric hindrance.

In chapter 3, another novel polymeric precursor for Si_3N_4-SiC-Y_2O_3 ceramics, Y-PCSOPHPS was designed and synthesized to study the effect of chemical structure of polymeric precursors on the microstructure development of Si_3N_4-based composite. Y-PCSOPHPS was synthesized by block copolymerization of PHPS with PCS-OH, followed by chemical modification with $Y(OCH_3)_3$. Fully dense SiC nano/micro particle-dispersed Si_3N_4-Y_2O_3 ceramics were successfully synthesized by pyrolysis of the precursors at 1000 °C, followed by hot pressing at 1800°C in N_2. The resulting ceramics revealed that β-SiC particles were dispersed in a size range of about 10 to 600 nm, and a large amount of β-SiC submicrion particles were segregated at the β-Si_3N_4 matrix grain boundaries. The microstructure comparison of the fully dense Si_3N_4-SiC-Y_2O_3 ceramics derived from Y-PCSOPHS and Y-DEOPHPS revealed that the β-SiC dispersibility was strongly influenced by the chemical structure of the polymeric precursors: when the molecular carbon source was introduced to PHPS followed by chemical modification with $Y(OCH_3)_3$, the polymeric precursor yielded a uniform microstructure of β-SiC nano/micro particle-dispersed β-Si_3N_4-Y_2O_3 ceramics, while the yttrium modified block copolymer of PHPS and PCS-OH yielded rather unique binary ceramics composed of β-SiC-Y_2O_3 and β-SiC nano/micro particle-dispersed β-Si_3N_4-Y_2O_3 ceramics. Theses results indicated that the β-SiC dispersibility could be in-situ controlled at nano/micrometer scale level by controlling the chemical structure of polymeric precursors at molecular level.

In chapter 4, poly-titanosilazanes for [Si-Ti-(C)-N] multicomponent ceramic system such as TiN or Ti(C,N) nano/micro particle-dispersed Si_3N_4 based-ceramics were designed and synthesized by chemical modification of PHPS with TiX_4 (X=$N(CH_3)_2$, Cl, $OCH(CH_3)_2$). The chemical modification reactions were studied using FT-IR, ^{1}H- and ^{29}Si-NMR techniques, and the

poly-titanosilazanes were found to contain some N-Ti bonds. [Si-Ti-O-C-N] multicomponent amorphous ceramics were synthesized by pyrolysis of the poly-titanosilazanes at 1000 °C in NH_3. The oxygen impurity in the multicomponent amorphous ceramics could be minimized by use of $Ti(N(CH_3)_2)_4$ as a molecular titanium source for the synthesis of the poly-titanosilazane.

The amorphous silicon nitride derived from as-received PHPS crystallized at 1200 °C, while poly-titanosilazane derived from PHPS and $Ti(N(CH_3)_2)_4$ (TNPHPS) yielded TiN nanoparticle-dispersed amorphous [Si-Ti-O-C-N] ceramics up to 1400 °C in N_2, and Ti element was found to suppress crystallization of Si_3N_4. At 1600 to 1800 °C, the TNPHPS yielded Si_3N_4-Ti(C,N) ceramics. Ti(C,N) was observed as particles with diameters smaller than 100 nm, and the TNPHPS was found to be suitable for the synthesis of TiN or Ti(C,N) nano/micro particle-dispersed Si_3N_4-based ceramics.

In chapter 5, the effect of Ti element on the crystallization and microstructure development of Si_3N_4-Ti(C,N)-Y_2O_3 ceramics were studied from a viewpoint of microstructure control of the Si_3N_4-based ceramics through polymeric precursor route. The poly-titanosilazanes with TiSi atomic ratios of 0.1 and 0.2 were prepared, then further modified with $Y(OCH(CH_3)_2)_3$. [Si-Y-Ti-O-C-N] multicomponent amorphous powders were synthesized by pyrolysis of the precursors at 1000 °C in NH_3. The crystallization and microstructure development of Si_3N_4-Ti(C,N)-Y_2O_3 ceramics from the polymeric precursor-derived [Si-Y-Ti-O-C-N] multicomponent amorphous powders were studied by comparison with the polymeric precursor-derived [Si-Y-O-C-N] amorphous powders.

Amorphous silicon nitride in the [Si-Y-Ti-O-C-N] powders was rather stable below 1400 °C in N_2. Above 1600 °C, Si-Y-Ti-O-N liquid phase accelerated the α-/β- phase transformation of Si_3N_4 and the [Si-Y-Ti-O-C-N] powders yielded β-Si_3N_4-Ti(C,N)-Y_2O_3 ceramics at 1800 °C. Fully dense β-Si_3N_4-Ti(C,N)-Y_2O_3 ceramics were successfully synthesized by hot pressing at 1800 °C in N_2. The resulting ceramics exhibited a uniform and fine-grained microstructure. Ti(C,N) phase was found to be dispersed as particles having a size range of 10 nm to 1.6 μm, and the large Ti(C,N) particles with diameters larger than 0.5 μm were located at the β-Si_3N_4 matrix boundaries. Based on the results obtained by the XRD and chemical composition analyses, it was concluded that the Ti element in the [Si-Y-Ti-O-C-N] powders could act as a catalyst to accelerate α-/β-Si_3N_4 phase transformation by the [Si-Ti-Y-O-N]] liquid phase formation as well as an in-situ source for nano/micro Ti(C,N) particles, which lead to the microstructure uniformity and refinement of Si_3N_4-Ti(C,N)-Y_2O_3 ceramics.

In chapter 6, a novel “self-binder” for SiC ceramics, chemically modified PCS containing fluoroalkoxy groups as side chains (PCSOCF1) was designed and synthesized from a commercially available PCS and $CF_2H(CF_2)_3CH_2OH$. This was expected to be essential for improving green density of SiC powder compacts when combined with SiC powders.

Coating of PCSOCF1 on SiC powders was found to be effective in increasing the green density of uniaxially pressed SiC powder compact, which was considered to be result in the increased fluidity given to PCS by the fluoroalkoxy groups. TGA and TEM studies revealed that the fluoroalkoxy groups in PCSOCF1 were removed from 300 °C to 500 °C, and PCSOCF1 yielded β-SiC microcrystallites at 1000 °C. These results suggested that the design concept of PCSOCF1 fitted with the development of a novel "self-binder" for fabrication of monolithic SiC ceramics with controlled microstructure.

In chapter 7, another commercially available PCS with higher molecular weight fraction was selected as a starting polymer for the synthesis of chemically modified PCS with high ceramic yield. The organofuluoric side chains was introduced to the PCS using $(CH_3O)_2Si(CH_3)CH_2CH_2(CF_2)_7CF_3$, which was expected to enhance the water repellency as well as the fluidity of the PCS. Then, the resulting chemically modified PCS, PCSOCF2 was applied for fabrication of monolithic SiC ceramics by the conventional powder processing.

Reasonably high ceramic yield of 75% was achieved in PCSOCF2 by use of commercially available PCS with higher molecular weight fractions as a starting polymer. The PCSOCF2 coating on the SiC powders was found to be very effective to improve in water repellency, fluidity and packing property of SiC powders. Additionally, small amount of PCSOCF2 on to the SiC powders (3 to 5 wt%) was found to be effective for controlling the uniform microstructure of SiC ceramics. These findings resulted in high reliability of the sintered body in terms of the less scatter of the fracture strength. Based on these results, it was concluded that the PCSOCF2 was useful as a novel "self-binder" for fabrication of monolithic SiC ceramics with uniform microstructure.

8.2. Future aspects

The synthesis and characterization of novel polymeric precursors containing elements other than Si, N, or C are of great interest with respect to the investigation of microstructure development and properties of the derived ceramics. The results in this study indicate that the design and chemical synthesis of polymeric precursors can lead to develop novel thermally stable amorphous ceramic matrix composites as well as polycrystalline ceramics with tailored microstructure.

Further study on the polymerization and cross-linking conditions of the polymeric precursors developed in this study will be expected to control the solubility, fusibility or viscosity of the polymeric precursors, which can provide the versatility in shaping components like coatings and fibers. Additionally, the polymeric precursors can be expected to apply for the new processing method, direct transformation of polymeric green bodies into monolithic ceramics first reported by Riedel *et al*. in 1992 [1]. This method involves cross-linking of polymeric precursors into infusible

solids, milling the precursor-derived solids into fine powders, shaping green bodies followed by pyrolysis. This new process can take advantages of the polymeric precursor route for fabrication of ceramic components with complicated shapes. Furthermore, the warm pressing technique at cross-linking temperatures [2,3] can be expected to apply for further densification of SiC green compacts containing novel "self-binders" for SiC ceramics, which leads to enhance the reliability of the SiC bulk ceramic components. These further study on the polymeric precursor route for these Si-based non-oxide ceramics would promise to develop various components for high-temperature applications.

References

[1] R. Riedel, G. Passing, H. Schonfelder and R. J. Brooks, Nature, **355**, 714-716 (1992).

[2] J. Sienz and J. Bill, J. Mater. Sci. Lett., **15**, 391-393 (1995).

[3] C. Konetschny, D. Galusek, S. Reschke, C. Fasel and R. Riedel, J .Europ. Ceram. Soc., **19**, 2789-96 (1999).

Acknowledgements

The author would like to express his deepest appreciation to Associate Professor Takahisa Yamamoto at The University of Tokyo for reviewing this Ph.D. thesis. Likewise, the author would like to express his sincere garatitude to Associate Professor Minoru Nohara, Associate Professor Hatsumi Mori, Associate Professor Hiroyuki Inoue and Professor Yuichi Ikuhara at The University of Tokyo for the invigorating discussions presented during the cross examination of this dissertation which have been very helpful in completing this thesis.

The author wishes to express his special gratitude to Professor Shin-ichi Hirano and Associate Professor Ko-ichi Kikuta at Nagoya University for helpful discussions and advices throughout this research work at Precursor Design Group, Synergy Ceramics Laboratory. The author would like to express his appreciation to Dr. Hiroaki Yanagida, Senior Advisor at Japan Fine Ceramics Center (Professor Emeritus, The University of Tokyo), for providing me with the opportunity to study and work on this research at Precursor Design Group, Synergy Ceramics Laboratory. The auothor also would like to express his appreciation to Professor Dr. Ralf Riedel at Technische Universität Darmstadt (TUD), Germany for helpful discussions on the precursor chemistry during his stay at TUD.

The author would like to express his thanks to Mr. Tomohiro Saito for analytical TEM analyses at Japan Fine Ceramics Center, and Dr. Yuichi Sawai and Ms. Sachiko Okuzaki for helpful discussions on the development of a novel “self-binder” for SiC ceramics at Precursor Design Group, Synergy Ceramics Laboratory.

Lastly, I wish to express my sincere gratitude to my familes (Iwamoto and Hayami) who have always been close at heart throughout this research work. Without all their love and sacrifice, this dissertation would not be possible. Finally, I would like to dedicate my dissertation to my wife, Masami and my daughters, Ayaka and Lena.

This work was supported by NEDO as part of the Synergy Ceramics Project under the Industrial Science and Technology Frontier (ISTF) Program promoted by AIST, MITI, Japan. This research work was carried out at Precursor Design Group, Fine Ceramics Research Association, Synergy Ceramics Laboratory.

Yuji Iwamoto
July 2004

List of publications

I. List of publications related to this research

(1) Yuji Iwamoto, Ko-ichi Kikuta and Shin-ichi Hirano, "Microstructural development of Si_3N_4-SiC-Y_2O_3 ceramics derived from polymeric precursors", J. Mater. Res., **13**[2], 353-361 (1998).

(2) Yuji Iwamoto, Ko-ichi Kikuta and Shin-ichi Hirano, "[Si-Ti-Y-O-N] multicomponent ceramics derived from polymeric precursors", Ceram. Trans., **83**, 63-70 (1998).

(3) Yuji Iwamoto, Sachiko Okuzaki, Ko-ichi Kikuta and Shin-ichi Hirano, "Processing of SiC ceramics using chemically modified polycarbosilane containing fluoroalkoxy groups as binder", Ceram. Trans., **83**, 77-82 (1998).

(4) Yuji Iwamoto, Ko-ichi Kikuta and Shin-ichi Hirano, "Si_3N_4-SiC-Y_2O_3 ceramics derived from yttrium-modified block copolymer of perhydropolysilazane and hydroxy-polycarbosilane", J. Mater. Res., **14**[5], 1886-95 (1999).

(5) Yuichi Sawai, Yuji Iwamoto, Sachiko Okuzaki, Yoshiyuki Yasutomi, Koichi Kikuta and Shin-ichi Hirano, "Synthesis of silicon carbide ceramics using chemically modified polycarbosilanes as a compaction binder", J. Am. Ceram. Soc., **82**[8], 2121-2125 (1999).

(6) Yuichi Sawai, Yuji Iwamoto, Sachiko Okuzaki, Yoshiyuki Yasutomi, Koichi Kikuta and Shin-ichi Hirano, "Processing of SiC ceramics with high reliability using chemically modified polycarbosilane as a compaction binder", J. Ceram. Soc. Japan, **107**[11], 1001-1006 (1999).

(7) Yuji Iwamoto, Ko-ichi Kikuta and Shin-ichi Hirano, "Si_3N_4-TiN-Y_2O_3 ceramics derived from chemically modified perhydropolysilazane", J. Mater. Res., **14**[11], 4294-4301 (1999).

(8) Yuji Iwamoto, Ko-ichi Kikuta and Shin-ichi Hirano, "Synthesis of poly-titanosilazanes and conversion into Si_3N_4-TiN ceramics", J. Ceram. Soc. Japan, **108**[4], 350-356 (2000).

(9) Yuji Iwamoto, Ko-ichi Kikuta and Shin-ichi Hirano, "Crystallization and microstructure development of Si_3N_4-Ti(C,N)-Y_2O_3 ceramics derived from chemically modified perhydropolysilazane", J. Ceram. Soc. Japan, **108**[12], 1072-1078 (2000).

II. General list of publications

(1) Toyohiko Aoyama, Yuji Iwamoto and Takayuki Shioiri, “New methods and reagents in organic synthesis. 59. Lithum trimethylsilyldiazomethane: A new synthon for the preparation of 5-substituted 1,2,3-thiadaiazoles”, Heterocycles, **24**, 589-592 (1986).

(2) Takayuki Shioiri, Yuji Iwamoto and Toyohiko Aoyama, “New methods and reagents in organic synthesis. 68. Reaction of thioketones with lithum trimethylsilyldiazomethane”, Heterocycles, **26**, 1467-1470 (1987).

(3) Toyohiko Aoyama, Yuji Iwamoto, Satoshi Nishizaki and Takayuki Shioiri, “New methods and reagents in organic synthesis. 78. Reaction of trimethylsilyldiazomethane with olefines”, Chem. Pharm. Bull., **37**[1], 253-256 (1989).

(4) Yuji Iwamoto, Akira Kuibira, Isao Sugiura and Jun-ichiro Tsubaki,“Effect of powder properties on thermal conductivity of aluminum nitride”, J. Ceram. Soc. Japan, **100**[5], 652-656 (1992).

(5) Yuji Iwamoto, Hiroshi Nomura, Isao Sugiura, Jun-ichiro Tsubaki, Hideo Takahashi, Kimiharu Ishikawa, Nobuhiro Shinohara, Masatarou Okumiya, Tetsuo Yamada, Hidehiro Kamiya and Keizo Uematsu, “Microstructure evolution and mechanical strength of silicon nitride ceramics”, J. Mater. Res., **9**[5], 1208-1213 (1994).

(6) Yuji Iwamoto, Hideaki Matsubara and Richard J. Brook, Microstructural development of Si_3N_4-Y_2O_3 ceramics derived from polymer precursors”, Ceram. Trans., **51**, 193-197 (1995).

(7) Hideo Takahashi, Nobuhiro Shinohara, Masatarou Okumiya, Keizo Uematsu, Jun-ichiro Tsubaki, Yuji Iwamoto and Hidehiro Kamiya, “Influence of slurry flocculation on the character and compaction of spry-dried silicon nitride granules”, J. Am. Ceram. Soc., **78**[4], 903-908 (1995).

(8) Yuji Iwamoto, Sun-Gi Shin and Hideaki Matsubara, “Grain growth behavior of ceramics under the existence of a liquid phase”, Ceram. Trans., **71**, 483-490 (1997).

(9) Yumi H. Ikuhara, Yuji Iwamoto, Ko-ichi Kikuta and Shin-ichi Hirano, “Processing of $LiMn_2O_4$ powders by precursor method”, Ceram. Trans., **83**, 53-59 (1998).

(10) Koji Sato, Yuji Iwamoto, Ko-ichi Kikuta and Shin-ichi Hirano, “Preparation of alumina-chromia solid solution powder and thin film through precursor method”, Ceram. Trans., **83**, 451-457 (1998).

(11) Sachiko Okuzaki, Yuji Iwamoto, Shinji Kondoh, Ko-ichi Kikuta and Shin-ichi Hirano, “Processing of silicon carbide ceramics using chemically modified polycarbosilanes”, J. Mater. Res., **14**[1], 189-195 (1999).

(12) Sachiko Okuzaki, Yuji Iwamoto, Ko-ichi Kikuta and Shin-ichi Hirano, “Synthesis and properties of chemically modified polycarbosilane containing organofluoric groups”, J. Mater. Res., **14**[4], 1353-1358 (1999).

(13) Shinji Kondoh, Yuji Iwamoto, Ko-ichi Kikuta and Shin-ichi Hirano, “Novel processing of mesoporous silica films with one-dimensional through channels normal to the substrate surface”, J. Am. Ceram. Soc., **82**[1], 209-212 (1999).

(14) Yumi H. Ikuhara, Yuji Iwamoto, Ko-ichi Kikuta and Shin-ichi Hirano, “Synthesis, electrochemical and microstructural study of precursor-derived $LiMn_2O_4$ powders”, J. Mater. Res., **14**[7], 3102-3110 (1999).

(15) Katsuyuki Matsunaga, Yuji Iwamoto, Craig A. J. Fisher and Hideaki Matsubara, “Molecular dynamics study of atomic structures in amorphous Si-C-N ceramics”, J. Ceram. Soc. Japan, **107**[11], 1025-1031 (1999).

(16) Katsuyuki Matsunaga, Yuji Iwamoto and Hideaki Matsubara, “Molecular orbital calculations of chemical bonding states of solute elements in amorphous silicon nitride”, J. Mater. Res., **15**[2], 429-436 (2000).

(17) Yumi H. Ikuhara, Yuji Iwamoto, Ko-ichi Kikuta and Shin-ichi Hirano, “Precursor derived $LiMn_2O_4$ thin films as ionic conductor”, Ionics, **6**, 156-160 (2000).

(18) Takaaki Nagaoka, Yuji Iwamoto, Ko-ichi Kikuta and Shin-ichi Hirano, “Forming and sintering of in-situ alumina composite with hydraulic inorganic binder”, J. Am. Ceram. Soc., **83**[7], 1613-1616 (2000).

(19) Issei Hayakawa, Yuji Iwamoto, Ko-ichi Kikuta and Shin-ichi Hirano, “Gas sensing properties of platinum dispersed-TiO_2 thin film fired in NH_3”, Sens. Acutuators, **B 62**, 55-60 (2000).

(20) Issei Hayakawa, Yuji Iwamoto, Ko-ichi Kikuta and Shin-ichi Hirano, “Gas sensing properties of metal-organics derived Pt dispersed-TiO_2 thin film derived from precursor”, Sens. Acutuators, **B 67**, 270-274 (2000).

(21) Koji Sato, Yuji Iwamoto, Ko-ichi Kikuta and Shin-ichi Hirano, “Effect of UV-irradiation on processing of lead titanate thin film derived from photoreactive [Pb-Ti] precursor modified with alkanolamine”, J. Ceram. Soc. Japan, **108**[11], 998-1002 (2000).

(22) Yumi H. Ikuhara, Yuji Iwamoto, Ko-ichi Kikuta and Shin-ichi Hirano, “Processing of epitaxial $LiMn_2O_4$ thin film on MgO(110) through metallorganic precursor”, J. Mater. Res., **15**[12], 2750-57 (2000).

(23) Issei Hayakawa, Yuji Iwamoto, Ko-ichi Kikuta and Shin-ichi Hirano, “Microstructural evolution of metallorganic derived Pt-doped TiO_2”, J. Mater. Res., **15**[12], 2794-99 (2000).

(24) Takaaki Nagaoka, Yuji Iwamoto, Ko-ichi Kikuta and Shin-ichi Hirano, “Forming and sintering of alumina with hydraulic inorganic binder”, Ceram. Trans., 112, 831-836 (2001).

(25) Yuji Iwamoto, Katsuyuki Matsunaga, Tomohiro Saito, Wolfgang Völger, Edwin Kroke and Ralf Riedel, “Crystallization behaviors of amorphous Si-C-N ceramics derived from organometallic precursors”, J. Am. Ceram. Soc., **84**[10], 2170-78 (2001).

(26) Katsuyuki Matsunaga and Yuji Iwamoto, “Molecular dynamics study of atomic structure and diffusion behavior of boron containing amorphous silicon nitride”, J. Am. Ceram. Soc., **84**[10], 2213-19 (2001).

(27) Yumi H. Ikuhara, Xiuliang Ma, Yuji Iwamoto, Ko-ichi Kikuta and Shin-ichi Hirano, “Interfaces between solution-derived $LiMn_2O_4$ thin film and MgO and Au/MgO substrates”, J. Mater. Res., **17**[2], 358-366 (2002).

(28) Katsuyuki Matsunaga, Yuji Iwamoto and Yuichi Ikuhara, “Atomic structure and diffusion in Si-B-C-N by molecular dynamics simulation”, Mater. Trans-JIM, **43**, 1506-11 (2002).

(29) Wolfgang Völger, Edwin Kroke, Christel Gervais, Tomohiro Saito, Florence Babonnau, Ralf Riedel, Yuji Iwamoto and Tsukasa Hirayama, “B/C/N materials and B_4C synthesized by a non-oxide sol-gel process”, Chem. Mater., **15**[3], 755-764 (2003).

(30) Masato Yoshiya, Craig A. J. Fisher, Yuji Iwamoto, Minoru Asanuma, Takashi Anyashiki and Kazuya Yabuta, “Phase stability of $BaCo_{1-y}Fe_yO_{3-\delta}$ by first principles calculations”, Solid State Ionics, in press.

(31) M. D. Hasan Zahir, Takeshi Inada, and Yuji Iwamoto, “Development of hydrothermally stable sol-gel derived La_2O_3-doped Ga_2O_3-Al_2O_3 composite mesoporous membrane”, submitted to J. Membr. Sci..

(32) Craig A. J. Fisher, Yuji Iwamoto, Minoru Asanuma, Takashi Anyashiki and Kazuya Yabuta, “Atomic simulations of oxide ion diffusion in heavily doped $LaCoO_3$”, submitted to J. Europ. Ceram. Soc..

(33) Takeshi Inada, Takeharu Kato and Yuji Iwamoto, “Mesoporous alumina capillary tube as a fine support for high-temperature gas separation membranes by novel pulse sequential anodic oxidation technique” , submitted to J. Mater. Res..

(34) Yuji Iwamoto, Koji Sato, Takeharu Kato, Takeshi Inada and Yukio Kubo, “A hydrogen permselective amorphous silica membrane derived from polysilazane”, submitted to J. Europ. Ceram. Soc..